Mechanisms of Epithelial Polarity in *Drosophila*

Francisca Geraldes Coelho Nunes de Almeida

A thesis presented for the degree of

Doctor of Philosophy

MRC Laboratory for Molecular Cell Biology

University College London

June 2018

Declaration

I, Francisca Geraldes Coelho Nunes de Almeida, confirm that the work presented in this thesis is my own. Where information has been derived from other sources, I confirm that this has been indicated in the thesis.

Signature:

Name:

Date:

Abstract

In epithelial cells, establishment of apical-basal polarity and specification of distinct membrane domains, such as cell-cell contacts, are fundamental processes during organogenesis. Polarised epithelial morphogenesis relies on a set of conserved polarity factors, namely Cdc42-Par6-aPKC-Baz/Par3 (the Par complex) and Crumbs-Stardust-Patj (the Crumbs complex). My work addresses how these two complexes cooperate in specifying and developing the apical membrane and epithelial cell contacts. Within the Par complex, Par6 is an effector of the small GTPase Cdc42 and is thought of as a regulatory unit for aPKC, which is the signalling component of the complex. My work indicates that in epithelial cells, Par6 assumes a novel and essential role in coupling cortical polarity with membrane delivery to drive epithelial morphogenesis. More specifically, Par6 binding to Cdc42 directs the assembly of the Par complex and enables the apical localisation of Par6-aPKC. In addition, Cdc42 enables apical retention of Par6-aPKC through promoting Par6 binding to Crumbs, which defines the boundaries of epithelial cell contacts. During this process, a link between the Par complex and the exocyst, couples polarity at the apical cortex with cargo delivery, including Crumbs. This coupling between Par6 and Crumbs defines a feedback loop that drives apical membrane and epithelial cell contact morphogenesis. In parallel, another Cdc42 effector, Mbt/Pak4, regulates the accumulation of junctional proteins at the cell contacts and enables a retention mechanism for Baz/Par3 that prevents ectopic Par complex assembly at the lateral cortex. Altogether, my work elucidates how two Cdc42 effectors, Par6 and Mbt, coordinate the specification and maturation of the apical membrane and cell contacts, via exocyst-dependent membrane delivery and multiple retention mechanisms.

Impact Statement

Epithelial tissues are an essential component of the human body, lining both the inside and outside of our organs. It is crucial that epithelial tissues maintain a well-established architecture in order to contribute to the accurate development and homeostasis of the human body. The establishment and maintenance of apical-basal polarity plays a central role in supporting epithelial tissue architecture. Therefore, it is not surprising that loss of apical-basal polarity is a hallmark of cancer, particularly considering that most cancers have an epithelial origin. Model organisms such as *Drosophila melanogaster* have been widely used to study the mechanisms that regulate apical-basal polarity. A detailed comprehension of how these apical-basal polarity mechanisms regulate normal tissue organisation is essential to understand how tissue architecture is lost during cancer progression.

The work I have developed during my PhD contributes to the understanding of the basic mechanisms that regulate apical-basal polarity and tissue architecture. In particular, my work has shed new light on how epithelial cells generate and spatially separate distinct membrane domains. Two chapters of this thesis focus on Par6 and present evidence that it coordinates polarity at the cell cortex and regulates plasma membrane delivery, therefore promoting apical membrane and cell-cell contact morphogenesis. Interestingly, Par6 overexpression has been observed in multiple cancer patients, such as breast and liver cancer patients (Nolan et al., 2008, Zhang et al., 2016). In addition, Par6 is a regulator of aPKC, a kinase that is a well known proto-oncogene (Lee and Vasioukhin, 2008). Understanding novel roles for Par6 in epithelial cell polarity will enable the launch of more applied studies with the aim of circumventing Par6-related polarity deficiencies

observed in many cancers.

In addition, my PhD work further elucidates how epithelial cells establish cell-cell contacts and clearly separate these contacts from the apical and basolateral domains. The formation of these intercellular contact sites is essential for the development of epithelial tissues in order to maintain their integrity, and is in part controlled by intracellular polarity regulators. Importantly, loss of key components of these contact sites is known to occur at later stages of cancer progression and is thought to be involved in epithelial-mesenchymal transition (EMT) and consequent metastasis (Royer and Lu, 2011).

My work helps understanding the basic mechanisms of apical-basal polarity. New research in this field is essential to understand the mechanisms that regulate apical-basal polarity and their role in tissue architecture, as well as during cancer progression. This knowledge will be the starting point for groundbreaking applied research and subsequent clinical experiments towards the development of novel cancer therapies.

Acknowledgements

This work would not have been possible without the financial support of the **Medical Research Council (MRC)**.

I am truly grateful to my supervisor, **Franck Pichaud**, for mentoring me during this 4-year journey of my PhD. Your support, motivation and enthusiasm made it much easier to go through the ups and downs of a PhD.

I am also profoundly grateful to all the members of my PhD committee: **Ewa Paluch**, **Julie Pitcher** and **Buzz Baum**. Your insightful comments, hard questions and encouragement were invaluable throughout my PhD. A special thanks to Ewa for being the chair of my PhD committee.

My research would have been impossible without the aid and support of **Rhian Walther**. You taught me more than I can ever give you credit for (like, pretty much ALL I know about flies) and it has been an honour to learn it from the best. I am tremendously grateful for your guidance, help and most of all, generosity, sharing your projects with me during the past years. You have shown me, by your example, how a good scientist should be.

I thank my fellow labmates at the Pichaud lab for all the support they gave me during my PhD. **Laura**, you know you are the best! We started and finished this journey at the same time, you are basically my PhD twin-sister and I am truly grateful for your help, wisdom, insightful comments and patience throughout this journey. **Chiara**, you have been a true example of perseverance and discipline to which I am really grateful. Many thanks for all the scientific (and non-scientific) discussions we had in the past

years. **Evi**, thanks for your help, feedback and for bringing such a great atmosphere to the lab while you were around. **Tim**, thanks for all the help during the first years of my PhD and the most important, for always staying later in the pub for that one more pint. **Kate** and **Mubarik**, thanks for all the discussions we had (mostly while flipping flies). A special thanks to Rhian and Laura for going through the painful task of reading this thesis. Also, my sincere thanks to **David Ish-Horowicz** for generously infiltrating our lab meetings, giving me valuable feedback throughout my PhD.

I would like to thank a few people at the LMCB that made the past years a lot easier and very enjoyable. **Cristina** as much as I thank you, it will never be enough. You have not only mentored me as a scientist, allowing me to learn biochemistry from the best, but you have also been an inspiration as a person. Thanks for always being there and for all your wisdom during the past years. **Mafalda** and **Joana** thanks for all the support and fun, especially during our coffee breaks at the LMCB. **Alex**, **Christian**, **Georgina**, **Beth** and (again!) **Laura**, thanks for being the best "PhD programme mates" ever and for all the fun we had in the past 5 years. Also, I want to thank to all my office mates, especially **Hamish** for your support and wise discussions.

Rita, thanks for teaming up with Cristina in dragging me out of the lab most weekends for that amazing brunch, pint or just a coffee break and some great chat.

To my "UK family": **André**, **Bárbara**, **Cabeleira**, **Carmen**, **Carol**, **Eduardo**, **Inês Mota**, **Inês Vale**, **Miguel** and **Queirós**, you made London feel like home during the past 5 years and thanks for listening and being there every time I felt frustrated during my PhD. Obrigada!

Nobody has been more supportive in the pursuit of this project than the members of my family. To my parents: these were particularly tough years and you are an example of mental and physical strength, an inspiration of ethics and integrity. Thanks for being my ultimate role model. **João** thanks for always supporting me, no matter what. **Marina** thanks for being so patient and supportive, especially during the writing of this thesis.

Table of Contents

Declaration **1**

Abstract **2**

Impact Statement **3**

Acknowledgements **5**

List of Figures **11**

List of Tables **13**

1 Introduction **17**

1.1 Polarity in epithelial cells 18

1.2 *Drosophila melanogaster* as a model system 20

1.2.1 The *Drosophila* photoreceptor 21

1.2.2 The *Drosophila* follicular epithelium 23

1.3 Epithelial polarity determinants 24

1.3.1 The small GTPase Cdc42 29

1.3.2 The Par complex 33

1.3.3 The Crumbs complex 36

1.3.4 The Scribble complex 40

1.3.5 Par1 42

1.4 *Zonula Adherens* morphogenesis 42

1.4.1 Adherens junction components 43

1.4.2 Mbt as a regulator of AJ morphogenesis 45

1.5 Trafficking 46

1.5.1 The exocyst 47

1.5.2 Regulation of E-cad trafficking 48

1.5.3 Regulation of Crb trafficking 49
1.6 Epithelial cell polarity and cancer 50

2 Aims **53**

3 Materials and Methods **54**
3.1 Fly food and stocks 55
3.2 Genotypes 55
3.3 Genetic techniques 57
3.3.1 *GAL4-UAS* system 57
3.3.2 Genetic Mosaics 58
The FLP-FRT system 58
The MARCM system 59
The *coinFLP-GAL4* system 60
3.3.3 P-element imprecise excision 61
3.4 Reagents 62
3.4.1 Antibodies 62
3.4.2 Plasmids 63
3.5 Molecular Cloning 64
3.5.1 Generation of competent bacteria 64
3.5.2 Restriction enzyme based cloning 64
3.5.3 Gateway system cloning 65
3.5.4 Site-directed mutagenesis 65
3.5.5 *Drosophila* genomic DNA extraction 66
3.5.6 DNA sequencing and analysis 66
3.6 Cell culture 67
3.6.1 Cell lines and maintenance 67
3.6.2 Transient transfection 67
3.7 Biochemistry 67
3.7.1 Expression and purification of recombinant proteins 67
3.7.2 *In vitro* binding assay 68
3.7.3 GST Pulldowns 68
3.7.4 Co-immunoprecipitation 69

3.7.5 *Drosophila* protein extraction 69
3.7.6 Western Blotting 69
3.7.7 Kinase Assay 70
3.8 Microscopy 71
3.8.1 S2 cell aggregation assay 71
3.8.2 Immunofluorescence of *Drosophila* pupal retinae 71
3.8.3 Immunofluorescence of *Drosophila* adult retinae 72
3.8.4 Cryosectioning of *Drosophila* adult retinae 72
3.8.5 Immunofluorescence of *Drosophila* follicle cells 73
3.8.6 Fluorescence recovery after photobleaching (FRAP) 74
3.9 Data analysis and Statistics 76
3.9.1 Western blot quantification 76
3.9.2 FRAP data analysis 76
3.9.3 Confocal data analysis 76
Area and pixel intensity quantifications 77
Intensity profiles 77
3.9.4 Protein sequence alignment 77

4 Par6 regulation during epithelial morphogenesis 78
4.1 Polarity protein network in two epithelial tissues 79
4.2 Par6 is essential during epithelial morphogenesis 80
4.3 aPKC regulates the apical localisation and stability of Par6 84
4.4 Binding to Cdc42 regulates Par6 apical recruitment and localisation . . 87
4.5 Crb mediates Cdc42-dependent apical retention of Par6-aPKC 89
4.6 Crb stabilizes Par6 at the apical membrane 91
4.7 Discussion 92

5 The Par complex regulates Crb delivery via the exocyst 98
5.1 The Par complex has multiple links to the exocyst 99
5.2 *exo84* is required for Crb apical delivery 101
5.3 The exocyst regulates apical membrane morphogenesis 105
5.4 RalA is required for Crb delivery 105
5.5 RalA regulates vesicle tethering redundantly via Exo84 and Sec5 108

5.6 Discussion 111

6 Mbt regulation during *ZA* morphogenesis **114**

6.1 Mbt is a core component of the AJ 115

6.2 Mbt regulates *ZA* morphogenesis through Arm phosphorylation 116

6.3 Discussion 120

7 Discussion and Perspectives **123**

References **127**

Appendix A **147**

Reagents: Plasmids 147

Appendix B **153**

Complementary data to Chapter 4 153

Appendix C **157**

Published Manuscript:

Pak4 Is Required during Epithelial Polarity Remodeling through Regulating *AJ* Stability and Bazooka Retention at the *ZA* 157

List of Figures

1.1 Cell polarity in different organisms 19
1.2 *Drosophila* and vertebrate epithelial cells 20
1.3 The *Drosophila* developing photoreceptor 22
1.4 Structure of the *Drosophila* ovariole 24
1.5 Structure and interactions of proteins that regulate epithelial cell polarity in *Drosophila* 28
1.6 The Cdc42 GTPase cycle 30
1.7 Cell-cell adhesion molecules in *Drosophila* epithelial cells 44

3.1 The *GAL4-UAS* system 58
3.2 The FLP-FRT system 59
3.3 The MARCM system 60
3.4 The coinFLP system 61
3.5 Sample preparation for FRAP 75

4.1 Polarity protein network in the follicular epithelium 79
4.2 Par6 is essential for plasma membrane partitioning into different domains 81
4.3 Interactions between Par6 transgenes and polarity determinants. 83
4.4 Expression of the *par6* transgenes *in vivo* 84
4.5 aPKC binding is essential for Par6 apical accumulation 85
4.6 aPKC binding promotes Par6 apical localisation 86
4.7 Par6 binding to Cdc42 is required for the apical localisation of Par6-aPKC 88
4.8 $Par6^{SE}$::GFP overexpression leads to severe polarity defects 89
4.9 Crb promotes the apical retention of Par6-aPKC 90
4.10 Par6 binding to Crb is required for the accumulation of Par6-aPKC at the apical cortex 91
4.11 Par6 binding to Crb slows down the recovery of Par6 after photobleaching 92

4.12 Par6 regulates apical membrane and *ZA* morphogenesis 94

5.1 Ed-Exo84 recruits Par6 to the cell-cell junctions 100
5.2 The Par complex is linked to the exocyst via Par6 and Baz 100
5.3 The Drosophila *exo84* gene 102
5.4 *exo84* is required for Crb acummulation at the apical membrane 103
5.5 *exo84* is required for Crb delivery to the apical membrane 104
5.6 Sec5 is required for Crb delivery to the apical membrane 105
5.7 RalA is required for Crb accumulation at the apical membrane 106
5.8 RalA does not regulate the delivery of the apical cargoes Rh1 and Eys . 107
5.9 Individual uncoupling of RalA from Exo84 and Sec5 109
5.10 RalA binding to at least one exocyst component is sufficient to rescue the *ralA*^{EE1} rough eye phenotype 110
5.11 RalA is localised at the cell cortex 110
5.12 Par6 couples cortical polarity to plasma membrane morphogenesis . . . 112

6.1 Mbt phosphorylates Arm, but not Par6 117
6.2 E-cad::GFP recovery after photobleaching at the apical and basal tips of the *ZA* 118
6.3 Arm phosphorylation regulates E-cad stability during *ZA* morphogenesis 119
6.4 Mbt regulates AJ stability and Baz retention at the *za* 121

7.1 Par6 binding to Cdc42 is required to separate Par6 from Baz 154
7.2 Par6-aPKC distributes between the Par and Cdc42-Par6-aPKC complexes 155
7.3 Par6 binding to Crb promotes the accumulation of both Par6-aPKC and Crb 156

List of Tables

1.1 Polarity protein complexes 25

1.2 Protein-protein interactions between polarity determinants 27

3.1 Primary antibodies and dilutions used for western blotting. 62

3.2 Secondary antibodies and dilutions used for western blotting. 62

3.3 Primary antibodies and dilutions used for immunofluorescence. 63

3.4 Secondary antibodies and dilutions used for immunofluorescence. 63

3.5 Primers used for RalA mutagenesis. 66

4.1 Par6 transgenes generated to individually uncouple Par6 binding aPKC, Crb and Cdc42. 82

7.1 Plasmids constructed for this thesis. 148

7.2 Plasmids kindly provided by colleagues. 150

Abbreviations

AJ Adherens Junction

APF After Puparium Formation

aPKC Atypical Protein Kinase C

Arm Armadillo

Baz Bazooka

BDSC Bloomington Drosophila Stock Center

Cno Canoe

Crb Crumbs

CRIB Cdc42/Rac-interactive-binding

DGRC Drosophila Genomics Resource Center

Dlg Discs large

DSHB Developmental Studies Hybridoma Bank

E-cad E-cadherin

ECM extracellular matrix

ECR evolutionary conserved region

Ed Echinoid

EGF epidermal growth factor

EMT Epithelial-Mesenchymal Transition

ER endoplasmic reticulum

ey *eyeless*

Eys Eyes shut

FC follicle cell

FE follicular epithelium

FERM four-point-one, ezrin, radixin, moesin

Flp Flip-recombinase

FRAP Fluorescence recovery after photobleaching

FRT *Flippase recognition target*

GAP GTPase activating protein

GDI guanine nucleotide dissociation inhibitor

GEF guanine nucleotide exchange factor

GMR *Glass Multimer Reporter*

GUK guanylate kinase

Lgl Lethal giant larvae

LIMK1 LIM domain kinase 1

Lin27 Lin-2/Lin-7

LRD lysine-rich domain

MAGUK membrane-associated guanylate kinase

MARCM mosaic analysis with a repressible cell marker

Mbt Mushroom bodies tiny

MDCK Madin-Darby canine kidney

MET Mesenchymal-Epithelial Transition

OD oligomerisation domain

Pak p21-activated kinase

Par Partitioning-defective

Patj Protein associated with tight junction

PB1 Phox/Bem 1

PCP planar cell polarity

PDZ PSD95/Discs-large/ZO1

PI3K phosphatidylinositol 3-kinase

PIP_2 phosphatidylinositol (4,5)-biphosphate

PIP_3 phosphatidylinositol (3,4,5)-triphosphate

Ral Ras-like

Rh1 Rhodopsin-1

ROI Region of Interest

RT Room Temperature

Scrib Scribble

Sdt Stardust

SH3 Src homology 3

SJ Septate Junction

TGN trans-Golgi network

TJ Tight Junction

UAS *Upstream Activation Sequence*

VDRC Vienna Drosophila Resource Center

WASp Wiskott-Aldrich Syndrome protein

ZA *Zonula Adherens*

Chapter 1

Introduction

Polarity is defined in the *Oxford English Dictionaries* as "the tendency of living organisms or parts to develop with distinct anterior and posterior (or uppermost and lowermost) ends, or to grow or orientate in a particular direction" (n.d. *Oxford English Dictionaries*. Retrieved April 16, 2018, from https://en.oxforddictionaries.com). In other words, in cells, polarity can be described as the generation of cell asymmetry, which is translated by a different structure, composition or function between at least two poles of the cell (Chen and Zhang, 2013). Most cells are polarised, from simple unicellular organisms, such as bacteria or budding yeast, to the more complex multicellular invertebrates and vertebrates (Figure 1.1) (Nelson, 2003). In all of these different organisms, cell polarity is required to perform a variety of cellular functions, such as growth of budding yeast, cell division, cell migration, vectorial transport of molecules across epithelial cell layers and long-range transmission of nerve impulses (Assémat et al., 2008, Mellman and Nelson, 2008). Such a diverse range of cell types and functions suggests that the regulatory mechanisms that establish cell polarity have evolved differently amongst different organisms. However, from budding yeast to epithelial tissues, the basic mechanisms and regulators that generate polarity are highly conserved in both their structure and function (Nelson, 2003). In this chapter, I will give an overview of the mechanisms that regulate cell polarity, with a particular focus on epithelial tissues in *Drosophila*.

1.1 Polarity in epithelial cells

Polarity is a feature of a variety of cell types and plays distinct roles in many cellular functions. There are a number of well-defined examples of polarised cells that offer an opportunity to study the mechanisms that regulate cell polarity (Figure 1.1). Within these different cell types, cell polarity can be further designated as apical-basal polarity in epithelial cells, planar cell polarity (PCP) during tissue morphogenesis, anterior-posterior polarity in the *Caenorhabditis elegans* embryo or transient polarity in migrating cells (Figure 1.1) (Chen and Zhang, 2013).

A classical example of polarised cells is found in epithelia, which line the surface of a variety of organs in our body (*e.g.* in the respiratory, digestive and urinary systems). Epithelial cells are the most common cell-type in multicellular organisms and provide a diffusion barrier between the interior and exterior surfaces of our body (Chen and Zhang, 2013). These cells are closely packed together, forming an impermeable sheet of epithelial cells. Adherens Junctions (AJs), the cell-cell contact regions that provide a mechanical and signalling link to neighbouring cells, play a key role in maintaining tissue architecture, while Tight Junctions (TJs) (Septate Junctions (SJs) in *Drosophila*) act as paracellular diffusion barriers (Figure 1.2) (Chen and Zhang, 2013). Additional cell-cell junctions include gap junctions, which form intercellular channels that allow the exchange of small molecules between neighbouring cells, and desmosomes, which provide a link to the intermediate filament cytoskeleton and are absent in *Drosophila* (Tepass et al., 2001). Importantly, epithelial cells are highly polarised along an apical-basal axis, which allow the vectorial transport of molecules between opposite sides of the epithelium, thus regulating compartment composition and the function of different organs (Tepass, 2012).

Polarity in epithelial cells results in the establishment of at least two distinct membrane domains that are physically separated by the *Zonula Adherens* (*ZA*), the intercellular signalling and adhesion belt of AJs that maintains cells together. These two domains are the apical surface, facing the lumen or the external free surface, and the basolateral surface, which is in contact with the neighbouring cells, as well as with the basement membrane (Figure 1.2). The formation of these domains (*i.e.* apical domain, *ZA* and basolateral domain) is highly conserved amongst metazoans. However, the paracellular

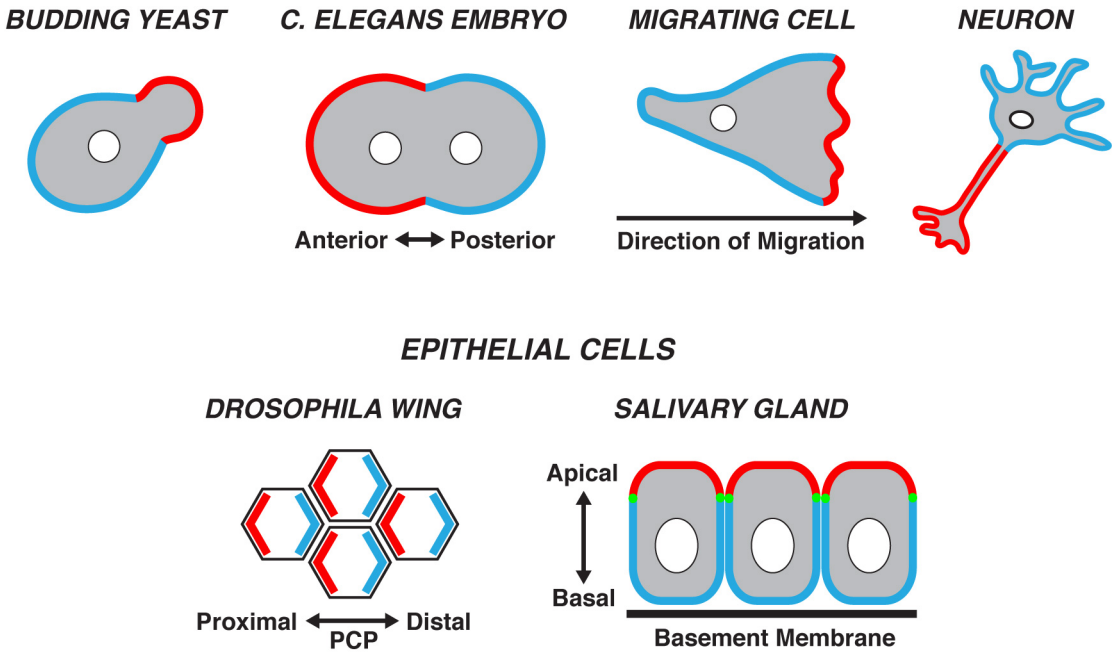

Figure 1.1: Cell polarity in different organisms. Budding yeast (*Saccharomyces cerevisiae*) is a simple and well-studied example of a cell that grows isotropically until it forms a polarised bud and undergoes cell division (Pruyne et al., 2004). The *C. elegans* one-cell embryo divides asymmetrically along the anterior-posterior axis, to generate two distinct cells that will give rise to different founder cells (Johnston and Ahringer, 2010). Migrating fibroblasts are polarised along the direction of migration, developing two distinct membrane domains at the front and rear ends of the cell (Watanabe et al., 2005). Neurons are highly polarised cells that transmit a unidirectional signal from their dendrites along their axon (Arimura and Kaibuchi, 2007). Epithelial cells are polarised along two axes: proximal-distal and apical-basal axes. In the *Drosophila* wing, planar cell polarity (PCP) regulates epithelial cell polarity within the plane of the epithelium, giving cells a sense of direction that properly orients the bristles in the fly wing (Diaz de la Loza and Thompson, 2017). Epithelial cells are also polarised along an apical (top)-basal (bottom) axis, which allows these cells to develop into a continuous sheet of cells that forms a barrier between two different compartments within an organism (Assémat et al., 2008). Different colours (red/blue) represent distinct membrane domains.

barriers between cells differ between some organisms. For instance, vertebrate epithelial cells contain TJs, which localise apical to the AJs (Chen and Zhang, 2013). On the other hand, *Drosophila* epithelial cells do not have TJs, but have a functionally similar structure, the SJs, which localise basal to the AJs (Figure 1.2) (Chen and Zhang, 2013).

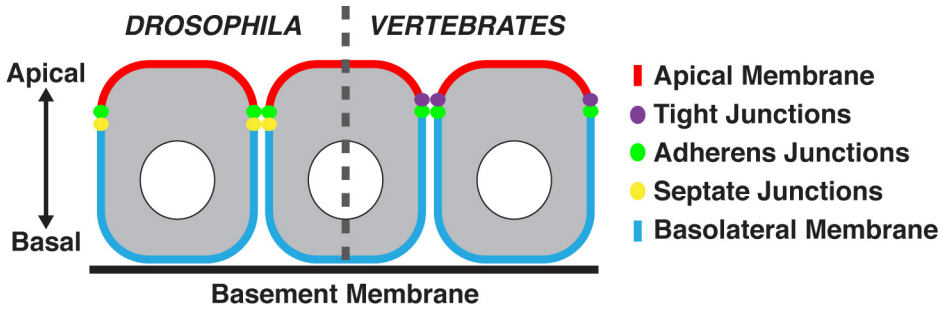

Figure 1.2: *Drosophila* and vertebrate epithelial cells. In all organisms, epithelial cells are physically linked to the neighbouring cells. Amongst different types of cell-cell junctions, the AJs (green) form a circular adhesive belt (the *ZA*) that maintains tissue integrity. The *ZA* separates the apical (red) from the basolateral domain (blue). Paracellular barriers are known as TJs (purple) in vertebrates or SJs (yellow) in *Drosophila* and localise apical or basal to the AJs, respectively.

1.2 *Drosophila melanogaster* as a model system

The fruit fly *Drosophila melanogaster* was initially used as a tool to study genetics at the early stages of the 20th century. However, its extensive number of appealing characteristics (*e.g.* low cost maintenance, rapid generation time and easily genetically modifiable), soon elected *Drosophila* as one of the most commonly used model systems in multiple areas of biology.

At 25 °C, fruit flies take approximately 10 days to develop from eggs into adults. *Drosophila* epithelia can derive from the blastoderm or from Mesenchymal-Epithelial Transition (MET) (Tepass et al., 2001). In the wake of fertilisation, the embryo follows a series of 13 nuclear divisions without cytokinesis (Tepass et al., 2001). With thousands of nuclei aligned at the surface of the one-cell embryo, at cell cycle 14, a process termed "cellularisation" occurs, in which the plasma membrane invaginates surrounding each nucleus and forming a sheet of individual epithelial cells (Tepass et al., 2001). At this stage (*i.e.* 4h post-fertilisation), the *Drosophila* blastoderm contains approximately 6,000 cells (Gilbert, 2000). During gastrulation, the blastoderm is re-organised into the three germ layers ectoderm, mesoderm and endoderm (Gilbert, 2000). One day after egg laying, larvae hatch and undergo three moulting stages known as instar stages that take approximately 4 days in total. During these three larval stages, the imaginal discs originate from the ectoderm, forming groups of undifferentiated cells that will undergo

metamorphosis and develop into different adult structures, such as the wings, legs or the fly head, among others (Müller, 2000). At conclusion of the third instar stage, larvae enter a metamorphic state known as pupation. Nearly 5 days after entering pupation, adult flies emerge. Within 10-12h the adults are sexually mature and able to initiate a new cycle.

Drosophila's genome is distributed over four pairs of chromosomes: a pair of sex chromosomes and three pairs of autosomes (*i.e.* 2nd, 3rd, and 4th chromosomes). Its small sized, fully sequenced genome and low gene redundancy allow the development of powerful genetic tools and large-scale genetic screens. Importantly, many proteins in *Drosophila* are evolutionarily conserved in higher organisms, in both their structure and function. In fact, *Drosophila*'s genome encodes for more than 75% of the proteins involved in human diseases, thus making *Drosophila* a very powerful tool to study human disease (Reiter et al., 2001).

There are many epithelia in *Drosophila* that can be used as models in the study of cell polarity, from simple undifferentiated epithelia (*e.g.* embryo, larval imaginal discs and follicular epithelium) to differentiated specialised tissues (*e.g.* pupal and adult retina) (Tepass, 2012).

1.2.1 The *Drosophila* photoreceptor

In *Drosophila*, the adult retina follows an extremely organised pattern, with repetitions of nearly 750 hexagonal subunits called ommatidia. Similarly to many other structures in flies, the retina develops from a simple monolayer epithelium, the eye-antennal imaginal disc.

Each ommatidium is organised as an hexagonal cluster with the 8 photoreceptors organised as a circular cluster within each ommatidium. The photoreceptors R1 to R7 form this circular cluster, with R8 sitting beneath R7 (Figure 1.3A-B). During pupal development, photoreceptors undergo extensive remodelling. At the initial stages of development, the apical-basal axis is aligned with the proximal-distal axis of the retina (Figure 1.3C). However, during pupal stage, the photoreceptors undergo a 90° rotation at the apical side towards the centre of the cluster, which establishes a new asymmetry axis (Figure 1.3C). At this stage, the photoreceptors become re-arranged with their

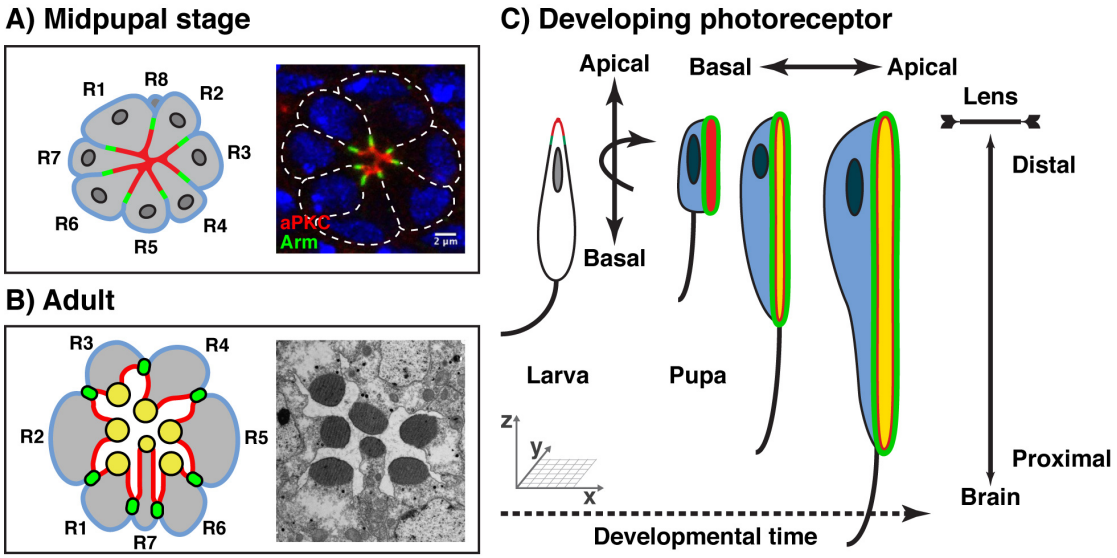

Figure 1.3: The *Drosophila* developing photoreceptor. (A and B) Schematic representation of a developing ommatidium at midpupal (A) and adult (B) stages. Confocal image of a *wild-type* ommatidium at midpupal stage (A) stained for aPKC (red) and Arm (green). Electron micrograph of a *wild-type* ommatidium at adult stage (B). **(C)** Developing photoreceptor from larval stage (left) to adult stage (right). During pupal stage, there is a 90° rotation of the photoreceptor polarity axis followed by its elongation. The axon (black line) projects to the optic lobe. From A to C, distinct membrane domains are represented in different colours: *ZA* in green, apical membrane (marginal zone) in red, rabdomeres in yellow and basolateral membrane in blue. Adapted from Walther et al. (2016).

apical membrane facing the centre of the cluster, which is followed by expansion of the membrane along the proximal-distal axis until it reaches the floor of the retina (Figure 1.3A-C). This is a remarkable morphogenetic step, as the apical membrane of the photoreceptors expands from a few µm to nearly 100 µm in length (Tepass and Harris, 2007). Concurrently, at the centre of the photoreceptor cluster, the apical membranes create a luminal space and differentiate to form the light-sensing, microvilli-rich structures called rhabdomeres (Figure 1.3B) (Tepass and Harris, 2007). Therefore, at the adult stage, the apical membrane of the photoreceptors is made up of the rhabdomere and a portion of subapical plasma membrane, the stalk membrane, that connects the rhabdomere to the *ZA* (Figure 1.3B) (Tepass and Harris, 2007).

The developing *Drosophila* photoreceptor has been extensively used as a model tissue to investigate the regulatory events involved in epithelial cell polarisation and membrane morphogenesis (Pichaud, 2018). There are two main reasons why the retina is widely

used for these studies. Firstly, it allows the study of embryonic lethal mutations *in vivo*, as the eye is not essential for the fly survival (Walther and Pichaud, 2006). Secondly, it allows the imaging in the *xy* axis of the clearly separated distinct plasma membrane domains (Walther et al., 2018).

1.2.2 The *Drosophila* follicular epithelium

The *Drosophila* follicular epithelium (FE) is an example of an epithelium that is generated from MET. In female flies, each ovary contains approximately 15 ovarioles, which consist of a series of progressively older egg chambers, reflecting the multiple stages of oogenesis (Figure 1.4) (Wu et al., 2008). At the anterior end of the germarium, a pair of germline stem cells undergo 4 mitotic divisions, forming a 16-cell cyst (Wu et al., 2008). From these 16 cells, one will become the oocyte, while the remaining will become nurse cells (Wu et al., 2008). In the middle region of the germarium, follicle stem cells form precursor follicle cells (FCs) that migrate towards the posterior region of the germarium and surround the 16-cell cyst, creating an epithelial monolayer around the germline cells (Figure 1.4) (Margolis and Spradling, 1995). The newly formed egg chamber leaves the germarium, while remaining connected to the neighbouring egg chambers through a stalk of 5-8 FCs (Figure 1.4) (Margolis and Spradling, 1995).

At the initial stages of oogenesis, the FCs form a cuboidal epithelium; however, between stages 8 and 10, the FCs start migrating towards the posterior pole of the egg chamber, forming a columnar epithelium at the posterior pole (*i.e.* around the oocyte) and a squamous epithelium at the anterior pole (*i.e.* around the nurse cells) (Figure 1.4) (Wu et al., 2008). From stage 10B to 14, the nurse cells deposit their cytoplasmic content in the oocyte, while the FCs secrete the vitelline membrane around the oocyte (Wu et al., 2008). Ultimately, as oocyte maturation is complete, both nurse cells and FCs undergo appoptosis (Wu et al., 2008). Similarly to the fly photoreceptor, FCs are highly polarised along an apical-basal axis, with an apical membrane facing the inner cyst and a basal membrane facing the outer region of the egg chamber (Figure 1.4).

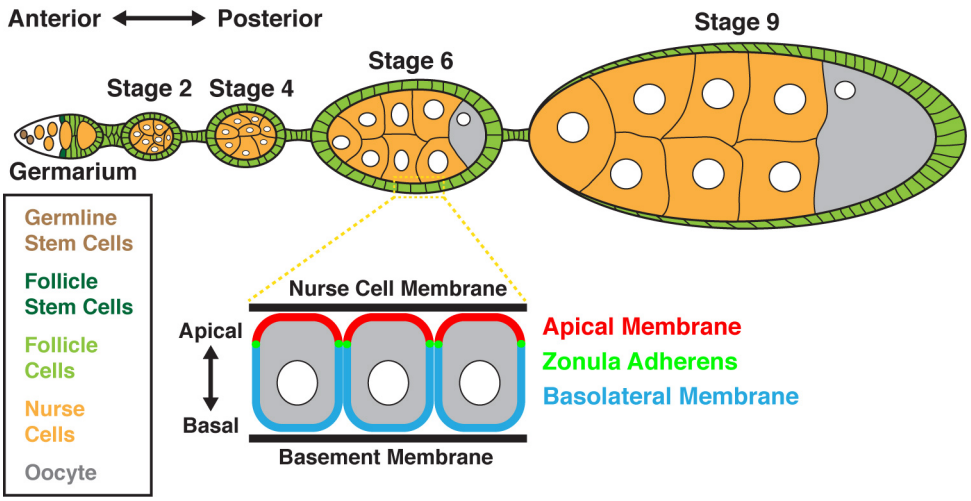

Figure 1.4: Structure of the *Drosophila* ovariole. At the anterior end, the germarium contains germline stem cells (brown) and follicle stem cells (dark green), which will form the different egg chambers, each including 15 nurse cells (yellow) and one oocyte (grey) surrounded by FCs (light green). FCs are initially cuboidal, but at stage 9 form a columnar epithelium at the posterior end and a squamous epithelium at the anterior end of the egg chamber. FCs are highly polarised along an apical-basal axis, displaying an apical membrane in contact with the inner cyst and a basal membrane facing the exterior of the egg chamber.

1.3 Epithelial polarity determinants

When forming an epithelium, cells are thought to start by sensing their environment in order to properly orientate their polarity. This is based on the communication not only with the extracellular matrix (ECM) (*e.g.* through integrins), but also with neighbouring cells (*e.g.* via cadherins) (Bryant and Mostov, 2008). Additionally, cells need to polarise protein complexes to specific cortical and membrane domains, which creates the asymmetry axis. This process is highly dependent on the polarisation of two cell machineries: the cytoskeleton and vesicle-trafficking (Bryant and Mostov, 2008).

Extensive work mainly in *C. elegans* and *Drosophila* strongly contributed to the discovery of the main regulators of epithelial cell polarity. These regulators are usually grouped into three main protein complexes, the Partitioning-defective (Par) protein complex, the Crumbs (Crb) complex and the Scribble (Scrib) complex, as in Table 1.1.

The *par* genes were first identified in the nematode *C. elegans* and encode six different proteins, from PAR-1 to PAR-6 (Kemphues et al., 1988, Watts et al., 1996). Together with the serine/threonine kinase aPKC ortholog, PKC-3, these proteins are key regula-

Table 1.1: Polarity protein complexes. The three main protein complexes that regulate cell polarity are: (1) the Par complex that consists of Cdc42, Par6, Atypical Protein Kinase C (aPKC) and Bazooka (Baz) (Par3 in vertebrates); (2) the Crb complex with the proteins Crb (Crb1-3 in vertebrates), Stardust (Sdt) (PALS1 in vertebrates), Protein associated with tight junction (Patj) and Lin-7; and (3) the Scrib complex containing Scrib, Lethal giant larvae (Lgl) and Discs large (Dlg).

Complex	***Drosophila***	**Vertebrates**
Par complex	Cdc42	Cdc42
	Par6	Par6
	aPKC	PKCζ, PKCλ/ι
	Baz	Par3
Crb complex	Crb	Crb1-3
	Sdt	PALS1
	Patj	Patj
	Lin-7	Lin-7
Scrib complex	Scrib	Scrib
	Lgl	Lgl
	Dlg	Dlg

tors of cell polarity in the *C. elegans* embryo (Tabuse et al., 1998). During *C. elegans* embryogenesis, the zygote undergoes a series of five asymmetric cell divisions that give rise to the six founder cells of the embryo (Gotta and Ahringer, 2001). During the first division, a specific set of PAR proteins localise asymmetrically, as PAR-3, PAR-6 and PKC-3 are restricted to the anterior pole, whereas PAR-1, PAR-2 and LGL-1 localise to the posterior pole of the one-cell embryo (Gotta and Ahringer, 2001). This segregation of PAR proteins defines the anterior-posterior axis of the zygote. In this system, the small GTPase CDC-42 maintains cell polarity by activating PKC-3, which then phosphorylates and restricts PAR-1, PAR-2 and LGL-1 to the posterior pole (Hao et al., 2006, Rodriguez et al., 2017). Similarly, PAR-2 and PAR-1 prevent the accumulation of anterior PARs at the posterior pole of the zygote (Hao et al., 2006). This recip-

rocal inhibition creates a mutually antagonistic regulatory mechanism responsible for maintaining polarity in the one-cell embryo.

The Par complex (Cdc42-Par6-aPKC-Par3) and its mutual antagonism with proteins such as Par1, were later on shown to be conserved in multiple organisms, playing a key role in polarity establishment, from *Drosophila* neuroblasts (Huynh et al., 2001), to *Xenopus laevis* oocytes (Nakaya et al., 2000), and importantly in the establishment of apical-basal polarity in epithelial cells (Benton and Johnston, 2003b). While the precise mechanisms may vary between different organisms or even between tissues, in most cases, the Par complex polarises at one side of the cell to drive asymmetry of its downstream effectors (Johnston and Ahringer, 2010, Rodriguez et al., 2017). In epithelial cells, while the Crb and Par complexes are restricted to the apical membrane, the Scrib complex, as well as the kinase Par1, are specific to the basolateral membrane (Tepass, 2012). The interactions between proteins of these different complexes are quite complex, yet highly conserved (Table 1.2). Importantly, the apical Par and Crb complexes, the basolateral Scrib complex and the kinase Par1 regulate each other in a mutually antagonistic manner, such as previously described in the *C. elegans* embryo.

Although most polarity proteins mentioned above are grouped into different complexes, in reality, the interaction between these proteins is extremely dynamic, potentially presenting varying stoichiometry (Figure 1.5 and Table 1.2). These dynamic interactions may be regulated tissue-specifically, during developmental time, or in response to environmental cues, increasing the complexity of polarity establishment and maintenance (Pires and Boxem, 2017). A very good example is the adaptor protein Par6, which is part of the Par complex where it binds Cdc42, aPKC and Baz/Par3 (Betschinger et al., 2003, Hutterer et al., 2004, Joberty et al., 2000, Lin et al., 2000, Petronczki and Knoblich, 2001, Qiu et al., 2000); however, it can also bind to Crb, Sdt/Pals1 and Patj at the apical side (Hurd et al., 2003, Kempkens et al., 2006, Lemmers et al., 2004, Nam and Choi, 2003, Wang et al., 2004), as well as to the basolateral protein Lgl (Betschinger et al., 2003, Plant et al., 2003, Yamanaka et al., 2003). Therefore, to fully understand how polarity regulators cooperate to establish and maintain epithelial cell polarity, we require a detailed knowledge of the structure of all these proteins, the detail of these molecular interactions and of the underlying genetic interactions. For the remainder of this subsection of my introduction, I will give an overview of these proteins that reg-

Table 1.2: Protein-protein interactions between polarity determinants. The different references that biochemically support these direct interactions in both *Drosophila* and vertebrates are listed following to the proteins involved. Proteins in **blue** mean that the kinase has been shown to phosphorylate its binding partner, which is shown in the references in **blue**.

Protein interactions	***Drosophila***	**Vertebrates**
Par6-aPKC	Betschinger et al. (2003)	Joberty et al. (2000), Lin et al. (2000), Qiu et al. (2000)
Par6-Cdc42	Hutterer et al. (2004)	Joberty et al. (2000), Lin et al. (2000), Qiu et al. (2000)
Par6-Baz/Par3	Petronczki and Knoblich (2001)	Joberty et al. (2000), Lin et al. (2000), Qiu et al. (2000)
Par6-Crb	Kempkens et al. (2006)	Lemmers et al. (2004)
Par6-Sdt/Pals1	Kempkens et al. (2006)	Hurd et al. (2003), Wang et al. (2004)
Par6-Patj	Nam and Choi (2003)	
Par6-Lgl	Betschinger et al. (2003)	Plant et al. (2003), Yamanaka et al. (2003)
aPKC-Crb	Sotillos et al. (2004)	
aPKC-Baz/Par3	Morais-de Sá et al. (2010), Walther and Pichaud (2010)	Izumi et al. (1998), Lin et al. (2000), Nagai-Tamai et al. (2002)
aPKC-Lgl	Betschinger et al. (2003)	Plant et al. (2003), Yamanaka et al. (2003)
aPKC-Patj	Sotillos et al. (2004)	
Crb-Sdt/Pals1	Bachmann et al. (2001), Hong et al. (2001)	Roh et al. (2002)
Sdt/Pals1-Patj	Bulgakova et al. (2008)	Roh et al. (2002)
Sdt/Pals1-Baz/Par3	Krahn et al. (2010a)	
Sdt/Pals1-Lin-7	Bachmann et al. (2004)	
Par1-Baz/Par3	Benton and Johnston (2003b)	

ulate the establishment, remodelling and maintenance of epithelial cell polarity, more specifically in *Drosophila* epithelial cells.

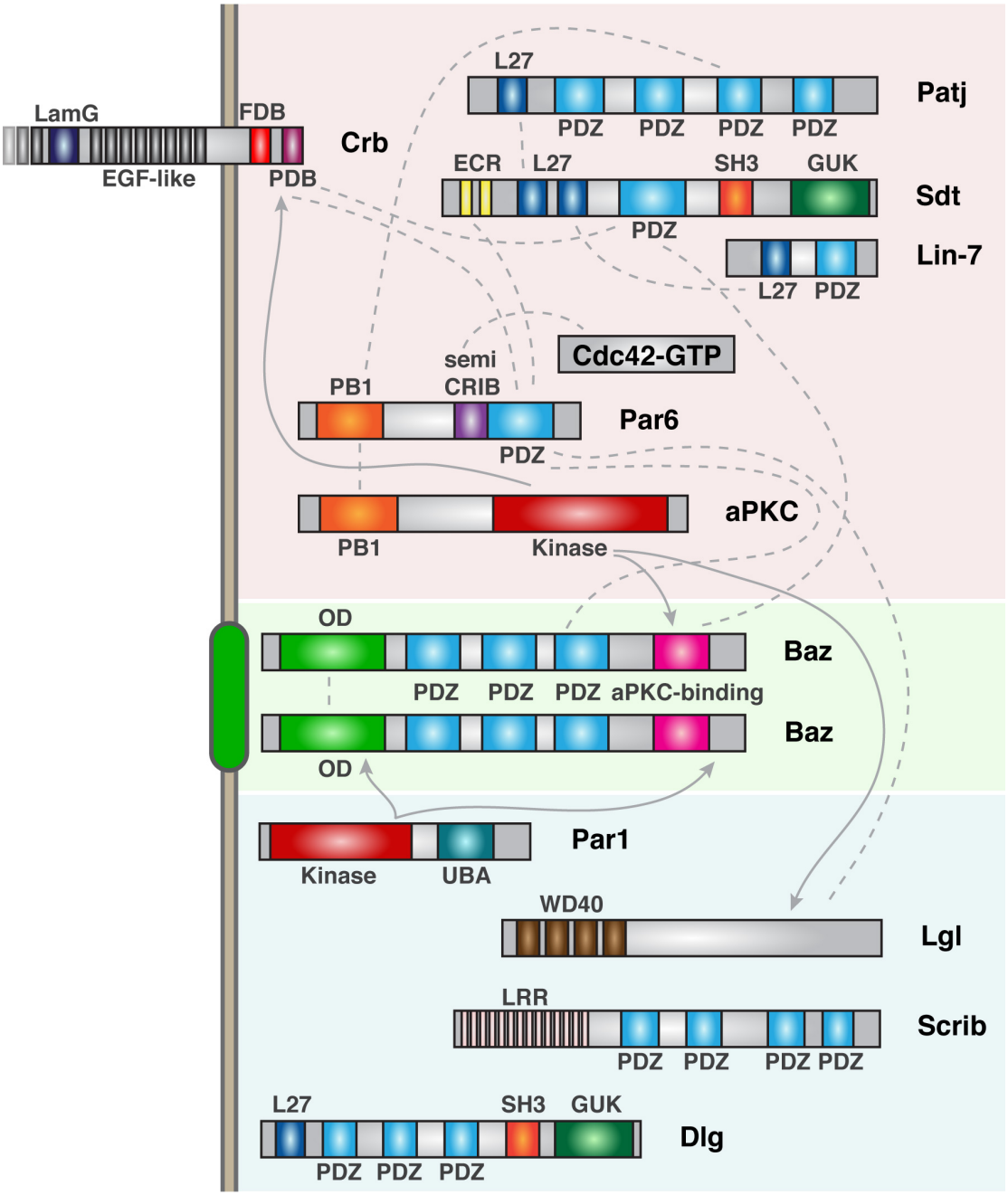

Figure 1.5: Structure and interactions of proteins that regulate epithelial cell polarity in *Drosophila*. Polarity determinants are shown in their respective domain at the cell cortex: apical (red), *ZA* (green) and basolateral (blue). Direct protein-protein interactions are shown with a dashed grey line, while grey arrows indicate protein phosphorylations. Abbreviations: CRIB, Cdc42/Rac-interactive-binding; ECR, evolutionary conserved region; EGF, epidermal growth factor; FDB, FERM domain binding; FERM, four-point-one, ezrin, radixin, moesin; GUK, guanylate-kinase; L27, Lin2/Lin7; LamG, Laminin-A globular domain; LRR, leucine-rich repeats; OD, oligomerization domain; PB1, Phox/Bem1; PDB, PDZ domain binding; PDZ, PSD95/Discs-large/ZO1; SH3, Src homology 3; UBA, ubiquitin-associated.

1.3.1 The small GTPase Cdc42

Cdc42 belongs to the Rho family (Ras superfamily) of small GTPases (Etienne-Manneville, 2004). This evolutionarily conserved protein is considered a master regulator of cell polarity, from yeast to more complex multicellular organisms (Etienne-Manneville, 2004). Like other Rho GTPases, Cdc42 cycles between an active, GTP-bound state and an inactive, GDP-bound state (Figure 1.6) (Etienne-Manneville and Hall, 2002). This cycle is regulated by three types of proteins: guanine nucleotide exchange factors (GEFs) activate Cdc42, while GTPase activating proteins (GAPs) and guanine nucleotide dissociation inhibitors (GDIs) inactivate this GTPase by hydrolysing GTP to GDP or by sequestering Cdc42 in the cytosol, respectively (Figure 1.6) (Etienne-Manneville, 2004). When in the GTP bound state, Cdc42 can activate a large set of downstream effectors, which generate a variety of cellular responses, mainly linked to the regulation of the actin cytoskeleton (Etienne-Manneville and Hall, 2002). Cdc42 is known to interact with proteins that contain the conserved Cdc42/Rac-interactive-binding (CRIB) domain in a GTP-dependent manner (Burbelo et al., 1995).

While being a key regulator of the actin cytoskeleton, Cdc42 has been linked to many cellular functions, including the regulation of cell polarity. The first link between Cdc42 and cell polarity came from studies in budding yeast, which showed that Cdc42p localises to the bud site at the early stages of cell cycle, being required for polarised growth (Ziman et al., 1993). In these unicellular organisms, lack of Cdc42p leads to isotropic growth and failure to establish a bud site (Adams et al., 1990). Since these studies, Cdc42 has been shown to be a master regulator of cell polarity in a variety of other organisms and cell types, from the *C. elegans* embryo, to the *Drosophila* neuroblast, and importantly, in all epithelial cells (Etienne-Manneville and Hall, 2002).

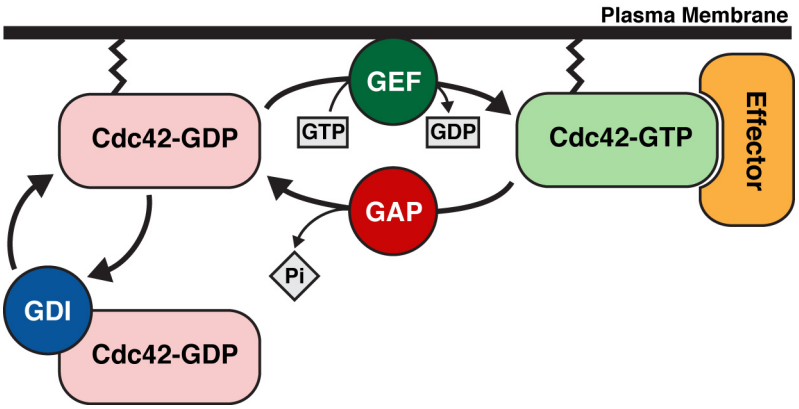

Figure 1.6: The Cdc42 GTPase cycle. Cdc42 cycles between an active, GTP-bound state and an inactive, GDP-bound state. This cycle is regulated by GEFs, which activate Cdc42, or by GAPs and GDIs, which inactivate this GTPase by hydrolysing GTP to GDP or by sequestering Cdc42 in the cytosol, respectively. Cdc42-GTP can activate a large set of downstream effectors.

Effectors of Cdc42 in epithelial cells

Cdc42 is mostly known for its role in the regulation of the actin cytoskeleton. In fact, activation of Cdc42 is mostly associated with the formation of actin protrusions known as filopodia (Nobes and Hall, 1995). Within Cdc42 numerous effector proteins that are known to regulate actin dynamics, the Wiskott-Aldrich Syndrome protein (WASp) family is of a particular interest, as WASp proteins bind to Cdc42 but not to other Rho GTPases (Symons et al., 1996). Binding to GTP-bound Cdc42 releases WASp proteins from their autoinhibition, which results in the activation of the Arp2/3 actin-nucleating complex, therefore promoting Arp2/3-dependent actin polymerisation (Kim et al., 2000, Rohatgi et al., 1999).

Another protein family that mediates Cdc42 activity towards regulating the actin cytoskeleton is the p21-activated kinase (Pak) family of serine/threonine kinases. Pak proteins can be divided into two groups: the type I Pak1-3 and the type II Pak4-6, which are regulated by different mechanisms (Arias-Romero and Chernoff, 2008). In type I Pak proteins, binding of Cdc42-GTP to their CRIB domain dissociates the autoinhibitory domain from their catalytic domain (Lei et al., 2000). In turn, this allows the autophosphorylation of type I Pak proteins, which is required for their kinase activity (Gatti et al., 1999). On the other hand, binding of type II Pak proteins to Cdc42-GTP does not enhance their kinase activity and is thought to be involved in the regulation of

their subcellular localisation (Ha et al., 2015). Pak4, or Mushroom bodies tiny (Mbt) in flies, is a particularly relevant Pak for this thesis, due to its role in the regulation of cell adhesion (Menzel et al., 2008, Schneeberger and Raabe, 2003). The role of Mbt/Pak4 in cell adhesion is further reviewed in subsection 1.4.2.

During epithelial morphogenesis, Cdc42 binds to Baz/Par3-Par6-aPKC, thus forming the quaternary Par complex that localises at the apical domain of epithelial cells (Hutterer et al., 2004, Joberty et al., 2000, Lin et al., 2000). Cdc42 is required for the recruitment of Par6-aPKC to the apical cortex of epithelial cells in the *Drosophila* embryo (Hutterer et al., 2004). In vertebrates, upon binding to Par6, Cdc42 has been shown to generate a conformational change in Par6 (Garrard et al., 2003). This conformational change has been suggested to relieve the inhibitory effect of Par6 on aPKC, therefore enhancing the kinase activity of aPKC and promoting the phosphorylation of its substrates, such as Crb, Baz and Lgl, therefore contributing to apical membrane differentiation (Garrard et al., 2003, Yamanaka et al., 2001). As discussed in more detail in the following subsections, in *Drosophila* photoreceptors, Cdc42 is necessary for the apical localisation of the transmembrane protein Crb, which in turn is required for the apical exclusion of Baz and consequent *ZA* morphogenesis (Walther and Pichaud, 2010). Altogether, Cdc42 seems to be required in epithelial cells, where it promotes both apical and *ZA* morphogenesis via its effector Par6.

In addition to the regulation of the actin cytoskeleton, cell adhesion and cell polarity, Cdc42 is also known to regulate cellular trafficking. In fact, extensive work from yeast to mammalian cells has shown that the polarisation of the trafficking machinery is essential to establish and maintain cell polarity and Cdc42 plays a key function in this process (Harris and Tepass, 2010). This role of Cdc42 in the regulation of different trafficking events is discussed in more detail in section 1.5.

Cdc42 activation and symmetry breaking

Since Cdc42 regulates such a wide range of cellular functions, its activation must be tightly restricted, in both time and space. A current challenge is to understand how Cdc42 is recruited and/or activated at the correct domain to activate the appropriate effectors. For instance, at the four-cell stage of *C. elegans* embryonic development,

CDC42 activation is spatially regulated by a distinct localisation of its GEF and GAP. In this system, CDC42 activation is restricted to the contact-free surface by the GEF ECT-2, while the GAP PAC-1 inactivates CDC42 at the cell-cell contacts (Anderson et al., 2008, Chan and Nance, 2013). A similar mechanism might presumably operate in *Drosophila* epithelial cells, however, the exact mechanism that spatially regulates the activation of Cdc42 is less understood in these cells. A system of positive feedback loops has been identified in budding yeast to regulate and amplify the activation of Cdc42. For example, during the polarised division of budding yeast, local activation of Cdc42 by its GEF Cdc24 recruits the scaffolding protein Bem1, which in turn recruits the GEF Cdc24 and generates more active Cdc42 (Butty et al., 2002). In this positive feedback loop, active Cdc42 promotes its activation via recruiting its own GEF, therefore locally increasing the pool of Cdc42-GTP. Recent work in yeast examined how many feedback loops are required for symmetry breaking and found that a single positive feedback loop is not sufficient to polarise cells, instead multiple feedback loops that are converging or cooperating are required (Goryachev and Leda, 2017). An example of such feedback loops includes a scenario where active Cdc42 recruits a Cdc42 GEF, which in turn recruits Cdc42-GDP and activates it (Goryachev and Leda, 2017). Previous work in yeast suggests that polarity establishment requires local activation of Cdc42, rather than local delivery (Woods et al., 2015).

Although positive feedback loops play an important role in amplifying Cdc42-dependent cell polarity, a key question in the field of cell polarity is which event creates the initial asymmetry that polarises cells. In the particular case of budding yeast, symmetry break is set by internal cues. While diploid yeast cells bud from their poles, haploid yeast cells rely on cues provided from the previous bud site (Pruyne et al., 2004). In the *C. elegans* oocyte, polarity cues are provided by the sperm centrosome at the posterior pole of the cell (Johnston and Ahringer, 2010). This symmetry breaking event initiates an actomyosin cortical flow that localises anterior PAR proteins at the anterior pole, while promoting the microtubule-dependent loading of PAR2 at the posterior pole (Goehring et al., 2011, Motegi et al., 2011, Munro et al., 2004). In unicellular organisms polarity can be stochastically generated or determined by intrinsic cues and amplified by a positive feedback loop, however, in multicellular organisms polarity is dictated initially by external cues, via contact regions with the basement membrane

and neighbouring cells. The symmetry breaking step is less understood in epithelial cells, as it also differs according to tissue type and context (Johnston and Ahringer, 2010). Our current knowledge of this process relies mostly in experimental studies from Madin-Darby canine kidney (MDCK) cells in culture, which revealed that polarisation of these cells requires cadherin-dependent cell-cell adhesion and integrin-mediated cell-ECM adhesion (Balcarova-Ständer et al., 1984, Johnston and Ahringer, 2010, Vega-Salas et al., 1987, Wang et al., 1990, Yeaman et al., 1999). In MDCK cells, impaired cell-cell adhesion results in the random accumulation of basolateral determinants at the cell surface, despite cell-ECM adhesion (Vega-Salas et al., 1987, Yeaman et al., 1999). In fact, cell-ECM adhesion is not sufficient to polarise MDCK cells, emphasising the role of cadherin-dependent cell-cell adhesion in symmetry break (Wang et al., 1990). Further investigation is required to uncover the detailed symmetry breaking mechanisms, as well as which GEFs and GAPs regulate Cdc42 in *Drosophila* epithelial cells.

1.3.2 The Par complex

Par6-aPKC

The *par6* gene is located on the X chromosome in *Drosophila* and encodes for a small adaptor protein of approximately 38 kDa. This protein contains three conserved domains: a Phox/Bem 1 (PB1), a semi-CRIB and a PSD95/Discs-large/ZO1 (PDZ) domain (Figure 1.5). At the N-terminus, the PB1 domain is known to bind the PB1 domain of aPKC (Betschinger et al., 2003). Par6 also interacts with the small GTPase Cdc42, when in its active GTP-bound conformation (Hutterer et al., 2004). Cdc42 is known to interact with proteins that contain the conserved CRIB domain in a GTP-dependent manner (Burbelo et al., 1995). Interestingly, the CRIB domain of Par6 is incomplete and lacks two conserved histidines at the C-terminus (Joberty et al., 2000). As a result, this semi-CRIB domain is not sufficient to bind to Cdc42-GTP and instead requires the adjacent PDZ domain to establish the interaction with Cdc42-GTP (Joberty et al., 2000, Lin et al., 2000). In addition, the PDZ domain of Par6 is also known to interact with multiple proteins, such as Baz, Crb, Sdt, Patj and Lgl (Figure 1.5 and Table 1.2) (Betschinger et al., 2003, Kempkens et al., 2006, Nam and Choi, 2003, Petronczki and Knoblich, 2001).

aPKC is a serine/threonine kinase and is considered the active component of the Par complex. The kinase activity of aPKC has been shown to play a key role in the establishment of epithelial cell polarity. Reducing aPKC activity leads to severe defects, such as loss of Crb and Patj from the membrane and apical expansion of basolateral proteins (Sotillos et al., 2004). Furthermore, ectopic expression of aPKC recruits other apical determinants, such as Crb, Patj and Baz, to the basolateral membrane (Sotillos et al., 2004). Importantly, this kinase-dependent role of aPKC during epithelial polarity establishment is conserved in vertebrates (Suzuki et al., 2001).

aPKC is known to phosphorylate various polarity proteins, such as Baz/Par3, Crb and Lgl (Figure 1.5 and Table 1.2). aPKC can phosphorylate Baz/Par3 at a conserved serine residue, S980 in flies or S827 in mammals, which excludes Baz/Par3 from the apical domain of epithelial cells and promotes its localisation at the developing *ZA* (Lin et al., 2000, Morais-de Sá et al., 2010, Nagai-Tamai et al., 2002, Walther and Pichaud, 2010). This is a critical event in both apical and *ZA* morphogenesis. On the other hand, Lgl phosphorylation promotes its dissociation from Par6-aPKC and restricts Lgl localisation to the basolateral membrane (Betschinger et al., 2003, Plant et al., 2003). As a result, Lgl activity is restricted to the basal cortex. Lastly, aPKC is also known to phosphorylate the cytoplasmic tail of the transmembrane protein Crb at two conserved threonine residues, T6 and T9 (Sotillos et al., 2004). Although the *in vivo* role of this phosphorylation requires further study, it has been proposed that the phosphorylation of Crb by aPKC is important for Crb function, as the gain-of-function phenotype observed upon overexpressing the intracellular domain of Crb is decreased by reducing aPKC activity (Sotillos et al., 2004).

Generally, Par6 is thought of as a small adaptor protein that is essential to allow the interaction between aPKC and its phosphorylation targets (Table 1.2). However, there is also evidence that Par6 regulates the localisation of aPKC, as well as its activity. While Par6 has been suggested to negatively modulate aPKC activity (Atwood et al., 2007), *par6* loss-of-function does not show any aPKC hyper-activation phenotype (Petronczki and Knoblich, 2001, Wodarz et al., 2000). Instead, it presents an *aPKC* loss-of-function phenotype, thus indicating that Par6 mainly regulates aPKC localisation (Petronczki and Knoblich, 2001, Wodarz et al., 2000). The apical localisation of Par6-aPKC depends on Cdc42-GTP (Atwood et al., 2007); however, the mechanisms that recruit and activate

Cdc42 apically in *Drosophila* epithelia are still not clear. In addition, the initial apical recruitment of Par6-aPKC requires the assembly of the Par complex, which occurs with Par6-aPKC binding to Baz (Harris and Peifer, 2005).

Bazooka

Baz/Par3 is a scaffolding protein that, together with Par6, aPKC and Cdc42, forms the Par complex. Vertebrate work has shown that Baz/Par3 binds aPKC via its C-terminal region and binds Par6 via two of its three PDZ domains: PDZ1 or PDZ3 (Izumi et al., 1998, Renschler et al., 2018). Further work in flies has shown that the recruitment of Baz to the cell cortex is independent of Par6-aPKC (Harris and Peifer, 2005, Nam et al., 2007). Its localisation at the apical cortex requires its self-association, via the N-terminal oligomerisation domain (OD) (Benton and Johnston, 2003a, Feng et al., 2007), as well as binding to phosphoinositide lipids via its C-terminal region (Krahn et al., 2010b).

Baz is not always observed co-localised with the remaining proteins of the Par complex. While Par6 and aPKC are restricted to the apical domain of polarised *Drosophila* epithelial cells, Baz has been shown to localise in a more basal position, at the level of the *ZA* (Johnston and Ahringer, 2010). This dissociation of the Par complex is triggered by aPKC phosphorylation of Baz at S980 (Morais-de Sá et al., 2010, Walther and Pichaud, 2010). Furthermore, this phosphorylation event dissociates Baz from Sdt, contributing to the assembly of the Crb complex (Krahn et al., 2010a). In mammalian cells, Par3 has been observed to reduce the kinase activity of aPKC, which could prevent its ectopic activation until the Par complex is properly assembled (Henrique and Schweisguth, 2003, Lin et al., 2000). Baz junctional localisation is also regulated by the kinase Par1, which phosphorylates Baz at two conserved serines, S151 and S1085 in flies, and prevents both Baz oligomerisation and binding to aPKC at the basolateral domain in various cell types (Benton and Johnston, 2003b, Walther et al., 2016).

Baz is required to assemble the Par complex and recruit Par6-aPKC to the apical domain; however, *ZA* assembly depends on Baz apical exclusion. At the developing *ZA*, phosphorylated Baz (P-Baz) plays a key role in promoting cell-cell adhesion, presumably by recruiting multiple proteins via its PDZ domains. In particular, at the *ZA*, Baz is able to bind to the β-catenin *Drosophila* orthologue Armadillo (Arm), as well as to the

Drosophila nectin, the transmembrane protein Echinoid (Ed) (Wei et al., 2005). This is thought to cluster both Cadherin and Ed adhesion complexes, to promote AJ morphogenesis. Similarly, in vertebrates, P-Par3 is able to bind JAM1-3 and nectin, thus promoting tight junction maturation (Ebnet et al., 2001, Itoh et al., 2001, Takekuni et al., 2003).

Lastly, Baz is also known to bind to the lipid phosphatase PTEN via its PDZ domains, which is required for PTEN localisation (Pinal et al., 2006, Stein et al., 2005). PTEN dephosphorylates phosphatidylinositol (3,4,5)-triphosphate (PIP_3) to phosphatidylinositol (4,5)-biphosphate (PIP_2). Both these phospholipids have been shown to regulate apical-basal polarity, as PIP_2 promotes apical membrane morphogenesis, while PIP_3 promotes basolateral membrane identity (Tepass, 2012). In fact, the addition of exogenous PIP_3 to the apical domain of MDCK cells leads to its transformation into a basolateral membrane, with accumulation of basolateral proteins at the apical side of these cells (Gassama-Diagne et al., 2006). Similarly, the addition of ectopic PIP_2 to the basolateral domain causes mistargeting of apical proteins to the basolateral surface (Martin-Belmonte et al., 2007). This suggests that Baz might play a role in establishing this PIP_2/PIP_3 asymmetry, which in turn is key for the differentiation of the plasma membrane into distinct domains.

1.3.3 The Crumbs complex

In addition to the Par complex, another evolutionarily conserved group of proteins forms at the apical membrane: the Crb complex. Its core components are the transmembrane protein Crb, the scaffolding protein Sdt, Patj and Lin-7 (Table 1.1) (Bulgakova and Knust, 2009). However, besides these core components, additional proteins can associate with this complex, contributing to the complexity and flexibility of this protein complex. In particular, there is an evident cross-talk between members of the Par and Crb complexes; however, further studies are required to understand the functional role of these interactions.

Crumbs

Crb is a type-I transmembrane protein that contains a very large extracellular domain composed of 29 epidermal growth factor (EGF)-like repeats and 4 laminin-A globular domains, as well as a small cytoplasmic tail with 37 amino acids that includes a four-point-one, ezrin, radixin, moesin (FERM)-binding domain and a PDZ-binding motif (ERLI) (Figure 1.5) (Bulgakova and Knust, 2009). Being a key regulator of apical epithelial cell polarity, in flies, *crb* mutant cells lose their apical-membrane identity, while cells overexpressing Crb show an increased apical domain at the expense of the basolateral domain (Pellikka et al., 2002, Tepass, 2012). Moreover, *crb* mutant cells show abnormally longer AJ domains (Izaddoost et al., 2002). In vertebrate cells, CRB3 localises to TJs and its overexpression delays the formation of these paracellular barriers (Lemmers et al., 2004, Roh et al., 2003).

The short intracellular domain is essential for Crb function, as a premature stop codon eliminating the last 23 amino acids leads to the same phenotype as *crb* null mutants (Knust et al., 1993, Wodarz et al., 1993). In addition, overexpression of the intracellular domain of Crb (Crb^{intra}) has the same phenotype as overexpressing the full-length protein, and *crb* mutant fly embryos are equally rescued with Crb full-length and Crb^{intra} (Wodarz et al., 1995). As previously mentioned, the intracellular region of Crb comprises a FERM-binding and a PDZ-binding domain. The FERM-binding domain binds directly to Yurt, which negatively regulates Crb and limits the growth of the apical membrane (Laprise et al., 2006). The C-terminal ERLI motif binds to the PDZ domains of Sdt or Par6 (Table 1.2 and Figure 1.5). In addition, Crb is a substrate of the kinase aPKC, being phosphorylated at two conserved threonine residues, T6 and T9 (Sotillos et al., 2004). Importantly, this phosphorylation has been proposed to maintain Crb at the membrane, as reduced aPKC activity causes loss of Crb from the plasma membrane (Sotillos et al., 2004). Also, reducing aPKC activity suppresses the effect of Crb^{intra} overexpression, suggesting that aPKC regulates Crb function (Sotillos et al., 2004).

Stardust

Sdt is a membrane-associated guanylate kinase (MAGUK) protein that includes two evolutionary conserved regions (ECRs), two Lin-2/Lin-7 (Lin27) domains, a PDZ domain, a Src homology 3 (SH3) domain and a guanylate kinase (GUK) domain (Figure 1.5) (Bulgakova and Knust, 2009). Sdt functions as a scaffolding protein, binding to the C-terminal ERLI domain of Crb via its PDZ domain and binding to both Patj and Lin-7 with its two Lin27 domains (Bachmann et al., 2001, 2004, Bulgakova et al., 2008). The ECR1 of Sdt can also interact with the PDZ domain of Par6, which prevents Sdt binding to Patj (Kempkens et al., 2006, Wang et al., 2004). In addition, the PDZ domain of Sdt binds to Baz and, as mentioned earlier, this binding is regulated by phosphorylation of Baz S980 (Krahn et al., 2010a).

The Baz-Sdt interaction is required for Sdt localisation at the membrane in the absence of Crb (Krahn et al., 2010a). In the *Drosophila* embryo, Crb staining is not detected at the early stages of embryonic development; however, Sdt can be previously visualised co-localising with Baz at the *ZA* (Krahn et al., 2010a). In fact, after Crb expression onset, Sdt is observed mainly co-localising with Crb in *wild-type* cells, while co-localising with Baz in *crb* mutant cells and is not detected at all in *baz* mutant cells, which reinforces the role of Baz in the localisation of Sdt in this tissue (Krahn et al., 2010a). Interestingly, Bachmann et al. (2001) had previously shown that in the fly embryo, although at later stages of embryonic development, Sdt is completely lost from the membrane in *crb* mutant cells. This suggests that there are different regulatory mechanisms through developmental time, which has also been observed in other tissues, such as the fly retina (Nam and Choi, 2003). More specifically, in *Drosophila* photoreceptors, Patj and Sdt mislocalisation in *crb* mutant cells is age-dependent and occurs from 35 % After Puparium Formation (APF) (Nam and Choi, 2003). Altogether, previous work in both the fly embryo and retina suggests that Sdt localisation requires Baz at the initial stages of development, while binding to Crb is required for Sdt apical membrane localisation at later developmental stages.

After addressing the dependence of Sdt on Crb, another important question that is not very clear is how Sdt affects Crb localisation. Krahn et al. (2010a) have shown that Crb is mislocalised in *sdt* mutant cells of the *Drosophila* embryo, subsequent to the

onset of Crb expression (Krahn et al., 2010a). However, additional studies in the fly retina show that, in *sdt* mutant photoreceptors, Crb is properly localised although its levels are strongly decreased (Walther and Pichaud, 2010). In fact, further studies in the fly retina support that Crb and Sdt might act independently, being required only in a specific subset of photoreceptors (Hwa and Clandinin, 2012). While Crb is essential in R2 and R4 cells and mostly dispensable in the remainder photoreceptors, Sdt is mostly required in R3 and R4 during apical membrane morphogenesis (Hwa and Clandinin, 2012). In addition, during midpupal stage, both Crb and Sdt appear to be expressed at higher levels in photoreceptors that have a longer stalk membrane (*i.e.* R2, R4, R5 and R7) (Hwa and Clandinin, 2012). In vertebrate cells, a western blot analysis shows that CRB3 levels are maintained in the presence and absence of Sdt (Straight et al., 2004). The mutual dependence of Crb and Sdt is not clear, being a subject that requires further investigation in different model tissues.

Patj

Fly Patj is a PDZ-domain protein composed of four PDZ domains in addition to a single N-terminal Lin27 domain (Figure 1.5) (Nam and Choi, 2006). In flies, the third PDZ of Patj binds to the PB1 domain of Par6 (Nam and Choi, 2003), which suggest that Par6 might be able to link Sdt and Patj. Altogether, this means that Crb could theoretically be found in multiple different complexes, besides the canonical Crb-Sdt-Patj complex, such as Crb-Sdt-Par6, Crb-Par6-aPKC, Crb-Par6-Patj and Crb-Sdt-Par6-Patj (Bulgakova and Knust, 2009). However, further studies are necessary to confirm if all these interactions occur *in vivo* and what their role is during epithelial morphogenesis.

In *Drosophila*, *patj* null mutants are lethal during the second instar stage of larval development (Nam and Choi, 2006). In more detail, analysis of *patj* mutant photoreceptors shows that, while the N-terminal region of Patj is required for fly viability and photoreceptor morphogenesis, the C-terminal region (*i.e.* from PDZ2 to PDZ4) is not essential for development and is required to prevent late-onset retinal degeneration (Nam and Choi, 2006). In addition, these studies suggest that Patj is required for stabilising the Crb complex, as in a *patj* mutant background, the levels of both Crb and Sdt are greatly

reduced (Nam and Choi, 2006). Complementary studies in the fly embryo suggest that Patj is not required for the establishment of apical-basal polarity in this tissue and that its loss results in lethality during early pupal stages (Sen et al., 2012). However, in the FE, loss of Patj also resulted in weaker accumulation of Crb and Sdt, as in the fly retina (Nam and Choi, 2006, Sen et al., 2012). Overall, these studies in *patj* mutant cells suggest that Patj might have a different role in distinct cell types.

Lin-7

Lin-7 is a small protein that includes a Lin27 domain at the N-terminus and a single PDZ domain at the C-terminus (Figure 1.5) (Bachmann et al., 2004). Mutations in *lin-7* do not seem to affect the localisation of the remaining core components of the Crb complex and results in viable animals (Bachmann et al., 2008). However, Lin-7 is lost in *crb*, *sdt* and *patj* mutants (Bachmann et al., 2008). In addition, overexpression of Lin-7 does not affect the distribution of the remaining polarity proteins (Bachmann et al., 2008). Further studies in the fly retina suggest that Lin-7 is required to prevent light-dependent retinal degeneration, similarly to Crb (Bachmann et al., 2008).

1.3.4 The Scribble complex

The Scrib complex includes the proteins Scrib, Lgl and Dlg (Table 1.1). Localised at the the lateral membrane (more specifically, at the SJs), the Scrib complex excludes the Par and Crb complexes from the lateral domain, restricting their localisation to the apical domain of epithelial cells (Assémat et al., 2008, Johnston and Ahringer, 2010). So far, there is no evidence for a direct physical interaction between the different components of the Scrib complex (Johnston and Ahringer, 2010). However, their strong functional and genetic interaction, *i.e.*, their co-localisation and their similarity in terms of mutant phenotype, groups these proteins in the same complex (Henrique and Schweisguth, 2003, Johnston and Ahringer, 2010).

Scribble

Scrib is a scaffolding protein that contains 16 LRRs and four PDZ domains (Figure 1.5). In *Drosophila*, *scrib* mutant cells show ectopic localisation of apical and junctional markers, such as Crb, Arm and the transmembrane adhesion molecule E-cadherin (E-cad) at the lateral membrane (Bilder and Perrimon, 2000). The localisation of basolateral markers, such as Coracle, is not affected in *scrib* mutants (Bilder and Perrimon, 2000). Therefore, Scrib plays an important role in restricting apical proteins to the apical domain of epithelial cells, segregating them from the basolateral domain and thus contributing to the accurate placement of the *ZA*. However, the exact mechanism by which Scrib confines apical proteins to their respective domain is not clear.

Dlg

Dlg is a MAGUK protein that contains a Lin27 domain, three PDZ domains, an SH3 domain and a GUK domain (Figure 1.5). *dlg* mutant larvae die before reaching pupal stage due to overgrowth of their imaginal discs (Perrimon, 1988). Dlg seems to play an important role in maintaining the asymmetric distribution of PIP_2 and PIP_3 in epithelial cells. In mammalian cells, the second PDZ domain of Dlg binds to the phosphatase PTEN and this binding is disrupted upon phosphorylation of PTEN (Adey et al., 2000, Assémat et al., 2008). In addition, phosphorylation of Dlg negatively regulates its binding to phosphatidylinositol 3-kinase (PI3K) in mammalian cells (Laprise et al., 2004). Further studies are necessary to reveal which kinases regulate the binding of Dlg to both PTEN and PI3K in epithelial cells, possibly revealing a role for Dlg in the regulation of PIP_2/PIP_3 levels at the lateral membrane.

Lgl

Lgl is a tumour suppressor protein that plays an essential role in cell proliferation, polarity and growth (Tanentzapf and Tepass, 2003). The basolateral localisation of Lgl is regulated by aPKC, which prevents Lgl apical accumulation by phosphorylating 3 conserved residues in Lgl (Betschinger et al., 2003, Yamanaka et al., 2003). In both *Drosophila* neuroblasts and mammalian cells, Lgl competes with Par3 to form a tran-

sient complex with Par6-aPKC (Betschinger et al., 2003, Yamanaka et al., 2003). This complex is disrupted upon Lgl phosphorylation by aPKC (Betschinger et al., 2003, Yamanaka et al., 2003). In addition to the Par complex, *lgl* genetically interacts with *crb*, as these two pathways compete to define the apical and basolateral domains of epithelial cells (Tanentzapf and Tepass, 2003).

1.3.5 Par1

In addition to the Scrib complex, the serine/threonine kinase Par1 also plays a key role as a lateral determinant. Similarly to Lgl, at least in vertebrates, the localisation and activity of Par1 is also regulated by the kinase aPKC (Hurov et al., 2004). Importantly, the phosphorylated residue (T564 in Par1a and T595 in Par1b), is also conserved in both *Drosophila* and *C. elegans*, suggesting a similar regulatory mechanism in these organisms (Doerflinger et al., 2010, Hurov et al., 2004). In fact, expression of a version of Par1 that escapes aPKC phosphorylation displays an ectopic localisation at the apical domain (Doerflinger et al., 2010). Par1 localisation to the lateral membrane is essential during polarity establishment, as in turn Par1 has been shown to regulate the localisation of other proteins, such as Baz (Benton and Johnston, 2003b). As previously mentioned, Par1 is known to phosphorylate Baz at two conserved serine residues, S151 and S1085 in flies, which prevents Baz accumulation at the basolateral domain (Benton and Johnston, 2003b, Sotillos et al., 2004, Walther et al., 2016). In both FCs and photoreceptors, mutation of the Par1 phosphorylation sites of Baz cause a lateral displacement of Baz (Benton and Johnston, 2003b, Walther et al., 2016). Despite Par1's role in Baz lateral exclusion, at least in the fly retina, *par1* mutants display a mild phenotype (Walther et al., 2016), suggesting that other mechanisms operate in parallel to Par1 towards promoting the lateral exclusion of Baz.

1.4 *Zonula Adherens* morphogenesis

The organisation of distinct apical and basolateral membrane domains is marked by the establishment and positioning of the *ZA*. The *ZA* is the circular adhesive and intercellular signalling belt that maintains epithelial cell contact, while providing cells with spatial

cues during tissue morphogenesis (Bryant and Mostov, 2008). The establishment of the *ZA* requires both aPKC and Crb, with subsequent exclusion of Baz from the apical domain (Morais-de Sá et al., 2010, Walther and Pichaud, 2010). A prevalent model is that the Par complex assembles at the apical domain of epithelial cells. This cortical recruitment and assembly of the Par complex has been shown to require GTP-bound Cdc42, as well as Baz (Atwood et al., 2007, Harris and Peifer, 2005, Hutterer et al., 2004). Upon Par complex assembly, aPKC phosphorylates Baz at S980, which dissociates Baz from both Sdt and Par6-aPKC (Krahn et al., 2010a, Morais-de Sá et al., 2010, Walther and Pichaud, 2010). This dissociation of Baz from Sdt contributes to the assembly of the Crb complex (Krahn et al., 2010a). Importantly, Crb is required in this process to prevent the interaction between Par6 and Baz, thus acting together with aPKC towards excluding Baz from the Par complex (Morais-de Sá et al., 2010, Walther and Pichaud, 2010). aPKC and Crb-dependent apical exclusion of Baz re-positions this protein at the boundary between the apical and basolateral domains (Morais-de Sá et al., 2010, Walther and Pichaud, 2010). In the fly embryo, microtubules and the motor protein Dynein position Baz clusters at the apico-lateral domain (Harris and Peifer, 2005). These Baz clusters establish the positioning of the *ZA* by recruiting AJ material, namely Arm (*Drosophila* β-catenin) and Ed (the fly nectin). Concurrently, a lateral displacement of Baz is prevented by Par1 (Benton and Johnston, 2003b). The kinase Par1 phosphorylates Baz at two serine residues, S151 and S1085, which prevents both Baz oligomerisation and binding to aPKC at the basolateral membrane (Benton and Johnston, 2003b).

The sequence of events that regulate the apical recruitment of Par6-aPKC via Cdc42, Baz and how Par6-aPKC is then transferred onto the Crb complex is not well understood. Answering these questions is necessary to understand the molecular basis of polarity establishment, as well as how this leads to the differentiation of specialised membrane domains such as the *ZA*.

1.4.1 Adherens junction components

The core components of the AJs are known as Cadherins. Classic cadherins, such as E-cadherin (E-cad, also known as DE-cadherin or shotgun in *Drosophila*), are Ca^{2+}-

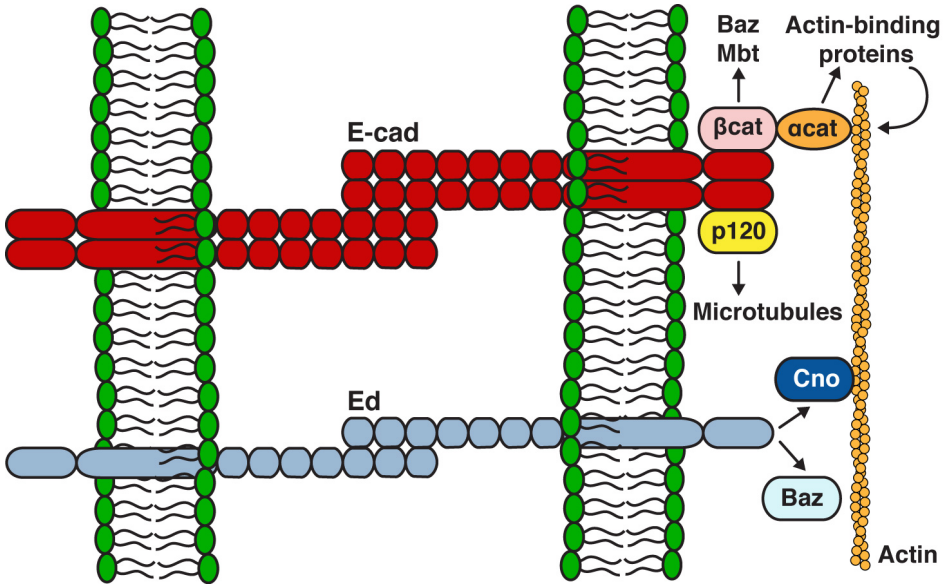

Figure 1.7: Cell-cell adhesion molecules in *Drosophila* epithelial cells. E-cad and Ed establish homophilic interactions with neighbouring cells, both contributing to cell-cell adhesion. E-cad binds β-catenin/Arm, which binds α-catenin to establish the link to the actin cytoskeleton. E-cad is also linked to microtubules via p120-catenin. β-catenin/Arm can also link the cadherin-catenin complex to other proteins, such as Baz and Mbt. Similarly, Ed is associated with the actin cytoskeleton via the protein Cno. Ed binding to both Cno and Baz is mutually exclusive.

dependent adhesion molecules that contain essentially three domains: an extracellular domain that establishes adhesion with neighbouring cells via homophilic interactions, a transmembrane domain, and an intracellular domain that links to the actin cytoskeleton (Harris and Tepass, 2010, Kemler, 1992, Tepass and Harris, 2007). The cytoplasmic domain of cadherins is highly conserved and binds to catenins, in particular to Arm/β-catenin and to p120-catenin (Figure 1.7) (Aberle et al., 1994, Kemler, 1992).

In MDCK cells, E-cad binding to β-catenin has been shown to occur in the endoplasmic reticulum (ER) and is coupled to an efficient exit from the ER and delivery to the plasma membrane (Chen et al., 1999). At the plasma membrane, β-catenin recruits α-catenin, which enriches α-catenin at the AJs (Aberle et al., 1994, Harris and Tepass, 2010). Importantly, α-catenin is also able to bind F-actin directly or via actin-binding proteins, such as α-actinin, formin or afadin (Harris and Tepass, 2010). However, the formation of a stable cadherin-catenin-F-actin complex requires tension, which causes a force-driven conformational change on α-catenin that allows the link of the cadherin-catenin complex to the actin cytoskeleton (Buckley et al., 2014). In turn, p120-catenin

links cadherins to microtubules and has been shown to increase the amount of E-cad at the plasma membrane by preventing its endocytosis and degradation (Davis et al., 2003, Harris and Tepass, 2010).

In the fly embryo, the positioning of the cadherin-catenin complex at the apico-lateral border is regulated by Baz (Harris and Peifer, 2005). Work in the fly embryo suggests that distinct clusters of Baz and E-cad/Arm are formed independently in epithelial cells, presumably based on Baz oligomerisation and E-cad homophilic interactions, respectively (Benton and Johnston, 2003b, Kemler, 1992, McGill et al., 2009). Baz clusters position the E-cad/Arm clusters at AJ sites, via the Baz-Arm interaction (McGill et al., 2009). In *baz* mutant embryos, E-cad/Arm clusters fail to localise to the developing AJs, which leads to a loss of epithelial tissue integrity (McGill et al., 2009).

In addition to the cadherin-catenin complex, another adhesion complex has been identified at the AJs: the Ed-Canoe (Cno) complex in *Drosophila* or Nectin-Afadin in vertebrates. Ed is an immunoglobulin domain-containing adhesion protein that cooperates with E-cad towards promoting cell adhesion. Ed is known to bind Baz via its C-terminal PDZ domain, and to bind Cno, which links Ed to the actin cytoskeleton (Figure 1.7) (Tepass and Harris, 2007, Wei et al., 2005). Both adhesion complexes can signal through Rho GTPases to further regulate the cell cytoskeleton (Harris and Tepass, 2010).

1.4.2 Mbt as a regulator of AJ morphogenesis

The apical exclusion of Baz sets the positioning of the *ZA* by recruiting the AJ proteins Arm and Ed. However, *baz* mutant cells still accumulate these adhesion molecules, suggesting that other *baz*-independent mechanisms might operate in epithelial cells to assemble AJs (Shahab et al., 2015, Walther and Pichaud, 2010, Wei et al., 2005).

One possible mechanism could involve the Pak, Pak4, or Mbt in flies, which has been shown to regulate cell adhesion and photoreceptor morphogenesis in *Drosophila* (Menzel et al., 2008). Pak4/Mbt is a serine/threonine kinase and an effector of the GTPase Cdc42 (Schneeberger and Raabe, 2003). In the fly photoreceptor, Mbt has been shown to localise at the developing *ZA* (Menzel et al., 2008, Schneeberger and Raabe, 2003). Moreover, Mbt phosphorylates Arm *in vitro* at the serine residues S561 and S688, which has been proposed to inhibit Arm binding to E-cad and ultimately to decrease E-cad-

mediated cell adhesion (Menzel et al., 2008). In mice, loss of Pak4 results in embryonic lethality; however, its conditional deletion correlates with a failure to assemble AJs in neuroepithelial cells (Tian et al., 2011). In human bronchial cells, Pak4 also promotes AJ assembly and maturation (Wallace et al., 2010). Interestingly, in these cells, the initial recruitment of Pak4 to nascent AJs is Cdc42-dependent, but its maintenance during AJs maturation requires Par6B-aPKC, suggesting a cross-talk between the Par complex and Pak4 (Wallace et al., 2010). Additional studies are required to further investigate the functional link between Pak4/Mbt and AJ morphogenesis, in the context of epithelial cell polarity.

1.5 Trafficking

Tissue morphogenesis highly depends on vesicle-trafficking. For example, recent studies show that E-cad maintains a high turnover at the AJs, requiring a highly regulated balance between its membrane delivery and endocytosis (Beco et al., 2009). This is crucial not only to maintain tissue integrity, but especially to facilitate epithelial tissue remodelling (Baum and Georgiou, 2011).

In most polarised epithelial cells, proteins and lipids are produced in the ER and directly sorted in the trans-Golgi network (TGN) to their final membrane domain (Griffiths and Simons, 1986, Keller et al., 2001). For example, in *Drosophila* photoreceptors, Rab11 promotes the delivery of Rhodopsin-1 (Rh1) from the TGN to the very apical membrane comprised of thousands of microvilli known as the rhabdomere (Satoh et al., 2005). This direct route to the apical surface ensures that Rh1 is properly delivered to the rhabdomere, maintaining a functional development of the retina (Satoh et al., 2005). However, it has been shown that in hepatocytes, the major epithelial cell type in the liver, most molecules follow an indirect route to the apical membrane: first from the TGN to the basolateral membrane, and then to the apical membrane (Bastaki et al., 2002). A well-studied example of a transcytosed molecule is the polymeric immunoglobulin receptor, pIgR. pIgR is initially sorted to the basolateral membrane where it binds its ligand. It is then internalised and transcytosed to the apical membrane (Mostov, 1994). In addition to these polarised delivery mechanisms, the asymmetric distribution of molecules can also be regulated at the plasma membrane by different retention mech-

anisms. One such example is the Na/K-ATPase. In MDCK cells, the Na/K-ATPase has an increased residence time at the basolateral membrane compared to at the apical membrane, which is a consequence of a retention mechanism through binding to ankyrin and the spectrin-like protein fodrin (Hammerton et al., 1991).

1.5.1 The exocyst

A particularly important step that is common to all polarised delivery mechanisms is the docking and fusion of the delivery vesicles at the appropriate plasma membrane site. Before SNARE-mediated fusion with the membrane, the fundamental docking event is mediated by the exocyst (Heider and Munson, 2012). The exocyst was first identified in yeast as a complex of eight proteins: Sec3p, Sec5p, Sec6p, Sec8p, Sec10p, Sec15p, Exo70 and Exo84 (Guo et al., 1999, TerBush et al., 1996). Although highly conserved in eukaryotes, it is still not clear how all these proteins are organised in a complex while tethering the exocytic vesicle to the plasma membrane. A prevalent model is that there are exocyst subcomplexes, both at the plasma membrane and at vesicles (Heider and Munson, 2012). Even though it has been commonly accepted that both Sec3 and Exo70 localise at the plasma membrane, while the remaining components of the exocyst localise at vesicles, very recently published data suggests that only Sec3 is localised at the plasma membrane (Boyd et al., 2004, Mei et al., 2018).

In both models, it is the assembly of these subcomplexes into a complete octameric exocyst complex that ensures that the tethering between membranes occurs at the right place (Heider and Munson, 2012). These tethering events are mainly regulated by GTPases, as many of the exocyst subunits act downstream of Rho, Ral and Rab GTPases (Wu et al., 2010). For example, both Sec5 and Exo84 subunits are regulated by a Ras-like (Ral) GTPase, RalA, which has been shown to regulate the assembly of the exocyst at the plasma membrane (Moskalenko et al., 2002, 2003). The Rho GTPase Cdc42 has also been implicated in exocyst function. In vertebrate cells, Cdc42 activates RalA (Sugihara et al., 2002), while in yeast, Cdc42 has been linked to at least two exocyst subunits, Sec3 and Exo70 (Wu et al., 2010, Zhang et al., 2008).

One of the main questions in this field is related to whether the exocyst is recruited to specific membrane domains and how it is maintained at those domains. In the past years,

the number of links between polarised proteins/lipids and exocyst subunits continues to grow. Exo84 has been shown to bind Par6 in vertebrate cells, thus providing the first evidence of a possible link between the exocyst and the polarity Par complex (Das et al., 2014). Moreover, the exocyst has been linked to the apical protein Crb in the *Drosophila* embryo (Blankenship et al., 2007). *exo84* mutant embryos show deffects in Crb trafficking, as well as mislocalisation of the AJ proteins Baz and Arm, similarly to *crb* mutant embryos (Blankenship et al., 2007). Recently, the Macara lab has suggested that, in mouse mammary epithelial cells, Par3 acts as a receptor for the exocyst at the plasma membrane, via binding to the exocyst subunit Exo70 (Ahmed and Macara, 2017). Interestingly, in cortical neurons, both Par3 and aPKC co-immunoprecipitate with several components of the exocyst, namely with Sec6, Sec8 and Exo84, and the GTPase RalA is a regulator of these interactions (Lalli, 2009). In addition, it has also been suggested that lipids are involved in the polarisation of the exocyst. In both yeast and mammals, the exocyst subunits Sec3 and Exo70 bind to PIP_2 at the plasma membrane (He et al., 2007, Zhang et al., 2008). Further studies are required to dissect the exact mechanisms that couple exocyst subunits to phosphoinositides and polarity determinants, in the delivery of different cargoes to distinct sites at the plasma membrane.

1.5.2 Regulation of E-cad trafficking

At the *ZA*, the cell-cell adhesion complexes signal through Rho GTPases. During development, AJs must be constantly assembled and disassembled to allow tissue dynamics, in a process known as AJ remodelling (Baum and Georgiou, 2011). E-cad is continuously internalised and recycled back to the plasma membrane and Cdc42 regulates AJ remodelling by promoting E-cad endocytosis. In the fly notum, Cdc42-Par6-aPKC regulate CIP4 function towards promoting E-cad endocytosis (Georgiou et al., 2008, Harris and Tepass, 2010, Leibfried et al., 2008). In this process, the Cdc42 effector CIP4 recruits the scission protein Dynamin and promotes Arp2/3-dependent actin polymerisation via WASp, thus regulating dynamin- and actin-dependent E-cad endocytosis (Georgiou et al., 2008, Leibfried et al., 2008). Upon endocytosis, E-cad accumulates in Rab5-positive early endosomes and can either follow a degradation pathway or a recycling route back to the plasma membrane (Baum and Georgiou, 2011). Ubiquitin-tagged E-cad is sorted to the lysosome for degradation (Fujita et al., 2002, Palacios

et al., 2005). Alternatively, Rab11 and the exocyst have been implicated in recycling E-cad to the plasma membrane (Langevin et al., 2005, Lock and Stow, 2005).

1.5.3 Regulation of Crb trafficking

In addition to the junctional protein E-cad, the apical transmembrane protein Crb is also thought to undergo active recycling in epithelial cells. Blocking endocytosis, exocytosis or disrupting recycling endosomes has been shown to alter Crb levels at the apical membrane (Blankenship et al., 2007, Lu and Bilder, 2005, Roeth et al., 2009). Crb apical localisation is known to require a whole set of proteins that are related to vesicular trafficking, such as Cdc42, the retromer, Rab11 and the exocyst subunit Exo84.

Cdc42 has been shown to regulate Crb endocytosis at two distinct stages in *Drosophila* (Harris and Tepass, 2008). Firstly, Cdc42 regulates Rab5- and syntaxin-dependent endocytosis of Crb via Par6-aPKC (Harris and Tepass, 2008, Lu and Bilder, 2005). While loss of Cdc42 increases Crb endocytosis, this phenotype can be suppressed by the expression of constitutively active aPKC, suggesting that Par6-aPKC act downstream of Cdc42 in the regulation of Crb endocytosis (Harris and Tepass, 2008). In addition, loss of Rab5 or the syntaxin Avalanche, which localise to early endosomes, result in expansion of the apical membrane, as a consequence of failure to endocytose Crb (Lu and Bilder, 2005). Secondly, loss of Cdc42 blocks the progression of Crb from early to late endosomes (Harris and Tepass, 2008). Altogether, Cdc42 regulates Crb apical localisation by reducing its endocytosis and promoting its progression from early to late endosomes (Harris and Tepass, 2008).

The retromer is a protein complex involved in the retrograde transport of transmembrane proteins from endosomes to the *trans*-Golgi network. Work in the fly embryo, FE and wing discs shows that the retromer regulates the retrograde recycling of Crb. Upon loss of retromer function, Crb is mis-targeted to lysosomes, thus following a degradation pathway that causes severe phenotypes in apical-basal polarity (Pocha et al., 2011, Zhou et al., 2011).

Lastly, the apical delivery of Crb has been suggested to be a Rab11- and exocyst-dependent process (Blankenship et al., 2007, Roeth et al., 2009). In fact disrupting *rab11* function results in a very similar phenotype to *crb* loss-of-function and reveals defects

in the apical accumulation of Crb (Roeth et al., 2009). Similarly, in the *Drosophila* embryo, *exo84* loss-of-function shows similarities to the *crb* loss-of-function (Blankenship et al., 2007). In *exo84* embryos, Crb accumulates in recycling endosomes instead of accumulating at the apical membrane (Blankenship et al., 2007).

Although we currently have a view of the different cellular machineries that regulate Crb trafficking, we still lack an integrated view of how these machineries are polarised and coordinated during the establishment of epithelial cell polarity.

1.6 Epithelial cell polarity and cancer

Tumours derived from epithelial cells are known as carcinomas and account for 80-90 % of human tumours (Molitoris and Nelson, 1990). Loss of cell polarity and adhesiveness are two hallmarks of cancer malignancy, therefore, it is not surprising that several proteins involved in polarity regulation are known tumour suppressors or proto-oncoproteins (Martin-Belmonte and Perez-Moreno, 2012). In addition, many of these polarity proteins crosstalk with a variety of other signalling pathways, such as the Wnt, Hedgehog and Hippo pathways, which regulate cell proliferation, differentiation and growth (Martin-Belmonte and Perez-Moreno, 2012).

In the Par complex, both Par6 and aPKC overexpression has been observed in multiple cancer patients, such as breast and liver cancer patients (Lee and Vasioukhin, 2008, Nolan et al., 2008, Zhang et al., 2016). In addition, more classical oncogenes, such as ErbB2, can associate with Par6-aPKC, which interferes with the regulation of the Par complex and promotes loss of epithelial polarity in breast cancer (Aranda et al., 2006). Also at the apical domain, Crb has also been implicated in cancer progression and metastasis. In immortalised mouse epithelial cells selected *in vivo* for tumourogenicity, CRB3 expression is considerably reduced and these cells display several Epithelial-Mesenchymal Transition (EMT) related characteristics, such as impaired TJ formation, loss of cell polarity and loss of contact inhibition (Bergstralh and Johnston, 2012, Karp et al., 2008, Martin-Belmonte and Perez-Moreno, 2012). In this context, re-introducing CRB3 reduces cell migration while preventing metastasis (Karp et al., 2008). Par3 also seems to act as a tumour suppressor, being reduced or mutated in squamous carcinomas

and glioblastomas (Rothenberg et al., 2010). Similarly, expressing Par3 in these cells restores TJs and reduces cell proliferation (Rothenberg et al., 2010).

All three proteins of the Scrib complex (Scrib, Lgl and Dlg) are known tumour suppressors and their expression is frequently lost in many advanced tumours (Martin-Belmonte and Perez-Moreno, 2012). In flies, *scrib*, *lgl* and *dlg* loss-of-function promotes tissue over-proliferation, which is similar to human tumourogenesis (Bergstralh and Johnston, 2012). In *Drosophila* eye-antennal discs, *scrib* mutants in combination with activated Ras develop metastatic tumours (Brumby and Richardson, 2003). Similarly, human cancers identified by the absence of *scrib* are characterised by cancer cell migration and invasion, a process that seems to be a consequence of Rac1 activation (Martin-Belmonte and Perez-Moreno, 2012). In breast and colorectal cancers, the ZEB1 transcription factor represses Lgl2 transcription, also leading to metastasis and invasion (Spaderna et al., 2008). Importantly, in melanoma cells, re-introducing Lgl decreases cell migration and increases cell adhesion, suggesting that Lgl is involved in melanoma progression (Kuphal et al., 2006).

Being largely involved in the regulation of cytoskeletal organisation, cell adhesion and cell migration, it is not surprising that Pak proteins are also frequently related to cancer. Although mutations in Pak proteins are not commonly found in human cancers, the expression or activation of these proteins is largely increased in certain types of cancer (Rane and Minden, 2014, Ye and Field, 2012). Both *pak1* and *pak4* genes are localised in chromosomal regions that are typically amplified in cancer cells (Rane and Minden, 2014, Ye and Field, 2012). While the *pak1* locus is frequently amplified in bladder, ovary and breast cancers, the *pak4* gene is found to be amplified in colorectal and pancreatic cancers (Bostner et al., 2007, Brown et al., 2008, Ito et al., 2007, Mahlamäki et al., 2004, Ye and Field, 2012). In the particular case of Pak4, it has been found overexpressed in 75 % of a total of 60 human tumour cell lines of different origins, where it has been implicated in both oncogenic transformation and anchorage-independent growth (Callow et al., 2002).

There is an evident link between cancer progression and epithelial cell polarity regulation. Loss of cell polarity and cell adhesion is a hallmark of cancer malignancy, and loss, mutation or overexpression of polarity regulators is observed in several human cancers.

However, so far, most of our knowledge resides from correlative studies. Further investigation is required to understand the detailed mechanisms that connect the regulation of polarity complexes to cancer progression. Only then we will be able to manipulate these networks in a disease background, through a tailored therapeutic approach. The use of both genetic and biochemical techniques to study in great detail the relationship between all these polarity factors is definitely necessary, possibly being the starting point for the development of novel cancer therapies.

Chapter 2

Aims

During my PhD, I aimed to understand how epithelial cells polarise their cortex and plasma membrane in order to build their apical membrane and intercellular junctions. The GTPase Cdc42 is known to play a central role in the regulation of cell polarity. Therefore, during my PhD I investigated whether Cdc42 is essential to separate the apical and junctional domains. To test this hypothesis, I have focused on the role of two effectors of Cdc42: Par6 (Chapter 4) and Mbt/Pak4 (Chapter 6).

Both Par6 and Mbt are cortical proteins, therefore regulating primarily polarity at the cell cortex. However, during epithelial morphogenesis, cortical polarity must be translated into plasma membrane specialisation. As a result, during part of my PhD, I investigated how polarity is coordinated between the cell cortex and the plasma membrane in epithelial cells. More specifically, I was interested in understanding the link between cortical polarity complexes (such as the Par complex) and the delivery of transmembrane proteins (such as Crb), while focusing on the role of the exocyst complex in the process (Chapter 5).

Chapter 3

Materials and Methods

3.1 Fly food and stocks

Drosophila melanogaster stocks were maintained at 18 °C in disposable plastic vials containing standard cornmeal fly food. Crosses and staging were carried at 25 °C unless otherwise stated. For routine fly work, flies were anaesthetised with CO_2.

3.2 Genotypes

Canton S and *yw* flies were used as *wild-type* flies for control experiments.

Fly lines used in Chapter 4

par6$^{\Delta 226}$, *FRT9.2* (Petronczki and Knoblich, 2001)

; GMR-GAL4 ; (Freeman, 1996)

;; GR1-GAL4 (Goentoro et al., 2006)

w ; FRTG13, aPKC^{psu69} (Kim et al., 2009)

Fly lines generated in Chapter 4

w ;; UAS-Par6^{WT}*::GFP*

w ;; UAS-Par6^{K23A}*::GFP*

w ;; UAS-Par6$^{KPLG\text{-}AAAA}$*::GFP*

w ;; UAS-Par6^{S146E}*::GFP*

UAS-Par6::GFP strains were generated by injecting the appropriate DNA constructs for standard P-element transformation (BestGene Inc.) (Rubin and Spradling, 1982).

w ;; par6-Par6^{WT}*::GFP*

w ;; par6-Par6^{K23A}*::GFP*

w ;; par6-Par6$^{KPLG\text{-}AAAA}$*::GFP*

w ;; par6-Par6$^{\Delta P139}$*::GFP*

w ;; par6-Par6^{S146E}::GFP

To generate *par6-Par6::GFP* rescue strains, the appropriate DNA constructs were injected into the parent strain *y[1] w[67c23] ;; PCary attP2* (Bloomington Drosophila Stock Center (BDSC) 8622) for PhiC31 mediated recombination (Groth et al., 2004) by BestGene Inc. The use of the PhiC31 integrase to target the insertion of different transgenes to the same genomic site enables the control of local genomic environment, allowing similar expression levels for different transgenes.

Fly lines used in Chapter 5

; Ubi-Ecad::GFP ; (Oda and Tsukita, 2001)

w ;; exo84^{IR} / TM3 (Vienna Drosophila Resource Center (VDRC) 30112)

w ; ubi-DECad::GFP, sec5^{E10}, FRT40A ; (Murthy et al., 2003)

ralA^{EE1} / FM7 (BDSC 25095, Eun et al. (2007))

eyFLP ; actGAL4, UAS-GFP ; FRT82B, tubGAL80 (Lee and Luo, 2001)

w[*] ; Py[+t7.7] w[+mC]=CoinFLP-GAL4attP40 / CyO ; Dr[1] / TM6C, Sb[1] (BDSC 58750) (Bosch et al., 2015)

w[*] ; Py[+t7.7] w[+mC]=CoinFLP-GAL4attP40 Pw[+mC]=UAS-2xEGFPAH2 ; (BDSC 58751) (Bosch et al., 2015)

Fly lines generated in Chapter 5

;; FRT82B exo84$^{\Delta 11}$ / TM6

;; FRT82B exo84$^{\Delta 14}$ / TM6

Both *exo84* mutant strains were generated as described in subsection 3.3.3.

;; UAS GFP::RalA^{WT}

;; UAS GFP::RalA^{E35R}

;; UAS GFP::RalA^{K44E}

To generate *UAS GFP::RalA* rescue strains, the appropriate DNA constructs were injected into the parent strain *y[1] w[67c23] ;; PCary attP2* (BDSC 8622) for PhiC31 mediated recombination (Groth et al., 2004) by BestGene Inc.

Fly lines used in Chapter 6

mbt^{P1} / mbt^{P1} ;; (Schneeberger and Raabe, 2003)

; GMR-GAL4 ; (Freeman, 1996)

Fly lines generated in Chapter 6

;; UAS-arm^{SA561,688}*::myc / +* was generated by injecting the appropriate DNA constructs for standard P-element transformation (BestGene Inc.) (Rubin and Spradling, 1982).

3.3 Genetic techniques

3.3.1 *GAL4-UAS* system

Ectopic gene expression was achieved using the *GAL4-UAS* system, which enables the overexpression or RNAi-induced knock-down of different genes in specific tissues at a controlled developmental time (Brand and Perrimon, 1993). A variety of promoters can be used to drive the expression of the yeast transcriptional activator *GAL4* in specific tissues. In this thesis, the *Glass Multimer Reporter* (*GMR*) promoter was used to drive *GAL4* expression in cells behind the morphogenetic furrow in *Drosophila* imaginal discs (Freeman, 1996), while the *GR1* promoter was used to drive *GAL4* expression in FCs including FC stem cells (Goentoro et al., 2006). Tissue specific GAL4 protein can then bind the *Upstream Activation Sequence* (*UAS*) and enhance transcription of transgenes under the control of the *UAS* sequence (Brand and Perrimon, 1993). As a consequence, transgenes under the control of a *UAS* sequence are expressed only in cells containing GAL4, *i.e.* in all cells behind the morphogenetic furrow in *Drosophila* imaginal discs or in all FCs (Figure 3.1).

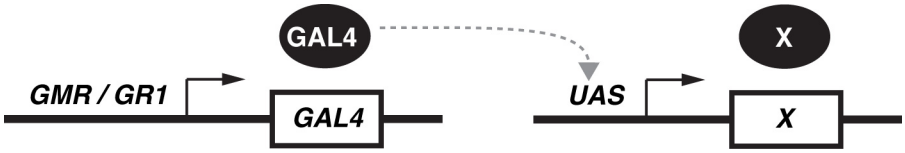

Figure 3.1: The *GAL4-UAS* system. The *GAL4* gene is under the control of the driver *GMR* or *GR1*, for expression in the retina or follicular epithelium, respectively. The protein GAL4 binds to the enhancer *UAS* and activates the transcription of gene *X*.

3.3.2 Genetic Mosaics

The FLP-FRT system

The FLP-FRT system is a site-directed recombination technique and was used to generate genetic mosaics in the fly retina. Tissue-specific Flip-recombinase (Flp) binds to *Flippase recognition target* (*FRT*) sites and promotes recombination between two homologous chromosomes: one harbouring the mutant allele and the other containing the marker gene *ubi-GFP* (Golic and Lindquist, 1989). This generates two genetically different cell populations: (1) a non-GFP population that is homozygous for the mutation, and (2) a population with two copies of the GFP marker, which is *wild-type* twin-spot (Figure 3.2) (Stocker and Gallant, 2008, Xu and Rubin, 1993). In this thesis, Flp was placed under the control of the *eyeless* (*ey*) promoter, therefore restricting these recombination events to the developing eye-antennal imaginal disc (Newsome et al., 2000). The expression of *ey* starts at stage 15 of embryonic development in the 6-23 cell eye-disc primordium and continues until the final cell divisions at late third instar larvae (Newsome et al., 2000).

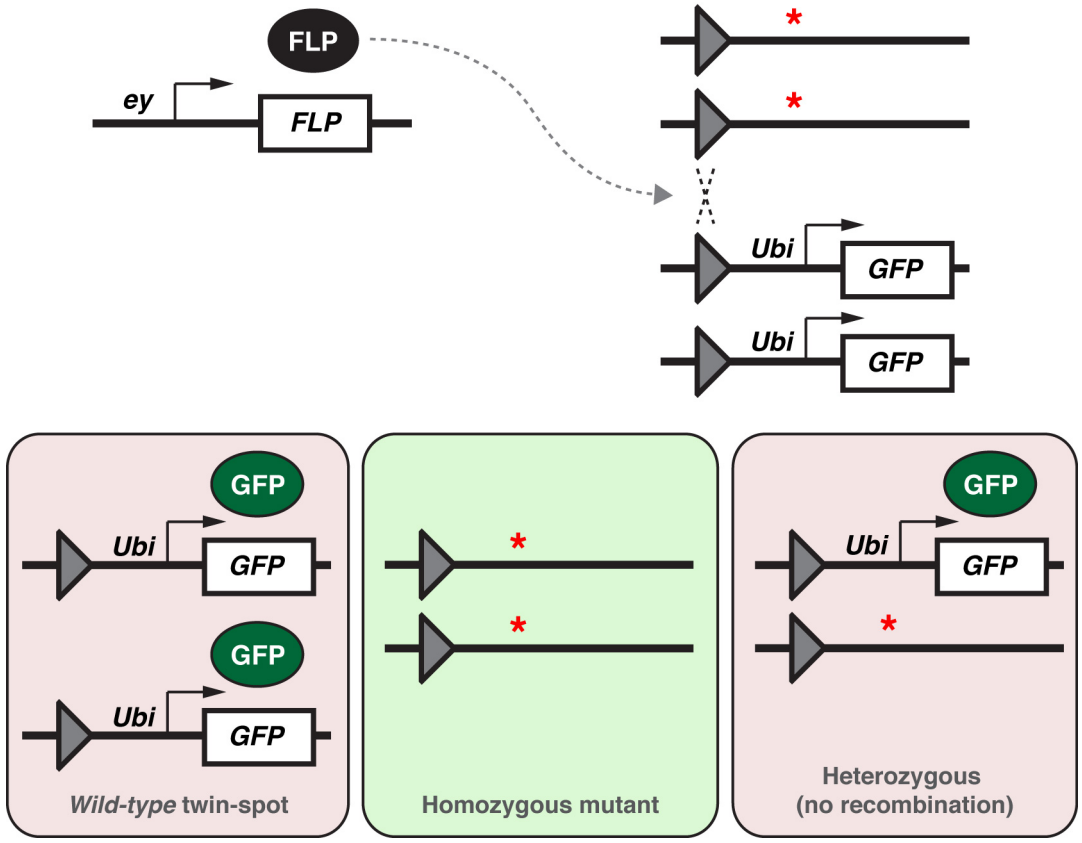

Figure 3.2: The FLP-FRT system. *ey* drives the expression of *FLP* in the eye-antennal disc, which in turn binds to identical *FRT* sites (grey triangles) and mediates site-specific recombination between two homologous chromosomes, one containing a lethal mutation (red asterisk) and another containing a GFP marker. As a consequence, cells that undergo recombination are *wild-type* twin-spot with two copies of the GFP marker, or homozygous mutant lacking GFP signal. There is potentially a population of cells that does not undergo recombination and contains one copy of each chromosome, similarly to the parent cell.

The MARCM system

The mosaic analysis with a repressible cell marker (MARCM) system is based on the previously mentioned FLP-FRT system; however, the mutant cells are marked by the presence of the GFP marker. In this system, GAL4 is ubiquitously expressed, driving the expression of a GFP marker placed under the control of a *UAS* sequence. Using the GAL4-repressor transgene *GAL80*, it is possible to repress *GFP* expression in *wild-type* cells, while mutant cells lacking GAL80 are marked by the expression of the *GFP* marker (Figure 3.3) (Lee and Luo, 1999). Similar to the previous subsection, Flp was expressed specifically in the fly eye using the *ey* promoter (Newsome et al., 2000).

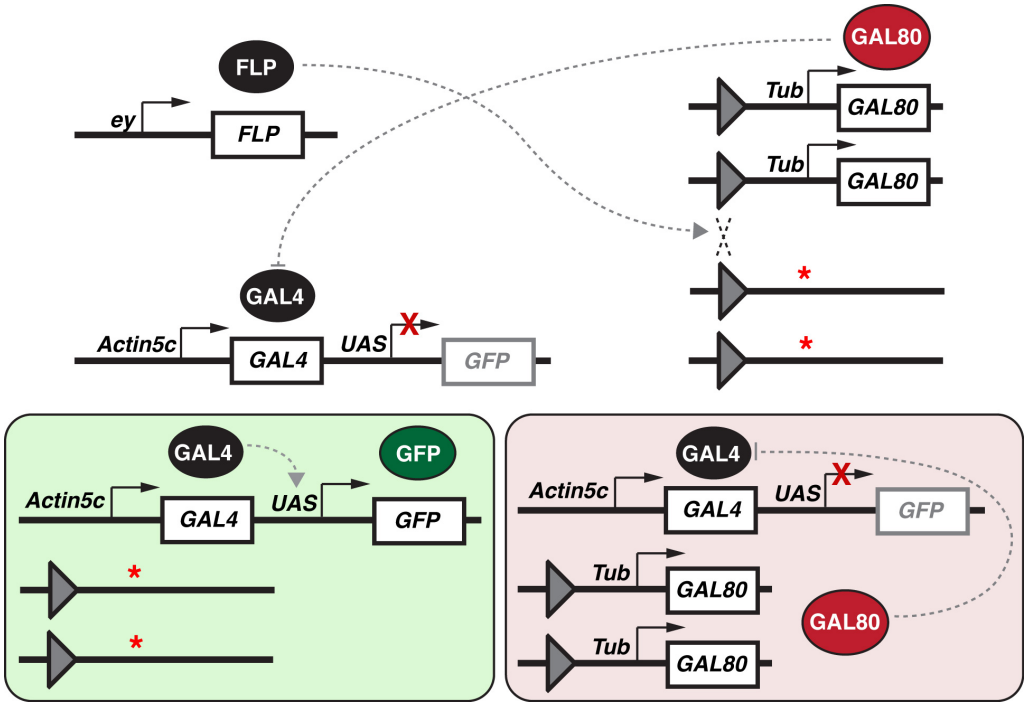

Figure 3.3: The MARCM system. *ey* drives the expression of *FLP* in the eye-antennal disc, which in turn binds to identical *FRT* sites (grey triangles) and mediates site-specific recombination between two homologous chromosomes, one containing a lethal mutation (red asterisk) and another containing the *GAL80* gene. GAL4 is ubiquitously expressed, enhancing the expression of *UAS GFP* in the absence of its repressor GAL80. As a consequence, cells that undergo recombination are homozygous mutant and GFP-positive, or *wild-type* and express *GAL80*, therefore lacking GFP signal.

The *coinFLP-GAL4* system

The *coinFLP-GAL4* system enables the overexpression or RNAi-induced knock-down of different genes in mosaic tissues (Bosch et al., 2015). Based on stochastic recombination events induced by the recombinase Flp, it is possible to combine both *wild-type* and mutant cells in the same tissue expressing Flp (Bosch et al., 2015). The eye-specific promoter *ey* was used to generate mosaics in the fly eye without affecting the rest of the animal (Newsome et al., 2000).

BDSC stock 58750 – *w[*] ; Py[+t7.7] w[+mC]=CoinFLP-GAL4attP40 / CyO ; Dr[1] / TM6C, Sb[1]* – was used to generate mosaic retina overexpressing fluorescently tagged proteins, while stock 58751 – *w[*] ; Py[+t7.7] w[+mC]=CoinFLP-GAL4attP40 Pw[+mC] =UAS-2xEGFPAH2* ; – was used to generate RNAi-induced knock-down clones where mutant cells are marked by the presence of GFP signal.

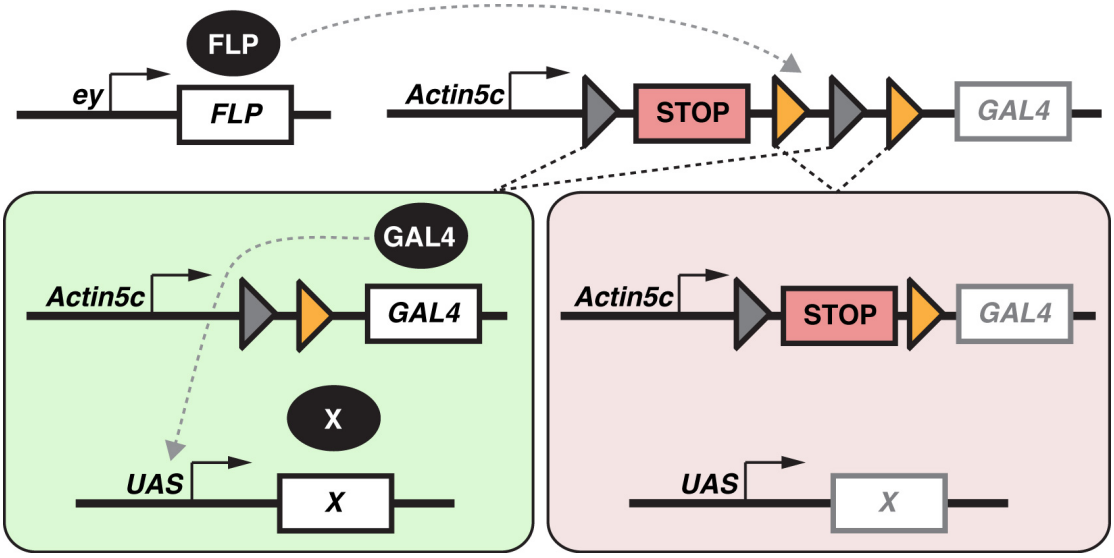

Figure 3.4: The coinFLP system. *ey* drives the expression of *FLP* in the eye-antennal disc, which in turn mediates site-specific recombination between one of the two existing pairs of mutually exclusive *FRT* sites: canonical *FRT* (grey triangle) or *FRT3* (orange triangle). Recombination between the canonical *FRT* sites excises a STOP codon, leading to the expression of *GAL4* and subsequent expression of gene *X*. On the other hand, recombination between the *FRT3* sites excises one of the canonical *FRT* sites, preventing further recombination events, while maintaining the STOP codon that prevents the expression of *GAL4* and as a consequence, also prevents the expression of gene *X*.

3.3.3 P-element imprecise excision

The *exo84* mutant flies were generated by P-element imprecise excision. Chromosomal P-element excision forms a double-stranded break in the DNA. Importantly, in approximately 1 % of these excision events, the ends of this double-stranded break are degraded before DNA repair, leading to removal of the flanking regions together with the P-element (Stocker and Gallant, 2008). This unpredictable process known as P-element imprecise excision can lead to the formation of mutants.

The Exo84 line w^{1118} ;; $exo84^{HP35566}$ (BDSC 21984) was used as a starting point to generate *exo84* mutant flies. The $exo84^{HP35566}$ line belongs to a library of EP-element insertions, which have been generated by the insertion of an *UAS* that can activate the transcription of an endogenous neighbouring gene in a GAL4-dependent manner (Staudt et al., 2005). The EP-element HP35566 is inserted in the first exon of the *exo84* gene (Figure 5.3A). The imprecise excision of this P-element was induced by the Δ2,3

transposase (BDSC 3629) and individual males were used to establish individual stocks. These stocks were screened for lethality and then by PCR using the following primer pair: 5'-TGAATTAGCAACAGGTGGAAAA-3' and 5'-AAACACATCTGTGGTGTA GAC-3'. Deletions were verified by sequencing the PCR product, which confirmed the characterisation of two independent mutant lines that we called *exo84*$^{\Delta 11}$ and *exo84*$^{\Delta 14}$. These *exo84* mutant lines were finally recombined onto FRT82B chromosomes (BDSC 5619).

3.4 Reagents

3.4.1 Antibodies

Table 3.1: Primary antibodies and dilutions used for western blotting.

Target	Host species	Supplier	Cat. No. (Clone)	Dilution
alpha-Tubulin	Mouse	DSHB*	AA4.3	1/100
Flag	Mouse	Sigma	F3165 (M2)	1/1,000
GFP	Rabbit	Cell Signaling	2956S (D5.1)	1/1,000
GST	Rabbit	Sigma	G7781 (polyclonal)	1/100,000
MBP	Mouse	New England Biolabs	E8032S	1/80,000
Myc	Mouse	Santa Cruz	sc-40 (9E10)	1/1,000
PKCζ	Rabbit	Santa Cruz	sc-216 (C-20)	1/500

* Developmental Studies Hybridoma Bank (DSHB)

Table 3.2: Secondary antibodies and dilutions used for western blotting.

Conjugation	Target species	Host species	Supplier	Cat. No.	Dilution
HRP	Mouse	Rabbit	Sigma	A0545	1/10,000 - 1/80,000
HRP	Rabbit	Goat	Sigma	A9044	1/10,000 - 1/100,000
Veriblot HRP	Mouse	Rat	Abcam	Ab131368	1/4,000

Table 3.3: Primary antibodies and dilutions used for immunofluorescence.

Target	Host species	Supplier	Cat. No.	Dilution
Arm	Mouse	DSHB	N27A1	1/200
Baz	Rabbit	Wodarz et al. (1999)		1/2,000
Crb	Mouse	DSHB	Cq4	1/50
Crb	Rat	Walther et al. (2016)		1/200
E-cad	Rat	DSHB	DCAD2	1/20
Eys	Mouse	DSHB	mAB21A6	1/10
Mbt	Guinea Pig	Walther et al. (2016)		1/200
Par6	Guinea Pig	Walther et al. (2016)		1/1,000
PKCζ	Rabbit	Sigma	SAB4502380	1/500
PS980-Baz	Rabbit	Morais-de Sá et al. (2010)		1/200
Rab11	Mouse	BD Transduction Laboratories	610657	1/100
Rab5	Rabbit	Abcam	ab31261	1/500
Rhodopsin-1	Mouse	DSHB	4C5	1/10
Sec5	Mouse	Murthy et al. (2003)	22A2	1/35

Table 3.4: Secondary antibodies and dilutions used for immunofluorescence.

Conjugation	Target species	Host species	Supplier	Cat. No.	Dilution
DyLight 405	Mouse	Donkey	Jackson ImmunoResearch	715-475-151	1/200
DyLight 405	Rabbit	Donkey	Jackson ImmunoResearch	711-475-152	1/200
AlexaFluor 488	Mouse	Donkey	Jackson ImmunoResearch	715-545-151	1/200
Cy3	Rabbit	Donkey	Jackson ImmunoResearch	711-165-152	1/200
Texas red	Rat	Donkey	Jackson ImmunoResearch	712-075-150	1/200
AlexaFluor 647	Rat	Donkey	Jackson ImmunoResearch	712-605-153	1/200
AlexaFluor 647	Guinea pig	Donkey	Jackson ImmunoResearch	706-605-148	1/200
Phalloidin TRITC	n/a	n/a	Sigma	P1951	1/200

3.4.2 Plasmids

A full list of the plasmids used in this thesis is listed in Appendix Tables 7.1 and 7.2, with a brief description of how they were engineered. Plasmid DNA purification was performed with the QIAprep Spin Miniprep Kit (Cat. No. 27104, Qiagen). Plasmid

DNA concentration was measured using a NanoDrop^{TM}2000 Spectrophotometer (ThermoFisher).

3.5 Molecular Cloning

3.5.1 Generation of competent bacteria

Bacteria (NEB 5-alpha Competent *E. coli* [Cat. No. C2987I, New England Biolabs] , BL21-AI One Shot Chemically Competent [Cat. No. C607003, Invitrogen] or One Shot *ccdB* Survival 2 T1R Competent Cells [Cat. No. A10460, Invitrogen]) were streaked from a glycerol stock onto an LB plate and incubated overnight at 37 °C. A single colony was used to inoculate 5 mL of LB media and incubated overnight at 37 °C. The overnight culture was used to inoculate 500 mL of LB media and grown at 37 °C until OD_{600} was between 0.4-0.55. The culture was then transferred to a cold sterile centrifuge bottle, incubated on ice for 10 min and centrifuged at 1,700 x g for 10 min at 4 °C. The bacterial pellet was resuspended in 1/3 of the original volume with RF1 buffer (100 mM rubidium chloride, 50 mM manganese (II) chloride tetrahydrate, 30 mM potassium acetate, 10 mM Calcium chloride dihydrate and 15 % wt/vol glycerol, pH 5.8). Bacteria in RF1 buffer were incubated on ice for 15 min and centrifuged at 580 x g for 15 min at 4 °C. The bacterial pellet was then resuspended in 1/25 of the original volume with RF2 buffer (10 mM MOPS, 10 mM rubidium chloride, 75 mM calcium chloride dihydrate and 15 % wt/vol glycerol, pH 6.8). Bacteria in RF2 buffer were incubated on ice for 15 min, aliquoted in eppendorf tubes and frozen at -80 °C.

3.5.2 Restriction enzyme based cloning

DNA fragments were amplified by PCR using the proof-reading enzyme PfuUltra II Fusion HS DNA Polymerase (Cat. No. 600670, Agilent). The quality of the PCR product was confirmed by agarose gel electrophoresis and then PCR purified (Monarch PCR & DNA Cleanup Kit. Cat. No. T1030S, New England Biolabs) or gel extracted (Monarch DNA Gel Extraction Kit, Cat. No. T1020S, New England Biolabs) as appropriate. All restriction digests were performed using enzymes and buffers from New England Biolabs. Ligations were performed overnight at 16 °C with T4 DNA ligase (Cat. No. M0202S,

New England Biolabs). Post-cloning plasmid screening was performed by colony PCR with BioMix^{TM}Red (Cat. No. BIO-25006, Bioline).

3.5.3 Gateway system cloning

pENTR directional TOPO cloning

Gateway cloning was performed according to manufacturer's instructions (Invitrogen). Primers were designed to amplify the region of interest from a template DNA and containing a CACC sequence at the 5' end of the Forward Primer. The DNA fragment was amplified by PCR using the proof-reading enzyme PfuUltra II Fusion HS DNA Polymerase (Cat. No. 600670, Agilent). The quality and quantity of the PCR product was confirmed by agarose gel electrophoresis and was then TOPO cloned into the *pENTR^{TM}/D-TOPO* vector (Cat. No. K240020, Invitrogen). For the TOPO cloning reaction, up to 5 µL of PCR product were incubated with 1 µL of salt solution and 1 µL of vector for 30 min at Room Temperature (RT). The recombinant vector was transformed into One Shot competent *E. coli* (Cat. No. K240020, Invitrogen) and plated onto LB agar plates with kanamycin. The obtained pENTR vectors were validated by Sanger sequencing.

LR recombination

The LR recombination reactions were performed by mixing 1 µL of the *pENTR* vector at 20 ng/µL, 0.5 µL of the Destination Vector at 75 ng/µL, 0.5 µL of TE buffer and 0.5 µL LR Clonase II enzyme mix (Cat. No. 11791-019, Invitrogen). The previous reactions were incubated for 1h at 25 °C and then further 10 min at 37 °C with 0.25 µL of Proteinase K to terminate the reaction. DH5α competent *E. coli* were transformed with 1 µL of the LR reaction and plated onto LB agar plates with ampicillin. The final products were validated by Sanger sequencing.

3.5.4 Site-directed mutagenesis

The QuikChange Lightning Site-Directed Mutagenesis Kit (Cat. No. 210518, Agilent) was used to generate mutant plasmids according to manufacturer's instructions.

Table 3.5: Primers used for RalA mutagenesis.

Primer	Sequence
RalA G20V forward	5'-atggtgggcagtgtcggcgtgggaaag-3'
RalA G20V reverse	5'-ctttcccacgccgacactgcccaccat-3'
RalA E35R forward	5'-cgccctcacactgcagtttatgtacgatcgattcgtcgaggactac-3'
RalA E35R reverse	5'-gtagtcctcgacgaatcgatcgtacataaactgcagtgtgagggcg-3'
RalA K44E forward	5'-gactacgagcccaccgaggccgatagctata -3'
RalA K44E reverse	5'- tatagctatcggcctcggtgggctcgtagtc -3'

3.5.5 *Drosophila* genomic DNA extraction

Fly genomic DNA was extracted from 25 fly heads per condition. First, flies were beheaded and their heads were kept on ice in 250 µL of extraction buffer (0.1 M Tris HCl, pH 9.0, 0.1 M EDTA and 1 % SDS). The heads were homogenised using a motor mixer with pestles and incubated 30 min at 70 °C, followed by addition of 35 µL of KAc 8 M and incubation on ice for further 30 min. Samples were centrifuged for 15 min at 13,000 rpm, and for each sample, the supernatant was transferred to a new tube to which was added the same volume of Phenol-Chloroform. After vigorous shaking, the samples were centrifuged again 5 min at 13,000 rpm, the supernatant was transferred to a new tube to which was added again the same volume of Phenol-Chloroform. Again, after shaking the samples were centrifuged 5 min at 13,000 rpm, the supernatant was transferred to a new tube to which was added 150 µL of Isopropanol. After shaking, the samples were centrifuged 5 min at 10,000 rpm, the supernatants were discarded and the pellets were washed with 1 mL 70 % EtOH. The samples were centrifuged 5 min at 13,000 rpm, the EtOH was removed and the pellets were allowed to air-dry for approximately 5 min before being resuspended in 100 µL of TE buffer.

3.5.6 DNA sequencing and analysis

Sanger sequencing was performed either by Eurofins Genomics (Ebersberg, Germany) or by Genewiz (Takeley , UK). Sequences were analysed with the DNASTAR Lasergene package.

3.6 Cell culture

3.6.1 Cell lines and maintenance

S2 cells from Drosophila Genomics Resource Center (DGRC) were maintained at 26 °C in Schneider's medium (Cat. No. 21720001, ThermoFisher Scientific) with 10 % FBS and 1 % Penicillin/Streptomycin.

3.6.2 Transient transfection

S2 cells were transiently transfected with Effectene Transfection Reagent (Cat. No. 301427, Qiagen). Approximately 1 x 10^6 cells in 600 µL were plated per well of a 12-well plate. After 24h, S2 cells were transfected with 1 µg of DNA, 65 µL of EC Buffer, 8 µL of enhancer, 10 µL of effectene and 107 µL of Schneider's medium. S2 cells were incubated for 48h in this transfection mix and then used for further experiments. For pulldown experiments, a total of 4 wells were transfected per experimental condition.

For plasmids with the metallothionein gene promoter, expression of the gene of interest was induced by addition of 0.5 mM copper sulfate to the culture medium 24h post-transfection and incubation for 24h, before being used for further experiments.

3.7 Biochemistry

3.7.1 Expression and purification of recombinant proteins

To express GST-fusion proteins, *E. coli* BL21 was transformed with the appropriate plasmid and induced with 0.2 % L-arabinose or 1 mM IPTG as appropriate for 4h at 30 °C. Bacteria were lysed by sonication in 50 mM Tris HCl pH 7.6, 50 mM NaCl, 5 mM $MgCl_2$, 0.5 % Triton X-100, 10 mM DTT and protease inhibitor (EDTA-free Complete Protease Inhibitor [Cat. No. 04693132001, Roche]). GST-fusion proteins were purified using Glutathione Sepharose 4 Fast Flow beads (Cat. No. 17-5132-01, GE Healthcare). Lysates were incubated with the beads for 1h at 4 °C in an end-over-end rotator, washed in lysis buffer and kept on beads in lysis buffer with 1 mM DTT at 4 °C for further experiments.

To express MBP-fusion proteins *E. coli* BL21 was transformed with the appropriate plasmids and induced with 0.3 mM IPTG for 2h at 37 °C. Bacteria were lysed in 20 mM Tris HCl pH 7.4, 200 mM NaCl, 1 mM EDTA, 1 mM DTT. MBP-fusion proteins were purified using Amylose resin (Cat. No. E8021S, New England Biolabs). Lysates were incubated with the beads for 1h at 4 °C in an end-over-end rotator, washed in lysis buffer, eluted in lysis buffer containing 10 mM Maltose, dialysed to 50 mM Tris HCl pH 7.5, 150 mM NaCl, 5 mM $MgCl_2$, 40 % Glycerol and stored at -80 °C for further experiments.

Before further experiments, all proteins were separated by SDS-PAGE followed by Instant Blue (Cat. No. HG773010, Expedeon) or Coomassie R-250 staining, to confirm the quantity and quality of the purified proteins.

3.7.2 *In vitro* binding assay

Approximately 1 µg of recombinant GST-fusion protein in beads and 0.5 µg of recombinant MBP-fusion protein were mixed together with binding buffer (50 mM Tris HCl pH 7.5, 150 mM NaCl, 5 mM $MgCl_2$, 0.5 % Triton X-100) in a total volume of 100 µL. From this, 30 % were saved as the input control, where 25 % were loaded into a gel for Coomassie staining and 5 % were loaded into a separate gel for Western Blot analysis as in subsection 3.7.6. The remaining 70 % were incubated for 1h at 4 °C in an end-over-end rotator, washed three times in binding buffer and 58 % were loaded into a gel for Coomassie staining while the remaining 12 % were loaded into a separate gel for Western Blot analysis as in subsection 3.7.6.

3.7.3 GST Pulldowns

S2 cells were washed in PBS and lysed in 50 mM Tris HCl pH 7.5, 150 mM NaCl, 0.5 % Triton X-100, 1 mM EDTA, protease inhibitor (EDTA-free Complete Protease Inhibitor [Cat. No. 04693159001, Roche]) and phosphatase inhibitor cocktail (Cat. No. P5726, Sigma). Protein concentration was determined with the Pierce BCA Protein Assay Kit (Cat. No. 23227, ThermoFisher Scientific) and samples were diluted accordingly to have the same final concentration. A small amount (approximately 2 % of the total cell lysate, *i.e.* roughly 10 µg) of cell lysate was diluted in SDS sample buffer (with a final

concentration in the sample of 62.5 mM Tris-Cl pH 6.8, 2 % SDS, 7.5 % glycerol, 2.5 % β-mercaptoethanol and 0.005 % bromophenol blue) and stored at -20 °C. With the remaining cell lysate, equal amounts (approximately 500 µg of total cell lysate) were added to roughly 1 µg of previously purified GST-tagged protein in beads. Cell lysates were incubated with the beads for 1h at 4 °C in an end-over-end rotator, washed three times in lysis buffer and analysed by Western blotting as in subsection 3.7.6.

3.7.4 Co-immunoprecipitation

S2 cells were washed in PBS and lysed as in subsection 3.7.3. Cell lysates were treated as in subsection 3.7.3. Flag-tagged proteins were immunoprecipitated with anti-FLAG M2 magnetic beads (Cat. No. M8823, Sigma), while myc-tagged proteins were immunoprecipitated with anti-myc agarose beads (Cat. No. A7470, Sigma). Equal amounts of cell lysate (approximately 500 µg of total cell lysate) were added to 30 µL of beads and incubated 1h at 4 °C in an end-over-end rotator. Proteins in the beads were then washed three times in lysis buffer and analysed by Western blotting as in subsection 3.7.6.

3.7.5 *Drosophila* protein extraction

Protein extractions were preformed from eight fly heads homogenised in 30 µL of extraction buffer (125 mM NaCl, 50 mM Tris HCl pH 7.5, 5 % glycerol, 1 mM $MgCl_2$, 1 mM EDTA, 0.2 % NP-40, 0.5 mM DTT, EDTA-free Complete Protease Inhibitor [Cat. No. 04693159001, Roche] and phosphatase inhibitor cocktail [Cat. No. P5726, Sigma]), using a motor mixer with pestles. Samples were centrifuged at 13,000 rpm for 10 min using a bench-top centrifuge and the supernatants were analysed by Western blotting as in subsection 3.7.6.

3.7.6 Western Blotting

Samples in SDS sample buffer were boiled for 5 min at 95 °C and loaded into a NuPAGE^{TM}10 % or 4-12 % Bis-Tris Protein Gel (Cat. No. NP0321BOX, Invitrogen). The gel assembly and tank were filled with MOPS running buffer (Cat. No.

NP0001, Invitrogen) and run at 120-180 V constant until proteins were properly separated. SeeBlue^{TM}Plus2 Pre-stained Protein Standard (Cat. No. LC5925, Invitrogen) was loaded adjacent to samples to estimate the molecular weight of detected proteins. Proteins were transferred onto a nitrocellulose membrane with a pore size of 0.45 µm (Cat. No. 10600008, GE Healthcare) using a wet transfer system running at 100 V constant for 1h or at 30 V overnight, at 4 °C. Ponceau S was used to reversibly stain the membrane and confirm transfer efficiency. Membranes were then blocked in 5 % skimmed milk powder in PBST (PBS with 0.1 % Tween20) for 1h at RT and incubated with primary antibody diluted in 3 % skimmed milk powder in PBST for 1h at RT or overnight at 4 °C. A list of the primary antibodies and dilutions used is shown in table 3.1. Membranes were washed three times with PBST for 15 min, before incubation with secondary antibody diluted in 3 % skimmed milk powder in PBST for 1h at RT. A list of the secondary antibodies and dilutions used is shown in table 3.2. Membranes were washed as above, incubated 5 min with the Luminata Crescendo Western HRP substrate (Cat. No. WBLUR0100, Merck) and developed on Amersham Hyperfilm ECL (Cat. No. 28906837, GE Healthcare).

3.7.7 Kinase Assay

GST-tagged proteins were expressed and purified as in subsection 3.7.1, but instead of being stored in the beads, proteins were eluted with 40 mM Glutathione, 50 mM Tris HCl, pH 8.0 and dialysed against lysis buffer with 40 % glycerol. S2 cells were transfected as in subsection 3.6.2 and lysed as in subsection 3.7.3. The lysates were incubated with 4 µg of anti-myc agarose beads (Cat. No. A7470, Sigma) for 1h at 4 °C in an end-over-end rotator. The beads were washed with the kinase buffer (20 mM HEPES, pH 7.6, 150 mM NaCl, 20 mM $MgCl_2$, 10 µL/mL phosphatase inhibitor [Cat. No. P5726, Sigma], 20 µM ATP). Beads with kinase were split in 20 µL fractions and then mixed with 30 µg of each substrate GST fusion protein as well as 1 µL of [γ-32P]-ATP (5 µCi). Each condition was incubated at 30 °C for 30 min. The proteins were separated by SDS-PAGE and visualized by autoradiography.

3.8 Microscopy

3.8.1 S2 cell aggregation assay

S2 cells were transfected as in subsection 3.6.2. S2 cells were collected, resuspended in fresh media and plated onto a 35 mm glass bottom dish (glass thickness 0.17 mm) (Cat. No. FD35-100, FluoroDish^{TM}, World Precision Instruments, Inc.). The dishes were incubated for 3h at 175 rpm at RT and then imaged with a Leica SP8 confocal microscope.

3.8.2 Immunofluorescence of *Drosophila* pupal retinae

Pupal retinae were dissected and prepared for imaging as in Walther and Pichaud (2006). Approximately 5 days after setting up a cross at 25 °C, white pupae (*i.e.* 0 % APF) were staged in a humid plastic Petri dish. Pupae were dissected at 40 % APF, which means 4 days at 18 °C, 42h APF at 25 °C or 32h APF at 29 °C. Each pupa was placed on a dissecting dish and using a pair of dissecting tweezers the pupal case was removed around the anterior side of the pupa. The pupa was placed in PBS and by inserting one tweezer at the top of the head, a whole was opened through which all head content was pipetted out with a P200 pipette. The content was expelled into a glass dish containing ice-cold PBS, the two retina with optic lobes and brain were located and transferred onto a new glass dish with ice-cold PBS. Retinas were incubated in fixative solution (4 % formaldehyde in PBS) for 20 min at RT with gentle shaking and washed with PBT (PBS with 0.3 % Triton X-100) before proceeding to immunostaining.

Retinae were blocked in 5 % goat serum in PBT for 20 min at RT with shaking and incubated with primary antibodies diluted in PBT overnight at 4 °C with shaking. A list of the primary antibodies and dilutions used is shown in Table 3.3. Retina were washed three times 5 min in PBT and incubated with secondary antibodies diluted in PBT for 2-4h at RT with shaking. A list of the secondary antibodies and dilutions used is shown in Table 3.4. A final wash step was proceeded by incubating the retinas in PBT overnight at 4 °C. The specimens were pipetted onto a glass microscope slide with as least PBT as possible and covered with a droplet of Vectashield^{TM} with or without DAPI (Vector Laboratories) as appropriate. Lastly, using a dissecting pin, each retina

was pulled away from the optic lobe, positioned with the apical side facing upward and carefully covered with a rectangular coverslip. Nail varnish was used to seal the coverslip. Retinae were imaged with a Leica SP5 or SP8 confocal microscope.

3.8.3 Immunofluorescence of *Drosophila* adult retinae

Adult flies were anaesthetised with CO_2 and, using dissecting tweezers, their head was removed from the thorax and placed in ice-cold PBS in a dissecting dish. The heads were bisected by holding them at the proboscis and gently tearing both retinae apart. Excess brain material was removed except for the lamina, and retinae were transferred to ice-cold PBS. Retinae were fixed in 4 % formaldehyde in PBS for 20 min at RT with gentle shaking and washed with PBT. The lens was removed by gently inserting a hooked dissecting pin between the lens and the retina and gently dragging the hook along the lens to scoop the retina away from the lens. Retinae were immunostained as in subsection 3.8.2. Two squared coverslips were placed 1 cm apart on top of a glass microscope slide and the immunostained retinae were pipetted onto the space between the coverslips. Vectashield^{TM} with or without DAPI (Vector Laboratories) was pipetted onto the retinae as appropriate and a third coverslip was carefully placed on top, bridged by the other two coverslips, and covering the retinae. Nail varnish was used to seal the coverslip. Retinae were imaged with a Leica SP5 or SP8 confocal microscope.

3.8.4 Cryosectioning of *Drosophila* adult retinae

Adult flies were anaesthetised with CO_2 and, using dissecting tweezers, their head was removed from the thorax and placed in ice-cold PBS. Heads were fixed in 3 % formaldehyde for 2h at RT in an end-over-end rotator, washed 3 x 5 min in PBS and incubated in 15 % sucrose in PBS overnight at 4 °C rotating. Approximately 4-5 heads were transferred to the well of an embedding mold and completely covered with Tissue-Tek® O.C.T. Compound (Cat. No. 50-363-579, Fisher Scientific). The position of the heads was carefully adjusted to keep them at the bottom of the well with the neck facing downwards and the eyes facing sideways. The mold with fly heads in O.C.T. was stored overnight at -20 °C. On the following day, the O.C.T. frozen blocks with fly heads were removed from the mold and placed onto a metal grid inside the cryostat (Leica CM1850)

at -25 °C. Sections of 12 µm thickness were cut along the O.C.T. block and transferred one by one to a microscope slide at RT by gently touching the slide to the tissue. Sections were surrounded with an hydrophobic marker and kept with a PBS drop to avoid drying out. When all cuts were finished for a single block, the PBS was removed from the slides and sections were incubated first 10 min at RT in PBS + 0.1 % Triton X-100 and then 30 min at RT in Phalloidin TRITC (Table 3.4). The sections were washed three times in PBS + 0.1 % Triton X-100 and mounted in Vectashield^{TM} with DAPI (Vector Laboratories). Cryosections were imaged with a Leica SP5 or SP8 confocal microscope.

3.8.5 Immunofluorescence of *Drosophila* follicle cells

Drosophila eggs were dissected and prepared for imaging as in Haack et al. (2013). Young adult flies were fed with yeast 1-2 days prior to dissecting them to increase ovaries size. Flies were anaesthetised with CO_2 and their head was removed from the thorax using dissecting tweezers. Heads were discarded while the thorax and the abdomen were transferred to a dissecting dish with ice-cold PBS. Flies were grabbed by the lower thorax and opened until abdominal content was exposed. Ovaries were cleaned from remaining organs, opened in quarters with dissecting pins to expose the ovarioles and kept in ice-cold PBS. Ovaries were fixed in 4 % formaldehyde in PBS for 20 min at RT with gentle shaking, washed with PBST (PBS with 0.1 % Tween20) and blocked in 5 % goat serum in PBST for 20 min at RT with shaking before proceeding to immunostaining. For Crb stainings, ovaries were fixed in 4 % formaldehyde in PBS for 20 min at RT with shaking, incubated 2 min in 50 % methanol in PBST, 2 min in 100 % methanol, 2 min in 50 % methanol in PBST, washed three times 10 min in PBST and blocked 30 min in 10 % BSA in PBST.

For immunolabelling, ovaries were incubated with primary antibodies diluted in PBST overnight at 4 °C with shaking, washed four times 5 min in PBST, incubated with secondary antibodies diluted in PBST for 3h at RT with shaking and washed three times 10 min in PBST. A list of the primary and secondary antibodies and dilutions used is shown in Tables 3.3 and 3.4. The specimens were pipetted onto a glass microscope slide with as little PBST as possible, submerged with a droplet of Vectashield^{TM} with

or without DAPI (Vector Laboratories) as appropriate, and carefully covered with a rectangular coverslip. Nail varnish was used to seal the coverslip. *Drosophila* FCs were imaged with a Leica SP5 or SP8 confocal microscope. Stage 7 eggs are shown in all figures unless otherwise stated.

3.8.6 FRAP

Pupal retinae were mounted at 40 % APF by removing the pupal cuticle and carefully exposing the retina. A glass slide was prepared with a stripe of two-sided tape in the middle (Figure 3.5A) and the pupa was placed on top of the tape with the dorsal side facing upwards and ventral side downwards (Figure 3.5B). Pupal cuticle was carefully removed at the anterior side with a pair of tweezers exposing at least one of the retinae (Figure 3.5B). The pupa was carefully removed from the tape a set aside in the glass slide. Using Blu-Tack, two small balls and a pillow were made to cushion the coverslip (Figure 3.5C). Using a pair of tweezers, a small cavity was created in the Blu-Tack pillow to hold the pupa at approximately 45° (Figure 3.5D). The pupa was placed sideways in the Blu-Tack pillow at approximately 45° and, with the tweezers, a small amount of Blu-Tack was pulled around the pupa, holding it at the correct position (Figure 3.5E-F). A small drop of Oil 10 S, Voltalef® (Cat. No. 24627.188, VWR) was placed onto a squared high precision coverslip at the predicted position of the retina and the coverslip was carefully pressed against the Blu-Tack, until the eye was touching the oil and coverslip (Figure 3.5G-H).

Live imaging was performed on a Leica SP5 confocal with a 63x 1.4 numerical aperture (NA) oil immersion objective and the following settings: pixel resolution 512 x 512; speed 400 Hz; 10 % 488-nm laser power at 20 % argon laser intensity; and 5x zoom. FRAP analysis of E-cad::GFP was performed through a 5 pixel-diameter circle Region of Interest (ROI) at the basal tip of the AJ of the photoreceptors and photo-bleached with a single pulse using 90 % 488-nm laser power at 20 % argon laser intensity. AJ recovery was recorded every 1.293 s with the previously mentioned settings for 200 frames. FRAP of Par6::GFP and Par6^{AAAA}::GFP was performed through a 5 pixel-diameter circle ROI at the apical region of the photoreceptors, followed by photo-bleaching with 2 pulses using 90 % 488-nm laser power at 20 % argon laser intensity. GFP recovery was recorded

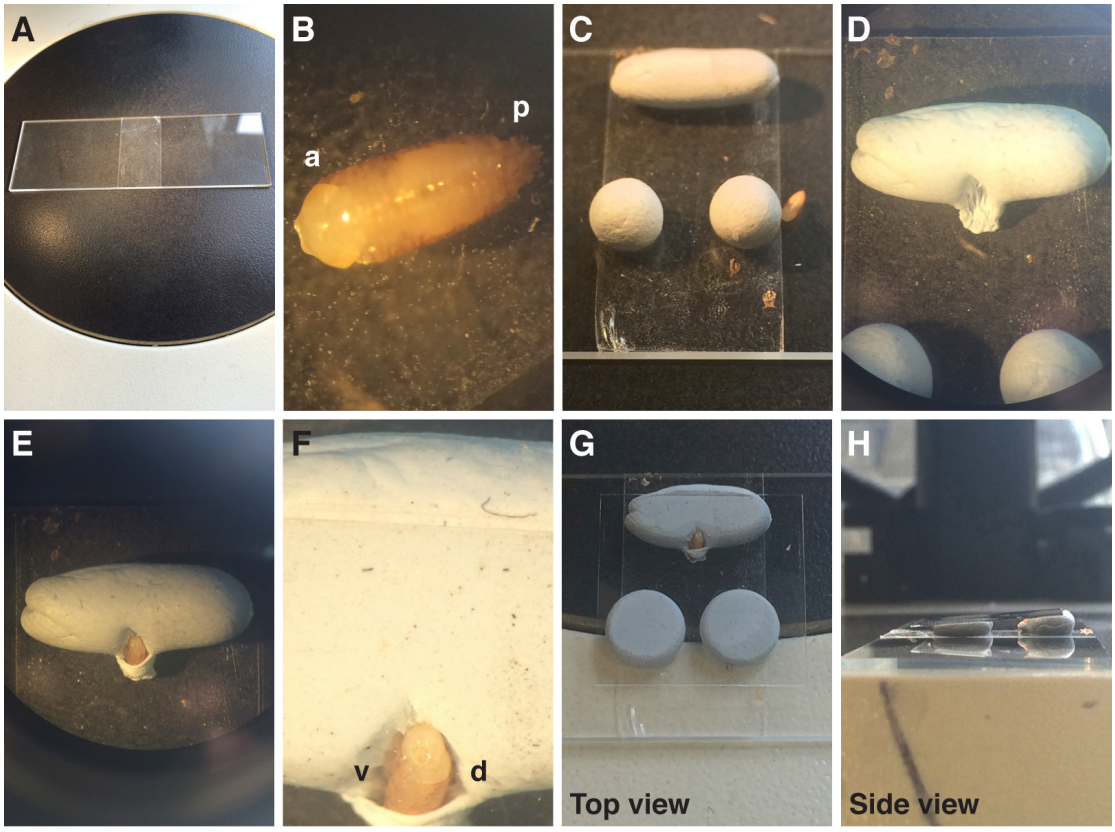

Figure 3.5: Sample preparation for FRAP. Sequence of steps performed to prepare 40 % APF pupae for FRAP. a: anterior, p: posterior, d: dorsal, v: ventral.

every 1.293 seconds with the previously mentioned settings for 200 frames.

3.9 Data analysis and Statistics

3.9.1 Western blot quantification

Western Blots were quantified using Fiji (Schindelin et al., 2012), while graphical representation and statistical analysis were performed in GraphPad Prism version 7.0 for Mac (GraphPad Software, San Diego California USA, www.graphpad.com). Columns represent mean, and error bars are the SEM of each dataset. The p values were calculated with a Kruskal Wallis test and corrected using Dunns multiple comparison test.

3.9.2 FRAP data analysis

When necessary, time series from FRAP were drift corrected in Fiji (Schindelin et al., 2012) using the the StackReg plugin. For each experiment three different z-axis profiles were plotted: (1) from the photo-bleached area, (2) from an equivalent area of a directly neighbouring non photo-bleached photoreceptor within the same ommatidium, and (3) from an equivalent area of background. The obtained data was normalized using easyFRAP (Rapsomaniki et al., 2012) and fitted to a one-phase or two-phase association curve in GraphPad Prism version 7.0 for Mac (GraphPad Software, San Diego California USA, www.graphpad.com) as appropriate. Each data point represents the mean and error bars the SEM. Half-time values were determined with Prism based on the fitting curves obtained and columns represent the mean and error bars the 95 % CI of each data set. Mobile fraction (*i.e.* y value at infinite times) was also determined with Prism and columns represent the mean and error bars the SEM of each data set. The p values were calculated with a two-way ANOVA test with Bonferonis correction or an unpaired two-tailed Student's t-test with Welch's correction, as appropriate.

3.9.3 Confocal data analysis

Confocal images were edited using Fiji (Schindelin et al., 2012) and Adobe Photoshop 7.0. All confocal images shown are representative images chosen from a pool of data containing stainings from more than three individuals.

Area and pixel intensity quantifications

All measurements were made in mosaic retina, where an ommatidium completely mutant for the indicated experimental condition was paired with an adjacent *wild-type* ommatidium. For quantifications in *exo84* mutant retinae it was not possible to obtain completely mutant ommatidia, therefore, all measurements were made in mutant photoreceptors from ommatidia at least 50 % mutant. For quantifications in $ralA^{EE1}$ whole mutant retinae, *Ubi Ecad::GFP* retinae stained and mounted together with the mutant retinae were used as a control. For area and intensity measurements, a threshold was applied to define the domain(s) of interest and then quantified using the wand (tracing) tool in Fiji (Schindelin et al., 2012). Statistical analysis was done using GraphPad Prism version 7.0 for Mac (GraphPad Software, San Diego California USA, www.graphpad.com). Data sets were tested for normality (DAgostino and Pearson normality test) and p-values were calculated using the students t-test or the Mann-Whitney test as appropriate.

Intensity profiles

The intensity profiles were measured in Fiji (Schindelin et al., 2012). For the follicle cells, a 2.6 µm line was drawn at the apical membrane, continued by another 2.6 µm segment along the lateral membrane and aligned so that the two segments align at the point of maximum intensity at the *ZA*. For each cell, pixel intensities were subjected to unity-based normalization and graphs were plotted in GraphPad Prism version 7.0 for Mac (GraphPad Software, San Diego California USA, www.graphpad.com).

3.9.4 Protein sequence alignment

Protein sequences were obtained from Flybase or UniProt and subsequently aligned using Clustal Omega (Sievers et al., 2011).

Chapter 4

Par6 regulation during epithelial morphogenesis

Par6 is thought of as a regulatory unit of aPKC, which in turn is the signalling component of the Par complex (Tepass, 2012). However, Par6 is known to bind multiple polarity determinants, in particular several components of the Par and Crb complexes, such as aPKC, Crb, Sdt, Cdc42 and Baz (Betschinger et al., 2003, Hutterer et al., 2004, Kempkens et al., 2006, Petronczki and Knoblich, 2001). This property of Par6 to bind multiple polarity proteins makes it an ideal candidate to coordinate the function of different polarity complexes during polarised morphogenesis. To understand the relative contribution of the different interactions with Par6 during polarised morphogenesis, we adopted a systematic approach and used a collection of transgenes that uncouple Par6 binding to the main polarity regulators Cdc42, Crb and aPKC.

4.1 Polarity protein network in two epithelial tissues

In this chapter, I examine the role of Par6 during epithelial morphogenesis in the follicular epithelium. This work has been complemented in the *Drosophila* pupal photoreceptor and further discussed in this chapter as courtesy of Dr. Rhian Walther. In this study, we used two complementary developing epithelia as there is evidence to suggest that different mechanisms operate during polarised morphogenesis in these two epithelial cell types (Shahab et al., 2015).

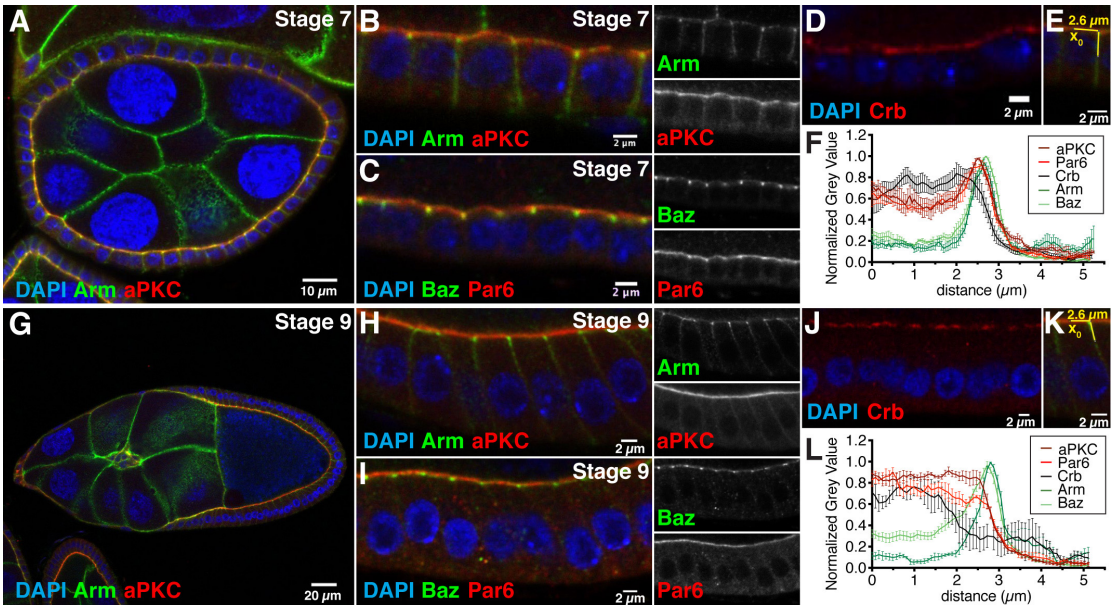

Figure 4.1: Polarity protein network in the follicular epithelium. (A-D) Stage 7 *wild-type* cuboidal FCs stained for DAPI (blue) and (A-B) Arm (green), aPKC (red), (C) Baz (green), Par6 (red), and (D) Crb (red). **(E)** Cuboidal FC where a 5.2 μm long yellow line shows the intensity values measured to plot the profiles in (F) from the apical (x_0) towards the lateral domain. **(F)** Intensity profiles of Arm, Baz, aPKC, Par6 and Crb at the cell cortex and plasma membrane from the apical domain towards the lateral domain in stage 7 FCs. Lines represent the mean value and error bars show the SEM (n = 4 for Par6/Baz, n = 5 for Crb and n = 6 for aPKC/Arm). **(G-J)** Stage 9 *wild-type* columnar FCs stained for DAPI (blue) and (G-H) Arm (green), aPKC (red), (I) Baz (green), Par6 (red), and (J) Crb (red). **(K)** Columnar FCs where a 5.2 μm long yellow line shows the intensity values measured to plot the profiles in (L) from the apical (x_0) to the lateral domain. Scale bars = 2 microns, except in (A) and (G), where scale bar = 10 microns and 20 microns, respectively. **(L)** Intensity profiles of Arm, Baz, aPKC, Par6 and Crb at the cell cortex and plasma membrane from the apical domain towards the lateral domain in stage 9 FCs. Lines represent the mean value and error bars show the SEM (n = 5 for Par6/Baz/Crb and n = 4 for aPKC/Arm).

I first examined the distribution of key polarity determinants in the FE. In this tissue, Crb, Par6 and aPKC were concentrated apical to the *ZA*, where Baz and Arm were found (Figure 4.1). Intensity profiles of Par6, aPKC, Crb, Arm and Baz were measured as in Figure 4.1E and K and then plotted together in the same graph (Figure 4.1F and L), to compare the distribution of these different proteins. This analysis showed that Crb, Par6 and aPKC are concentrated at the apical domain and further indicated that their levels sharply decrease within the *ZA* to reach near zero values at the basal boundary of the *ZA* (Figure 4.1F and L). We also noticed that Crb levels decreased more sharply at the apical-*ZA* boundary when compared to Par6-aPKC. These data suggest that mechanisms must exist to separate Crb, Par6 and aPKC from the *ZA*. This in turn is important for the maturation of both apical and *ZA* membrane domains.

4.2 Par6 is essential during epithelial morphogenesis

In order to examine the contribution of Par6 to epithelial morphogenesis and *ZA* specification and maturation, we assessed the requirement for Par6 to recruit the Par complex components Baz and aPKC, as well as Crb. We used the $par6^{\Delta 226}$ allele previously generated by the Knoblich lab by P-element imprecise excision, which led to the deletion of the start codon and first 121 amino acids, thus generating a null allele (Petronczki and Knoblich, 2001). Using the FLP-FRT system, I attempted to generate clones in the FE containing both *wild-type* and $par6^{\Delta 226}$ mutant cells. However, I was not able to recover such clones, presumably due the cell lethal nature of *par6*. As an alternative, we used the FLP-FRT system to generate clones in the fly retina. In this system, we observed that *par6* mutant cells lacked aPKC and Crb at the plasma membrane, but Baz and Arm domains were still present at the cell cortex (Figure 4.2). Notably, Crb staining showed punctate structures in the presumptive apical region of the *par6* mutant cells (Figure 4.2B). These results show that Baz and AJ material can be recruited at the cell cortex independently of Par6 and aPKC. They also confirm that Par6 is essential for Par complex assembly and subsequent partitioning of the plasma membrane into an apical pole and the *ZA*.

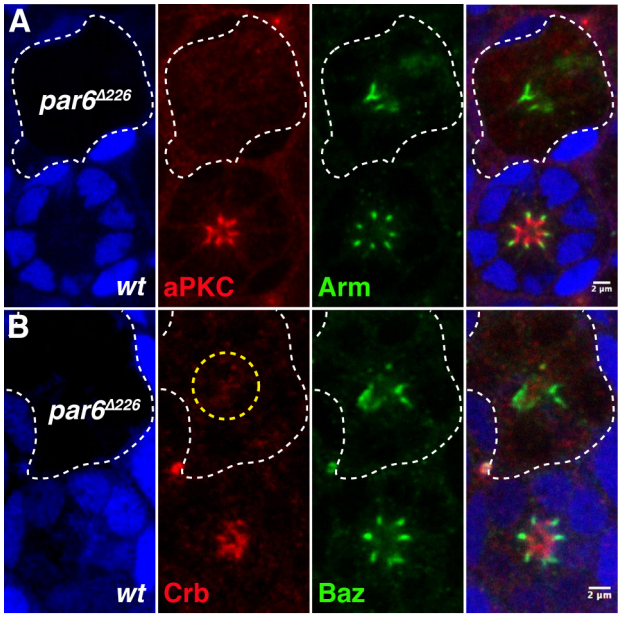

Figure 4.2: Par6 is essential for plasma membrane partitioning into different domains. *par6*$^{\Delta 226}$ mutant cells are labeled by loss of GFP (blue) and stained for **(A)** aPKC (red), Arm (green) and **(B)** Crb (red), Baz (green). A dashed yellow circle indicates punctate structures stained for Crb, in the presumptive apical region of the *par6* mutant cells. Scale bars = 2 microns. Images courtesy of Dr. Rhian Walther. Nunes de Almeida and Walther *et al.*, under revision.

To further understand the role of Par6 during epithelial morphogenesis, we used directed mutagenesis to disrupt Par6 interaction with specific binding partners (Table 4.1). Based on previous work in *C. elegans*, *Drosophila* and vertebrate cells, we cloned a series of *par6* transgenes that we predicted to uncouple Par6 binding to Cdc42, Crb and aPKC (Figure 4.3A and Table 4.1). To disrupt Par6 binding to Cdc42, we generated Par6$^{\Delta P139}$ (Par6$^{\Delta P}$) (Hutterer et al., 2004, Lin et al., 2000) and Par6^{S146E} (Par6^{SE}) (Jin et al., 2015). Recombinant GST-Cdc42 was purified from *E. coli* and used to pulldown both Par6 mutant proteins from S2 cell lysates, showing that both Par6$^{\Delta P}$ and Par6^{SE} were not able to bind to Cdc42 (Figure 4.3B). In addition, using the intracellular domain of Crb GST-tagged (GST-Crb^{intra}) purified from *E. coli* and endogenous aPKC from S2 cells, I could confirm that interrupting Par6 binding to Cdc42 did not interfere with the ability of Par6$^{\Delta P}$ and Par6^{SE} to bind to Crb or aPKC (Figure 4.3C-D). To disrupt Par6 binding to Crb, we generated Par6$^{KPLG170\text{-}173AAAA}$ (Par6^{AAAA}) (Joberty et al., 2000, Li et al., 2010, Peterson et al., 2004, Whitney et al., 2016), a protein that retained its ability to bind to Cdc42 and aPKC, but cannot bind to Crb (Figure 4.3B-D). Finally, to

Table 4.1: Par6 transgenes generated to individually uncouple Par6 binding aPKC, Crb and Cdc42.

Par6 mutation	**Predicted from**	**Uncouples binding to**	**Binds to**
K23A	Noda et al. (2003), Wirtz-Peitz et al. (2008)	aPKC	Crb, Cdc42, Baz
KPLG170-173AAAA	Hurd et al. (2003), Joberty et al. (2000), Li et al. (2010)	Crb	aPKC, Cdc42, Baz
S146E	This work	Cdc42	aPKC, Crb, Baz
Δ139P	Hutterer et al. (2004)	Cdc42	aPKC, Crb, Baz

uncouple Par6 from aPKC, we generated $Par6^{K23A}$ (Noda et al., 2003), in which Par6 binding to aPKC was abolished without affecting its binding to Cdc42 or Crb (Figure 4.3B-D). In addition, I controlled that all transgenes maintain their ability to bind Baz (Figure 4.3E). All transgenes were GFP-tagged at the C-terminus and placed under the control of a *par6* minimal promoter or a *UAS* sequence in order to generate transgenic animals.

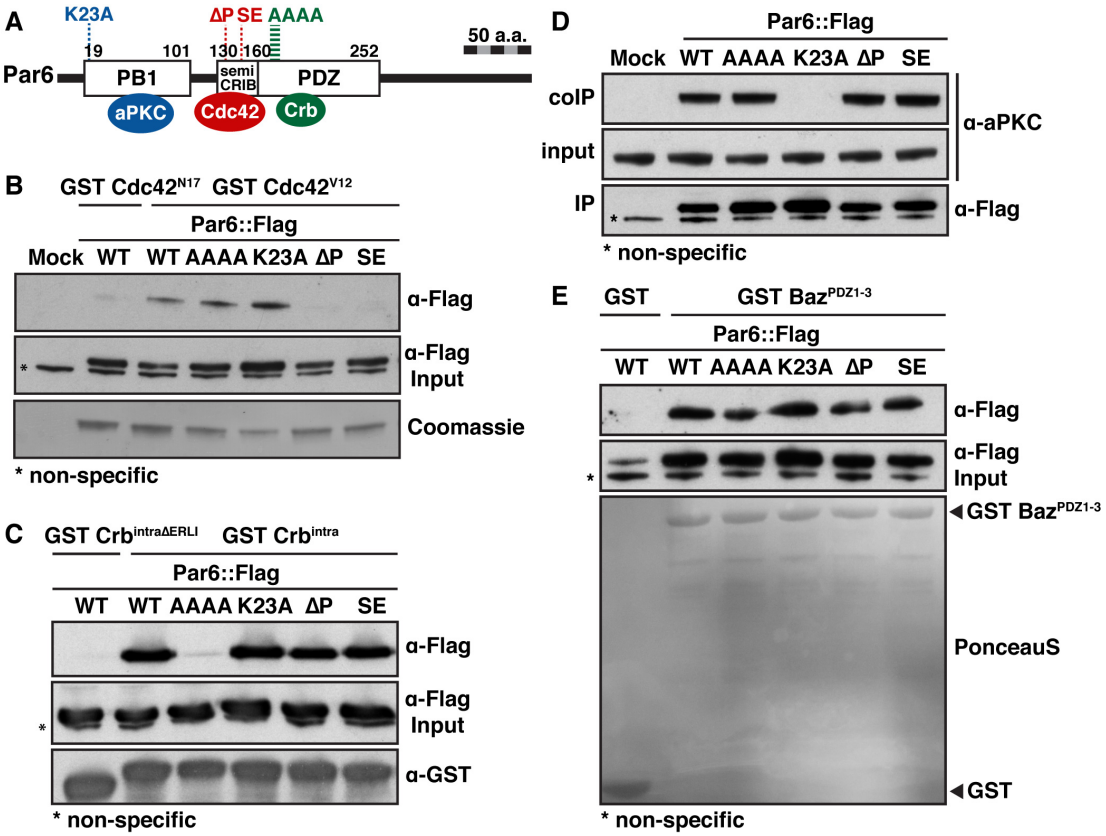

Figure 4.3: Interactions between Par6 transgenes and polarity determinants. (A) Schematic representation of Par6. Domains involved in direct protein-protein interactions with aPKC, Cdc42 and Crb are shown, as well as the mutagenised sites used to uncouple these interactions. **(B)** GST-pulldown between recombinant GST::Cdc42^{V12} and S2 cell extracts transfected with the various *par6::Flag* transgenes. Recombinant GST::Cdc42^{N17} was used as a control. **(C)** GST-pulldown between recombinant GST::Crb^{intra} and S2 cell extracts transfected with the various *par6::Flag* transgenes. Recombinant GST::Crb$^{intra\Delta ERLI}$ (Bachmann et al., 2001) was used as a control. **(D)** Endogenous aPKC was co-immunoprecipitated from S2 cells transfected with the various *par6::Flag* transgenes. **(E)** GST-pulldown between recombinant GST::Baz^{PDZ1-3} and S2 cell extracts transfected with the various *par6::Flag* transgenes. GST alone was used as a control. In (B) and (D), mock corresponds to samples transfected with empty Flag vector, to show the non-specific band below Par6::Flag (marked with an asterisk in B-E). n = 2 for B, D and E, n = 3 for C.

4.3 aPKC regulates the apical localisation and stability of Par6

Western blotting from *in vivo* extracts showed that all fusion proteins, except Par6^{K23A}, were stably expressed *in vivo* in the presence of endogenous Par6 (Figure 4.4). Because Par6^{K23A} was stably expressed in S2 cells (Figure 4.3), these *in vivo* experiments suggest that, during epithelial morphogenesis, binding to aPKC is required to stabilise Par6. Alternatively, the K23A mutation might lead to an unstable Par6 protein *in vivo*.

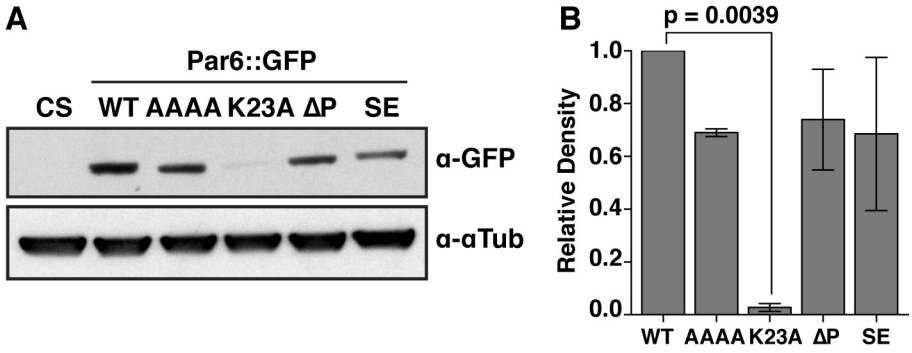

Figure 4.4: Expression of the *par6* transgenes *in vivo*. **(A)** Western blot of protein extracts from adult heads of animals expressing the various *par6-Par6::GFP* transgenes, probed with anti-GFP and quantified in **(B)**. *Wild-type Canton S* (CS) flies were used as a control. Bars represent mean and error bars represent the SEM from 3 independent experiments.

My biochemical results on Par6^{K23A} suggest that aPKC regulates the levels of Par6 during epithelial morphogenesis. To test this suggestion, we examined the expression of *par6-Par6^{K23A}::GFP in vivo*. As expected from our biochemical evidence (Figure 4.4), Par6^{K23A}::GFP failed to rescue the *par6$^{\Delta 226}$* phenotype (data not shown), as it was not recruited at the cortex, even when expressed in otherwise *wild-type* cells (Figure 4.5A-B). In addition, overexpressing Par6^{K23A} with the *GAL4-UAS* system did not lead to any noticeable gain-of-function phenotype (Figure 4.5C-D).

To complement this analysis, we made use of the *aPKC^{psu69}* allele, which encodes a version of aPKC that does not bind to Par6 (Kim et al., 2009). In *aPKC^{psu69}* mutant cells, aPKC was not detected at the membrane (Figure 4.6A-B), and Par6 levels were decreased (Figure 4.6C-D). In addition, most residual Par6 was found at the *ZA* instead of the apical cortex (Figure 4.6C), indicating that Par6 binding to aPKC is required to promote its apical localisation during epithelial morphogenesis. However, we noticed

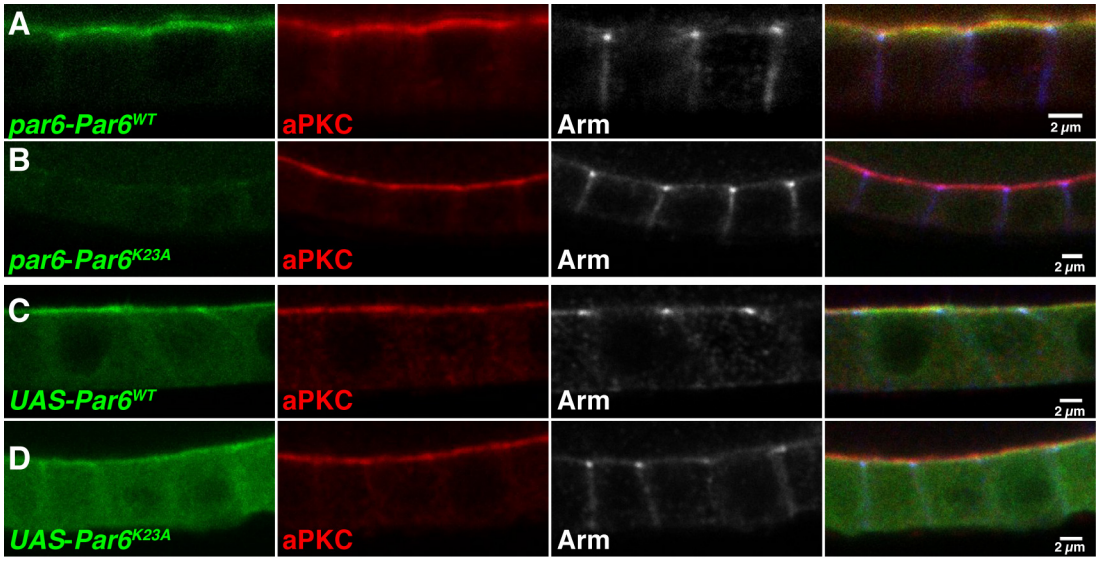

Figure 4.5: aPKC binding is essential for Par6 apical accumulation. **(A)** *par6-Par6^{WT}::GFP* (green), **(B)** *par6-Par6^{K23A}::GFP* (green), **(C)** *UAS-Par6^{WT}::GFP* (green) and **(D)** *UAS-Par6^{K23A}::GFP* (green) expressed in otherwise *wild-type* FCs and stained for aPKC (red) and Arm (grey; blue in the merged channel). Scale bars = 2 microns.

that even though aPKC seemed to be absent from *aPKC^{psu69}* mutant photoreceptors, the observed phenotype was quite mild, presenting an almost *wild-type* localisation of apically excluded Baz (Figure 4.6C). Because junctional Baz requires its phosphorylation and consequent apical exclusion, we asked whether P-Baz was detected in *aPKC^{psu69}* mutant cells. This was indeed the case, as not only P-Baz could be detected in these cells, but also Crb at the apical domain, albeit at presumably lower levels (Figure 4.6E-F). The accumulation of P-Baz and Crb is thought to be dependent on the kinase activity of aPKC (Morais-de Sá et al., 2010, Sotillos et al., 2004, Walther and Pichaud, 2010). Therefore, our result suggests that, although aPKC cannot be detected in our stainings of *aPKC^{psu69}* mutant photoreceptors, there might be a basal level of this kinase that is sufficient to phosphorylate its downstream targets. Alternatively, these data might suggest that a second kinase could phosphorylate these proteins in a semi-redundant pathway to aPKC.

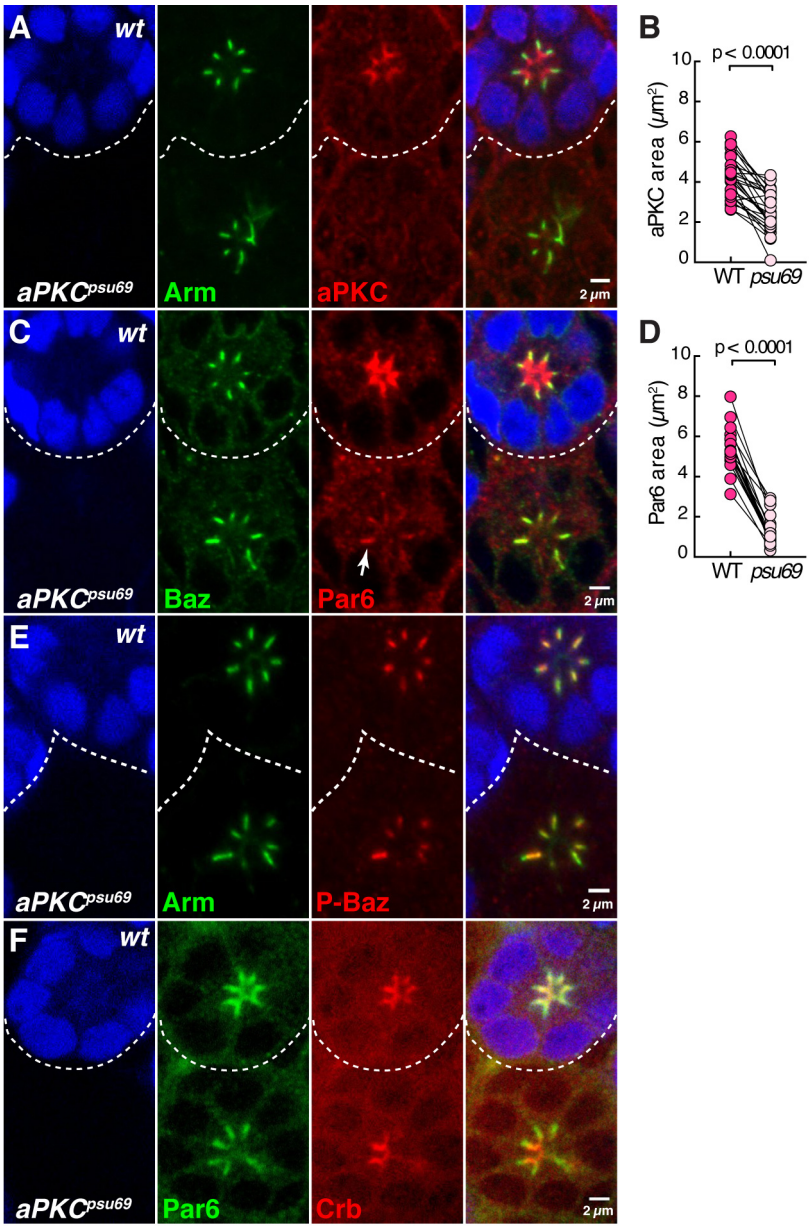

Figure 4.6: aPKC binding promotes Par6 apical localisation. (A) *aPKC*^{psu69} mutant photoreceptors lacking nuclear GFP (blue) signal and stained for Arm (green) and aPKC (red). **(B)** Quantification of aPKC area. **(C)** *aPKC*^{psu69} mutant photoreceptors lacking nuclear GFP (blue) signal and stained for Baz (green) and Par6 (red). Note residual Par6 staining localises predominantly at the *ZA* (white arrow). **(D)** Quantification of Par6 area. For each quantification, at least 17 ommatidia pairs were analyzed from 3 retinas. **(E-F)** *aPKC*^{psu69} mutant photoreceptors lacking nuclear GFP (blue) signal and stained for (E) Arm (green), phospho-Baz (red) and (F) Par6 (green), Crb (red). Scale bars = 2 microns. Images courtesy of Dr. Rhian Walther. Nunes de Almeida and Walther *et al.*, under revision.

4.4 Binding to Cdc42 regulates Par6 apical recruitment and localisation

Cdc42 is a key regulator of the Par complex through Par6. To better understand how Par6 binding to Cdc42 regulates Par complex assembly and overall epithelial morphogenesis, we made use of both *Par6$^{\Delta P}$::GFP* and *Par6^{SE}::GFP* transgenes. I first expressed Par6$^{\Delta P}$::GFP and Par6^{SE}::GFP under the control of the *par6* minimal promoter in otherwise *wild-type* cells. As a control, I expressed *wild-type* Par6::GFP under the control of the *par6* minimal promoter. I observed that Par6::GFP localised as endogenous Par6, concentrated at the apical membrane (Figure 4.7A, D, F). In contrast, both Par6$^{\Delta P}$::GFP and Par6^{SE}::GFP were found at the *ZA* (Figure 4.7B-C, E, G-H). Importantly, I found that failure of Par6$^{\Delta P}$::GFP and Par6^{SE}::GFP to accumulate at the apical membrane occurred even though Crb was present at this membrane domain (Figure 4.7F-H). Similar results were obtained in the pupal photoreceptor (Nunes de Ameida and Walther *et al.*, under revision). From these experiments, we conclude that Par6 binding to Cdc42 is required for the recruitment and accumulation of Par6 at the apical membrane.

While expressing Par6$^{\Delta P}$::GFP and Par6^{SE}::GFP under the *par6* minimal promoter did not lead to any notable gain-of-function phenotype in photoreceptors and FCs, expressing high levels of these proteins using the *GAL4-UAS* system led to severe polarity defects. In FCs, I found that Par6^{SE}::GFP overexpression led to the formation of gaps in the FE, with consequent exposure of the underlying nurse cells (Figure 4.8A-C). In addition, while Par6::GFP localised to the apical domain, overexpressed Par6^{SE}::GFP was found at the *ZA* together with Arm (Figure 4.8A-C). In these experiments, Par6^{SE}::GFP outcompetes endogenous Par6, thus leading to a gain-of-function phenotype. Altogether, our results support the notion that Par6 binding to Cdc42 is a mandatory step in the separation of the apical and *ZA* domains during epithelial cell morphogenesis.

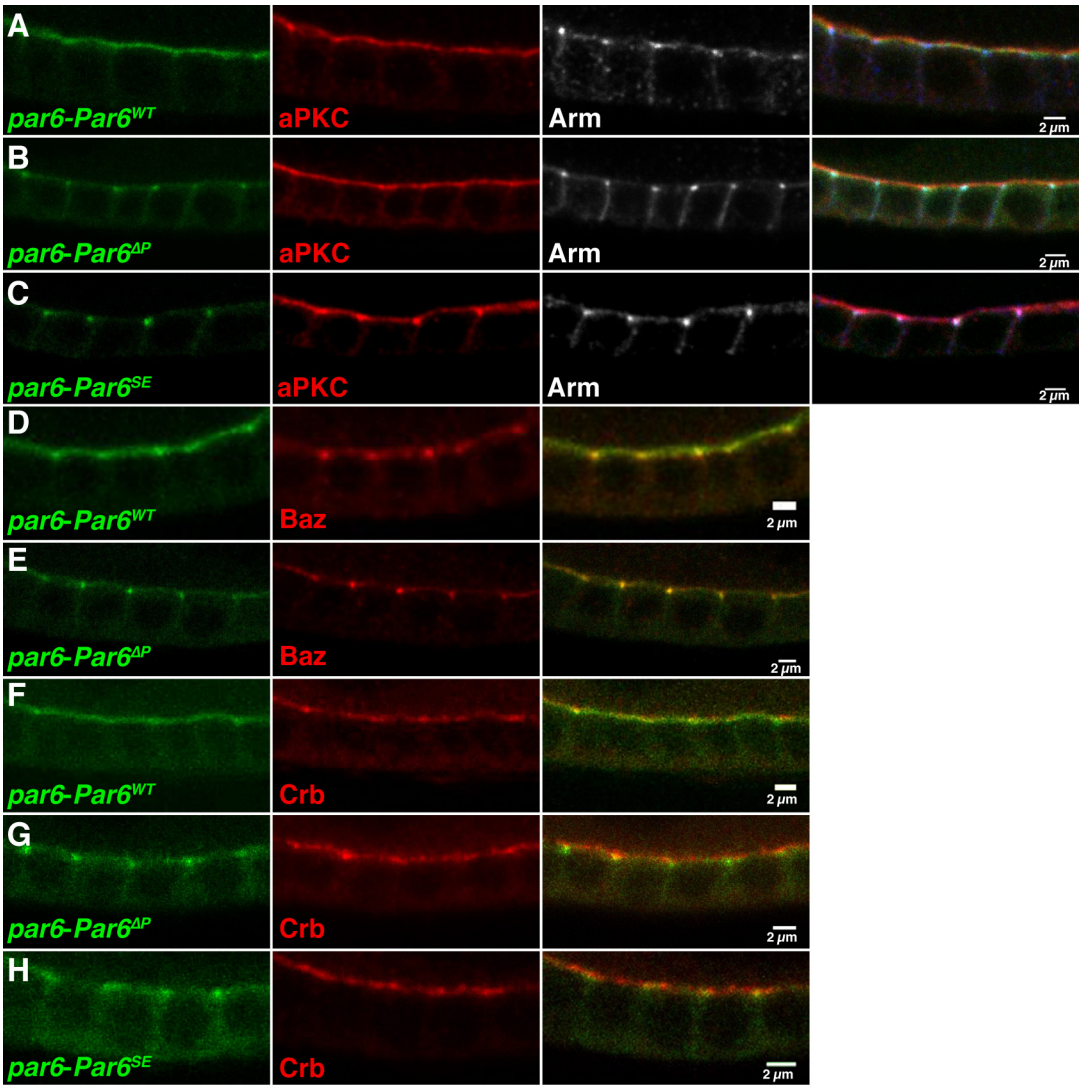

Figure 4.7: Par6 binding to Cdc42 is required for the apical localisation of Par6-aPKC. (A-C) *Wild-type* FCs expressing (A) *par6-Par6::GFP* (green), (B) *par6-Par6*$^{\Delta P}$*::GFP* (green), or (C) *par6-Par6*^{SE}*::GFP* (green), and stained for aPKC (red) and Arm (grey). **(D-E)** *wild-type* FCs expressing (D) *par6-Par6::GFP* (green) or (E) *par6-Par6*$^{\Delta P}$*::GFP* (green) and stained for Baz (red). **(F-H)** *wild-type* FCs expressing (D) *par6-Par6::GFP* (green), (E) *par6-Par6*$^{\Delta P}$*::GFP* (green), or (F) *par6-Par6*^{SE}*::GFP* (green), and stained for Crb (red). In all panels, the grey channel is shown in blue in the merge. Scale bars = 2 microns.

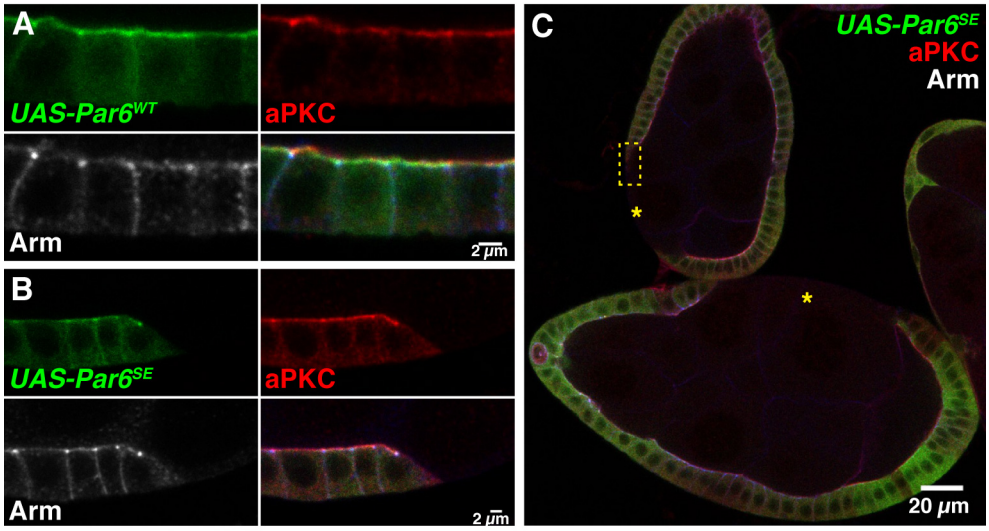

Figure 4.8: Par6^{SE}::GFP overexpression leads to severe polarity defects. *Wild-type* FCs expressing **(A)** *UAS-Par6::GFP* and **(B-C)** *UAS-Par6^{SE}::GFP*, stained for aPKC (red) and Arm (grey, blue in th merged channel). (B) is a zoomed imaged of the yellow dashed rectangle in (C). Yellow asterisks show gaps in FE. Scale bars = 2 microns in (A-B), 20 microns in (C).

4.5 Crb mediates Cdc42-dependent apical retention of Par6-aPKC

To probe the relationship between Crb and Par6, we re-examined *crb* mutant cells in the pupal photoreceptor. According to previous work in our lab (Walther and Pichaud, 2010), in *crb* mutant cells, Baz and Arm overlap with aPKC, thus leading to the formation of domains where the Par complex co-localises with Arm. These findings support the idea that exclusion of P-S980Baz from the Par complex is achieved through aPKC phosphorylation of Baz and through Crb (Morais-de Sá et al., 2010, Walther and Pichaud, 2010). However, we noticed that in the absence of Crb, a reproducible fraction of Par6-aPKC was separated from Baz (Walther and Pichaud (2010) and Appendix B Figure 7.2A-B, Nunes de Almeida and Walther *et al.*, under revision.), suggesting that Par6-aPKC can segregate from P-S980Baz in the absence of Crb and that this apical Par6-aPKC fraction might consist of the ternary Cdc42-Par6-aPKC complex. Quantification of Par6-aPKC levels in *crb* mutant photoreceptors indicates that Crb is required for their apical accumulation (Appendix B Figure 7.2E-F, Nunes de Almeida and Walther *et al.*, under revision.).

Next, to assess the contribution of Par6 binding to Crb in Par6-aPKC localisation, we used the *par6-Par6^{AAAA}::GFP* transgene, which uncouples Par6 binding to Crb. Rescue experiments performed in the fly retina showed that Par6^{AAAA}::GFP cannot support the accumulation of Par6, aPKC and Crb at the apical domain to *wild-type* levels (Appendix B Figure 7.3, Nunes de Almeida and Walther *et al.*, under revision.). This suggests that Par6 binding to Crb is required for the accumulation of Par6-aPKC at the apical membrane. In addition, when expressed in FCs, I observed a displacement of Par6^{AAAA}::GFP signal along the lateral membrane (Figure 4.9A-D). This was quantified in intensity profiles, showing that Par6::GFP signal reaches near zero values at the

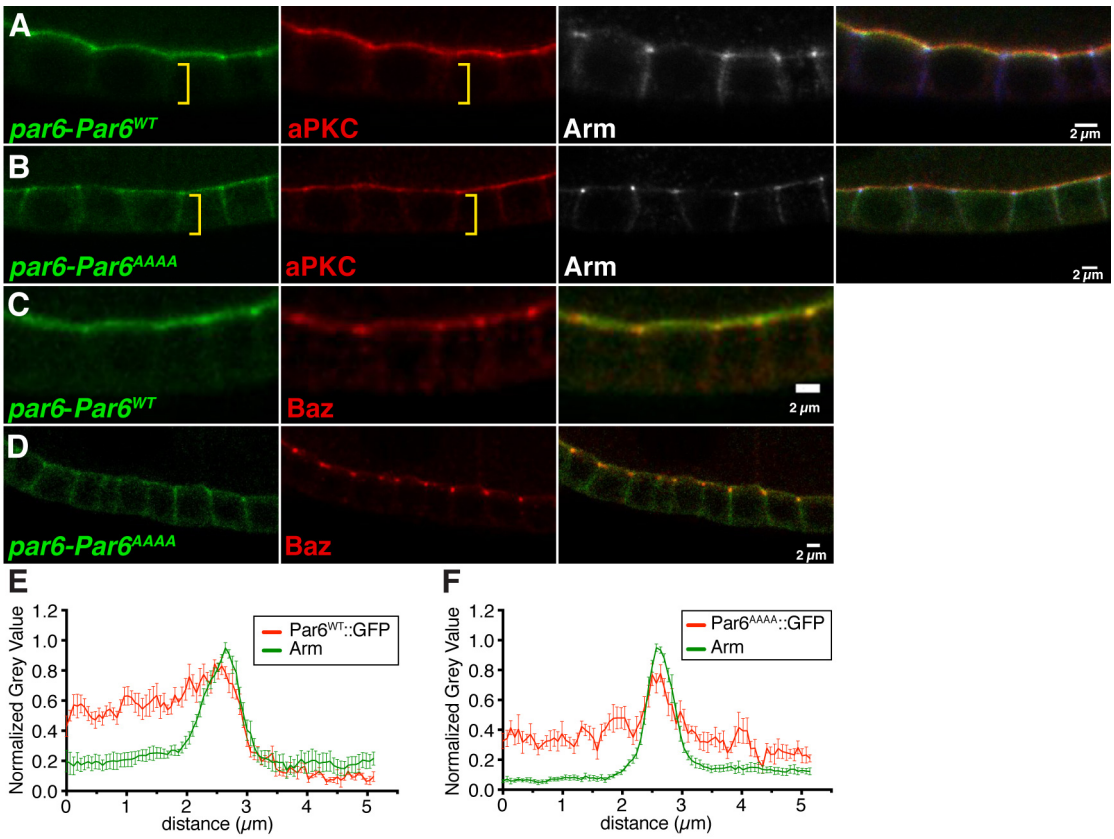

Figure 4.9: Crb promotes the apical retention of Par6-aPKC. (A-B) *Wild-type* FCs expressing (A) *par6-Par6::GFP* (green) or (B) *par6-Par6^{AAAA}::GFP* (green) and stained for aPKC (red) and Arm (grey; blue in the merged channel). **(C-D)** *Wild-type* FCs expressing (C) *par6-Par6::GFP* (green) or (D) *par6-Par6^{AAAA}::GFP* (green) and stained for Baz (red). Scale bar = 2 microns. **(E-F)** Intensity profiles of Arm and Par6 at the cell cortex and plasma membrane from the apical domain towards the lateral domain of *wild-type* FCs expressing (E) *par6-Par6::GFP* or (F) *par6-Par6^{AAAA}::GFP*. Lines represent the mean value and error bars show the SEM (n = 6 and n = 9, receptively).

lateral membrane, contrary to Par6^{AAAA}::GFP (Figure 4.9E-F). These results indicate that the contribution of Par6 binding to Crb is to promote the apical retention and accumulation of Cdc42-Par6-aPKC at the developing apical membrane.

Overexpression of Par6^{AAAA}::GFP using the *GAL4-UAS* system did not show any morphological defects (Figure 4.10). However, the apical accumulation of Par6^{AAAA}::GFP and endogenous aPKC was impaired, with these proteins showing a more diffused and cytosolic distribution within FCs (Figure 4.10). Together, these results support a model where Par6 binding to Crb is necessary for the apical retention and accumulation of Par6-aPKC at the apical membrane.

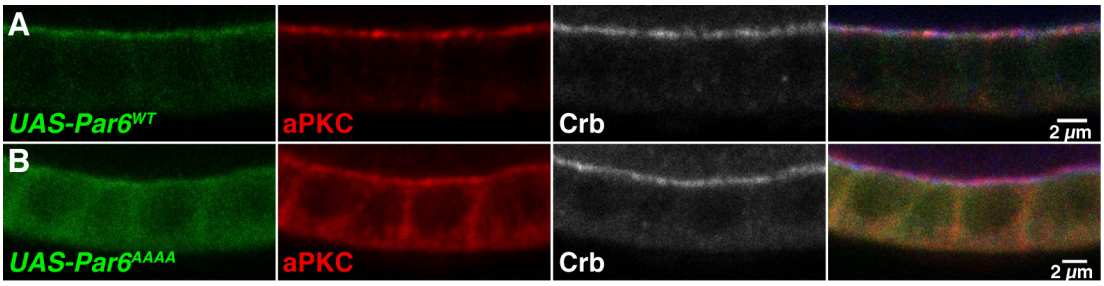

Figure 4.10: Par6 binding to Crb is required for the accumulation of Par6-aPKC at the apical cortex. *Wild-type* FCs expressing **(A)** *UAS-Par6::GFP* (green) or **(B)** *UAS-Par6^{AAAA}::GFP* (green) and stained for aPKC (red) and Crb (grey; blue in the merged channel). Scale bar = 2 microns.

4.6 Crb stabilizes Par6 at the apical membrane

Our results indicate that, upon Par complex assembly, differentiation of the *ZA* from the apical membrane is driven by the apical retention of Par6-aPKC. We also find that Crb mediates this retention and accumulation of Par6-aPKC presumably by anchoring these proteins to the plasma membrane. To test this hypothesis, we used FRAP to assess the turnover of Par6::GFP and Par6^{AAAA}::GFP. FRAP experiments showed that Par6^{AAAA}::GFP recovered twice as fast as Par6::GFP after photobleaching (Figure 4.11). Using double exponential fitting, we estimated that the half-time recovery of the fast-phase was not significantly different between Par6::GFP and Par6^{AAAA}::GFP (Figure 4.11B). However, this was not the case for the slow-phase of the half-time of recovery (Figure 4.11B). Our FRAP data are therefore consistent with a model in which there are

at least two Par6 pools: one that recovers or exchanges quickly with the cytosol (Par6 not associated with Crb) and another that recovers more slowly (Par6 associated with Crb). Altogether, this part of our work suggests that Crb promotes apical retention of Par6 by slowing down its rate of diffusion at the cortex or decreasing its exchange rate with the cytosol. In turn, this allows for Par6-aPKC and P-Baz to segregate from each other.

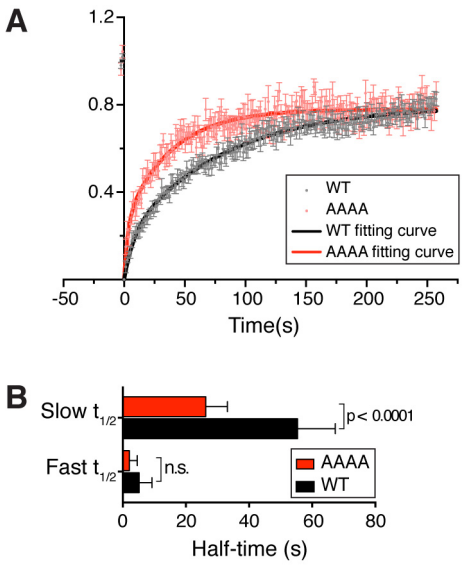

Figure 4.11: Par6 binding to Crb slows down the recovery of Par6 after photobleaching. FRAP on photoreceptors overexpressing Par6::GFP and Par6^{AAAA}::GFP using the *GAL4-UAS* system. **(A)** Graph shows mean normalized fluorescence intensity for Par6::GFP (grey, n = 14 from 3 individuals) and Par6^{AAAA}::GFP (red, n = 16 from 3 individuals); error bars represent SEM. Fluorescence recovery curves of Par6::GFP were calculated using a double exponential fit of the FRAP data. **(B)** Slow and fast half-time recovery of Par6::GFP (black) and Par6^{AAAA}::GFP (red). Images courtesy of Dr. Rhian Walther. Nunes de Almeida and Walther *et al.*, under revision.

4.7 Discussion

The Par complex (Cdc42-Par6-aPKC-Baz) is one of the main regulators of epithelial cell polarity. Yet, the exact function of each of its components during epithelial cell polarisation is not fully understood. Within the Par complex, the kinase aPKC is the

signalling component; however, further work is required to understand how its activity and localisation are regulated. A common feature in various cell types is the requirement for Baz/Par3, Par6 and Cdc42 in the cortical localisation of aPKC (Walther and Pichaud, 2010). Previous work in the *Drosophila* pupal photoreceptor suggests that, within the Par complex, Baz sits upstream of the remaining components to recruit the Par complex to the cell cortex (Walther and Pichaud (2010) and Figure 4.2). However, this does not seem to be the case in the FE, where Baz actually seems to be dispensable (Shahab et al., 2015). Also, we observed that *par6* mutants appear to have a stronger effect in the FE compared to the retina. As a consequence of at least these two differences between the fly retina and FE, we acknowledged that distinct tissues might have different regulatory mechanism during polarity establishment and maintenance. Therefore, all experiments performed in the FE in this chapter have been complemented in the fly retina. In addition, rescue experiments have been performed only in the fly retina, as a consequence of our limitation in obtaining *par6* mutant FCs.

In the fly retina, in the absence of *baz* function, Par6 is strongly decreased but not abolished, presumably due to Crb ability to recruit Par6-aPKC independently of Baz (Walther et al., 2016). Our work shows that Cdc42 is essential during epithelial polarisation of photoreceptors and FCs to segregate Baz from Par6-aPKC and promote Par6-aPKC accumulation at the apical membrane. Accordingly, when Cdc42 is uncoupled from Par6, Par6-aPKC localise at the *ZA*, presumably with Baz. This has been further demonstrated in our lab, as in *par6* mutant photoreceptors, Par6$^{\Delta P}$::GFP colocalises with Baz; however, no Par6$^{\Delta P}$::GFP or aPKC are detected when expressed in a *baz* mutant background (*i.e.* when we uncouple both Baz and Cdc42 interfaces) (Appendix B, Figure 7.1, Nunes de Almeida and Walther *et al.*, under revision). Altogether, we suggest that Cdc42, Baz and Crb synergize in recruiting Par6-aPKC to the apical domain of epithelial cells.

All interdependent modes of recruitment of Par6-aPKC are required for the correct assembly and function of the Par complex. In *wild-type* cells, the quaternary complex (Cdc42-Par6-aPKC-Baz) assembles transiently. Our results support a model whereby Baz/Par3 oligomerises to form large domains of Par complex and possibly amplifying the recruitment of the Par complex to the cortex. In addition, the presence of Baz/Par3 in this complex inhibits the activity of aPKC (Graybill et al., 2012), preventing phos-

phorylation of other substrates. A similar mode of operation has been observed in the *C. elegans* zygote, where PAR-6/PKC-3 cycle between an inactive PAR-3-associated complex and an active CDC-42-bound complex (Rodriguez et al., 2017). Segregation of Baz/Par3 from Cdc42-Par6-aPKC is essential for both apical membrane and *ZA* morphogenesis and requires Baz phosphorylation by aPKC (Morais-de Sá et al., 2010, Walther and Pichaud, 2010). Our data show that Cdc42 is required to maintain the apical localisation of Par6-aPKC and prevent their re-localisation at the *ZA* together with Baz (Figure 4.12A).

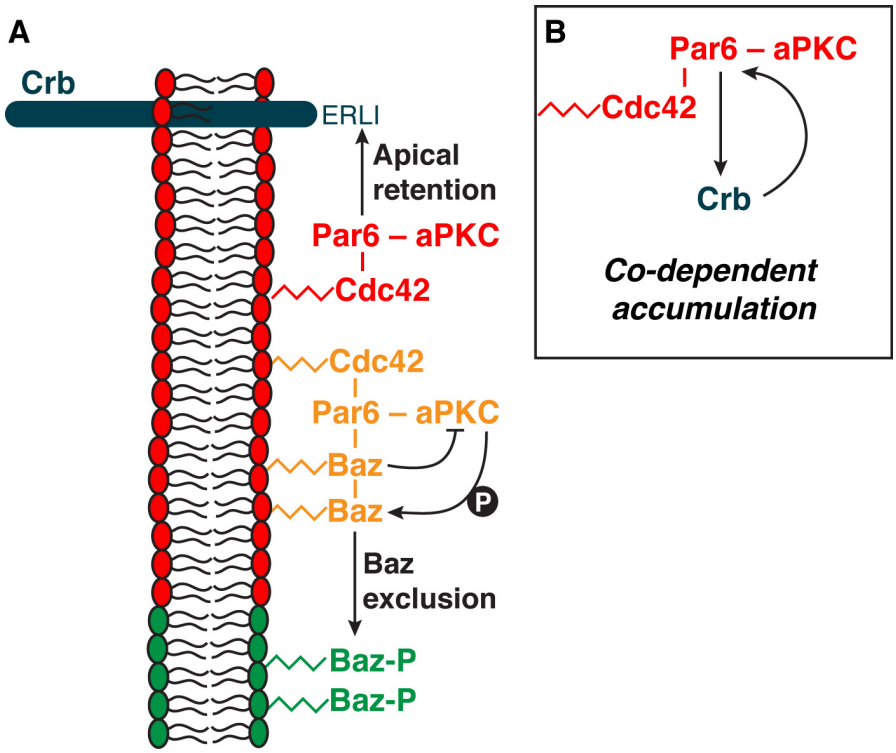

Figure 4.12: Par6 regulates apical membrane and *ZA* morphogenesis. (A) Baz and Cdc42 recruit Par6-aPKC to the apical cortex, forming the quaternary Par complex (orange). This quaternary complex is inactive, as Baz inhibits aPKC activity. *ZA* morphogenesis requires Baz apical exclusion, which is triggered by aPKC phosphorylation of Baz. Upon Baz phosphorylation, this protein localises to the developing *ZA* (green), while Par6-aPKC remain at the apical domain as a consequence of Cdc42 action. In this ternary complex, the kinase aPKC is relieved from Baz inhibition and is in its active state (red). Crb (dark blue) binds Par6, which retains Par6-aPKC at the apical pole of the cell and contributes to the establishment of sharp apical and basal boundaries between the *ZA* and the apical and lateral domains, respectively. **(B)** Crb binds Par6, which contributes to the accumulation and retention of Par6-aPKC at the apical pole. In turn, Par6-aPKC are essential to maintain elevated levels of Crb. This creates a co-dependence in the accumulation of these proteins.

Current knowledge in the field of epithelial cell polarity suggests that Crb is required, together with aPKC-dependent phosphorylation of Baz/Par3, to apically exclude Baz/Par3 and separate the quaternary Par complex (Morais-de Sá et al., 2010, Walther and Pichaud, 2010). However, two striking observations contradict this model. Firstly, we detect a pool of Par6-aPKC that separates from Baz-Arm in photoreceptors lacking *crb* function, indicating that Par6-aPKC can segregate from Baz in the absence of Crb. Secondly, when Par6 is uncoupled from Cdc42 in both photoreceptors and FCs, it localises at the *ZA*, even in the presence of Crb. Altogether, we propose a model whereby, upon aPKC-dependent Baz apical exclusion, Cdc42 initially maintains the ternary Cdc42-Par6-aPKC complex at the apical domain (Figure 4.12A). We suggest this is the Par6-aPKC pool detected in *crb* mutant photoreceptors that segregates from Baz.

Our *in vivo* data suggest that the interaction between Par6 and Crb is regulated by Cdc42. However, this is not what we observe *in vitro*. In fact, the pulldown experiments show similar binding to Crb when $Par6^{\Delta P}$/$Par6^{SE}$ are compared to *wild-type* Par6. It is possible that Cdc42 facilitates the interaction between Par6 and Crb *in vivo*, although no differential binding is observed in *in vitro*. However, further experiments are required to confirm if such mechanism operates in epithelial cells. Alternatively, Par6 could have a higher binding affinity to Crb, when compared to Cdc42. In this second model, Cdc42 would act as an initial recruitment mechanism to localise Par6-aPKC at the apical domain, preventing the accumulation of Par6-aPKC at the *ZA* with Baz, and concurrently positioning Par6-aPKC at the same subcellular localisation as Crb, to allow their interaction.

Cdc42 contains a conserved C-terminal CAAX box, which is subjected to a post-translational covalent modification called prenylation that allows the association of Cdc42 with the plasma membrane (Ziman et al., 1993). In Cdc42, this CAAX box is formed by the amino acids Cys-Xaa-Xaa-Leu, where Xaa consists usually of an aliphatic amino acid (Ziman et al., 1993). Protein prenylation is thought to direct the localisation of the modified protein to a specific membrane location in the cell (Cox and Der, 1992). Therefore, Cdc42 could function as a localisation mechanism, to direct Par6-aPKC to the apical domain of epithelial cells. However, our data suggest that this might not be sufficient to maintain Par6-aPKC strictly at the apical domain, as upon uncoupling the

Par6-Crb interaction, Par6 is still able to bind Cdc42 while showing a lateral spreading in both photoreceptors and FCs. Our data suggest that Crb regulates an additional retention mechanism that maintains Par6-aPKC at the apical domain of epithelial cells (Figure 4.12A).

Crb-dependent retention of Par6-aPKC seems to play an important function setting up a clear boundary between the *ZA* and the apical or basolateral domains. Additional data from our lab shows that in *crb* mutant photoreceptors, both the apical and basal boundaries of the *ZA* are displaced apically and basally, respectively (Appendix B, Figure 7.2C, Nunes de Almeida and Walther *et al.*, under revision). The lateral kinase Par1 defines the basal boundary of the *ZA* by phosphorylating Baz and displacing it form the lateral membrane (Benton and Johnston, 2003b, Walther et al., 2016). As Par1 is a substrate of aPKC, we propose that the lateral spreading of Par6-aPKC in *crb* mutant photoreceptors inhibits Par1 cortical localisation and promotes the basal expansion of the *ZA*. As a consequence, our data suggest that Crb regulates *ZA* morphogenesis, in addition to its established function during apical membrane morphogenesis.

Additional experiments performed in our lab show that the interaction between Par6 and Crb is required not only for the retention of Par6-aPKC at the apical domain, but also for their accumulation, which is demonstrated by quantifications of Par6-aPKC levels in *crb* mutant photoreceptors and in *par6* mutant rescue experiments with $Par6^{AAAA}$::GFP (Appendix B, Figures 7.2E-F and 7.3A-C, Nunes de Almeida and Walther *et al.*, under revision). Furthermore, our quantifications in $Par6^{AAAA}$::GFP rescue experiments show evidence that the interaction between Par6 and Crb is required to maintain high levels of Crb itself (Appendix B, Figure 7.3D, Nunes de Almeida and Walther *et al.*, under revision). This establishes a co-dependence in the accumulation of both Crb and Par6-aPKC, in which Crb retains Par6-aPKC, while in turn, Par6-aPKC sustain the levels of Crb at the apical pole of the cell (Figure 4.12B). Previous published work suggests that aPKC phosphorylates the cytoplasmic tail of Crb, which is required to maintain Crb at the plasma membrane (Sotillos et al., 2004), possibly explaining why Crb accumulation depends on Par6-aPKC. In addition, the Par complex could control Crb levels by regulating its delivery. Very little is known about Crb delivery or possible links between the Par complex and Crb delivery, and this is a topic I will be addressing in the next chapter.

Lastly, we also investigated the interface between Par6 and aPKC. Our results suggest that this interface is required to sustain the levels of both Par6 and aPKC at the apical domain. Interestingly, we observe that when we disrupt the Par6-aPKC interface using the $aPKC^{psu69}$ allele, even though aPKC is not detected, Baz is still apically excluded. This is very surprising, as the apical exclusion of Baz requires its phosphorylation by aPKC. In fact, although aPKC cannot be detected in the absence of the interface between Par6 and aPKC, we were still able to detect P-Baz and Crb. One possible explanation is that the $aPKC^{psu69}$ allele does not completely prevent binding of Par6 to aPKC. Alternatively, aPKC might be present in the cytosol at very low levels, with an on-off rate that could be sufficient to phosphorylate some of its targets. A third possibility includes the role of a second kinase that could function semi-redundantly to aPKC. An important information from these experiments on Par6 and aPKC is the fact that aPKC might be only required at very low levels to perform its function, phosphorylate its targets and support the formation of distinct apical and *ZA* domains. Another surprising observation is the localisation of Par6 at the *ZA* together with Baz, when Par6 binding to aPKC is abolished. This is an unexpected result, as Par6 should still maintain its binding to Cdc42 and therefore, should be maintained at the apical domain upon Baz apical exclusion. Moreover, as we detect Crb in the apical domain of $aPKC^{psu69}$ mutant cells, Par6 should also be retained apically via binding to Crb. Altogether, our results indicate that binding of Par6 to both aPKC and Cdc42 is required for Par6 apical localisation mediated by Crb. Further studies will be required to understand in more detail why Par6 localises mostly to the *ZA* in the absence of its interface with the kinase aPKC.

Our work addresses the individual contribution of Par6, aPKC, Cdc42 and Crb during epithelial morphogenesis. We propose that the small adaptor protein Par6 plays an essential role in linking different components of the Par and Crb complexes. As we have demonstrated, this regulates the levels, localisation, and as shown by others, the activity of the active signalling component of the Par complex, the kinase aPKC. Importantly, we have validated these results in two complementary epithelial tissues, the *Drosophila* retina and FE, suggesting that these are common regulatory mechanisms among epithelial tissues.

Chapter 5

The Par complex regulates Crb delivery via the exocyst

Crb is required to support the apical retention of Par6-aPKC, while Par6-aPKC in turn promote Crb accumulation at the apical plasma membrane. However, how exactly Par6-aPKC promote Crb accumulation is not fully understood. Previous work in vertebrate cells has shown that Par6 binds to the exocyst subunit Exo84 (Das et al., 2014). In addition, in the fly embryo, *exo84* mutant cells present defects in Crb localisation (Blankenship et al., 2007). Therefore, one possibility is that Par6 binding to Exo84 might promote Crb delivery. A recent genetic screen performed in our lab aiming at identifying novel genes involved in epithelial cell polarity, identified that both *exo84* and its binding partner *ralA* genetically interact with *crb* (Pichaud lab, unpublished). In this chapter, I will explore in more detail the possible link between Par6, the Par complex and the exocyst, in particular with respect to Crb delivery and epithelial morphogenesis.

5.1 The Par complex has multiple links to the exocyst

To confirm whether the interaction observed in vertebrate cells between Par6 and Exo84 is conserved in *Drosophila*, I performed an S2 cell aggregation assay as previously used by Johnston et al. (2009). In this assay, the localisation of a protein of interest, such as Par6, is polarised within S2 cells by fusing it to the transmembrane and extracellular domains of the transmembrane adhesion molecule Echinoid (Ed) (Figure 5.1A-D, red channel). Upon formation of S2 cell aggregates, Ed is mostly localised at the cell-cell contacts, therefore polarising the localisation of the protein of interest, Par6, to these regions (Figure 5.1A-D, red channel). Consequently, proteins that bind to Par6, such as aPKC, are polarised and co-localise at the cell-cell contacts with Par6 (Figure 5.1A-B, green channel). With this assay in mind, I tested whether junctional Ed-mCherry::Par6 was able to recruit GFP-tagged Exo84 (Figure 5.1C-D). However, this was not the case, as Exo84 localised to the cytoplasm and was not enriched at the cell-cell contact regions (Figure 5.1D). Yet, when I tested if GFP-tagged Par6 was recruited by junctional Ed-mCherry::Exo84, I found a detectable enrichment of Par6 at the cell-cell contacts (Figure 5.1E-G).

To further test the interaction between Par6 and Exo84 in flies, I co-immunoprecipitated Exo84::Myc from S2 cells co-transfected with Par6::Flag (Figure 5.2A). This biochemical approach revealed that Par6 and Exo84 interact with each other in flies (Figure 5.2A). Furthermore, a recent work in vertebrate epithelial cells showed that Par3 can bind to another exocyst component, Exo70, through its conserved lysine-rich domain (LRD) (Ahmed and Macara, 2017). To test this interaction in flies, I purified recombinant MBP-tagged Exo70 and the LRD of Baz tagged with GST from *E. coli*, to perform an *in vitro* binding assay. I found that in *Drosophila*, Baz also binds directly to Exo70 through its conserved LRD (Figure 5.2B-C). Together, these experiments show that multiple links exist between the Par complex and the exocyst.

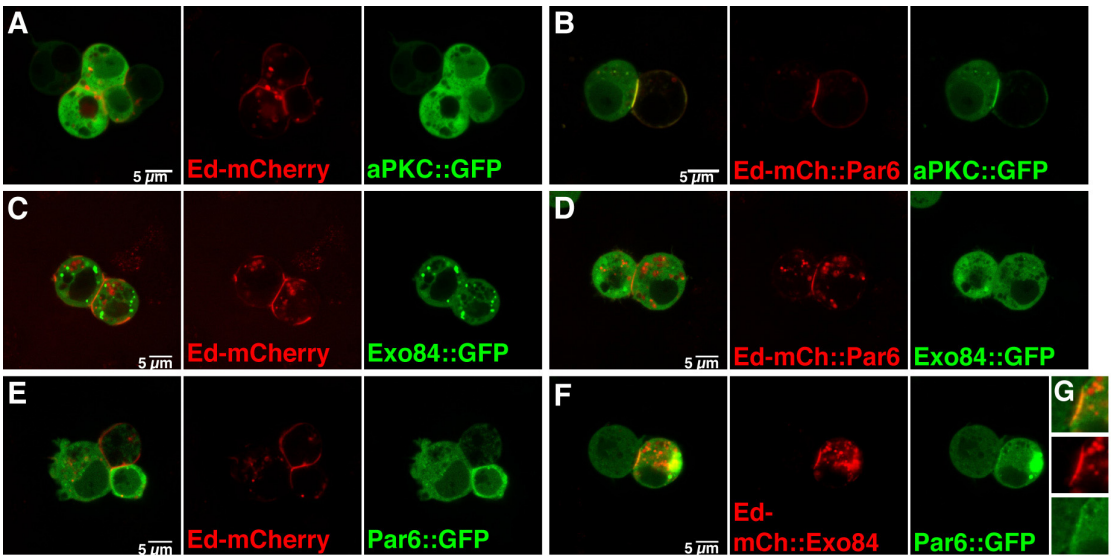

Figure 5.1: Ed-Exo84 recruits Par6 to the cell-cell junctions. **(A)** Ed was fused to mCherry to visualise its localisation at the cell-cell junctions and to control that it has no effect on GFP-tagged aPKC cytoplasmic localisation. **(B)** Ed was fused to both mCherry and Par6, recruits GFP-tagged aPKC to the cell-cell junctions of *Drosophila* S2 cells. **(C)** Ed-mCherry and **(D)** Ed-mCherry::Par6 were co-expressed with GFP-tagged Exo84 in *Drosophila* S2 cells. **(E)** Ed-mCherry and **(F)** Ed-mCherry::Exo84 were co-expressed with GFP-tagged Par6 in *Drosophila* S2 cells. **(G)** Zoomed-in cell-cell junction from (F). Scale bar = 5 microns.

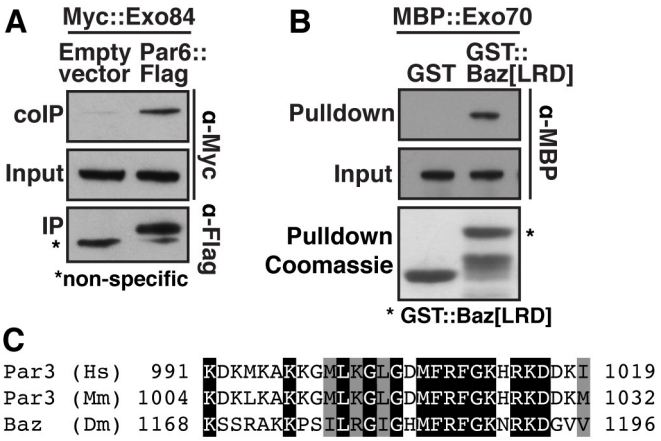

Figure 5.2: The Par complex is linked to the exocyst via Par6 and Baz. **(A)** Co-immunoprecipitation from S2 cells overexpressing Exo84::Myc and Par6::Flag. **(B)** *in vitro* binding assay between recombinant MBP::Exo70 and the LRD domain of Baz GST-tagged. **(C)** Protein sequence alignment of the LRD of Baz/Par3 in human (*Homo sapiens*, Hs), mouse (*Mus musculus*, Mm) and flies (*Drosophila melanogaster*, Dm). Black boxed amino acids are conserved amongst the three species compared, while grey boxed amino acids indicate conservation between groups of strongly similar properties.

5.2 *exo84* is required for Crb apical delivery

One possible model is that, at the cell cortex, Par6 and/or Baz/Par3 regulate the delivery of membrane polarity determinants, such as Crb and E-cad. To investigate a direct role for Exo84 (and the exocyst) in the delivery of Crb, I generated *exo84* mutant flies (as described in subsection 3.3.3). Over 100 males experienced the Δ2,3 transposase-induced excision of the EP-element HP35566, which were subsequently used to established individual stocks. These stocks were screened for lethality, which reduced the number of mutant candidates to 19 stocks. These 19 stocks were further screened by PCR, using a primer pair adjacent to the neighbouring genes *groucho* and *vps2*, to confirm that these genes were unaffected (Figure 5.3A, primers P1 and P2). The PCR confirmed two independent *exo84* mutant lines, identified as $exo84^{\Delta 11}$ and $exo84^{\Delta 14}$ (Figure 5.3A, agarose gels). Ultimately, both PCR products were sequenced to fully characterise these mutant lines. The sequencing results indicated a deletion of 887 bp in $exo84^{\Delta 11}$ and 757 bp in $exo84^{\Delta 14}$ (Figure 5.3A), both leading to premature stop codons in the translated protein (Figure 5.3B). Both mutants are embryonic lethal and fail to complement each other.

Both *exo84* alleles resulted in a very strong phenotype, indicating that *exo84* is required for cell viability, as expected from the broad role of the exocyst in promoting membrane delivery. However, at 18 °C, I could recover small clones of *exo84* mutant photoreceptors, which were characterised by a strong decrease in apical accumulation of Crb when compared to other epitopes, such as Arm (Figure 5.4A-C, quantified in D-E).

To bypass the strong *exo84* phenotype, I next made use of an *exo84* RNAi line ($exo84^{IR}$). A milder phenotype was observed, which allowed me to recover larger clones of photoreceptors deficient for *exo84*. In these clones, Crb localisation was more diffused compared to *wild-type* and overlapped with the vesicular distribution of Rab11 (Figure 5.5A-B). The accumulation of these Rab11-positive vesicles was increased in Exo84-depleted photoreceptors compared to *wild-type*, which is consistent with a role for Exo84 in docking exocytic vesicles to the plasma membrane (Figure 5.5B). In addition, the levels of another component of the exocyst complex, Sec5, were strongly reduced in $exo84^{IR}$ cells (Figure 5.5C). On rare occasions (approx. 15 %), I observed ectopic Arm accumulation at the basal membrane (Figure 5.5A). Nevertheless, in these experiments, *exo84*

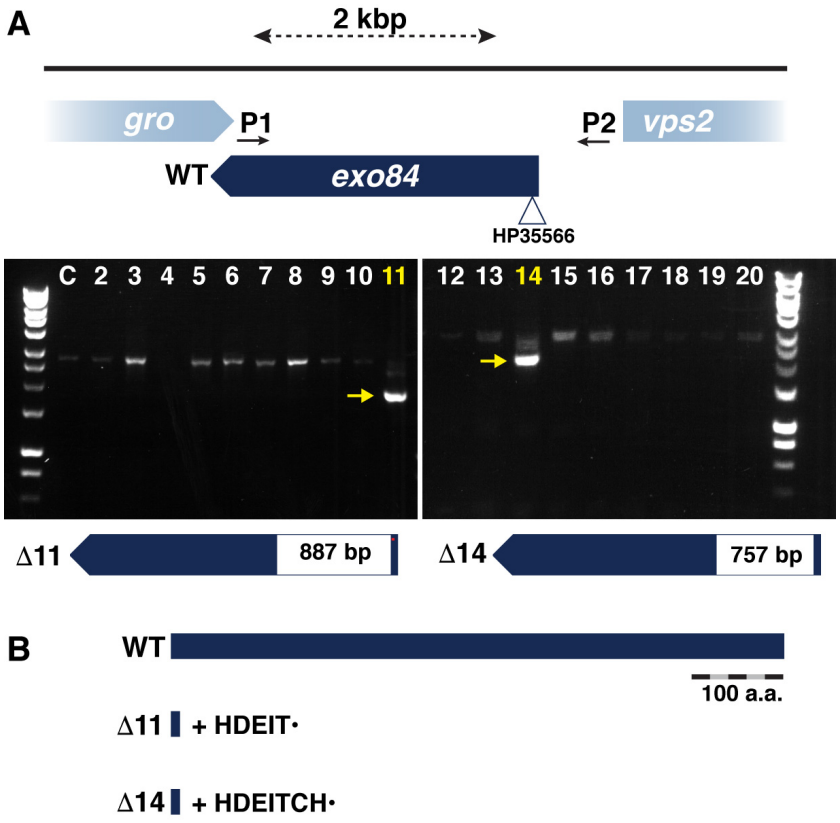

Figure 5.3: The Drosophila *exo84* gene. (A) Dark blue boxes show the coding region and direction of transcription of *exo84*, while light blue boxes show the neighbouring genes *groucho* (*gro*) and *vacuolar protein sorting 2* (*vps2*). The triangle indicates the insertion site of the EP-element HP35566 used for imprecise excision. The location of primers P1 and P2 used to screen and sequence the mutants is indicated by two arrows. Agarose gels showing the PCR products from the different *exo84* mutant candidate lines. C = *CantonS*. Yellow arrows point to shifted bands in stocks 11 and 14, suggesting that these stocks contain genomic deleted regions within the *exo84* gene. White boxes indicate the genomic deleted regions in *exo84* mutant alleles *Δ11* and *Δ14*. kbp = kilo base pairs. **(B)** Exo84 protein generated from *wild-type* and mutant alleles *Δ11* and *Δ14*.

knockdown did not interfere significantly with the formation of domains containing high levels of Arm, Baz and E-cad at the plasma membrane (Figure 5.5A and D). Altogether, our data suggest that *exo84* regulates the apical delivery of Crb to the plasma membrane.

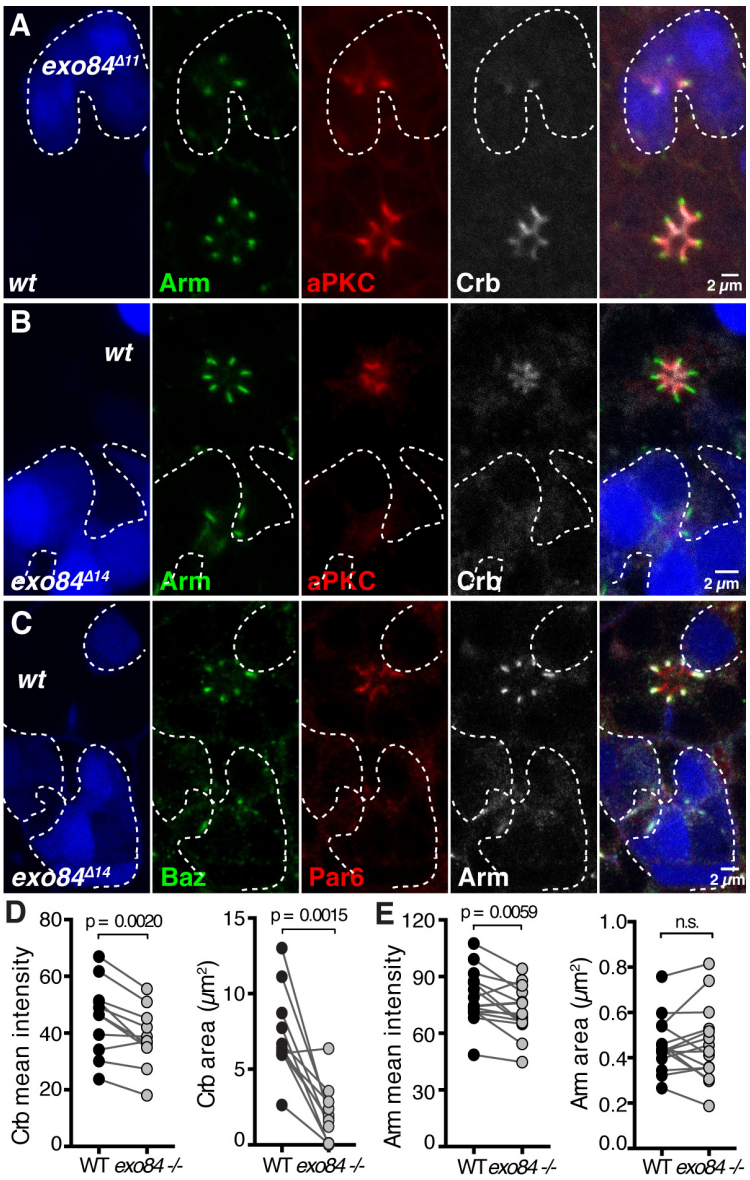

Figure 5.4: *exo84* is required for Crb acummulation at the apical membrane. (A) *exo84*$^{\Delta 11}$ mutant mid-pupal photoreceptors positively labeled with GFP (blue) and stained for Arm (green), aPKC (red) and Crb (grey). **(B-C)** *exo84*$^{\Delta 14}$ mutant photoreceptors positively labeled with GFP (blue) and stained for (B) Arm (green), aPKC (red), Crb (grey), and (C) Baz (green), Par6 (red) and Arm (grey). Scale bars = 2 microns. **(D-E)** Quantification of Crb and Arm mean intensity and area in *exo84* mutant photoreceptors compared to *wild-type* (n = 11 ommatidia for Crb and n = 15 ommatidia for Arm, both from at least 3 individuals).

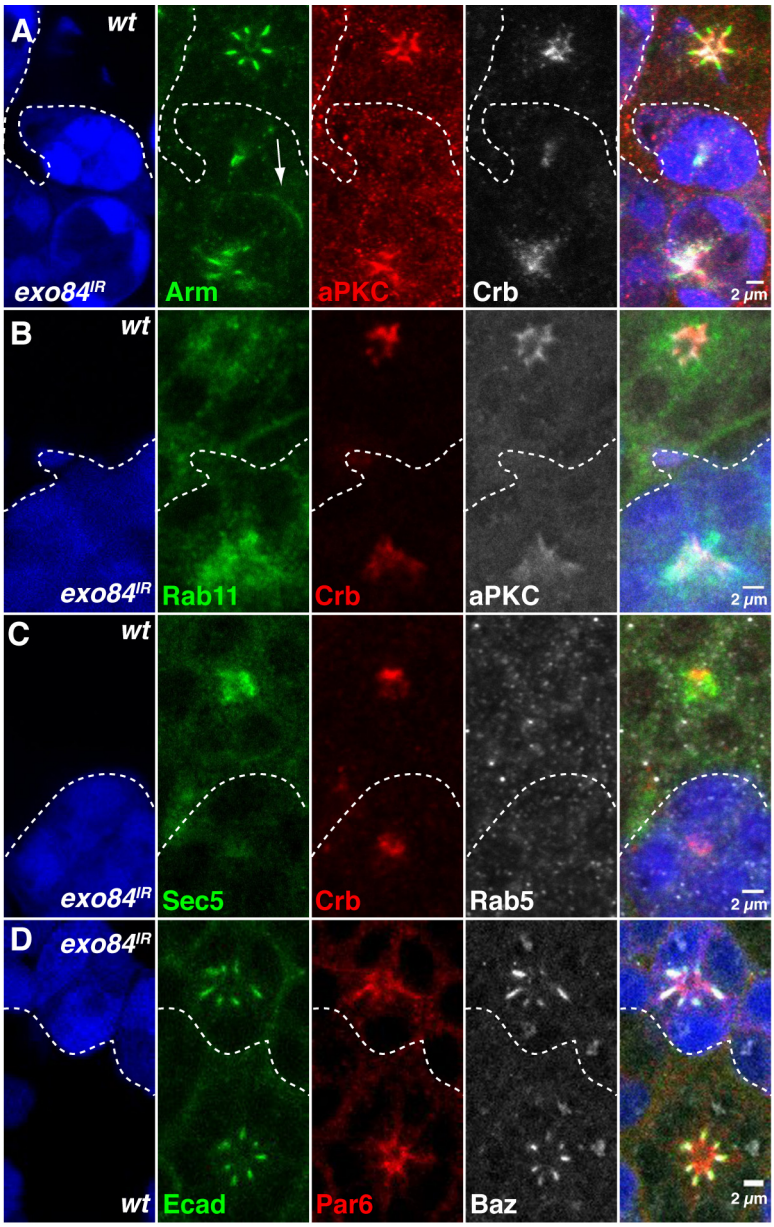

Figure 5.5: *exo84* is required for Crb delivery to the apical membrane. RNAi knockdown of Exo84 in mid-pupal photoreceptors positively labeled with GFP (blue) using the coin-FLP system and stained for **(A)** Arm (green), aPKC (red) and Crb (grey), **(B)** Rab11 (green), Crb (red) and aPKC (grey), **(C)** Sec5 (green), Crb (red) and Rab5 (grey), **(D)** E-cad (green), Par6 (red) and Baz (grey). White arrow shows ectopic Arm staining at the basal membrane. Scale bars = 2 microns.

5.3 The exocyst regulates apical membrane morphogenesis

To complement these experiments addressing the role of the exocyst during apical membrane morphogenesis, we examined polarity markers in *sec5* mutant photoreceptors, which is another component of the exocyst. To this end, we made use of the null allele $sec5^{E10}$, which contains a premature stop codon at amino acid 31 (Murthy et al., 2003). Similarly to *exo84* mutants, it was particularly difficult to recover large clones of *sec5* mutant photoreceptors. In this case, we observed a loss of the apical markers Crb, aPKC and Par6, and similarly to $exo84^{IR}$, instances where AJ markers were detected at the basal membrane of the cell (Figure 5.6).

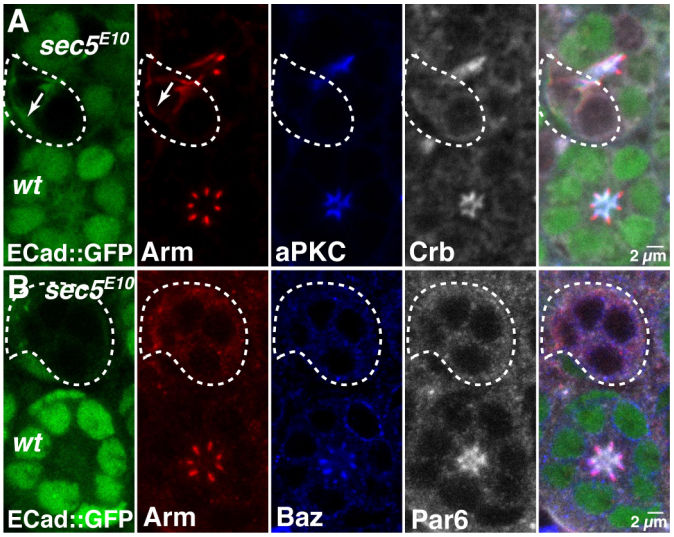

Figure 5.6: Sec5 is required for Crb delivery to the apical membrane. $sec5^{E10}$ mutant mid-pupal photoreceptors labelled by loss of nuclear GFP signal (green) and expressing E-cad::GFP (green). **(A)** Arm (red), aPKC (blue) and Crb (grey), **(B)** Arm (red), Baz (blue) and Par6 (grey). White arrow shows ectopic E-cad and Arm staining at the basal membrane. Scale bars = 2 microns. Images courtesy of Dr. Rhian Walther. Nunes de Almeida and Walther *et al.*, under revision.

5.4 RalA is required for Crb delivery

To further investigate how the exocyst regulates apical membrane morphogenesis I decided to examine RalA function. RalA is a GTPase that regulates the assembly of the

exocyst complex via binding to Exo84 and Sec5 (Moskalenko et al., 2002, 2003). The *ralA* gene is localised in the X chromosome and $ralA^{EE1}$ mutants are hemizygous viable, although males are sterile and display morphological defects, such as rough eyes and missing bristles in the notum, head and humerus (Eun et al., 2007). The $ralA^{EE1}$ allele contains a missense mutation, Ser^{154} (TCG) to Leu^{154} (TTG), which affects nucleotide binding to this GTPase, therefore interfering with the function of RalA (Eun et al., 2007). Confocal imaging of $ralA^{EE1}$ mid-pupal retinae from hemizygous males showed extensive morphogenetic defects, when compared to heterozygous female flies (Figure 5.7A-B). In addition to missing photoreceptors in $ralA^{EE1}$ retinae, I also observed a partial co-localisation of apical and AJ markers, which resembled the previously analysed *crb* mutant phenotype (Walther and Pichaud, 2010). Further quantification of Crb levels in $ralA^{EE1}$ mutant photoreceptors showed that these were significantly decreased, when compared to *Ubi-Ecad::GFP* control flies (Figure 5.7C).

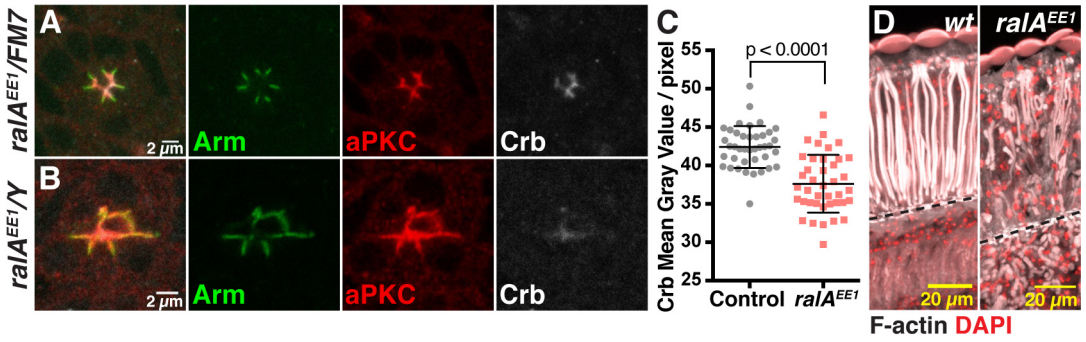

Figure 5.7: RalA is required for Crb accumulation at the apical membrane. Mid-pupal photoreceptors from **(A)** $ralA^{EE1}$ heterozygous female flies and **(B)** $ralA^{EE1}$ hemizygous males, stained for Arm (green), aPKC (red) and Crb (grey). Scale bar = 2 microns. **(C)** Quantification of the mean intensity levels of Crb staining in the retina of *Ubi-Ecad::GFP* control flies (grey, n=42 ommatidia from 2 retinae) compared to $ralA^{EE1}$ mutant flies (red, n=41 ommatidia from 2 retinae). Graph shows mean and SD, p value calculated with a two-tailed Mann-Whitney test. **(D)** Longitudinal sections from adult retinae of *wild-type (wt) CantonS* (left) and $ralA^{EE1}$ mutant flies (right), stained with Phalloidin (grey) and DAPI (red). Black dashed line indicates the floor of the retina. Scale bar = 20 microns.

To complement this analysis, I imaged cryosections from adult retinae of both $ralA^{EE1}$ and *wild-type* flies. Longitudinal sections showed that $ralA^{EE1}$ mutant photoreceptors did not fully elongate all the way down to the floor of the retina (Figure 5.7D), a phenotype that resembles that of *crb* mutant photoreceptors (Pellikka et al., 2002).

Furthermore, in *ralA*^{EE1} flies, there was a substantial amount of photoreceptors that felt below the floor of the retina (Figure 5.7D). Altogether, these data are compatible with RalA being involved in Crb apical accumulation, therefore being necessary for apical membrane morphogenesis.

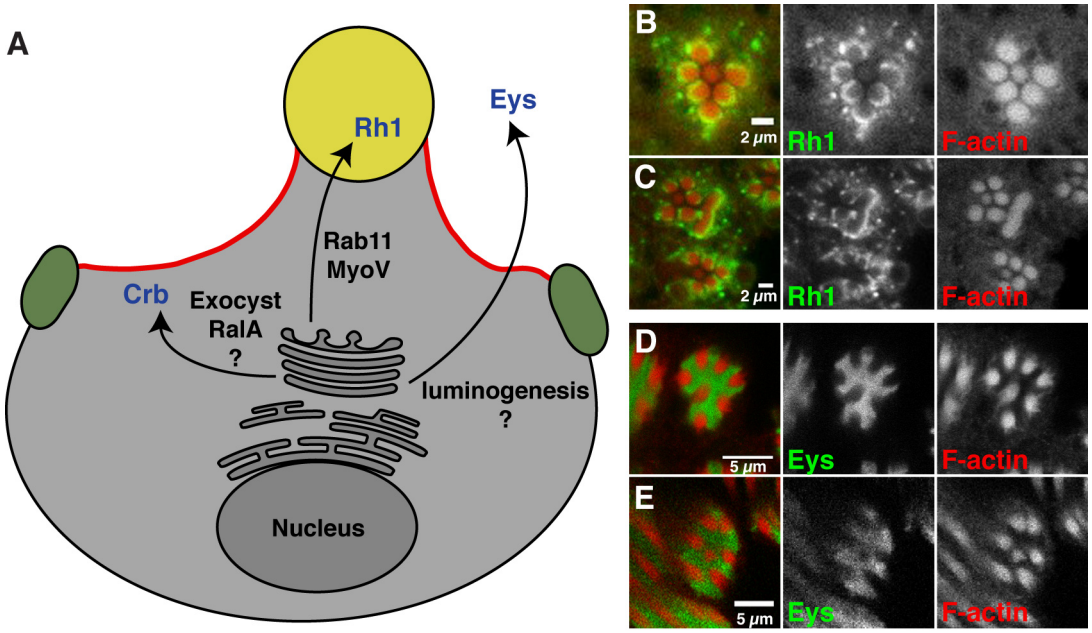

Figure 5.8: RalA does not regulate the delivery of the apical cargoes Rh1 and Eys. **(A)** Representation of a photoreceptor with three different trafficking pathways that deliver apical cargoes: (1) RalA and the exocyst potentially deliver Crb to the apical membrane (our testing hypothesis), (2) Rab11 and Myosin V regulate the delivery of Rh1 to the rhabdomere, and (3) a poorly studied pathway secretes Eyes shut (Eys) to the luminal space between photoreceptors. *ZA* in green, stalk membrane in red and rhabdomere in yellow. **(B)** *wild-type CantonS* and **(C)** *ralA*^{EE1} mutant retinae stained for Rh1 (green) and F-actin (red). Scale bar = 2 microns. **(D)** *wild-type CantonS* and **(E)** *ralA*^{EE1} mutant retinae stained for Eys (green) and F-actin (red). Scale bar = 5 microns.

Next, I asked whether RalA was involved in regulating the delivery of other apical cargoes besides Crb. The post-Golgi to rhabdomere route is regulated by both Rab11 and Myosin V, which delivers rhabdomeric proteins such as Rh1 (Figure 5.8A) (Li et al., 2007, Satoh et al., 2005). We tested whether RalA also regulates the delivery of Rh1. Despite the clear morphological defects in *ralA*^{EE1} mutant photoreceptors, Rh1 localised as a crescent at the base of the rhabdomeres in both *wild-type* and *ralA*^{EE1} mutant photoreceptors (Figure 5.8B-C). Alternatively, we tested the possibility that RalA and the exocyst could regulate the secretion of luminal proteins, such as the proteoglycan

Eys (Figure 5.8A) (Husain et al., 2006). I found that in both *wild-type* and *ralA*^{EE1} mutant photoreceptors, Eys was properly secreted to the central luminal space (Figure 5.8D-E). Based on examining *ralA*^{EE1} escapers, it appears that RalA does not regulate the delivery of apical cargoes in general, as both Rh1 and Eys were not affected in *ralA*^{EE1} mutants. Examining a stronger allele might reveal such phenoptypes.

5.5 RalA regulates vesicle tethering redundantly via Exo84 and Sec5

So far, my data indicate that the exocyst delivers Crb to the apical membrane. Both Exo84 and Sec5 are essential in Crb delivery, which could be by either physically linking the octameric exocyst complex together or as a consequence of their role in vesicle tethering (a process that is regulated by RalA). Therefore, I next asked whether both Exo84 and Sec5 are required for vesicle tethering to the plasma membrane. To this end, I have individually uncoupled RalA from Exo84 and Sec5 with the amino acid substitutions K44E and E35R, respectively (Figure 5.9A) (Hazelett and Yeaman, 2012). Firstly, I controlled that the different transgenes, *UAS-GFP::RalA*$^{WT/K44E/E35R}$, could be stably expressed in S2 cells and observed that the three proteins present a cortical distribution in these cells (Figure 5.9B-C). These amino acid substitutions (K44E and E35R) have been previously validated by Hazelett and Yeaman (2012) in an invasive human prostate cancer cell line (Hazelett and Yeaman, 2012), and I have further confirmed that RalA$^{\mathrm{K44E}}$ was not able to bind Exo84 in *Drosophila* S2 cells (Figure 5.9D). The GFP-tagged RalA transgenes were finally injected in flies and used to rescue the rough eye phenotype in *ralA*^{EE1} mutant flies. All three transgenes rescued the rough eye phenotype (Figure 5.10), suggesting that binding of RalA to Exo84 and Sec5 acts redundantly during exocyst function.

Lastly, I used these RalA transgenes to disrupt exocyst function using overexpression experiments in FCs. I hypothesised that, if RalA is required to bind both Exo84 and Sec5 during exocyst function, the overexpression of Exo84- or Sec5-uncoupled RalA could outcompete endogenous RalA, leading to gain-of-function phenotypes. However, this was not the case, as no gain-of-function phenotypes were observed and FCs formed

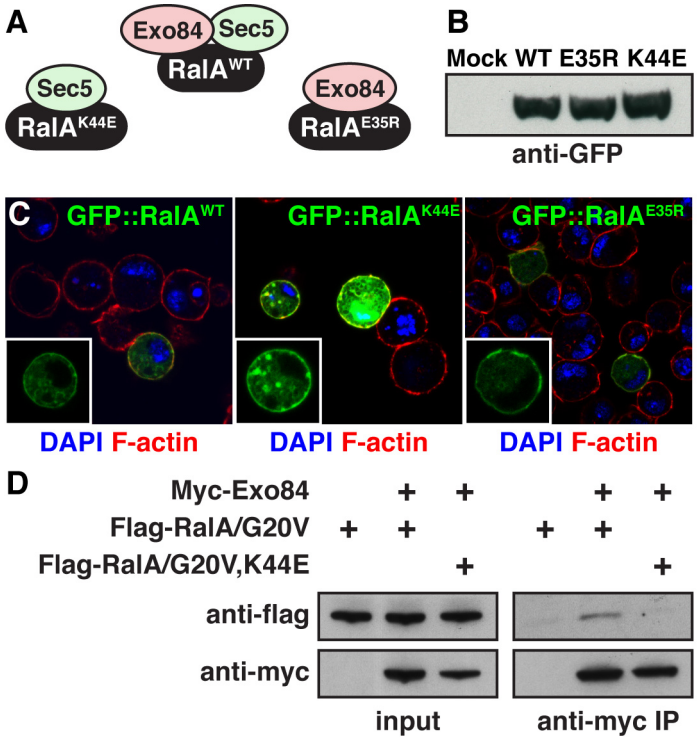

Figure 5.9: Individual uncoupling of RalA from Exo84 and Sec5. (A) *wild-type* RalA binds both Exo84 and Sec5, while RalA^{K44E} only binds Sec5 and RalA^{E35R} only binds to Exo84 (Hazelett and Yeaman, 2012). **(B-C)** The different GFP-tagged transgenes are expressed in S2 cells, as observed with (B) western blotting and (C) immunostaining. Mock = S2 cells transfected with salmon sperm DNA. S2 cells stained with Phalloidin (red) and DAPI (blue). **(D)** Co-immunoprecipitation from S2 cells shows that the K44E substitution uncouples constitutively active (G20V) RalA from Exo84.

a continuous monolayer around the egg chamber, with apical Par6/aPKC and junctional Arm/Baz organised in distinct domains (Figure 5.11). In addition, we noticed that all RalA proteins (WT, K44E and E35R) were detected at the apical and lateral membranes, suggesting that RalA is homogeneously distributed around the cell (Figure 5.11). Our experiments from this section strongly suggest that RalA regulates Exo84 and Sec5 in a redundant mechanism to tether vesicles to the plasma membrane.

Altogether, the results from this chapter indicate that the exocyst is required to regulate the apical delivery of Crb and to prevent basal delivery of AJ material. We propose that, at the cell cortex, the Par complex components Baz and Par6 coordinate cell polarity to membrane delivery via the exocyst. During this process RalA regulates vesicle tethering redundantly via Exo84 and Sec5.

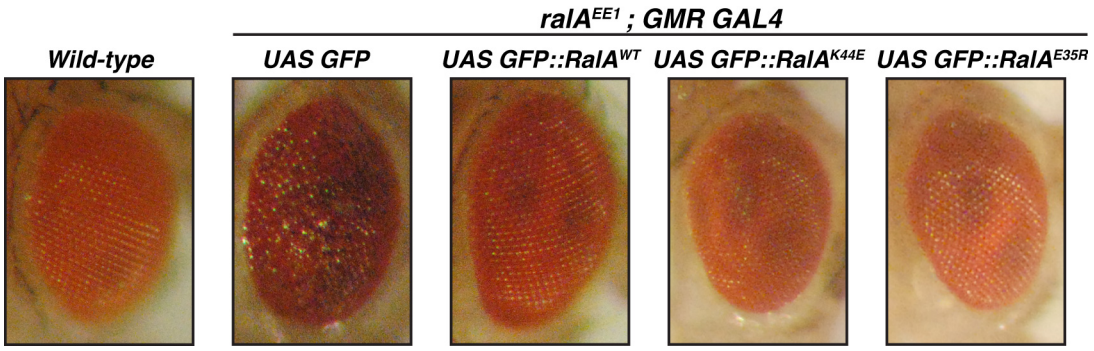

Figure 5.10: RalA binding to at least one exocyst component is sufficient to rescue the *ralA*^{EE1} rough eye phenotype. *ralA*^{EE1} */ FM7 ; GMR GAL4* female flies were crossed with males carrying the different *UAS-GFP::RalA* transgenes (or *UAS-GFP* as a control) and the roughness of adults eyes was examined, together with *wild-type CantonS* flies as a control.

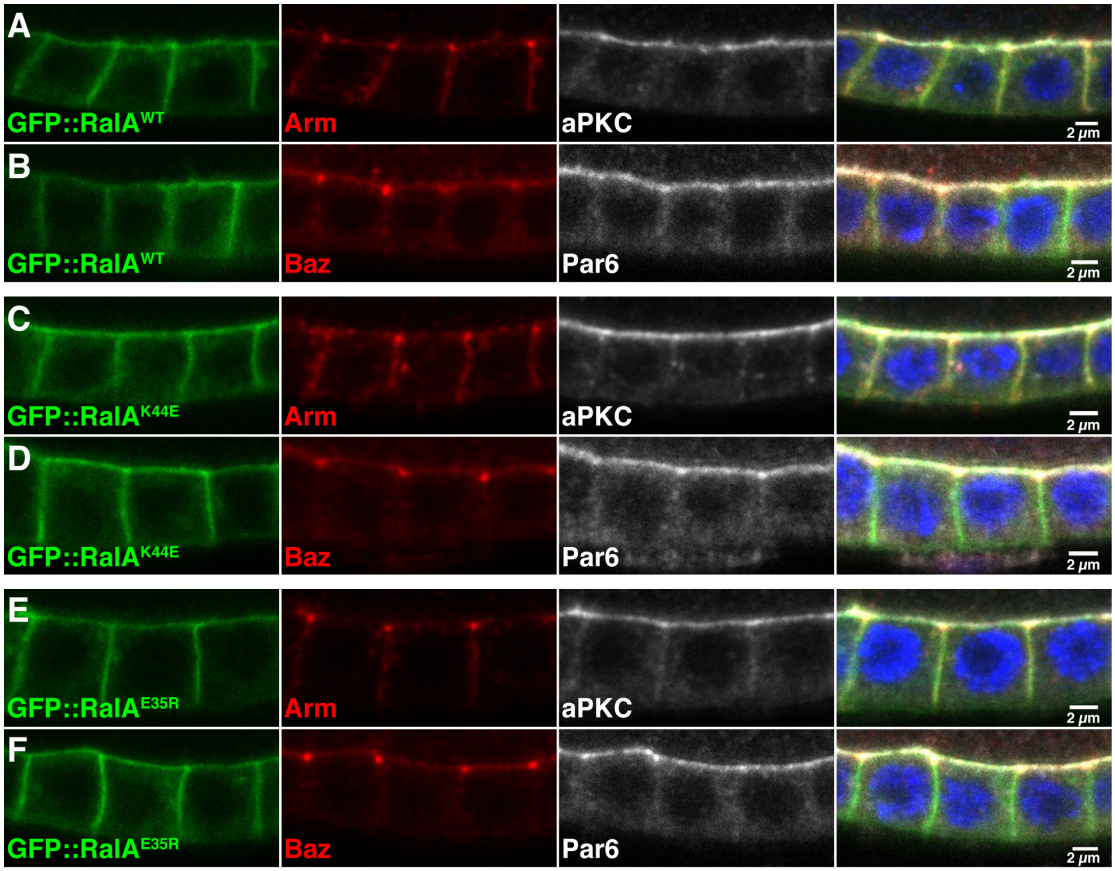

Figure 5.11: RalA is localised at the cell cortex. (A-B) GFP::RalA^{WT} (green) was overexpressed in FCs and stained for (A) Arm (red) and aPKC (grey) or (B) Baz (red) and Par6 (grey). **(C-D)** GFP::RalA^{K44E} (green) was overexpressed in FCs and stained for (C) Arm (red) and aPKC (grey) or (D) Baz (red) and Par6 (grey). **(E-F)** GFP::RalA^{E35R} (green) was overexpressed in FCs and stained for (E) Arm (red) and aPKC (grey) or (F) Baz (red) and Par6 (grey). DAPI staining is shown in blue in the merged channel. Scale bars = 2 microns.

5.6 Discussion

The exocyst is an essential cellular machinery that acts prior to vesicle fusion to link post-Golgi vesicles to the plasma membrane. Our work shows that, in *Drosophila*, at least two links exist between the exocyst and the Par complex. More specifically, we have shown that both Par6 and Baz bind to Exo84 and Exo70, respectively. While I have shown that the Baz-Exo70 interaction is direct, it is possible that Par6 binding to Exo84 occurs via Baz and Exo70, as Par6 binds Baz and, in vertebrates, Exo84 is known to bind Exo70 (Matern et al., 2001, Petronczki and Knoblich, 2001). However, we do not think this could be the case, as S2 cells express both *baz* and *exo70* at very weak levels (Celniker et al., 2009).

Previous work in vertebrate cells reports that Par3 acts as a receptor for the exocyst at the plasma membrane (Ahmed and Macara, 2017). Moreover, Ahmed and Macara (2017) report defects in E-cad trafficking in Par3 depleted mouse mammary cells, which could be rescued by expression of the LRD of Par3 (Ahmed and Macara, 2017). Our data suggest that, instead of a single receptor, there are multiple links that could dock the exocyst complex to the plasma membrane (Figure 5.12A). The reason for the existence of multiple links is not clear, as it could be a redundant mechanism to ensure recognition by multiple receptors at the plasma membrane, or instead, it could be a mechanism to polarise apical delivery via binding to Par6 and junctional delivery via binding to Baz/Par3. In this latest model, the fact that Par6 and Baz/Par3 are enriched at different locations along the apical-basal axis of epithelial cells suggests that these proteins regulate the delivery of specific cargoes independently. Still, further studies are necessary to understand if the exocyst requires binding to both Par6 and Baz/Par3 at the same time during cargo delivery or whether these are independent links.

We have further analysed the role of two exocyst components, Exo84 and Sec5, in the delivery of different cargoes. We have tested this directly using *exo84* and *sec5* mutant flies and indirectly, via their regulator RalA. Our analyses are compatible with previous studies that show a function for Baz-Exo70 in regulating E-cad delivery (Ahmed and Macara, 2017). However, we note that Sec5 and Exo84 are not strictly required for E-cad delivery to the *ZA*. Instead, these exocyst components appear to prevent the basal accumulation of E-cad. As a result, we suggest that while both apical and basal

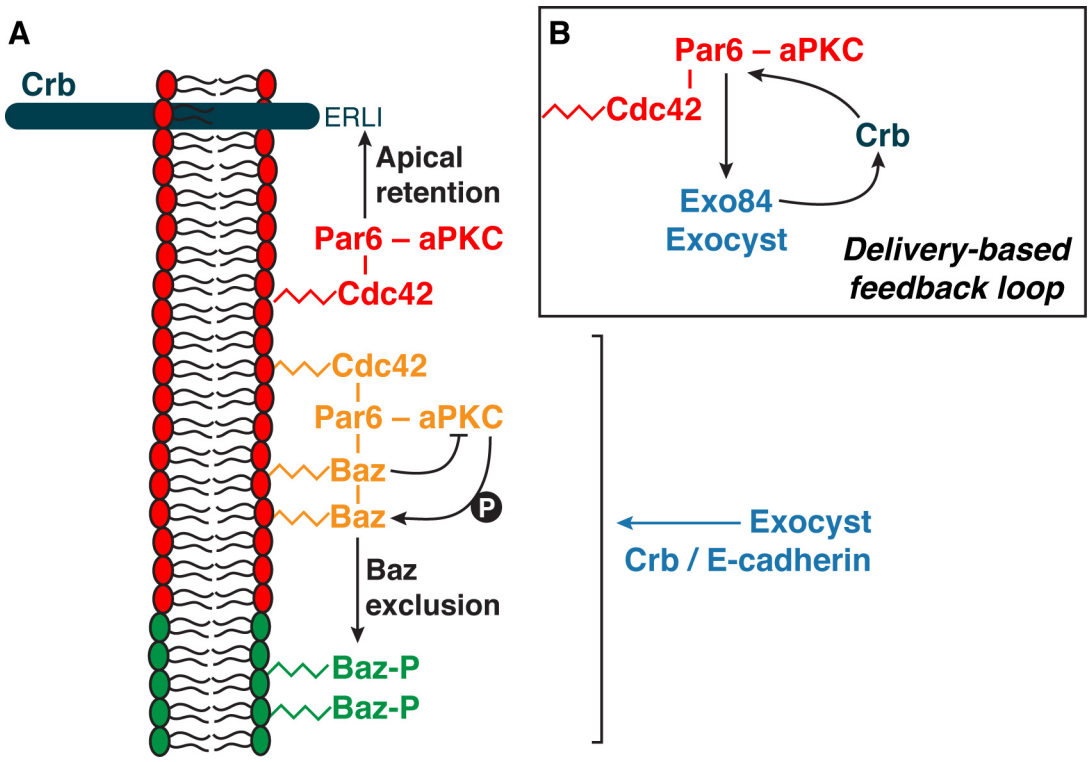

Figure 5.12: Par6 couples cortical polarity to plasma membrane morphogenesis. Complementing the model in Figure 4.12 with the data from this chapter, **(A)** we propose that, at the apical cortex, the Par complex functions as a receptor for the exocyst, promoting the delivery of different cargoes, including Crb and E-cad. **(B)** At the cell cortex, Par6 binds Exo84 promoting the delivery of Crb, which creates a delivery-based feedback loop.

domains can support E-cad delivery, the Baz-Exo70 interface serves to outcompete basal delivery, perhaps by increasing the probability of vesicle fusion at the apical pole of the cell.

Our studies on Exo84, Sec5 and RalA show that, in the absence of any of these proteins, Crb delivery is severely impaired. The apical determinant and transmembrane protein Crb has been shown to play a central role during apical membrane morphogenesis. In the previous chapter, we have shown that Crb regulates the retention of Par6-aPKC at the apical domain, which affects both apical and *ZA* morphogenesis. In turn, our data also suggested that Par6-aPKC regulate the accumulation of Crb at the plasma membrane. In this chapter, we show that Par6 binds the exocyst component Exo84. In addition, *exo84* depleted cells accumulate Crb in their cytosol, which was also observed in the previous chapter in *par6* mutant photoreceptors. As a result, we propose that Par6 binding to Exo84 regulates the delivery of Crb, which enables a delivery-based feedback

loop that drives polarised morphogenesis by coordinating cortical polarity and plasma membrane delivery (Figure 5.12B). In addition, Par6-aPKC have been shown to act downstream of Cdc42 to limit Crb endocytosis (Harris and Tepass, 2008). Therefore, this might suggest that Par6 can regulate the accumulation of Crb at the apical membrane, by two distinct mechanisms: by limiting Crb endocytosis as shown by Harris and Tepass (2008), as well as by promoting its delivery via the exocyst.

The GTPase RalA promotes the tethering of vesicles via regulating the exocyst components Exo84 and Sec5. I have individually uncoupled both RalA-Exo84 and RalA-Sec5 interfaces to analyse the role of each of these regulatory mechanisms. Surprisingly, disrupting each of these interfaces does not lead to gain-of-function phenotypes and, most importantly, both RalA mutant proteins rescue the *ralA* mutant rough eye phenotype. Therefore, this part of my work indicates that RalA regulates both Exo84 and Sec5 redundantly, possibly to ensure the tethering of vesicles to the plasma membrane. In the future, it would be important to confirm this redundancy, by creating double-mutants where RalA is uncoupled from both Exo84 and Sec5.

Altogether, our data suggest that there are multiple links between the exocyst and Par complexes. In flies, while Baz is largely dispensible for epithelial cell viability, this is not the case with Par6 or the exocyst. Based on this requirement for cell viability, we therefore favour a model in which, in flies, Par6 is the main link between the exocyst and the Par complex.

Chapter 6

Mbt regulation during *ZA* morphogenesis

In the previous two chapters of this thesis I investigated how epithelial cells build two distinct apical and *ZA* domains. My work suggests that a Crb-dependent retention mechanism takes place at the apical domain, which enables the separation of the apical domain from the *ZA* and morphogenesis of these two domains. In line with this model, in this last chapter, we investigate another retention mechanism that operates at the level of the *ZA* and that is regulated by the Cdc42-effector Mbt/Pak4.

6.1 Mbt is a core component of the AJ

Mbt is a component of the AJs and is localised at the developing *ZA* together with other junctional markers, such as Arm and Baz (Appendix C, Walther et al., 2016). We noted that Mbt localisation with AJ material is independent of apical polarity cues, as Mbt co-localises with junctional markers in the absence of *aPKC* or *crb* function (Appendix C, Walther et al., 2016).

In order to link Mbt to the epithelial polarity protein network we examined the requirement of baz for Mbt localization. AJ material, including Mbt, are present at the cell membrane in the absence of *baz* (Appendix C, Walther et al., 2016), suggesting that there must be at least one molecular pathway that can support AJ assembly independently of Baz. Based on its junctional localisation, we reasoned that Mbt could be part of that pathway. To this end, we compared baz^4 *and* mbt^{P1} single-mutants to baz^4, mbt^{P1} double-mutants (Appendix C, Walther et al., 2016). While junctional material is still detected in baz^4 and mbt^{P1} single-mutant photoreceptors, we found no AJ material at the cortex of baz^4, mbt^{P1} double-mutant photoreceptors. Moreover, analysis of mbt^{P1} single-mutant photoreceptors showed a significant decrease in both length and mean pixel intensity of Arm and Baz-positive domains at the developing *ZA*, when compared to *wild-type* cells (Appendix C, Walther et al., 2016). Altogether, our results indicate that Mbt and Baz converge in promoting AJ morphogenesis.

In addition to regulating the accumulation AJ material at the developing *ZA* of pupal photoreceptors, our work also showed that Mbt regulates apical membrane morphogenesis (Appendix C, Walther et al., 2016). We observed that a fraction of mbt^{P1} mutant photoreceptors showed poorly differentiated apical membranes that were found between the lamina and the floor of the retina (Appendix C, Walther et al., 2016). Importantly, the *mbt* loss-of-function phenotype was completely rescued when expressing a *wild-type* version of Mbt, but not with a version of Mbt that could not bind to Cdc42 or that lacked kinase activity (Appendix C, Walther et al., 2016). This suggests that the function of Mbt requires its kinase activity, as well as binding to Cdc42.

6.2 Mbt regulates *ZA* morphogenesis through Arm phosphorylation

To gain a mechanistic insight into how Mbt operates during polarity remodelling, we investigated the relationship between Mbt and both Par6 and Arm. Human Pak4 (hPak4) phosphorylates hPar6b at serine 143, which corresponds to serine 146 in *Drosophila* Par6 (Jin et al., 2015, Walther et al., 2016). However, the (-2) residue in *Drosophila* Par6 is a glutamine (Q), which differs from the proline (P) found in hPar6b (Figure 6.1A). In addition, previous *in vitro* studies have shown that Mbt can phosphorylate Arm at two conserved residues: serine 561 and 688 (Figure 6.1B) (Menzel et al., 2008). Altogether, these observations suggest a model in which Mbt regulates AJ morphogenesis via Arm and apical membrane morphogenesis via Par6. However, no *in vivo* relevance was shown for these interactions.

To test the link between Mbt, Par6 and Arm in *Drosophila*, I purified myc-tagged constitutively active Mbt from *Drosophila* S2 cells (Figure 6.1C) and used it to perform a kinase assay (Figure 6.1D) on recombinant Par6 and Arm as substrates. The kinase assay showed no evidence for Par6 S146 being phosphorylated by Mbt. However, I was able to confirm that Mbt phosphorylates Arm at S561 and S688 (Figure 6.1D) (Menzel et al., 2008).

One possible model is that Arm phosphorylation might regulate the interface between Arm and Baz. Since Baz binds to Arm, the phosphorylation of Arm could modulate this binding. Alternatively, Arm phosphorylation could regulate the stability of the AJs, which in turn could impact on Baz retention. To begin testing the *in vivo* role of Arm phosphorylation by Mbt, I made use of FRAP and analysed the recovery of E-cad::GFP after photobleaching. Bleaching the entire junction led to no recovery of E-cad::GFP. However, bleaching half of the junctional domain, allowed me to recover nearly 30 % of the E-cad::GFP signal (Figure 6.2). This suggests that the recovered pool of E-cad::GFP reflects exchange within the junctional domain or with a pool associated with the junction, instead of recovery from a more distant pool of E-cad::GFP. I then tested how homogeneous E-cad mobility is along the *ZA*. To this end, I analysed E-cad::GFP recovery after photobleaching the apical half of the *ZA* and compared it to the recovery

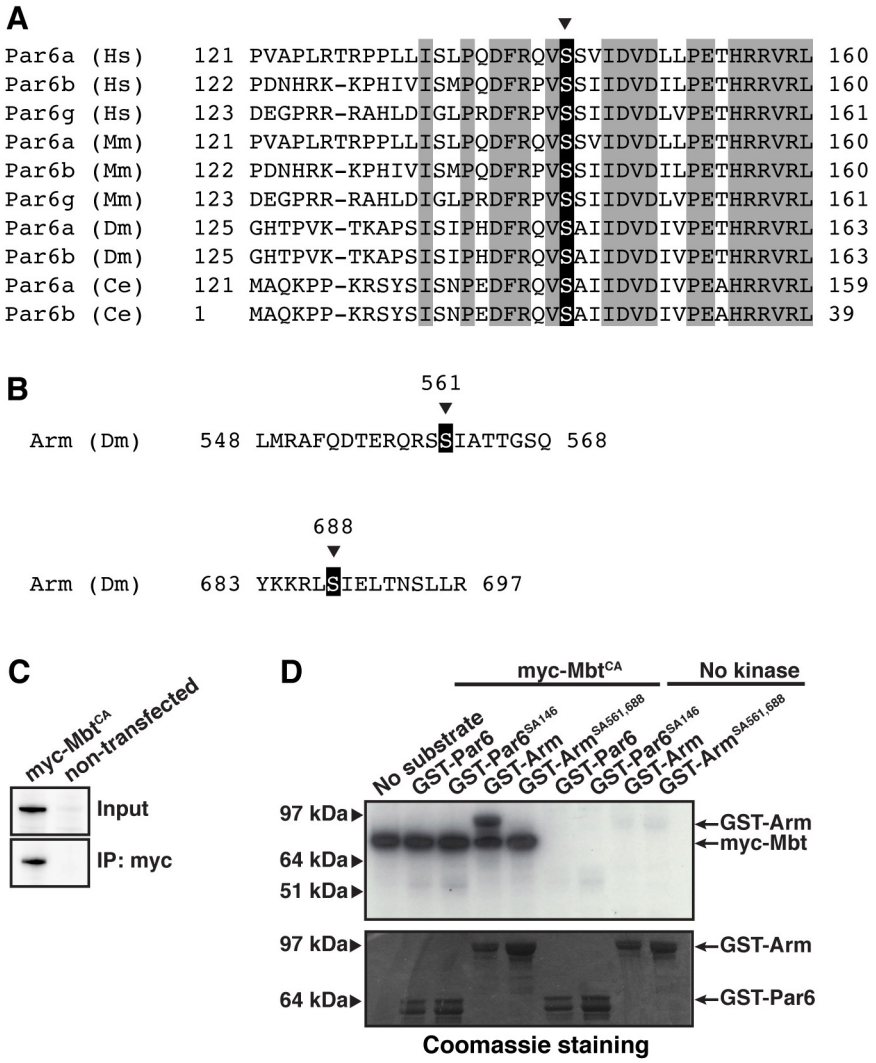

Figure 6.1: Mbt phosphorylates Arm, but not Par6. **(A)** Par6 sequence alignment, containing the conserved S143 that, in Par6b, is phosphorylated by hPak4 (Jin et al., 2015). **(B)** Arm sequence containing the two serine residues S561 and S688 that are phosphorylated by Mbt *in vitro* (Menzel et al., 2008). **(C)** Myc::Mbt^{CA} was expressed in S2 cells and immunoprecipitated to perform the kinase assay in (D). **(D)** *In vitro* kinase assay using Par6 and Arm substrates purified from *E. coli*. Adapted from Walther et al. (2016).

after photobleaching the basal half (Figure 6.2A). These experiments showed that the recovery of E-cad was identical at both these junctional subdomains (Figure 6.2B-C). Although the mobile fractions were statistically significantly different, this difference was considered minimal when compared to nearly doubled differences observed under specific genotypes (*e.g.* the difference observed later in *mbt* mutant flies).

Next, I estimated the recovery of E-cad::GFP after photobleaching the basal half of the *ZA* in *wild-type* cells and compared to that of *mbt*^{P1} mutant cells. I found that, in

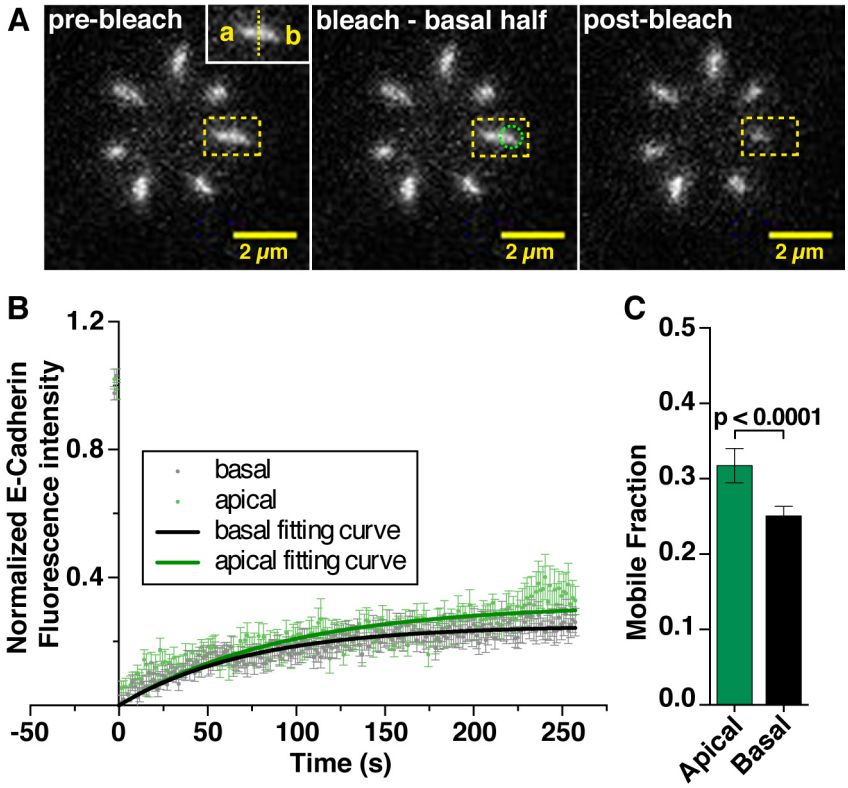

Figure 6.2: E-cad::GFP recovery after photobleaching at the apical and basal tips of the *ZA*. **(A)** *wild-type* ommatidium before (left) and after (right) photobleaching the basal half of the *ZA*. The photobleached *ZA* is shown within a yellow dashed rectangle and zoomed at the top right corner of the left image. a = apical and b = basal. The photobleached area is shown with a green dashed circle. **(B)** FRAP on Ecad::GFP in *wild-type* photoreceptors. Recovery at both apical and basal halves of the *ZA* was tested. Mean normalized fluorescence intensity at the apical half (green; n = 16 from three individuals) and at the basal half (grey; n = 32 from seven individuals) is shown; error bars represent SEM. Fluorescence recovery curves of E-cad::GFP after photobleaching were calculated using single exponential fitting. **(C)** Mobile fraction of E-cad::GFP at the apical (green) and basal (black) halves of the *ZA*. The p value was calculated with an unpaired two-tailed Students t test with Welchs correction.

wild-type photoreceptors, 23.3 % ± 0.6 % of E-cad::GFP was mobile with an evaluated half-time recovery of 47 sec (Figure 6.3A-B). In mbt^{P1} mutant cells, I found that the mobile fraction of E-cad::GFP at the developing *ZA* was increased to 45.7 % ± 1.2 %, with a half-time recovery of approximately 45 sec (Figure 6.3A-B). This indicates that Mbt is required to stabilise E-cad at the *ZA* during photoreceptor polarity remodelling. Interestingly, when I overexpressed a phospho-dead $Arm^{SA561,688}$::myc transgene in otherwise *wild-type* retinas, I was able to reproduce the increased mobility of E-cad

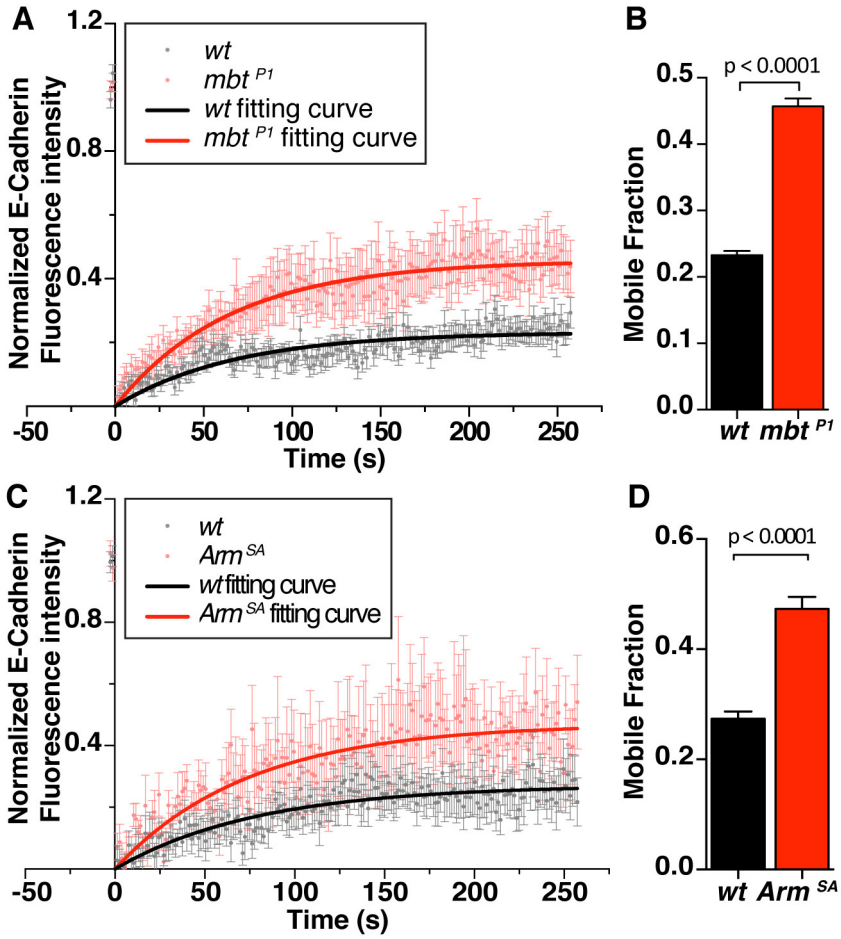

Figure 6.3: Arm phosphorylation regulates E-cad stability during *ZA* morphogenesis. **(A)** FRAP on Ecad::GFP in *wild-type* (grey; n = 18 from two individuals) and mbt^{P1} mutant (pink; n = 15 from three individuals) photoreceptors. **(B)** Mobile fraction of E-cad::GFP in a *wild-type* (black) or mbt^{P1} (red) background. **(C)** FRAP on Ecad::GFP in *wild-type* cells (grey; n = 14 from five individuals) and in cells expressing $Arm^{SA561,688}$*::myc* (pink; n = 9 from five individuals). (A) and (C) show the mean normalized fluorescence intensity; error bars represent SEM; fluorescence recovery curves of E-cad::GFP after photobleaching were calculated using single exponential fitting. **(D)** Mobile fraction of E-cad::GFP in a *wild-type* (black) or $Arm^{SA561,688}$*::myc* (red) background. In (B) and (D), the p value was calculated with an unpaired two-tailed Students t test with Welchs correction. Adapted from Walther et al. (2016).

estimated in mbt^{P1} mutant cells (Figure 6.3C-D). In fact, photoreceptors overexpressing $Arm^{SA561,688}$::myc also reproduced the mbt^{P1} mutant phenotype, showing lower levels of Arm/Baz and shorther Arm/Baz-positive domains at the developing *ZA* (Appendix C, Walther et al., 2016). Altogether, these data show that Mbt stabilises E-cad at the membrane and promotes the accumulation of both Arm and Baz through phosphorylation of Arm at S561 and S688.

6.3 Discussion

During epithelial tissue morphogenesis, the establishment of the *ZA* is a critical step that sets a barrier between the apical and basolateral domains, while creating a region of contact between neighbouring cells. The apical exclusion of Baz is a fundamental process in the establishment of the *ZA* (Morais-de Sá et al., 2010, Walther and Pichaud, 2010), by contributing to the coalescence of AJ material during *ZA* morphogenesis. However, the detailed mechanisms that regulate AJ morphogenesis are poorly understood. In this chapter, I presented work that suggests that Mbt is an essential regulator of *ZA* morphogenesis.

Mbt is a core component of the AJs, localising to this domain independently of *baz* (Walther et al., 2016). My work contributed to showing that Mbt functions by phosphorylating Arm and consequently promoting the accumulation of junctional proteins, such as Arm and Baz. In the absence of *mbt* function, photoreceptors display shorter junctional domains that contain less Arm and Baz, when compared to *wild-type* (Walther et al., 2016). My FRAP experiments suggest that Mbt limits the mobility of E-cad at the developing *ZA*, which I could also replicate by expressing a version of Arm that cannot be phosphorylated by Mbt in a *wild-type* background. My data therefore suggest that Mbt regulates AJ morphogenesis via phosphorylation of Arm at S561 and S688 *in vivo* (Figure 6.4). Although the obtained E-cad recovery is almost half than that measured in the *Drosophila* embryo (Bulgakova et al., 2013, Warrington et al., 2013), it is comparable to previously published data in MDCK cells (Yamada et al., 2005).

Previously published work argues that phosphorylation of Arm at S561 and S688 destabilises the interaction between E-cad and Arm in S2 cells, resulting in decreased E-cad-mediated adhesion (Menzel et al., 2008). Consequently, one would expect that loss of *mbt* should stabilise the E-cad-Arm interface. However, this is not the case *in vivo*, as we find that loss of *mbt* increases the mobility of E-cad and decreases the levels of Arm and Baz (as quantified in the length and pixel intensity of Baz/Arm positive junctional domains in Appendix C, Walther et al., 2016). One hypothesis is that Mbt promotes the stabilisation and accumulation of junctional proteins through modulation of the actin cytoskeleton. The cadherin-catenin complex is linked to F-actin, which is regulated by a vast set of actin-binding proteins. One of these proteins, Cofilin, is phosphorylated by a

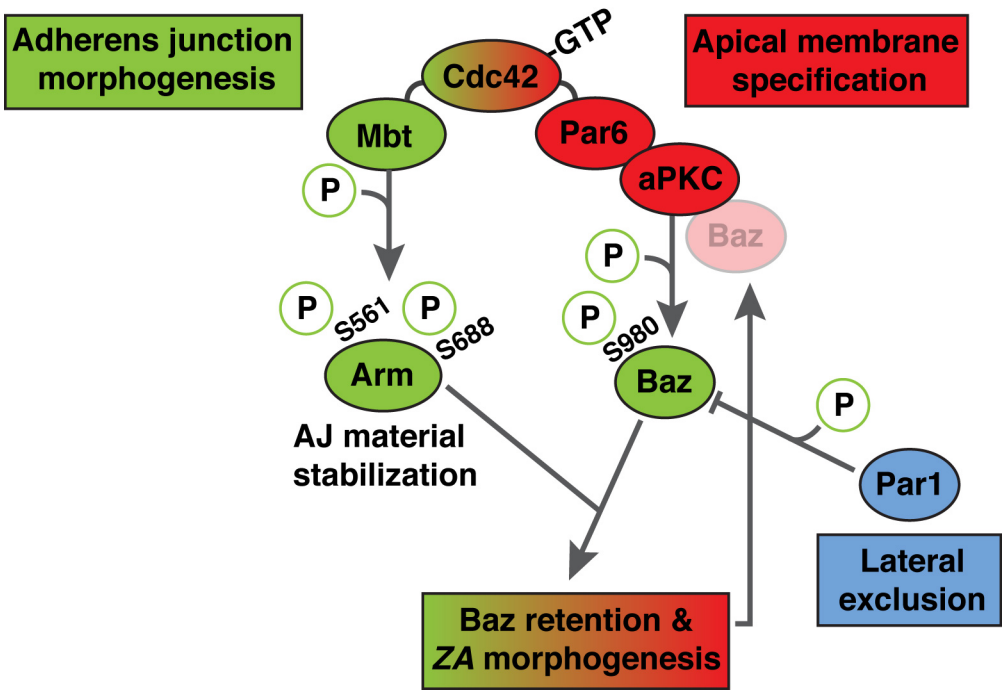

Figure 6.4: Mbt regulates AJ stability and Baz retention at the *za*. Mbt phosphorylates Arm at S561 and S688, which stabilises AJ material and promotes AJ morphogenesis. Mbt also promotes Baz retention at the *ZA*, in a mechanism that synergises with Par1-dependent lateral exclusion of Baz. Altogether, Mbt promotes *ZA* morphogenesis via regulating Arm and Baz, which in turn crosstalk with apical determinants to promote apical membrane specification.

Pak4 effector, the LIM domain kinase 1 (LIMK1) (Dan et al., 2001). More specifically, Pak4 phosphorylates LIMK1, stimulating the kinase LIMK1 to phosphorylate Cofilin, which in turn inactivates Cofilin and inhibits Cofilin-induced actin depolymerisation (Dan et al., 2001). Therefore, Pak4 has been shown to regulate actin dynamics via modulating the activity of the actin severing protein Cofilin (Dan et al., 2001). We propose that, upon loss of *mbt*, there is a decrease in Cofilin phosphorylation by LIMK1, which increases the activity of Cofilin and leads to actin depolimerisation. As a consequence, there is an increase in actin turnover that destabilises the cadherin-catenin complex and increases E-cad mobility.

In addition to regulating the dynamics of the cadherin-catenin complex, we have also shown that Mbt is required for the retention of Baz at the *ZA* (Appendix C, Walther et al., 2016). At the lateral membrane, the kinase Par1 phosphorylates Baz at two conserved serines (S151 and S1085), leading to Baz lateral exclusion (Benton and Johnston, 2003b). We showed that Mbt-dependent *ZA* retention and Par1-dependent lateral ex-

clusion of Baz are two redundant mechanisms in epithelial cells that synergise towards restricting Baz localisation to the developing *ZA* (Figure 6.4) (Appendix C, Walther et al., 2016).

Chapter 7

Discussion and Perspectives

Cdc42 is considered a master regulator of cell polarity in a variety of different organisms (Etienne-Manneville, 2004). This Rho GTPase regulates cell polarity via multiple effectors and in this thesis, I contributed to the characterisation of two of these effectors: Par6 and Mbt/Pak4. My work showed that the ability of Par6 to bind a large number of polarity determinants is crucial during development to promote apical membrane and *ZA* morphogenesis. I contributed to analysing in detail the different interfaces between Par6 and Crb, Cdc42 and aPKC, which gave us an in-depth knowledge of the individual mechanistic function of these interactions. In particular, my work showed that binding of Par6 to aPKC is required for the accumulation of both Par6 and aPKC at the apical membrane, while the interface between Par6 and Cdc42 is required to separate Par6-aPKC from P-Baz. In addition, my work has also contributed in showing that the Par6-Crb interface is required to retain Par6-aPKC at the apical domain, which promotes the establishment of clear boundaries between the *ZA* and the apical and lateral domains. Establishing this clear boundary is important for both *ZA* and apical membrane morphogenesis (Walther et al., 2016, Walther and Pichaud, 2010).

In addition, my results have shown that Par6 functions as a link between the Par complex and the exocyst, via binding to Exo84. Crb promotes apical membrane morphogenesis, and its overexpression leads to longer apical membrane domains (Pellikka et al., 2002). Altogether, I propose the Par6-Exo84 interface regulates the apical delivery of Crb, creating a delivery-based positive feedback loop that promotes apical membrane morphogenesis.

Finally, I have contributed to showing that Mbt regulates both apical membrane differentiation and *ZA* morphogenesis. My work indicates that Mbt functions by phosphorylating Arm, which promotes the accumulation of AJ material. In addition, Mbt function is redundant with that of the lateral kinase Par1 towards promoting the retention of Baz at the developing *ZA*. While *baz* and *mbt* single-mutants still present detectable levels of AJ material, *baz mbt* double-mutants on the contrary are completely depleted of junctional proteins, suggesting that Mbt and Baz function in parallel pathways towards promoting *ZA* morphogenesis.

The reason for the requirement for multiple retention mechanisms along the epithelial apical-basal axis is not clear. One possibility is the existence of a displacement flow operating in epithelial cells. According to this model, the segregation of P-Baz from Cdc42-Par6-aPKC would result from a selective basal displacement of P-Baz, which would be counterbalanced by the apical retention of Cdc42-Par6-aPKC through Crb. Similarly, at the *ZA*, Mbt would retain Baz to prevent the accumulation of ectopic microdomains of Baz at the lateral membrane. Further studies are required to validate this displacement flow and we are currently testing this approach with FRAP experiments, as well as by interfering with myosin-driven F-actin flows. Another possible model is that Par proteins are not recruited stably at the cell cortex and need to be anchored through transmembrane proteins. In line with this model, Crb would anchor Par6-aPKC at the apical membrane, while E-cad would maintain Baz at the *ZA*. These anchoring mechanisms would also act as sinks that titre Par6-aPKC and Baz, thus preventing these proteins from diffusing more basally.

One major open question is regarding the localisation of Cdc42, and more specifically, that of active GTP-bound Cdc42. Our data indicates that Cdc42 is required to assemble the Par complex, together with Baz, and to maintain Par6-aPKC at the apical domain upon Baz apical exclusion. For the Par complex to assemble at the apical membrane, Cdc42 needs to be in this domain. We have now developed a Cdc42 biosensor based on the CRIB domain of the protein WASp to allow us to visualise GTP-bound Cdc42 in *Drosophila* epithelial cells. I have recently contributed to validating this biosensor with a biochemical approach and preliminary results indicate that active Cdc42 is localised at the apical domain of the fly photoreceptor, showing a very similar distribution to Crb.

However, our recently published work shows that the Cdc42 effector, Mbt, is localised at the developing *ZA* in *Drosophila* photoreceptors. Moreover, we have shown that Mbt function requires its CRIB domain, which is known to bind to Cdc42. This might suggest that active Cdc42 is also required at the *ZA*. The Pak family of serine/threonine kinases is subdivided in two groups: type I Paks (Pak1, Pak2 and Pak3) and type II Paks (Pak4, Pak5 and Pak6) (Ha et al., 2015). While in type I Paks, binding to small GTPases activates their kinase activity, this is not the case for type II Paks (Ha et al., 2015). Most studies suggest that type II Paks are not directly activated by binding to small GTPases (Ha et al., 2015), but instead, interacting with GTPases regulates their subcellular localisation (Ha et al., 2015). Our data are in line with these studies, as we have observed that Mbt requires its CRIB domain to perform its function (Walther et al., 2016), presumably to interact with Cdc42 and properly localise at the developing *ZA*. However, this does not necessarily mean that Cdc42 must be also activated at the *ZA*, as type II Paks, such as Mbt/Pak4, do not require active Cdc42 to enhance their kinase activity.

We have proposed that the Par complex functions as a receptor for the exocyst at the plasma membrane. Components of both the Par and exocyst complexes have been linked to the phosphoinositides PIP_2 and PIP_3. Both Sec3 and Exo70 bind PIP_2, which has been shown to be essential for the polarisation of the exocyst machinery (He et al., 2007, Zhang et al., 2008). Baz is known to bind PTEN, which reduces the levels of PIP_3 in favour of PIP_2 accumulation (Pinal et al., 2006, Stein et al., 2005). Interestingly, neuroendocrine cells display microdomains at the plasma membrane with high concentrations of PIP_2, which correlate with sites of vesicle fusion (Kabachinski et al., 2014). In fact, PIP_2 has been shown to regulate exocytosis by recruiting and activating proteins like CAPS, Munc13 and synaptotagmin-1, which in turn regulate SNARE protein function during exocytosis (Kabachinski et al., 2014). One possibility is that in epithelial cells, Baz might increase the pool of membrane PIP_2 via recruiting PTEN, therefore regulating vesicle fusion.

This network of interactions between polarity determinants is extremely complex, increasing the difficulty in interpreting data. For instances, Cdc42 has a central role in trafficking, regulating for example the endocytosis of proteins such as Crb and E-cad (Georgiou et al., 2008, Harris and Tepass, 2008, Leibfried et al., 2008). Therefore, affect-

ing Cdc42 leads to massive polarity defects, not only because it affects directly the Par complex, but also as a consequence of affecting apical and junctional protein trafficking. By looking specifically at Par6 and uncoupling its interactions, one by one, we were able to overcome some of these limitations and analyse more clearly the role of different protein interactions in epithelial cell polarity.

There are still many open questions in the field of epithelial cell polarity. Even though Cdc42 is thought of as a master regulator of cell polarity, further studies are required to fully understand how symmetry is broken within epithelial cells and how polarity is initially established. For instances, how is Cdc42 activation polarised in epithelial cells? My thesis work has contributed to the field of epithelial cell polarity with in-depth knowledge of how different interfaces between polarity determinants contribute to maintain a polarised axis within epithelial cells. I have studied in detail how different proteins are retained, accumulated, localised or delivered to distinct domains of epithelial cells. Overall, understanding these mechanisms in detail is an important step towards acquiring an integrated view of how epithelial cells develop spatially distinct domains that are crucial for proper epithelial tissue morphogenesis.

References

Aberle, H., Butz, S., Stappert, J., Weissig, H., Kemler, R. and Hoschuetzky, H. (1994). Assembly of the cadherin-catenin complex in vitro with recombinant proteins. Journal of Cell Science *107*, 3655–3663.

Adams, A. E., Johnson, D. I., Longnecker, R. M., Sloat, B. F. and Pringle, J. R. (1990). CDC42 and CDC43, two additional genes involved in budding and the establishment of cell polarity in the yeast Saccharomyces cerevisiae. The Journal of Cell Biology *111*, 131–142.

Adey, N. B., Huang, L., Ormonde, P. A., Baumgard, M. L., Pero, R., Byreddy, D. V., Tavtigian, S. V. and Bartel, P. L. (2000). Threonine Phosphorylation of the MMAC1/PTEN PDZ Binding Domain Both Inhibits and Stimulates PDZ Binding. Cancer Research *60*, 35–37.

Ahmed, S. M. and Macara, I. G. (2017). The Par3 polarity protein is an exocyst receptor essential for mammary cell survival. Nature Communications *8*, 14867.

Anderson, D. C., Gill, J. S., Cinalli, R. M. and Nance, J. (2008). Polarization of the C. elegans Embryo by RhoGAP-Mediated Exclusion of PAR-6 from Cell Contacts. Science *320*, 1771–1774.

Aranda, V., Haire, T., Nolan, M. E., Calarco, J. P., Rosenberg, A. Z., Fawcett, J. P., Pawson, T. and Muthuswamy, S. K. (2006). Par6–aPKC uncouples ErbB2 induced disruption of polarized epithelial organization from proliferation control. Nature Cell Biology *8*, 1235–1245.

Arias-Romero, L. E. and Chernoff, J. (2008). A tale of two Paks. Biology of the Cell *100*, 97–108.

Arimura, N. and Kaibuchi, K. (2007). Neuronal polarity: from extracellular signals to intracellular mechanisms. Nature Reviews Neuroscience *8*, 194–205.

Assémat, E., Bazellières, E., Pallesi-Pocachard, E., Le Bivic, A. and Massey-Harroche, D. (2008). Polarity complex proteins. Biochimica et Biophysica Acta *1778*, 614–630.

Atwood, S. X., Chabu, C., Penkert, R. R., Doe, C. Q. and Prehoda, K. E. (2007). Cdc42 acts downstream of Bazooka to regulate neuroblast polarity through Par-6–aPKC. Journal of Cell Science *120*, 3200–3206.

Bachmann, A., Grawe, F., Johnson, K. and Knust, E. (2008). Drosophila Lin-7 is a component of the Crumbs complex in epithelia and photoreceptor cells and prevents light-induced retinal degeneration. European Journal of Cell Biology *87*, 123–136.

Bachmann, A., Schneider, M., Theilenberg, E., Grawe, F. and Knust, E. (2001). *Drosophila* Stardust is a partner of Crumbs in the control of epithelial cell polarity. Nature *414*, 638–643.

Bachmann, A., Timmer, M., Sierralta, J., Pietrini, G., Gundelfinger, E. D., Knust, E. and Thomas, U. (2004). Cell type-specific recruitment of Drosophila Lin-7 to distinct MAGUK-based protein complexes defines novel roles for Sdt and Dlg-S97. Journal of Cell Science *117*, 1899–1909.

Balcarova-Ständer, J., Pfeiffer, S. E., Fuller, S. D. and Simons, K. (1984). Development of cell surface polarity in the epithelial Madin-Darby canine kidney (MDCK) cell line. The EMBO Journal *3*, 2687–2694.

Bastaki, M., Braiterman, L. T., Johns, D. C., Chen, Y.-H. and Hubbard, A. L. (2002). Absence of Direct Delivery for Single Transmembrane Apical Proteins or Their "Secretory" Forms in Polarized Hepatic Cells. Molecular Biology of the Cell *13*, 225–237.

Baum, B. and Georgiou, M. (2011). Dynamics of adherens junctions in epithelial establishment, maintenance, and remodeling. The Journal of Cell Biology *192*, 907–917.

Beco, S. d., Gueudry, C., Amblard, F. and Coscoy, S. (2009). Endocytosis is required for E-cadherin redistribution at mature adherens junctions. Proceedings of the National Academy of Sciences *106*, 7010–7015.

Benton, R. and Johnston, D. S. (2003a). A Conserved Oligomerization Domain in Drosophila Bazooka/PAR-3 Is Important for Apical Localization and Epithelial Polarity. Current Biology *13*, 1330–1334.

Benton, R. and Johnston, D. S. (2003b). Drosophila PAR-1 and 14-3-3 Inhibit Bazooka/PAR-3 to Establish Complementary Cortical Domains in Polarized Cells. Cell *115*, 691–704.

Bergstralh, D. T. and Johnston, D. S. (2012). Epithelial cell polarity: what flies can teach us about cancer. Essays In Biochemistry *53*, 129–140.

Betschinger, J., Mechtler, K. and Knoblich, J. A. (2003). The Par complex directs asymmetric cell division by phosphorylating the cytoskeletal protein Lgl. Nature *422*, 326–330.

Bilder, D. and Perrimon, N. (2000). Localization of apical epithelial determinants by the basolateral PDZ protein Scribble. Nature *403*, 676–680.

Blankenship, J. T., Fuller, M. T. and Zallen, J. A. (2007). The Drosophila homolog of the Exo84 exocyst subunit promotes apical epithelial identity. Journal of Cell Science *120*, 3099–3110.

Bosch, J. A., Tran, N. H. and Hariharan, I. K. (2015). CoinFLP: a system for efficient mosaic screening and for visualizing clonal boundaries in Drosophila. Development *142*, 597–606.

Bostner, J., Waltersson, M. A., Fornander, T., Skoog, L., Nordenskjöld, B. and Stål, O. (2007). Amplification of *CCND1* and *PAK1* as predictors of recurrence and tamoxifen resistance in postmenopausal breast cancer. Oncogene *26*, 6997–7005.

Boyd, C., Hughes, T., Pypaert, M. and Novick, P. (2004). Vesicles carry most exocyst subunits to exocytic sites marked by the remaining two subunits, Sec3p and Exo70p. The Journal of Cell Biology *167*, 889–901.

Brand, A. H. and Perrimon, N. (1993). Targeted gene expression as a means of altering cell fates and generating dominant phenotypes. Development *118*, 401–415.

Brown, L. A., Kalloger, S. E., Miller, M. A., Shih, I.-M., McKinney, S. E., Santos, J. L., Swenerton, K., Spellman, P. T., Gray, J., Gilks, C. B. and Huntsman, D. G. (2008). Amplification of 11q13 in ovarian carcinoma. Genes, Chromosomes and Cancer *47*, 481–489.

Brumby, A. M. and Richardson, H. E. (2003). scribble mutants cooperate with oncogenic Ras or Notch to cause neoplastic overgrowth in Drosophila. The EMBO Journal *22*, 5769–5779.

Bryant, D. M. and Mostov, K. E. (2008). From cells to organs: building polarized tissue. Nature Reviews Molecular Cell Biology *9*, 887–901.

Buckley, C. D., Tan, J., Anderson, K. L., Hanein, D., Volkmann, N., Weis, W. I., Nelson, W. J. and Dunn, A. R. (2014). The minimal cadherin-catenin complex binds to actin filaments under force. Science *346*, 1254211.

Bulgakova, N. A., Grigoriev, I., Yap, A. S., Akhmanova, A. and Brown, N. H. (2013). Dynamic microtubules produce an asymmetric E-cadherin–Bazooka complex to maintain segment boundaries. J Cell Biol *201*, 887–901.

Bulgakova, N. A., Kempkens, Ö. and Knust, E. (2008). Multiple domains of Stardust differentially mediate localisation of the Crumbs-Stardust complex during photoreceptor development in Drosophila. Journal of Cell Science *121*, 2018–2026.

Bulgakova, N. A. and Knust, E. (2009). The Crumbs complex: from epithelial-cell polarity to retinal degeneration. Journal of Cell Science *122*, 2587–2596.

Burbelo, P. D., Drechsel, D. and Hall, A. (1995). A Conserved Binding Motif Defines Numerous Candidate Target Proteins for Both Cdc42 and Rac GTPases. Journal of Biological Chemistry *270*, 29071–29074.

Butty, A.-C., Perrinjaquet, N., Petit, A., Jaquenoud, M., Segall, J. E., Hofmann, K., Zwahlen, C. and Peter, M. (2002). A positive feedback loop stabilizes the guanine-nucleotide exchange factor Cdc24 at sites of polarization. The EMBO Journal *21*, 1565–1576.

Callow, M. G., Clairvoyant, F., Zhu, S., Schryver, B., Whyte, D. B., Bischoff, J. R., Jallal, B. and Smeal, T. (2002). Requirement for PAK4 in the Anchorage-independent Growth of Human Cancer Cell Lines. Journal of Biological Chemistry *277*, 550–558.

Celniker, S. E., Dillon, L. A. L., Gerstein, M. B., Gunsalus, K. C., Henikoff, S., Karpen, G. H., Kellis, M., Lai, E. C., Lieb, J. D., MacAlpine, D. M., Micklem, G., Piano, F., Snyder, M., Stein, L., White, K. P. and Waterston, R. H. (2009). Unlocking the secrets of the genome. Nature *459*, 927–930.

Chan, E. and Nance, J. (2013). Mechanisms of CDC-42 activation during contact-induced cell polarization. J Cell Sci *126*, 1692–1702.

Chen, J. and Zhang, M. (2013). The Par3/Par6/aPKC complex and epithelial cell polarity. Experimental Cell Research *319*, 1357–1364.

Chen, Y.-T., Stewart, D. B. and Nelson, W. J. (1999). Coupling Assembly of the E-Cadherin/β-Catenin Complex to Efficient Endoplasmic Reticulum Exit and Basal-lateral Membrane Targeting of E-Cadherin in Polarized MDCK Cells. The Journal of Cell Biology *144*, 687–699.

Cox, A. D. and Der, C. J. (1992). Protein prenylation: more than just glue? Current Opinion in Cell Biology *4*, 1008–1016.

Dan, C., Kelly, A., Bernard, O. and Minden, A. (2001). Cytoskeletal Changes Regulated by the PAK4 Serine/Threonine Kinase Are Mediated by LIM Kinase 1 and Cofilin. Journal of Biological Chemistry *276*, 32115–32121.

Das, A., Gajendra, S., Falenta, K., Oudin, M. J., Peschard, P., Feng, S., Wu, B., Marshall, C. J., Doherty, P., Guo, W. and Lalli, G. (2014). RalA promotes a direct exocyst–Par6 interaction to regulate polarity in neuronal development. J Cell Sci *127*, 686–699.

Davis, M. A., Ireton, R. C. and Reynolds, A. B. (2003). A core function for p120-catenin in cadherin turnover. J Cell Biol *163*, 525–534.

Diaz de la Loza, M. C. and Thompson, B. J. (2017). Forces shaping the Drosophila wing. Mechanisms of Development *144*, 23–32.

Doerflinger, H., Vogt, N., Torres, I. L., Mirouse, V., Koch, I., Nüsslein-Volhard, C. and Johnston, D. S. (2010). Bazooka is required for polarisation of the Drosophila anterior-posterior axis. Development *137*, 1765–1773.

Ebnet, K., Suzuki, A., Horikoshi, Y., Hirose, T., Meyer zu Brickwedde, M.-K., Ohno, S. and Vestweber, D. (2001). The cell polarity protein ASIP/PAR-3 directly associates with junctional adhesion molecule (JAM). The EMBO Journal *20*, 3738–3748.

Etienne-Manneville, S. (2004). Cdc42 - the centre of polarity. Journal of Cell Science *117*, 1291–1300.

Etienne-Manneville, S. and Hall, A. (2002). Rho GTPases in cell biology. Nature *420*, 629–635.

Eun, S. H., Lea, K., Overstreet, E., Stevens, S., Lee, J.-H. and Fischer, J. A. (2007). Identification of Genes That Interact With Drosophila liquid facets. Genetics *175*, 1163–1174.

Feng, W., Wu, H., Chan, L.-N. and Zhang, M. (2007). The Par-3 NTD adopts a PB1-like structure required for Par-3 oligomerization and membrane localization. The EMBO Journal *26*, 2786–2796.

Freeman, M. (1996). Reiterative Use of the EGF Receptor Triggers Differentiation of All Cell Types in the Drosophila Eye. Cell *87*, 651–660.

Fujita, Y., Krause, G., Scheffner, M., Zechner, D., Leddy, H. E. M., Behrens, J., Sommer, T. and Birchmeier, W. (2002). Hakai, a c-Cbl-like protein, ubiquitinates and induces endocytosis of the E-cadherin complex. Nature Cell Biology *4*, 222–231.

Garrard, S. M., Capaldo, C. T., Gao, L., Rosen, M. K., Macara, I. G. and Tomchick, D. R. (2003). Structure of Cdc42 in a complex with the GTPase-binding domain of the cell polarity protein, Par6. The EMBO Journal *22*, 1125–1133.

Gassama-Diagne, A., Yu, W., Beest, M. t., Martin-Belmonte, F., Kierbel, A., Engel, J. and Mostov, K. (2006). Phosphatidylinositol-3,4,5-trisphosphate regulates the formation of the basolateral plasma membrane in epithelial cells. Nature Cell Biology *8*, 963–970.

Gatti, A., Huang, Z., Tuazon, P. T. and Traugh, J. A. (1999). Multisite Autophosphorylation of p21-activated Protein Kinase γ-PAK as a Function of Activation. Journal of Biological Chemistry *274*, 8022–8028.

Georgiou, M., Marinari, E., Burden, J. and Baum, B. (2008). Cdc42, Par6, and aPKC regulate Arp2/3-mediated endocytosis to control local adherens junction stability. Current biology: CB *18*, 1631–1638.

Gilbert, S. F. (2000). Early Drosophila Development. 6th edition edition, Sinauer Associates, Sunderland (MA).

Goehring, N. W., Trong, P. K., Bois, J. S., Chowdhury, D., Nicola, E. M., Hyman, A. A. and Grill, S. W. (2011). Polarization of PAR Proteins by Advective Triggering of a Pattern-Forming System. Science *334*, 1137–1141.

Goentoro, L. A., Yakoby, N., Goodhouse, J., Schüpbach, T. and Shvartsman, S. Y. (2006). Quantitative analysis of the GAL4/UAS system in Drosophila oogenesis. genesis *44*, 66–74.

Golic, K. G. and Lindquist, S. (1989). The FLP recombinase of yeast catalyzes site-specific recombination in the drosophila genome. Cell *59*, 499–509.

Goryachev, A. B. and Leda, M. (2017). Many roads to symmetry breaking: molecular mechanisms and theoretical models of yeast cell polarity. Molecular Biology of the Cell *28*, 370–380.

Gotta, M. and Ahringer, J. (2001). Axis determination in C. elegans: initiating and transducing polarity. Current Opinion in Genetics & Development *11*, 367–373.

Graybill, C., Wee, B., Atwood, S. X. and Prehoda, K. E. (2012). Partitioning-defective Protein 6 (Par-6) Activates Atypical Protein Kinase C (aPKC) by Pseudosubstrate Displacement. Journal of Biological Chemistry *287*, 21003–21011.

Griffiths, G. and Simons, K. (1986). The trans Golgi network: sorting at the exit site of the Golgi complex. Science (New York, N.Y.) *234*, 438–443.

Groth, A. C., Fish, M., Nusse, R. and Calos, M. P. (2004). Construction of Transgenic Drosophila by Using the Site-Specific Integrase From Phage PhiC31. Genetics *166*, 1775–1782.

Guo, W., Grant, A. and Novick, P. (1999). Exo84p Is an Exocyst Protein Essential for Secretion. Journal of Biological Chemistry *274*, 23558–23564.

Ha, B. H., Morse, E. M., Turk, B. E. and Boggon, T. J. (2015). Signaling, Regulation, and Specificity of the Type II p21-activated Kinases. Journal of Biological Chemistry *290*, 12975–12983.

Haack, T., Bergstralh, D. T. and St Johnston, D. (2013). Damage to the Drosophila follicle cell epithelium produces "false clones" with apparent polarity phenotypes. Biology Open *2*, 1313–1320.

Hammerton, R. W., Krzeminski, K. A., Mays, R. W., Ryan, T. A., Wollner, D. A. and Nelson, W. J. (1991). Mechanism for regulating cell surface distribution of Na+,K(+)-ATPase in polarized epithelial cells. Science *254*, 847–850.

Hao, Y., Boyd, L. and Seydoux, G. (2006). Stabilization of Cell Polarity by the C. elegans RING Protein PAR-2. Developmental Cell *10*, 199–208.

Harris, K. P. and Tepass, U. (2008). Cdc42 and Par proteins stabilize dynamic adherens junctions in the Drosophila neuroectoderm through regulation of apical endocytosis. J Cell Biol *183*, 1129–1143.

Harris, K. P. and Tepass, U. (2010). Cdc42 and Vesicle Trafficking in Polarized Cells. Traffic *11*, 1272–1279.

Harris, T. J. C. and Peifer, M. (2005). The positioning and segregation of apical cues during epithelial polarity establishment in Drosophila. J Cell Biol *170*, 813–823.

Harris, T. J. C. and Tepass, U. (2010). Adherens junctions: from molecules to morphogenesis. Nature Reviews Molecular Cell Biology *11*, 502–514.

Hazelett, C. C. and Yeaman, C. (2012). Sec5 and Exo84 Mediate Distinct Aspects of RalA-Dependent Cell Polarization. PLoS ONE *7*, e39602.

He, B., Xi, F., Zhang, X., Zhang, J. and Guo, W. (2007). Exo70 interacts with phospholipids and mediates the targeting of the exocyst to the plasma membrane. The EMBO Journal *26*, 4053–4065.

Heider, M. R. and Munson, M. (2012). Exorcising the Exocyst Complex. Traffic (Copenhagen, Denmark) *13*, 898–907.

Henrique, D. and Schweisguth, F. (2003). Cell polarity: the ups and downs of the Par6/aPKC complex. Current Opinion in Genetics & Development *13*, 341–350.

Hong, Y., Stronach, B., Perrimon, N., Jan, L. Y. and Jan, Y. N. (2001). *Drosophila* Stardust interacts with Crumbs to control polarity of epithelia but not neuroblasts. Nature *414*, 634–638.

Hurd, T. W., Gao, L., Roh, M. H., Macara, I. G. and Margolis, B. (2003). Direct interaction of two polarity complexes implicated in epithelial tight junction assembly. Nature Cell Biology *5*, 137–142.

Hurov, J. B., Watkins, J. L. and Piwnica-Worms, H. (2004). Atypical PKC Phosphorylates PAR-1 Kinases to Regulate Localization and Activity. Current Biology *14*, 736–741.

Husain, N., Pellikka, M., Hong, H., Klimentova, T., Choe, K.-M., Clandinin, T. R. and Tepass, U. (2006). The Agrin/Perlecan-Related Protein Eyes Shut Is Essential for Epithelial Lumen Formation in the Drosophila Retina. Developmental Cell *11*, 483–493.

Hutterer, A., Betschinger, J., Petronczki, M. and Knoblich, J. A. (2004). Sequential Roles of

Cdc42, Par-6, aPKC, and Lgl in the Establishment of Epithelial Polarity during Drosophila Embryogenesis. Developmental Cell *6*, 845–854.

Huynh, J.-R., Petronczki, M., Knoblich, J. A. and Johnston, D. S. (2001). Bazooka and PAR-6 are required with PAR-1 for the maintenance of oocyte fate in Drosophila. Current Biology *11*, 901–906.

Hwa, J. J. and Clandinin, T. R. (2012). Apical-Basal Polarity Proteins Are Required Cell-Type Specifically to Direct Photoreceptor Morphogenesis. Current Biology *22*, 2319–2324.

Ito, M., Nishiyama, H., Kawanishi, H., Matsui, S., Guilford, P., Reeve, A. and Ogawa, O. (2007). P21-Activated Kinase 1: A New Molecular Marker for Intravesical Recurrence After Transurethral Resection of Bladder Cancer. The Journal of Urology *178*, 1073–1079.

Itoh, M., Sasaki, H., Furuse, M., Ozaki, H., Kita, T. and Tsukita, S. (2001). Junctional adhesion molecule (JAM) binds to PAR-3. The Journal of Cell Biology *154*, 491–498.

Izaddoost, S., Nam, S.-C., Bhat, M. A., Bellen, H. J. and Choi, K.-W. (2002). Drosophila Crumbs is a positional cue in photoreceptor adherens junctions and rhabdomeres. Nature *416*, 178–183.

Izumi, Y., Hirose, T., Tamai, Y., Hirai, S.-i., Nagashima, Y., Fujimoto, T., Tabuse, Y., Kemphues, K. J. and Ohno, S. (1998). An Atypical PKC Directly Associates and Colocalizes at the Epithelial Tight Junction with ASIP, a Mammalian Homologue of Caenorhabditis elegans Polarity Protein PAR-3. The Journal of Cell Biology *143*, 95–106.

Jin, D., Durgan, J. and Hall, A. (2015). Functional cross-talk between Cdc42 and two downstream targets, Par6B and PAK4. The Biochemical Journal *467*, 293–302.

Joberty, G., Petersen, C., Gao, L. and Macara, I. G. (2000). The cell-polarity protein Par6 links Par3 and atypical protein kinase C to Cdc42. Nature Cell Biology *2*, 531–539.

Johnston, C. A., Hirono, K., Prehoda, K. E. and Doe, C. Q. (2009). Identification of an Aurora-A/PinsLINKER/Dlg spindle orientation pathway using induced cell polarity in S2 cells. Cell *138*, 1150–1163.

Johnston, D. S. and Ahringer, J. (2010). Cell Polarity in Eggs and Epithelia: Parallels and Diversity. Cell *141*, 757–774.

Kabachinski, G., Yamaga, M., Kielar-Grevstad, D. M., Bruinsma, S. and Martin, T. F. J. (2014). CAPS and Munc13 utilize distinct PIP2-linked mechanisms to promote vesicle exocytosis. Molecular Biology of the Cell *25*, 508–521.

Karp, C. M., Tan, T. T., Mathew, R., Nelson, D., Mukherjee, C., Degenhardt, K., Karantza-

Wadsworth, V. and White, E. (2008). Role of the Polarity Determinant Crumbs in Suppressing Mammalian Epithelial Tumor Progression. Cancer research *68*, 4105–4115.

Keller, P., Toomre, D., Díaz, E., White, J. and Simons, K. (2001). Multicolour imaging of post-Golgi sorting and trafficking in live cells. Nature Cell Biology *3*, 140–149.

Kemler, R. (1992). Classical cadherins. Seminars in Cell Biology *3*, 149–155.

Kemphues, K. J., Priess, J. R., Morton, D. G. and Cheng, N. (1988). Identification of genes required for cytoplasmic localization in early C. elegans embryos. Cell *52*, 311–320.

Kempkens, Ö., Médina, E., Fernandez-Ballester, G., Özüyaman, S., Le Bivic, A., Serrano, L. and Knust, E. (2006). Computer modelling in combination with in vitro studies reveals similar binding affinities of Drosophila Crumbs for the PDZ domains of Stardust and DmPar-6. European Journal of Cell Biology *85*, 753–767.

Kim, A. S., Kakalis, L. T., Abdul-Manan, N., Liu, G. A. and Rosen, M. K. (2000). Autoinhibition and activation mechanisms of the Wiskott–Aldrich syndrome protein. Nature *404*, 151–158.

Kim, S., Gailite, I., Moussian, B., Luschnig, S., Goette, M., Fricke, K., Honemann-Capito, M., Grubmüller, H. and Wodarz, A. (2009). Kinase-activity-independent functions of atypical protein kinase C in Drosophila. Journal of Cell Science *122*, 3759–3771.

Knust, E., Tepaß, U. and Wodarz, A. (1993). crumbs and stardust, two genes of Drosophila required for the development of epithelial cell polarity. Development *119*, 261–268.

Krahn, M. P., Buckers, J., Kastrup, L. and Wodarz, A. (2010a). Formation of a Bazooka-Stardust complex is essential for plasma membrane polarity in epithelia. The Journal of Cell Biology *190*, 751–760.

Krahn, M. P., Klopfenstein, D. R., Fischer, N. and Wodarz, A. (2010b). Membrane Targeting of Bazooka/PAR-3 Is Mediated by Direct Binding to Phosphoinositide Lipids. Current Biology *20*, 636–642.

Kuphal, S., Wallner, S., Schimanski, C. C., Bataille, F., Hofer, P., Strand, S., Strand, D. and Bosserhoff, A. K. (2006). Expression of *Hugl-1* is strongly reduced in malignant melanoma. Oncogene *25*, 103–110.

Lalli, G. (2009). RalA and the exocyst complex influence neuronal polarity through PAR-3 and aPKC. Journal of Cell Science *122*, 1499–1506.

Langevin, J., Morgan, M. J., Rossé, C., Racine, V., Sibarita, J.-B., Aresta, S., Murthy, M., Schwarz, T., Camonis, J. and Bellaïche, Y. (2005). Drosophila Exocyst Components Sec5,

Sec6, and Sec15 Regulate DE-Cadherin Trafficking from Recycling Endosomes to the Plasma Membrane. Developmental Cell *9*, 365–376.

Laprise, P., Beronja, S., Silva-Gagliardi, N. F., Pellikka, M., Jensen, A. M., McGlade, C. J. and Tepass, U. (2006). The FERM Protein Yurt Is a Negative Regulatory Component of the Crumbs Complex that Controls Epithelial Polarity and Apical Membrane Size. Developmental cell *11*, 363–374.

Laprise, P., Viel, A. and Rivard, N. (2004). Human Homolog of Disc-large Is Required for Adherens Junction Assembly and Differentiation of Human Intestinal Epithelial Cells. Journal of Biological Chemistry *279*, 10157–10166.

Lee, M. and Vasioukhin, V. (2008). Cell polarity and cancer – cell and tissue polarity as a non-canonical tumor suppressor. Journal of Cell Science *121*, 1141–1150.

Lee, T. and Luo, L. (1999). Mosaic Analysis with a Repressible Cell Marker for Studies of Gene Function in Neuronal Morphogenesis. Neuron *22*, 451–461.

Lee, T. and Luo, L. (2001). Mosaic analysis with a repressible cell marker (MARCM) for Drosophila neural development. Trends in Neurosciences *24*, 251–254.

Lei, M., Lu, W., Meng, W., Parrini, M.-C., Eck, M. J., Mayer, B. J. and Harrison, S. C. (2000). Structure of PAK1 in an Autoinhibited Conformation Reveals a Multistage Activation Switch. Cell *102*, 387–397.

Leibfried, A., Fricke, R., Morgan, M. J., Bogdan, S. and Bellaiche, Y. (2008). Drosophila Cip4 and WASp Define a Branch of the Cdc42-Par6-aPKC Pathway Regulating E-Cadherin Endocytosis. Current Biology *18*, 1639–1648.

Lemmers, C., Michel, D., Lane-Guermonprez, L., Delgrossi, M.-H., Médina, E., Arsanto, J.-P. and Bivic, A. L. (2004). CRB3 Binds Directly to Par6 and Regulates the Morphogenesis of the Tight Junctions in Mammalian Epithelial Cells. Molecular Biology of the Cell *15*, 1324–1333.

Li, B. X., Satoh, A. K. and Ready, D. F. (2007). Myosin V, Rab11, and dRip11 direct apical secretion and cellular morphogenesis in developing Drosophila photoreceptors. The Journal of Cell Biology *177*, 659–669.

Li, J., Kim, H., Aceto, D. G., Hung, J., Aono, S. and Kemphues, K. J. (2010). Binding to PKC-3, but not to PAR-3 or to a conventional PDZ domain ligand, is required for PAR-6 function in C. elegans. Developmental Biology *340*, 88–98.

Lin, D., Edwards, A. S., Fawcett, J. P., Mbamalu, G., Scott, J. D. and Pawson, T. (2000). A mammalian PAR-3–PAR-6 complex implicated in Cdc42/Rac1 and aPKC signalling and cell polarity. Nature Cell Biology *2*, 540–547.

Lock, J. G. and Stow, J. L. (2005). Rab11 in Recycling Endosomes Regulates the Sorting and Basolateral Transport of E-Cadherin. Molecular Biology of the Cell *16*, 1744–1755.

Lu, H. and Bilder, D. (2005). Endocytic control of epithelial polarity and proliferation in *Drosophila*. Nature Cell Biology *7*, 1232–1239.

Mahlamäki, E. H., Kauraniemi, P., Monni, O., Wolf, M., Hautaniemi, S. and Kallioniemi, A. (2004). High-Resolution Genomic and Expression Profiling Reveals 105 Putative Amplification Target Genes in Pancreatic Cancer. Neoplasia (New York, N.Y.) *6*, 432–439.

Margolis, J. and Spradling, A. (1995). Identification and behavior of epithelial stem cells in the Drosophila ovary. Development *121*, 3797–3807.

Martin-Belmonte, F., Gassama, A., Datta, A., Yu, W., Rescher, U., Gerke, V. and Mostov, K. (2007). PTEN-mediated segregation of phosphoinositides at the apical membrane controls epithelial morphogenesis through Cdc42. Cell *128*, 383–397.

Martin-Belmonte, F. and Perez-Moreno, M. (2012). Epithelial cell polarity, stem cells and cancer. Nature Reviews Cancer *12*, 23–38.

Matern, H. T., Yeaman, C., Nelson, W. J. and Scheller, R. H. (2001). The Sec6/8 complex in mammalian cells: Characterization of mammalian Sec3, subunit interactions, and expression of subunits in polarized cells. Proceedings of the National Academy of Sciences *98*, 9648–9653.

McGill, M. A., McKinley, R. F. A. and Harris, T. J. C. (2009). Independent cadherin–catenin and Bazooka clusters interact to assemble adherens junctions. The Journal of Cell Biology *185*, 787–796.

Mei, K., Li, Y., Wang, S., Shao, G., Wang, J., Ding, Y., Luo, G., Yue, P., Liu, J.-J., Wang, X., Dong, M.-Q., Wang, H.-W. and Guo, W. (2018). Cryo-EM structure of the exocyst complex. Nature Structural & Molecular Biology *25*, 139–146.

Mellman, I. and Nelson, W. J. (2008). Coordinated protein sorting, targeting and distribution in polarized cells. Nature Reviews Molecular Cell Biology *9*, 833–845.

Menzel, N., Melzer, J., Waschke, J., Lenz, C., Wecklein, H., Lochnit, G., Drenckhahn, D. and Raabe, T. (2008). The Drosophila p21-activated kinase Mbt modulates DE-cadherin-mediated cell adhesion by phosphorylation of Armadillo. The Biochemical Journal *416*, 231–241.

Molitoris, B. A. and Nelson, W. J. (1990). Alterations in the establishment and maintenance of epithelial cell polarity as a basis for disease processes. Journal of Clinical Investigation *85*, 3–9.

Morais-de Sá, E., Mirouse, V. and St Johnston, D. (2010). aPKC Phosphorylation of Bazooka Defines the Apical/Lateral Border in Drosophila Epithelial Cells. Cell *141*, 509–523.

Moskalenko, S., Henry, D. O., Rosse, C., Mirey, G., Camonis, J. H. and White, M. A. (2002). The exocyst is a Ral effector complex. Nature Cell Biology *4*, 66–72.

Moskalenko, S., Tong, C., Rosse, C., Mirey, G., Formstecher, E., Daviet, L., Camonis, J. and White, M. A. (2003). Ral GTPases Regulate Exocyst Assembly through Dual Subunit Interactions. Journal of Biological Chemistry *278*, 51743–51748.

Mostov, K. E. (1994). Transepithelial Transport of Immunoglobulins. Annual Review of Immunology *12*, 63–84.

Motegi, F., Zonies, S., Hao, Y., Cuenca, A. A., Griffin, E. and Seydoux, G. (2011). Microtubules induce self-organization of polarized PAR domains in *Caenorhabditis elegans* zygotes. Nature Cell Biology *13*, 1361–1367.

Müller, H.-A. J. (2000). Genetic control of epithelial cell polarity: Lessons from Drosophila. Developmental Dynamics *218*, 52–67.

Munro, E., Nance, J. and Priess, J. R. (2004). Cortical Flows Powered by Asymmetrical Contraction Transport PAR Proteins to Establish and Maintain Anterior-Posterior Polarity in the Early C. elegans Embryo. Developmental Cell *7*, 413–424.

Murthy, M., Garza, D., Scheller, R. H. and Schwarz, T. L. (2003). Mutations in the exocyst component Sec5 disrupt neuronal membrane traffic, but neurotransmitter release persists. Neuron *37*, 433–447.

Nagai-Tamai, Y., Mizuno, K., Hirose, T., Suzuki, A. and Ohno, S. (2002). Regulated protein-protein interaction between aPKC and PAR-3 plays an essential role in the polarization of epithelial cells. Genes to Cells: Devoted to Molecular & Cellular Mechanisms *7*, 1161–1171.

Nakaya, M., Fukui, A., Izumi, Y., Akimoto, K., Asashima, M. and Ohno, S. (2000). Meiotic maturation induces animal-vegetal asymmetric distribution of aPKC and ASIP/PAR-3 in Xenopus oocytes. Development *127*, 5021–5031.

Nam, S.-C. and Choi, K.-W. (2003). Interaction of Par-6 and Crumbs complexes is essential for photoreceptor morphogenesis in Drosophila. Development *130*, 4363–4372.

Nam, S.-C. and Choi, K.-W. (2006). Domain-specific early and late function of Dpatj in Drosophila photoreceptor cells. Developmental Dynamics *235*, 1501–1507.

Nam, S.-C., Mukhopadhyay, B. and Choi, K.-W. (2007). Antagonistic functions of Par-1 ki-

nase and protein phosphatase 2A are required for localization of Bazooka and photoreceptor morphogenesis in Drosophila. Developmental biology *306*, 624–635.

Nelson, W. J. (2003). Adaptation of core mechanisms to generate cell polarity. Nature *422*, 766–774.

Newsome, T. P., Asling, B. and Dickson, B. J. (2000). Analysis of Drosophila photoreceptor axon guidance in eye-specific mosaics. Development *127*, 851–860.

Nobes, C. D. and Hall, A. (1995). Rho, rac, and cdc42 GTPases regulate the assembly of multimolecular focal complexes associated with actin stress fibers, lamellipodia, and filopodia. Cell *81*, 53–62.

Noda, Y., Kohjima, M., Izaki, T., Ota, K., Yoshinaga, S., Inagaki, F., Ito, T. and Sumimoto, H. (2003). Molecular Recognition in Dimerization between PB1 Domains. Journal of Biological Chemistry *278*, 43516–43524.

Nolan, M. E., Aranda, V., Lee, S., Lakshmi, B., Basu, S., Allred, D. C. and Muthuswamy, S. K. (2008). The Polarity Protein Par6 Induces Cell Proliferation and Is Overexpressed in Breast Cancer. Cancer Research *68*, 8201–8209.

Oda, H. and Tsukita, S. (2001). Real-time imaging of cell-cell adherens junctions reveals that Drosophila mesoderm invagination begins with two phases of apical constriction of cells. Journal of Cell Science *114*, 493–501.

Palacios, F., Tushir, J. S., Fujita, Y. and D'Souza-Schorey, C. (2005). Lysosomal Targeting of E-Cadherin: a Unique Mechanism for the Down-Regulation of Cell-Cell Adhesion during Epithelial to Mesenchymal Transitions. Molecular and Cellular Biology *25*, 389–402.

Pellikka, M., Tanentzapf, G., Pinto, M., Smith, C., McGlade, C. J., Ready, D. F. and Tepass, U. (2002). Crumbs, the Drosophila homologue of human CRB1/RP12, is essential for photoreceptor morphogenesis. Nature *416*, 143–149.

Perrimon, N. (1988). The maternal effect of lethal(1)discs-large-1: A recessive oncogene of Drosophila melanogaster. Developmental Biology *127*, 392–407.

Peterson, F. C., Penkert, R. R., Volkman, B. F. and Prehoda, K. E. (2004). Cdc42 Regulates the Par-6 PDZ Domain through an Allosteric CRIB-PDZ Transition. Molecular Cell *13*, 665–676.

Petronczki, M. and Knoblich, J. A. (2001). DmPAR-6 directs epithelial polarity and asymmetric cell division of neuroblasts in *Drosophila*. Nature Cell Biology *3*, 43.

Pichaud, F. (2018). PAR-Complex and Crumbs Function During Photoreceptor Morphogenesis and Retinal Degeneration. Frontiers in Cellular Neuroscience *12*.

Pinal, N., Goberdhan, D. C. I., Collinson, L., Fujita, Y., Cox, I. M., Wilson, C. and Pichaud, F. (2006). Regulated and Polarized PtdIns(3,4,5)P3 Accumulation Is Essential for Apical Membrane Morphogenesis in Photoreceptor Epithelial Cells. Current Biology *16*, 140–149.

Pires, H. R. and Boxem, M. (2017). Mapping the Polarity Interactome. Journal of Molecular Biology *https://doi.org/10.1016/j.jmb.2017.12.017*.

Plant, P. J., Fawcett, J. P., Lin, D. C. C., Holdorf, A. D., Binns, K., Kulkarni, S. and Pawson, T. (2003). A polarity complex of mPar-6 and atypical PKC binds, phosphorylates and regulates mammalian Lgl. Nature Cell Biology *5*, 301–308.

Pocha, S. M., Wassmer, T., Niehage, C., Hoflack, B. and Knust, E. (2011). Retromer Controls Epithelial Cell Polarity by Trafficking the Apical Determinant Crumbs. Current Biology *21*, 1111–1117.

Pruyne, D., Legesse-Miller, A., Gao, L., Dong, Y. and Bretscher, A. (2004). Mechanisms of Polarized Growth and Organelle Segregation in Yeast. Annual Review of Cell and Developmental Biology *20*, 559–591.

Qiu, R.-G., Abo, A. and Martin, G. S. (2000). A human homolog of the C. elegans polarity determinant Par-6 links Rac and Cdc42 to PKCζ signaling and cell transformation. Current Biology *10*, 697–707.

Rane, C. K. and Minden, A. (2014). P21 activated kinases. Small GTPases *5*, e28003.

Rapsomaniki, M. A., Kotsantis, P., Symeonidou, I.-E., Giakoumakis, N.-N., Taraviras, S. and Lygerou, Z. (2012). easyFRAP: an interactive, easy-to-use tool for qualitative and quantitative analysis of FRAP data. Bioinformatics *28*, 1800–1801.

Reiter, L. T., Potocki, L., Chien, S., Gribskov, M. and Bier, E. (2001). A Systematic Analysis of Human Disease-Associated Gene Sequences In Drosophila melanogaster. Genome Research *11*, 1114–1125.

Renschler, F. A., Bruekner, S. R., Salomon, P. L., Mukherjee, A., Kullmann, L., Schütz-Stoffregen, M. C., Henzler, C., Pawson, T., Krahn, M. P. and Wiesner, S. (2018). Structural basis for the interaction between the cell polarity proteins Par3 and Par6. Sci. Signal. *11*, eaam9899.

Rodriguez, J., Peglion, F., Martin, J., Hubatsch, L., Reich, J., Hirani, N., Gubieda, A. G., Roffey, J., Fernandes, A. R., Johnston, D. S., Ahringer, J. and Goehring, N. W. (2017). aPKC Cycles between Functionally Distinct PAR Protein Assemblies to Drive Cell Polarity. Developmental Cell *42*, 400–415.e9.

Roeth, J. F., Sawyer, J. K., Wilner, D. A. and Peifer, M. (2009). Rab11 Helps Maintain Apical

Crumbs and Adherens Junctions in the Drosophila Embryonic Ectoderm. PLOS ONE *4*, e7634.

Roh, M. H., Fan, S., Liu, C.-J. and Margolis, B. (2003). The Crumbs3-Pals1 complex participates in the establishment of polarity in mammalian epithelial cells. Journal of Cell Science *116*, 2895–2906.

Roh, M. H., Makarova, O., Liu, C.-J., Shin, Lee, S., Laurinec, S., Goyal, M., Wiggins, R. and Margolis, B. (2002). The Maguk protein, Pals1, functions as an adapter, linking mammalian homologues of Crumbs and Discs Lost. The Journal of Cell Biology *157*, 161–172.

Rohatgi, R., Ma, L., Miki, H., Lopez, M., Kirchhausen, T., Takenawa, T. and Kirschner, M. W. (1999). The Interaction between N-WASP and the Arp2/3 Complex Links Cdc42-Dependent Signals to Actin Assembly. Cell *97*, 221–231.

Rothenberg, S. M., Mohapatra, G., Rivera, M. N., Winokur, D., Greninger, P., Nitta, M., Sadow, P. M., Sooriyakumar, G., Brannigan, B. W., Ulman, M. J., Perera, R. M., Wang, R., Tam, A., Ma, X.-J., Erlander, M., Sgroi, D. C., Rocco, J. W., Lingen, M. W., Cohen, E. E., Louis, D. N., Settleman, J. and Haber, D. A. (2010). A genome-wide screen for microdeletions reveals disruption of polarity complex genes in diverse human cancers. Cancer research *70*, 2158–2164.

Royer, C. and Lu, X. (2011). Epithelial cell polarity: a major gatekeeper against cancer? Cell Death and Differentiation *18*, 1470–1477.

Rubin, G. M. and Spradling, A. C. (1982). Genetic transformation of Drosophila with transposable element vectors. Science *218*, 348–353.

Satoh, A. K., O'Tousa, J. E., Ozaki, K. and Ready, D. F. (2005). Rab11 mediates post-Golgi trafficking of rhodopsin to the photosensitive apical membrane of Drosophila photoreceptors. Development *132*, 1487–1497.

Schindelin, J., Arganda-Carreras, I., Frise, E., Kaynig, V., Longair, M., Pietzsch, T., Preibisch, S., Rueden, C., Saalfeld, S., Schmid, B., Tinevez, J.-Y., White, D. J., Hartenstein, V., Eliceiri, K., Tomancak, P. and Cardona, A. (2012). Fiji: an open-source platform for biological-image analysis. Nature Methods *9*, 676–682.

Schneeberger, D. and Raabe, T. (2003). Mbt, a Drosophila PAK protein, combines with Cdc42 to regulate photoreceptor cell morphogenesis. Development *130*, 427–437.

Sen, A., Nagy-Zsvér-Vadas, Z. and Krahn, M. P. (2012). Drosophila PATJ supports adherens junction stability by modulating Myosin light chain activity. J Cell Biol *199*, 685–698.

Shahab, J., Tiwari, M. D., Honemann-Capito, M., Krahn, M. P. and Wodarz, A. (2015).

Bazooka/PAR3 is dispensable for polarity in Drosophila follicular epithelial cells. Biology Open *4*, 528–541.

Sievers, F., Wilm, A., Dineen, D., Gibson, T. J., Karplus, K., Li, W., Lopez, R., McWilliam, H., Remmert, M., Söding, J., Thompson, J. D. and Higgins, D. G. (2011). Fast, scalable generation of high-quality protein multiple sequence alignments using Clustal Omega. Molecular Systems Biology *7*, 539.

Sotillos, S., Díaz-Meco, M. T., Caminero, E., Moscat, J. and Campuzano, S. (2004). DaPKC-dependent phosphorylation of Crumbs is required for epithelial cell polarity in Drosophila. The Journal of Cell Biology *166*, 549–557.

Spaderna, S., Schmalhofer, O., Wahlbuhl, M., Dimmler, A., Bauer, K., Sultan, A., Hlubek, F., Jung, A., Strand, D., Eger, A., Kirchner, T., Behrens, J. and Brabletz, T. (2008). The Transcriptional Repressor ZEB1 Promotes Metastasis and Loss of Cell Polarity in Cancer. Cancer Research *68*, 537–544.

Staudt, N., Molitor, A., Somogyi, K., Mata, J., Curado, S., Eulenberg, K., Meise, M., Siegmund, T., Häder, T., Hilfiker, A., Brönner, G., Ephrussi, A., Rørth, P., Cohen, S. M., Fellert, S., Chung, H.-R., Piepenburg, O., Schäfer, U., Jäckle, H. and Vorbrüggen, G. (2005). Gain-of-Function Screen for Genes That Affect Drosophila Muscle Pattern Formation. PLoS Genetics *1*.

Stein, W. v., Ramrath, A., Grimm, A., Müller-Borg, M. and Wodarz, A. (2005). Direct association of Bazooka/PAR-3 with the lipid phosphatase PTEN reveals a link between the PAR/aPKC complex and phosphoinositide signaling. Development *132*, 1675–1686.

Stocker, H. and Gallant, P. (2008). Getting Started. In Drosophila Methods in Molecular Biology pp. 27–44. Humana Press.

Straight, S. W., Shin, K., Fogg, V. C., Fan, S., Liu, C.-J., Roh, M. and Margolis, B. (2004). Loss of PALS1 Expression Leads to Tight Junction and Polarity Defects. Molecular Biology of the Cell *15*, 1981–1990.

Sugihara, K., Asano, S., Tanaka, K., Iwamatsu, A., Okawa, K. and Ohta, Y. (2002). The exocyst complex binds the small GTPase RalA to mediate filopodia formation. Nature Cell Biology *4*, 73–78.

Suzuki, A., Yamanaka, T., Hirose, T., Manabe, N., Mizuno, K., Shimizu, M., Akimoto, K., Izumi, Y., Ohnishi, T. and Ohno, S. (2001). Atypical Protein Kinase C Is Involved in the Evolutionarily Conserved Par Protein Complex and Plays a Critical Role in Establishing Epithelia-Specific Junctional Structures. The Journal of Cell Biology *152*, 1183–1196.

Symons, M., Derry, J. M. J., Karlak, B., Jiang, S., Lemahieu, V., McCormick, F., Francke, U. and Abo, A. (1996). Wiskott–Aldrich Syndrome Protein, a Novel Effector for the GTPase CDC42Hs, Is Implicated in Actin Polymerization. Cell *84*, 723–734.

Tabuse, Y., Izumi, Y., Piano, F., Kemphues, K. J., Miwa, J. and Ohno, S. (1998). Atypical protein kinase C cooperates with PAR-3 to establish embryonic polarity in Caenorhabditis elegans. Development *125*, 3607–3614.

Takekuni, K., Ikeda, W., Fujito, T., Morimoto, K., Takeuchi, M., Monden, M. and Takai, Y. (2003). Direct Binding of Cell Polarity Protein PAR-3 to Cell-Cell Adhesion Molecule Nectin at Neuroepithelial Cells of Developing Mouse. Journal of Biological Chemistry *278*, 5497–5500.

Tanentzapf, G. and Tepass, U. (2003). Interactions between the *crumbs*, *lethal giant larvae* and *bazooka* pathways in epithelial polarization. Nature Cell Biology *5*, 46–52.

Tepass, U. (2012). The Apical Polarity Protein Network in Drosophila Epithelial Cells: Regulation of Polarity, Junctions, Morphogenesis, Cell Growth, and Survival. Annual Review of Cell and Developmental Biology *28*, 655–685.

Tepass, U. and Harris, K. P. (2007). Adherens junctions in Drosophila retinal morphogenesis. Trends in Cell Biology *17*, 26–35.

Tepass, U., Tanentzapf, G., Ward, R. and Fehon, R. (2001). Epithelial Cell Polarity and Cell Junctions in Drosophila. Annual Review of Genetics *35*, 747–784.

TerBush, D. R., Maurice, T., Roth, D. and Novick, P. (1996). The Exocyst is a multiprotein complex required for exocytosis in Saccharomyces cerevisiae. The EMBO Journal *15*, 6483–6494.

Tian, Y., Lei, L. and Minden, A. (2011). A key role for Pak4 in proliferation and differentiation of neural progenitor cells. Developmental Biology *353*, 206–216.

Vega-Salas, D. E., Salas, P. J., Gundersen, D. and Rodriguez-Boulan, E. (1987). Formation of the apical pole of epithelial (Madin-Darby canine kidney) cells: polarity of an apical protein is independent of tight junctions while segregation of a basolateral marker requires cell-cell interactions. The Journal of Cell Biology *104*, 905–916.

Wallace, S. W., Durgan, J., Jin, D. and Hall, A. (2010). Cdc42 Regulates Apical Junction Formation in Human Bronchial Epithelial Cells through PAK4 and Par6B. Molecular Biology of the Cell *21*, 2996–3006.

Walther, R. F., Burki, M., Pinal, N., Rogerson, C. and Pichaud, F. (2018). Rap1, canoe and

Mbt cooperate with Bazooka to promote zonula adherens assembly in the fly photoreceptor. J Cell Sci *131*, jcs.207779.

Walther, R. F., Nunes de Almeida, F., Vlassaks, E., Burden, J. J. and Pichaud, F. (2016). Pak4 Is Required during Epithelial Polarity Remodeling through Regulating AJ Stability and Bazooka Retention at the ZA. Cell Reports *15*, 45–53.

Walther, R. F. and Pichaud, F. (2006). Immunofluorescent staining and imaging of the pupal and adult *Drosophila* visual system. Nature Protocols *1*, 2635–2642.

Walther, R. F. and Pichaud, F. (2010). Crumbs/DaPKC-Dependent Apical Exclusion of Bazooka Promotes Photoreceptor Polarity Remodeling. Current Biology *20*, 1065–1074.

Wang, A. Z., Ojakian, G. K. and Nelson, W. J. (1990). Steps in the morphogenesis of a polarized epithelium. I. Uncoupling the roles of cell-cell and cell-substratum contact in establishing plasma membrane polarity in multicellular epithelial (MDCK) cysts. Journal of Cell Science *95*, 137–151.

Wang, Q., Hurd, T. W. and Margolis, B. (2004). Tight Junction Protein Par6 Interacts with an Evolutionarily Conserved Region in the Amino Terminus of PALS1/Stardust. Journal of Biological Chemistry *279*, 30715–30721.

Warrington, S. J., Strutt, H. and Strutt, D. (2013). The Frizzled-dependent planar polarity pathway locally promotes E-cadherin turnover via recruitment of RhoGEF2. Development *140*, 1045–1054.

Watanabe, T., Noritake, J. and Kaibuchi, K. (2005). Regulation of microtubules in cell migration. Trends in Cell Biology *15*, 76–83.

Watts, J. L., Etemad-Moghadam, B., Guo, S., Boyd, L., Draper, B. W., Mello, C. C., Priess, J. R. and Kemphues, K. J. (1996). par-6, a gene involved in the establishment of asymmetry in early C. elegans embryos, mediates the asymmetric localization of PAR-3. Development *122*, 3133–3140.

Wee, B., Johnston, C. A., Prehoda, K. E. and Doe, C. Q. (2011). Canoe binds RanGTP to promote PinsTPR/Mud-mediated spindle orientation. J Cell Biol *195*, 369–376.

Wei, S.-Y., Escudero, L. M., Yu, F., Chang, L.-H., Chen, L.-Y., Ho, Y.-H., Lin, C.-M., Chou, C.-S., Chia, W., Modolell, J. and Hsu, J.-C. (2005). Echinoid Is a Component of Adherens Junctions That Cooperates with DE-Cadherin to Mediate Cell Adhesion. Developmental Cell *8*, 493–504.

Whitney, D. S., Peterson, F. C., Kittell, A. W., Egner, J. M., Prehoda, K. E. and Volkman, B. F.

(2016). Crumbs binding to the Par-6 CRIB-PDZ module is regulated by Cdc42. Biochemistry *55*, 1455–1461.

Wirtz-Peitz, F., Nishimura, T. and Knoblich, J. A. (2008). Linking Cell Cycle to Asymmetric Division: Aurora-A Phosphorylates the Par Complex to Regulate Numb Localization. Cell *135*, 161–173.

Wodarz, A., Grawe, F. and Knust, E. (1993). CRUMBS is involved in the control of apical protein targeting during Drosophila epithelial development. Mechanisms of Development *44*, 175–187.

Wodarz, A., Hinz, U., Engelbert, M. and Knust, E. (1995). Expression of crumbs confers apical character on plasma membrane domains of ectodermal epithelia of Drosophila. Cell *82*, 67–76.

Wodarz, A., Ramrath, A., Grimm, A. and Knust, E. (2000). Drosophila Atypical Protein Kinase C Associates with Bazooka and Controls Polarity of Epithelia and Neuroblasts. The Journal of Cell Biology *150*, 1361–1374.

Wodarz, A., Ramrath, A., Kuchinke, U. and Knust, E. (1999). Bazooka provides an apical cue for Inscuteable localization in *Drosophila* neuroblasts. Nature *402*, 544–547.

Woods, B., Kuo, C.-C., Wu, C.-F., Zyla, T. R. and Lew, D. J. (2015). Polarity establishment requires localized activation of Cdc42. J Cell Biol *211*, 19–26.

Wu, H., Turner, C., Gardner, J., Temple, B. and Brennwald, P. (2010). The Exo70 Subunit of the Exocyst Is an Effector for Both Cdc42 and Rho3 Function in Polarized Exocytosis. Molecular Biology of the Cell *21*, 430–442.

Wu, X., Tanwar, P. S. and Raftery, L. A. (2008). Drosophila follicle cells: morphogenesis in an eggshell. Seminars in cell & developmental biology *19*, 271–282.

Xu, T. and Rubin, G. M. (1993). Analysis of genetic mosaics in developing and adult Drosophila tissues. Development *117*, 1223–1237.

Yamada, S., Pokutta, S., Drees, F., Weis, W. I. and Nelson, W. J. (2005). Deconstructing the Cadherin-Catenin-Actin Complex. Cell *123*, 889–901.

Yamanaka, T., Horikoshi, Y., Sugiyama, Y., Ishiyama, C., Suzuki, A., Hirose, T., Iwamatsu, A., Shinohara, A. and Ohno, S. (2003). Mammalian Lgl Forms a Protein Complex with PAR-6 and aPKC Independently of PAR-3 to Regulate Epithelial Cell Polarity. Current Biology *13*, 734–743.

Yamanaka, T., Horikoshi, Y., Suzuki, A., Sugiyama, Y., Kitamura, K., Maniwa, R., Nagai, Y., Yamashita, A., Hirose, T., Ishikawa, H. and Ohno, S. (2001). PAR-6 regulates aPKC activity

in a novel way and mediates cell-cell contact-induced formation of the epithelial junctional complex. Genes to Cells *6*, 721–731.

Ye, D. Z. and Field, J. (2012). PAK signaling in cancer. Cellular Logistics *2*, 105–116.

Yeaman, C., Grindstaff, K. K. and Nelson, W. J. (1999). New Perspectives on Mechanisms Involved in Generating Epithelial Cell Polarity. Physiological Reviews *79*, 73–98.

Zhang, X., Choi, P. S., Francis, J. M., Imielinski, M., Watanabe, H., Cherniack, A. D. and Meyerson, M. (2016). Identification of focally amplified lineage-specific super-enhancers in human epithelial cancers. Nature genetics *48*, 176–182.

Zhang, X., Orlando, K., He, B., Xi, F., Zhang, J., Zajac, A. and Guo, W. (2008). Membrane association and functional regulation of Sec3 by phospholipids and Cdc42. The Journal of Cell Biology *180*, 145–158.

Zhou, B., Wu, Y. and Lin, X. (2011). Retromer regulates apical–basal polarity through recycling crumbs. Developmental Biology *360*, 87–95.

Ziman, M., Preuss, D., Mulholland, J., O'Brien, J. M., Botstein, D. and Johnson, D. I. (1993). Subcellular localization of Cdc42p, a Saccharomyces cerevisiae GTP-binding protein involved in the control of cell polarity. Molecular Biology of the Cell *4*, 1307–1316.

Appendix A

Reagents: Plasmids

Table 7.1: Plasmids constructed for this thesis.

No.	Plasmid	Source	Cloning method
1	*pDEST15 Cdc42^{V12}*	Destination vector *pDEST15* (Invitrogen) and *pENTR Cdc42^{V12}* (gift from Evi Vlassaks)	Gateway^{TM}cloning (Invitrogen)
2	*pDEST15 Cdc42^{N17}*	Destination vector *pDEST15* (Invitrogen) and *pENTR Cdc42^{N17}* (gift from Evi Vlassaks)	Gateway^{TM}cloning (Invitrogen)
3	*pENTR Exo84*	*pENTR^{TM}/D-TOPO* vector (Invitrogen) and *exo84* cDNA (clone FI18238, DGRC)	pENTR^{TM}Directional TOPO Cloning (Cat. No. K240020, Invitrogen)
4	*pActin myc::Exo84*	Destination vector *pAMW* (*Drosophila* Gateway Vector collection) and #3	Gateway^{TM}cloning (Invitrogen)
5	*pGEX-4T-2 Baz[LRD]*	*pGEX-4T-2* (GE Healthcare Life Sciences) and *baz* cDNA (Benton and Johnston, 2003b)	The LRD-containing fragment G1146-Q1219 was cloned into the *pGEXT-4T-2* vector using BamHI/NotI sites
6	*pMAL Exo70*	*pMAL-c2x* (New England Biolabs) and *exo70* cDNA (clone FI18254, DGRC)	*exo70* was cloned into the pMAL-c2x vector with an N-terminal MBP-tag using EcoRI/XbaI sites.
7	*pMT Ed-mCherry::Par6*	#21 and #2 from Table 7.2	*par6* was cloned downstream of the *mCherry* sequence in the *pMT Ed::mCherry* vector using NheI/NotI sites
8	*pMT Ed-mCherry::Exo84*	#21 from Table 7.2 and #3	*par6* was cloned downstream of the *mCherry* sequence in the *pMT Ed::mCherry* vector using NheI/NotI sites
9	*pUAS Exo84::GFP*	Destination vector *pUASP* (*Drosophila* Gateway Vector collection) and #3	Gateway^{TM}cloning (Invitrogen)

Table 7.1 continued from previous page

No.	Plasmid	Source	Cloning method
10	*pENTR RalA*	*pENTR^{TM}/D-TOPO* vector (Invitrogen) and *ralA* cDNA (clone LD21679, DGRC)	pENTR^{TM}Directional TOPO Cloning (Cat. No. K240020, Invitrogen)
11	*pENTR RalA^{G20V}*	#10	Site-directed mutagenesis (Agilent)
12	*pENTR RalA^{E35R}*	#10	Site-directed mutagenesis (Agilent)
13	*pENTR RalA^{K44E}*	#10	Site-directed mutagenesis (Agilent)
14	*pENTR RalA^{G20V,K44E}*	#10	Site-directed mutagenesis (Agilent)
15	*pUAST GFP::RalA^{WT}*	*pUAST-attB-NmGFP* (gift from Tony Southall) and #10	*ralA* was cloned downstream of the *GFP* sequence in the *pUAST-attB-NmGFP* vector using XhoI/NotI sites
16	*pUAST GFP::RalA^{E35R}*	*pUAST-attB-NmGFP* (gift from Tony Southall) and #12	*ralA* was cloned downstream of the *GFP* sequence in the *pUAST-attB-NmGFP* vector using XhoI/NotI sites
17	*pUAST GFP::RalA^{K44E}*	*pUAST-attB-NmGFP* (gift from Tony Southall) and #13	*ralA* was cloned downstream of the *GFP* sequence in the *pUAST-attB-NmGFP* vector using XhoI/NotI sites
18	*pActin Flag::RalA^{G20V}*	#1 from Table 7.2 and #11	Gateway^{TM}cloning (Invitrogen)
19	*pActin Flag::RalA^{G20V,K44E}*	#1 from Table 7.2 and #14	Gateway^{TM}cloning (Invitrogen)

Table 7.2: Plasmids kindly provided by colleagues.

No.	Plasmid	Source	Cloning method
1	*pActin Flag* (*pAWF*)	Gift from Yanxiang Zhou	Derived from the *Drosophila* Gateway Vector collection
2	*pENTR par6*	Gift from Rhian Walther	Derived from *pENTR*^{TM}*/D-TOPO* vector (Invitrogen) and *par6* cDNA (clone LD29223, DGRC)
3	*pActin Par6::Flag*	Gift from Rhian Walther. From #1 and #2	Gateway^{TM} cloning (Invitrogen)
4	*pActin Par6*^{K23A}*::Flag*	Gift from Rhian Walther. From #1 and #2	Gateway^{TM} cloning (Invitrogen) and site-directed mutagenesis (Agilent)
5	*pActin Par6*^{AAAA}*::Flag*	Gift from Rhian Walther. From #1 and #2	Gateway^{TM} cloning (Invitrogen) and site-directed mutagenesis (Agilent)
6	*pActin Par6*$^{\Delta P}$*::Flag*	Gift from Rhian Walther. From #1 and #2	Gateway^{TM} cloning (Invitrogen) and site-directed mutagenesis (Agilent)
7	*pActin Par6*^{SE}*::Flag*	Gift from Rhian Walther. From #1 and #2	Gateway^{TM} cloning (Invitrogen) and site-directed mutagenesis (Agilent)
8	*pENTR H427*	Gift from Frederick Wirtz-Peitz	Contains a minimal *par6* promoter, the *par6* coding region with a C-terminal GFP fusion and a minimal *par6* 3'UTR
9	*par6-Par6::GFP*	Gift from Rhian Walther. From destination vector *pBID* (Addgene 35195) and #8	Gateway^{TM} cloning (Invitrogen)
10	*par6-Par6*^{K23A}*::GFP*	Gift from Rhian Walther. From destination vector *pBID* (Addgene 35195) and #8	Gateway^{TM} cloning (Invitrogen) and site-directed mutagenesis (Agilent)

Table 7.2 continued from previous page

No.	Plasmid	Source	Cloning method
11	*par6-Par6^{AAAA}::GFP*	Gift from Rhian Walther. From destination vector *pBID* (Addgene 35195) and #8	Gateway^{TM} cloning (Invitrogen) and site-directed mutagenesis (Agilent)
12	*par6-Par6$^{\Delta P}$::GFP*	Gift from Rhian Walther. From destination vector *pBID* (Addgene 35195) and #8	Gateway^{TM} cloning (Invitrogen) and site-directed mutagenesis (Agilent)
13	*par6-Par6^{SE}::GFP*	Gift from Rhian Walther. From destination vector *pBID* (Addgene 35195) and #8	Gateway^{TM} cloning (Invitrogen) and site-directed mutagenesis (Agilent)
14	*pUASP Par6::GFP*	Gift from Rhian Walther. From destination vector *pUASP* (*Drosophila* Gateway Vector collection) and #2	Gateway^{TM} cloning (Invitrogen)
15	*pUASP-Par6^{K23A}::GFP*	Gift from Rhian Walther. From destination vector *pUASP* (*Drosophila* Gateway Vector collection) and #2	Gateway^{TM} cloning (Invitrogen) and site-directed mutagenesis (Agilent)
16	*pUASP-Par6^{AAAA}::GFP*	Gift from Rhian Walther. From destination vector *pUASP* (*Drosophila* Gateway Vector collection) and #2	Gateway^{TM} cloning (Invitrogen) and site-directed mutagenesis (Agilent)
17	*pUASP-Par6^{SE}::GFP*	Gift from Rhian Walther. From destination vector *pUASP* (*Drosophila* Gateway Vector collection) and #2	Gateway^{TM} cloning (Invitrogen) and site-directed mutagenesis (Agilent)
18	*pGEX-2T Crb^{intra}*	Gift from Elisabeth Knust	Kempkens et al. (2006)
19	*pGEX-2T Crb$^{intra\ \Delta ERLI}$*	Gift from Elisabeth Knust	Kempkens et al. (2006)
20	*pMT Ed::mCherry*	Gift from Chris Doe	Wee et al. (2011)
21	*pUAS aPKC::GFP*	Gift from Daniel St Johnston	
22	*pDEST15 Par6^{WT}*	Gift from Rhian Walther	Walther et al. (2016)

Table 7.2 continued from previous page

No.	Plasmid	Source	Cloning method
23	*pDEST15 Par6^{S146A}*	Gift from Rhian Walther	Walther et al. (2016)
24	*pDEST15 Arm^{WT}*	Gift from Rhian Walther	Walther et al. (2016)
25	*pDEST15 Arm^{S561,688A}*	Gift from Rhian Walther	Walther et al. (2016)
26	*pActin myc::mbt^{CA}*	Gift from Rhian Walther	Walther et al. (2016): mutations S492N and S521E

Appendix B

Complementary data to Chapter 4

The following experiments were performed by Dr. Rhian Walther and complement the data shown in Chapter 4.

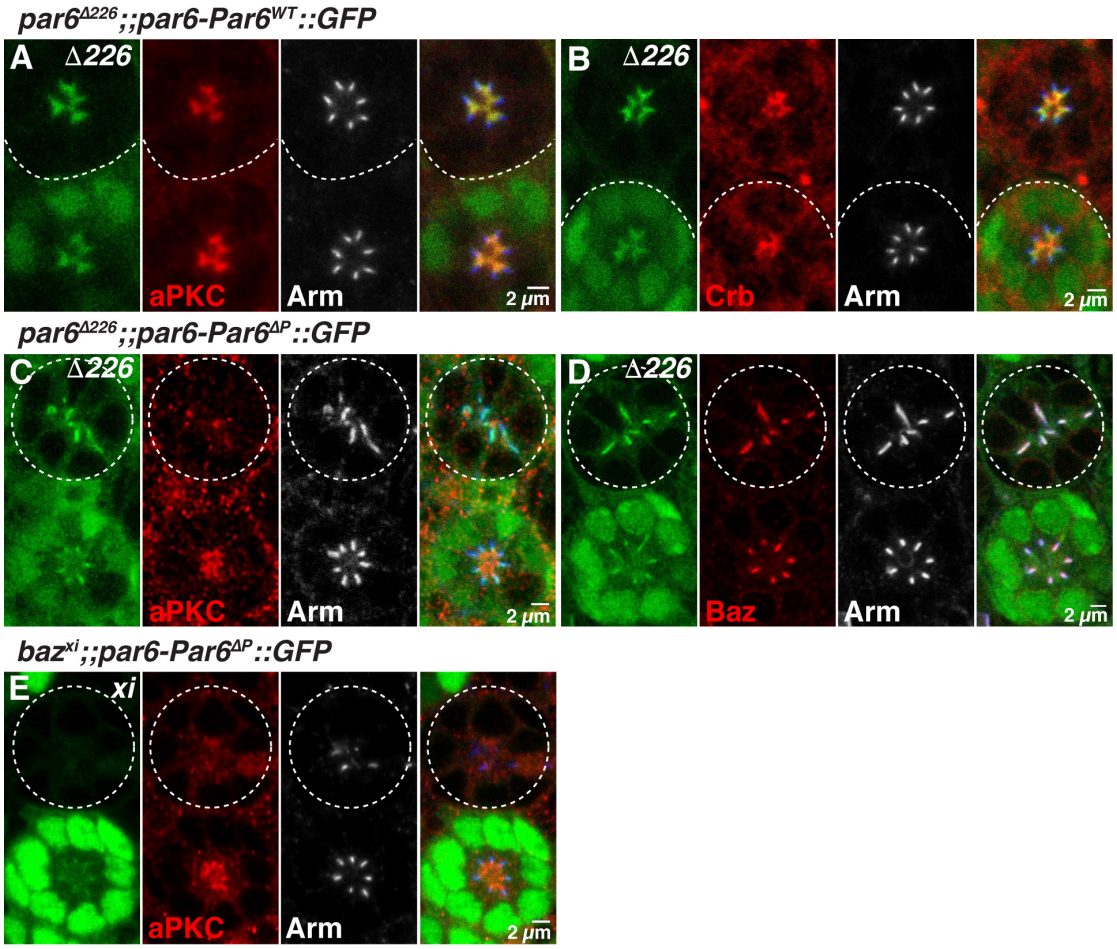

Figure 7.1: Par6 binding to Cdc42 is required to separate Par6 from Baz. *par6*$^{\Delta 226}$ pupal retinal clones labelled by loss of nuclear GFP signal (green), expressing **(A-B)** *par6-Par6::GFP* (green) or **(C-D)** *par6-Par6*$^{\Delta P}$*::GFP* (green) and stained for (A and C) aPKC (red) and Arm (grey), (B) Crb (red) and Arm (grey), (D) Baz (red) and Arm (grey). **(E)** *baz*^{xi} pupal retinal clones labelled by loss of nuclear GFP signal (green), expressing *par6-Par6*$^{\Delta P}$*::GFP* (green) and stained for aPKC (red) and Arm (grey). In all panels, the grey channel is shown in blue in the merge. Scale bars = 2 microns. Images courtesy of Dr. Rhian Walther.

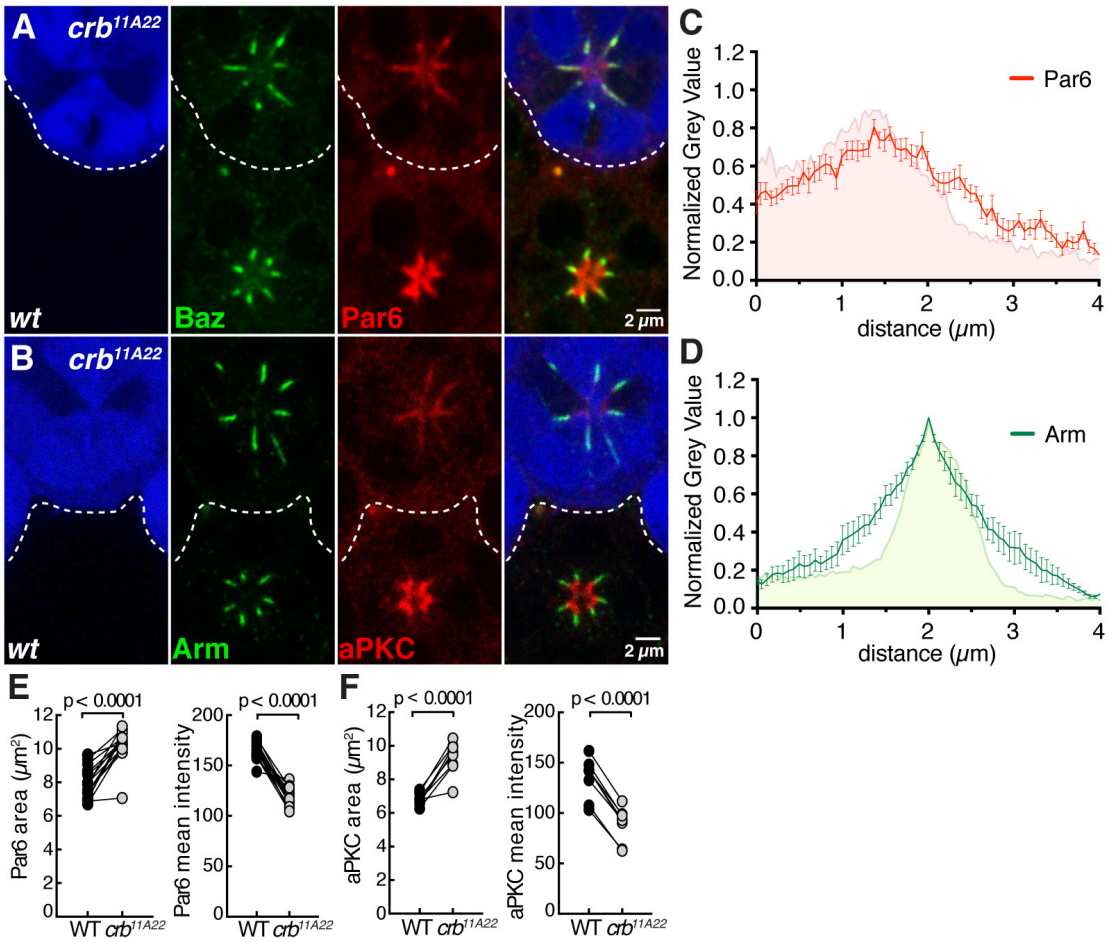

Figure 7.2: Par6-aPKC distributes between the Par and Cdc42-Par6-aPKC complexes. **(A-B)** crb^{11A22} mutant pupal photoreceptors positively labeled by GFP (blue) and stained for (A) Baz (green), Par6 (red) and (B) Arm (green), aPKC (red). Scale bars = 2 microns. **(C-D)** Intensity profiles of Par6 and Arm at the cell cortex of crb^{11A22} mutant photoreceptors from the apical to the lateral domains. *Wild-type* values of Par6 and Arm from *wild-type* retinae are shown (shaded) in the background of each respective graph for comparison with *crb* mutant values. For each condition a minimum of 9 photoreceptors from 3 retinas were measured. **(E-F)** Par6 and aPKC area and mean intensity quantifications in crb^{11A22} mutant photoreceptors compared to *wild-type*. 20 ommatidia pairs from 7 retinas and 9 ommatidia pairs from 3 retinas were measured for Par6 and aPKC, respectively. Images courtesy of Dr. Rhian Walther.

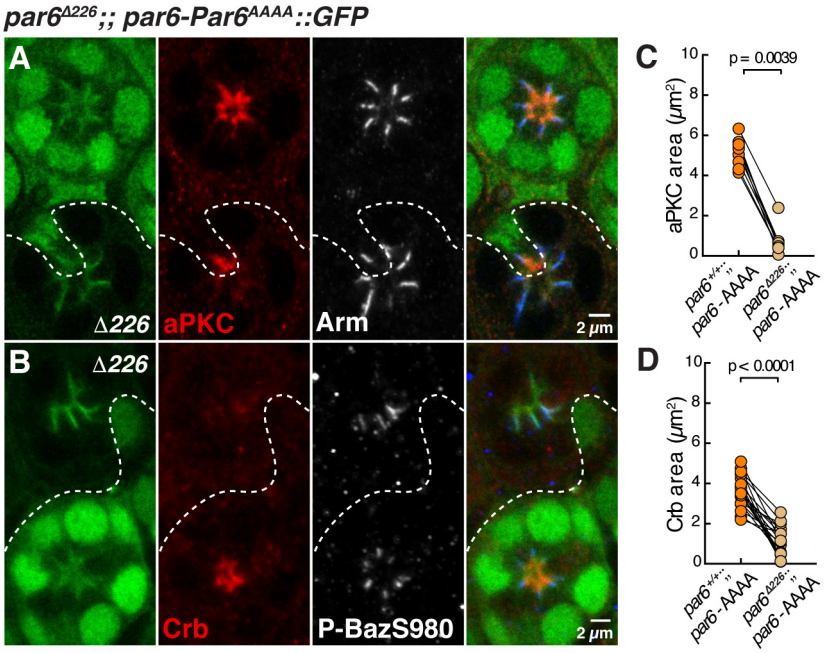

Figure 7.3: Par6 binding to Crb promotes the accumulation of both Par6-aPKC and Crb. (A-B) *par6*$^{\Delta 226}$ pupal retinal clones expressing *par6-Par6*^{AAAA}*::GFP* (green). *par6*$^{\Delta 226}$ mutant cells labelled by loss of nuclear GFP signal and stained for (A) aPKC (red), Arm (grey) and (B) Crb (red), P-S980Baz (grey). In both panels, the grey channel is shown in blue in the merge. Scale bar = 2 microns. **(C-D)** Quantification of aPKC and Crb area. 9 ommatidia pairs from 4 retinas and 19 ommatidia pairs from 6 retinas were analysed for aPKC and Crb, respectively. Images courtesy of Dr. Rhian Walther.

Appendix C

Published Manuscript:

Pak4 Is Required during Epithelial Polarity Remodeling through Regulating *AJ* Stability and Bazooka Retention at the *ZA*

Published in *Cell Reports* in April 5, 2016

Cell Reports
Report

OPEN ACCESS
CellPress

Pak4 Is Required during Epithelial Polarity Remodeling through Regulating AJ Stability and Bazooka Retention at the ZA

Rhian F. Walther,[1] Francisca Nunes de Almeida,[1] Evi Vlassaks,[1] Jemima J. Burden,[1] and Franck Pichaud[1,*]
[1]MRC Laboratory for Molecular Cell Biology, University College London, Gower Street, WC1E 6BT London, UK
*Correspondence: f.pichaud@ucl.ac.uk
http://dx.doi.org/10.1016/j.celrep.2016.03.014

SUMMARY

The ability of epithelial cells to assemble into sheets relies on their zonula adherens (ZA), a circumferential belt of adherens junction (AJ) material, which can be remodeled during development to shape organs. Here, we show that during ZA remodeling in a model neuroepithelial cell, the Cdc42 effector P21-activated kinase 4 (Pak4/Mbt) regulates AJ morphogenesis and stability through β-catenin (β-cat/Arm) phosphorylation. We find that β-catenin phosphorylation by Mbt, and associated AJ morphogenesis, is needed for the retention of the apical determinant Par3/Bazooka at the remodeling ZA. Importantly, this retention mechanism functions together with Par1-dependent lateral exclusion of Par3/Bazooka to regulate apical membrane differentiation. Our results reveal an important functional link between Pak4, AJ material morphogenesis, and polarity remodeling during organogenesis downstream of Par3.

INTRODUCTION

In vertebrate and invertebrate epithelial or neuroepithelial cells, apical membrane morphogenesis consists of the differentiation of the cell-cell junction (zonula adherens [ZA]) from the apical and lateral membrane domains. How this is achieved is not fully understood. In *Drosophila*, apical membrane morphogenesis and remodeling requires at least two processes: (1) the confinement of the conserved polarity proteins Par6-atypical protein kinase C (aPKC), Crumbs (Crb), and Stardust (Sdt) to the apical pole of the cell and (2) the exclusion of Baz (*Drosophila* Par3) from the apical membrane, such that this protein is positioned at the boundary between the apical and lateral membrane where the ZA assembles (Krahn et al., 2010; Morais-de-Sá et al., 2010; Walther and Pichaud, 2010). These two processes drive polarity specification and remodeling in the follicular epithelium, the cellularizing blastoderm, and the photoreceptor (St Johnston and Ahringer, 2010). Notably, the junctional configuration and localization of the apical proteins Par6-aPKC and Baz/Par3 relative to the apical-lateral border is conserved through evolution (Afonso and Henrique, 2006; Totong et al., 2007; Zihni et al., 2014).

In addition to the apical exclusion of Baz, and in order to limit apical membrane morphogenesis to one pole of the cell, Baz must be excluded from the lateral cortex. Lateral exclusion of Baz prevents its ectopic association with aPKC basal to the ZA and is mediated by the serine/threonine kinase Par1 in several model epithelial cell types (Benton and St Johnston, 2003b). However, the relatively mild *par1* loss-of-function polarity phenotype observed in the follicular epithelium, blastoderm, and photoreceptor suggests that other mechanisms might be at play (Benton and St Johnston, 2003b; McKinley and Harris, 2012; Nam et al., 2007). For example, in the blastoderm where polarity is established de novo, basal to apical transport of Baz and the presence of an apical scaffold of F-actin can act to localize Baz at the apical pole of the cortex (Harris and Peifer, 2004; McKinley and Harris, 2012). Whether these or other mechanisms regulate the ZA localization of Baz in a remodeling epithelium is not clear.

As Baz is confined to the apico-lateral border of the cell, it is thought to interact with adherens junction (AJ) material, possibly via binding to Arm and Echinoid (Wei et al., 2005). However, in the blastoderm, follicular epithelium, or photoreceptor, accumulation of AJ material at the plasma membrane does not strictly depend on Baz (Harris and Peifer, 2004; Shahab et al., 2015; Walther and Pichaud, 2010). This indicates that pathways must promote AJ assembly independently of *baz*. These pathways and their relation to the epithelial polarity gene network remain to be characterized in detail.

Among the factors that might regulate AJ morphogenesis is the Cdc42 effector P21-activated serine/threonine kinase, Pak4 (*Drosophila mushroom bodies tiny* [*mbt*]). In *Drosophila* photoreceptors, this kinase localizes at the developing ZA and is required for proper ZA morphogenesis (Schneeberger and Raabe, 2003). In addition, Mbt can phosphorylate β-cat/Arm in vitro, and in cell culture, this phosphorylation limits the association of Arm and E-cadherin (Menzel et al., 2008). Consistent with a conserved role for Mbt/Pak4 in regulating AJ morphogenesis, conditional deletion of mPak4 in the mouse nervous system leads to a loss of neuroepithelial AJs (Tian et al., 2011). In addition, hPak4 is required to promote tight junction and AJ maturation in human bronchial cells (Wallace et al., 2010). Thus, Pak4/Mbt plays an important role in regulating epithelial polarity across phyla. However, the functional relationship between this kinase, AJ morphogenesis, and the conserved epithelial polarity gene network remains to be examined in detail.

This is an open access article under the CC BY license (http://creativecommons.org/licenses/by/4.0/).

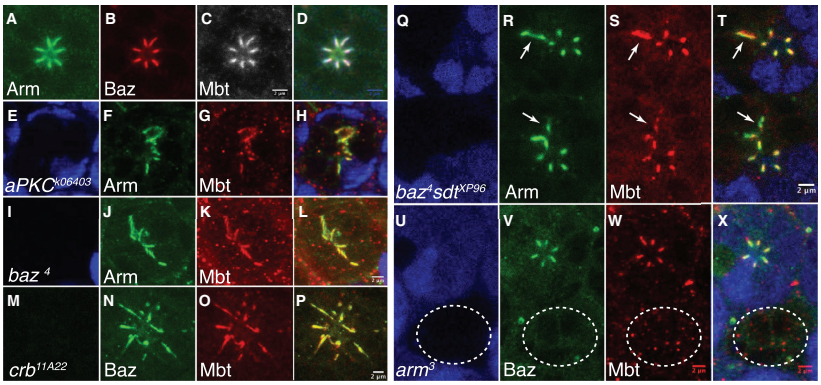

Figure 1. Mbt Is a Core Component of the AJ

(A–D) Wild-type ommatidium. Arm (green; A), Baz (red; B), Mbt (gray; C), and merge (D) are shown.
(E–H) *aPKC*^{k06403} *mutant*, lacking GFP (blue; E), Arm (green; F), Mbt (red; G), and merge (H).
(I–L) *baz*^{4} mutant, lacking GFP (blue; I), Arm (green; J), and Mbt (red; K), and merge (L).
(M–P) *crb*^{11A22} mutant, lacking GFP (blue; M), Baz (green; N), Mbt (red; O), and merge (P).
(Q–T) *baz*^{4}, *sdt*^{XP96} mutant, lacking GFP (blue; Q), Arm (green; R), Mbt (red; S), and merge (T). White arrows point to mutant cell-cell interfaces.
(U–X) *arm*^{3} *mutant*, lacking GFP (blue; U), Baz (green; V), Mbt (red; W), and merge (X). A mutant ommatidium is circled.
The scale bars represent 2 μm.

RESULTS

Baz Is Essential for Photoreceptor Polarity Remodeling

The *Drosophila* photoreceptor, which undergoes a sustained phase of apico-basal polarity remodeling during development, is a particularly attractive model to study the relationship between the conserved polarity determinants and the AJ during cortical polarity remodeling and plasma membrane morphogenesis (Figure S1A).

In light of recent work suggesting that *baz* might be dispensable in some instances of epithelial polarity remodeling in vivo (Shahab et al., 2015), we first re-examined the function of this factor in the remodeling photoreceptor using two new loss-of-function alleles: *baz*^{XR11} *and baz*^{EH747}. Both alleles lead to a strong reduction in aPKC, Crb, and Par6 staining (Figures S1A–S1J). In addition, most mutant photoreceptors fail to specify a clear ZA and AJ material invades what would normally be the apical pole of the cell (Figure S1E). These data confirm that Baz is required to support the recruitment of Par6-aPKC and Crb at the apical cortex and membrane, respectively (Walther and Pichaud, 2010). However, we note instances where the ZA is relatively well defined (Figure S1I). These instances correlate with residual apical Par6 accumulation (Figure S1H), which suggests that Par6 can be recruited at the apical pole of the cell independently of Baz, presumably through binding to Cdc42 or Crb (Hutterer et al., 2004; Morais-de-Sá et al., 2010).

Mbt Is a Core Component of the AJ

In the developing photoreceptor, Mbt localizes at the developing ZA (Schneeberger and Raabe, 2003; Figures 1A–1D). To test whether this localization depends on the apical epithelial gene network, we examined Mbt localization in *aPKC*^{k06403} (Figures 1E–1H), *baz*^{4} (Figures 1I–1L), *crb*^{11A22} (Figures 1M–1P), and *baz*^{4}, *sdt*^{XP96} double-mutant cells (Figures 1Q–1T). We found that AJ domains, which contain Mbt, are still present in all these conditions. The only condition that abolishes Mbt localization at the cell cortex is in *arm*^{3} mutant cells, where AJ material is absent (Figures 1U–1X).

From this set of data, we can therefore draw two main conclusions. First, Mbt is a core component of the AJ. Second, there must be at least one molecular pathway that can support AJ assembly independently of Baz and Crb. Due to its close association with AJ material, we reasoned that Mbt could be part of such pathway. To test this possibility, we generated *baz*^{4}, *mbt*^{P1} double-mutant cells and compared them to *baz*^{4} and *mbt* ^{P1} single-mutant cells. AJ material is detected in *baz*^{4} (Figure S1E) and in *mbt*^{P1} single-mutant photoreceptors (Figure 2A–D). In contrast, we found that no AJ material can be detected at the cortex of *baz*^{4}, *mbt*^{P1} double-mutant cells (Figures 2K–2N). Therefore, our results indicate that *mbt* can support AJ morphogenesis independently of *baz*.

Mbt Supports AJ Morphogenesis Independently of *baz*

Next, we sought to examine the role of *mbt* during photoreceptor polarity remodeling. Consistent with Mbt promoting ZA

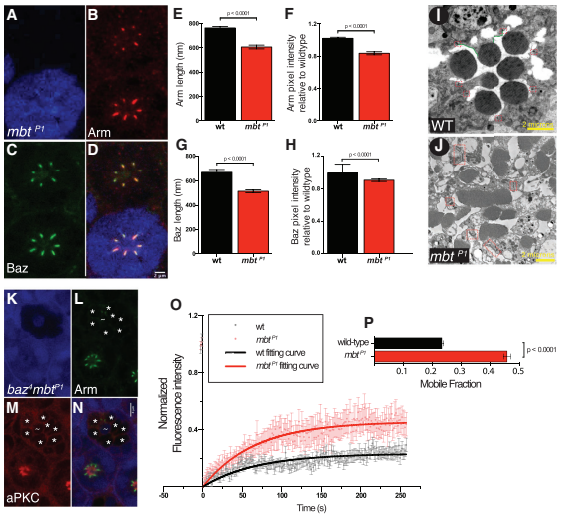

Figure 2. *mbt* Promotes AJ Morphogenesis Independently from Baz

(A–D) mbt^{P1} mutant, lacking GFP (blue; A), Arm (red; B), Baz (green; C), and merge (D). The scale bars represent 2 microns.

(E) Mean length of Arm cortical domain in wild-type and mbt^{P1} mutants.

(F) Mean pixel intensity of Arm in wild-type and mbt^{P1}. In (E) and (F), n = 202 (in four wild-type retinas) and n = 460 (in four mbt^{P1} retinas).

(G) Mean length of Baz cortical domain in wild-type and mbt^{P1} mutants.

(H) Mean pixel intensity of Baz in wild-type and mbt^{P1}. In both (G) and (H), n = 99 (wild-type) and n = 107 (mbt^{P1}), with measurements taken from five independent mbt^{P1} mosaic retina. In (E)–(H), columns represent mean and error bars represent the SEM of each dataset. Statistical significance was determined using an unpaired two-tailed Student's t test.

(I and J) Electron microscopy (I) on a wild-type ommatidium and (J) on the poorly developed apical membranes of an mbt^{P1} adult ommatidium. Ectopic AJ domains are boxed and sub-apical membranes in green. The scale bar represents 2 μm.

(K–N) baz^4, mbt^{P1} mutant lacking GFP (blue; K), Arm (green; L), aPKC (red; M), and merge (N). Asterisks highlight mutant cells. A tilde marks a wild-type cell. The scale bars represent 4 μm.

(O) FRAP on E-cadherin::GFP in wild-type or mbt^{P1}. Mean normalized fluorescence intensity in wild-type (gray; n = 18 from two individuals) and mbt^{P1} (pink; n = 15 from three individuals) is shown; error bars represent SEM. Fluorescence recovery curves of E-cad::GFP after photo-bleaching in wild-type (black) and mbt^{P1} (red) are shown.

(P) Mobile fraction of E-cadherin::GFP in a wild-type (black) or mbt^{P1} (red) background. The p value was calculated with an unpaired two-tailed Student's t test with Welch's correction.

morphogenesis, we measure a significant decrease in the length and mean pixel intensity of Arm and Baz at the developing ZA of mbt^{P1} mutant photoreceptors (Figures 2A–2H). In addition, *mbt* is required for overall apical membrane differentiation, albeit only in a fraction of the mutant cells (Figures 2I and 2J). We found that, in 40% of the mbt^{P1} mutant ommatidia (n = 2,662 from nine retinae), no ZA assembles along the photoreceptors proximo-distal axis, and instead, poorly differentiated apical membranes are found between the floor of the retina and the lamina part of the brain (Figures 2J and S2A–S2J). Whereas these membranes contain aPKC, Crb, Baz, and Arm, apico-basal polarity is severely compromised (Figures S2D–S2G″). These data indicate that Mbt promotes AJ morphogenesis and to some extent apical membrane morphogenesis. Importantly, the *mbt* phenotype can be fully rescued when expressing a wild-type version of this kinase (Figure S3A). In contrast, re-introducing a version of Mbt that can no longer bind to Cdc42 or lacks kinase activity (Schneeberger and Raabe, 2003) fails to rescue the *mbt* phenotype (Figure S3A). Therefore, Mbt functions through its kinase activity, which, as expected for this family of kinases, is regulated via binding to Cdc42 (Ha et al., 2015).

Mbt Does Not Phosphorylate Par6 in *Drosophila*

In order to gain mechanical insight into how Mbt might regulate apical membrane morphogenesis, we examined the relationship between Mbt and Par6. Human Pak4 (hPak4) can phosphorylate hPar6b at serine 143, which is found in *Drosophila* Par6 at position 146 (Jin et al., 2015). However, the (−2) residue in Par6 differs from that found in hPar6b, and in that, Par6 most resembles hPar6a, which is not phosphorylated by hPak4 (Figures S3B and S3C).

To test whether Mbt can phosphorylate Par6, we purified an activated version of Mbt from S2 cells and used it to perform kinase assays with *Drosophila* Par6. In our assays, we found no evidence for Mbt (or for recombinant hPak4) phosphorylating Par6S146 in vitro (Figures S3D and S3E). In addition, a version of Par6 in which S146 is mutated to an alanine (Par6-Par6SA146) can rescue the embryonic lethality of the $par6^{-d226}$ when expressed under the *par6* promoter (data not shown). Thus, our results indicate that phosphorylation of Par6S146 is not essential for Par6 function during *Drosophila* development.

Mbt Regulates the Stability of E-cadherin at the ZA

Mbt influences the stability of the E-cadherin-catenin complex in non-polarized S2 cells (Menzel et al., 2008). To examine whether this contributes to regulating ZA morphogenesis, we made use of fluorescence recovery after photobleaching (FRAP) to evaluate the mobile fraction and half-time recovery of E-cadherin. When photobleaching the basal tip of the wild-type ZA, we find that 23.3% ± 0.6% of E-cadherin::GFP is mobile with an evaluated

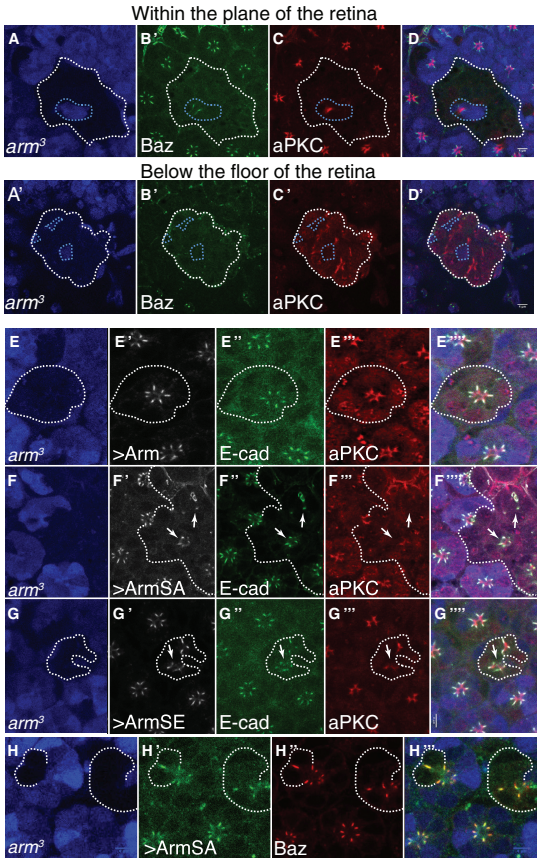

Figure 3. *mbt* Regulates ZA Remodeling through Arm Phosphorylation

(A–D') arm^3 mutant, lacking GFP (blue; A and A'), Baz (green; B and B'), aPKC (red; C and C'), and merge (D and D').

(E–G'''') Myc (gray), E-cadherin (green), aPKC (red). (E–E'''') Rescue of an arm^3 mutant ommatidium, lacking GFP (blue; E), by re-introduction of a wild-type version of the Arm::Myc transgene is shown. (F–F'''') Re-introduction of ArmSA561,688::Myc is shown. (G–G'''') Re-introduction of ArmSE561,688::Myc is shown.

(H–H''') arm^3 mutant lacking GFP (blue; H), ArmSA561,688::Myc (green; H'), Baz (red; H''), and merge (H''').

The scale bars represent 4 μm.

half-time recovery of 47 s (Figures 2O and 2P). In mbt^{P1} mutant ZA, we found that the mobile fraction of E-cadherin::GFP is 45.7% ± 1.2% with a half-time recovery of approximately 45 s (Figures 2O and 2P). Therefore, Mbt is required to stabilize E-cadherin at the ZA during photoreceptor polarity remodeling.

Mbt Regulates ZA Remodeling through Arm Phosphorylation

Phosphorylation of β-cat/Arm by Pak4/Mbt is conserved through evolution (Selamat et al., 2015), thus providing a potential mechanism for regulating AJ morphogenesis and E-cadherin mobility. Therefore, we next sought to re-examine the relationship between Mbt, Arm phosphorylation, and ZA morphogenesis. First, we confirmed that a constitutively active form of Mbt phosphorylates Arm at S561 and S688 (Figures S3D and S3E). Second, we generated transgenic animals bearing myc-tagged phospho-mimetic (*UAS-armSE561,688::myc*), phospho-dead (*UAS-armSA561,688::myc*), and wild-type (*UAS-arm::myc*) transgenes and asked whether these could rescue the arm^3 mutant phenotype. arm^3 mutant photoreceptors show defects in aPKC localization at their cortex, lack Baz altogether, and, similar to *mbt* mutant cells, tend to form cysts below the floor of the retina (Figures 3A–3D').

Re-introducing Arm::myc in arm^3 mutant cells rescues the photoreceptor polarity remodeling phenotype (Figure 3E). However, re-introducing either ArmSA561,688::myc or ArmSE561,688::myc in arm^3 mutant photoreceptors fails to support ZA morphogenesis, and instead, discrete AJ domains are found distributed along the proximo-distal axis of the cell. Both transgenes are able to form domains that contain E-cadherin and Baz (Figures 3F–3H). In the case of ArmSA561,688::myc, two of the ZA-like domains examined (n = 24) present ArmSA561,688::myc, but lack Baz entirely. Among the remaining 22 ZA-like domains, four include a region positive for ArmSA561,688::myc, but not Baz, and three include regions positive for Baz, but not ArmSA561,688::myc. These results suggest that the phosphorylation status of Arm regulates the interface between the AJ and Baz. In addition, we note that, with ArmSA561,688, several cells present poorly differentiated apical membranes including aPKC domains that are smaller than in the wild-type (Figures 3F'''–3G''' and S4).

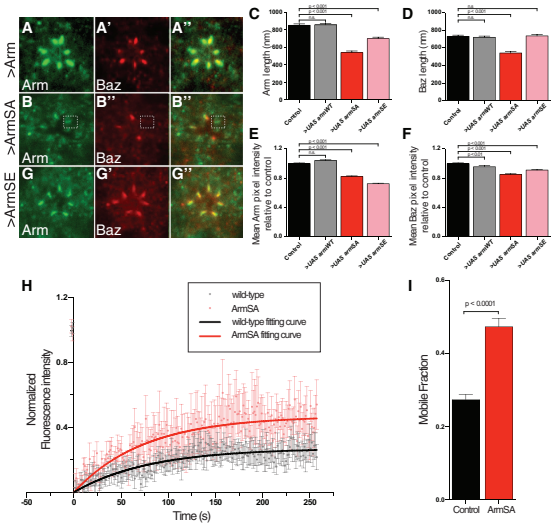

Figure 4. Arm Phosphorylation Regulates AJ Material Stability during ZA Morphogenesis

(A) Overexpression of Arm::myc. Arm (green) and Baz (red) are shown.

(B) Overexpression of ArmSA561,688::myc. Arm (green) and Baz (red) are shown. A dashed rectangle highlights a ZA that contains Arm, but not Baz.

(C and D) Length of the Arm (C) and Baz (D) domains in wild-type and in photoreceptors expressing Arm::myc, ArmSA561,688::myc, or ArmSE561,688::myc.

(E and F) Mean pixel intensity for Arm (E) and Baz (F) measured relative to that of control photoreceptors. In (C)–(F), columns indicate the mean whereas error bars indicate the SEM ($n > 200$). Statistical significance was determined using one-way ANOVA and the Kruskal-Wallis multiple comparison test for non-parametric samples.

(G–G'') Overexpression of ArmSE561,688::myc; Arm (green; G), Baz (red; G'), and merge (G'').

(H) FRAP on E-cadherin::GFP in wild-type cells and in cells expressing ArmSA561,688::myc. Mean normalized fluorescence intensity in wild-type (gray; n = 14 from five individuals) and ArmSA561,688::myc (red; n = 9 from five individuals) is shown. Error bars represent SEM. Fluorescence recovery curves of E-cadherin::GFP after photo-bleaching in wild-type (black) and ArmSA561,688::myc (red) are shown.

(I) Mobile fraction of E-cadherin::GFP in a wild-type (black) or ArmSA561,688::myc (red) background. The p value was calculated with an unpaired two-tailed Student's t test with Welch's correction.

Altogether, our results indicate that the developing ZA influences apical membrane differentiation. They also suggest that the fraction of phosphorylated Arm must be present in the correct proportion to support ZA morphogenesis. This notion is further supported by the fact that expressing an activated form of Mbt is detrimental to photoreceptor polarity remodeling and ZA maturation (Figures S3G–S3I).

Arm Phosphorylation Promotes the Accumulation of AJ Material at the ZA

If Arm phosphorylation must be finely tuned during ZA remodeling, then overexpressing ArmSA561,688 should lead to phenotypes resembling that of the *mbt* loss of function. To test this hypothesis, we overexpressed ArmSA561,688::myc in wild-type retinae. In this assay, overexpressing wild-type Arm::myc does not lead to significant phenotypes (Figures 4A, 4C–4F, and S4A). In contrast, overexpressing ArmSA561,688::myc leads to a decrease in Arm and Baz as well as a significant shortening of the ZA when compared to wild-type (Figures 4C–4F). We also note instances where Baz is missing from the ZA, while Arm is present (Figure 4B). This is specific, as expressing ArmSE561,688::myc or Arm::myc does not lead to such uncoupling between Arm and Baz (Figures 4A, 4G, S4C, and S4E). Expressing the ArmSE561,688::myc transgene leads to a significant decrease in length and mean pixel intensity for Arm. In this case, however, the length of the Baz domain is comparable to wild-type (Figure 4D). Finally, when overexpressing the ArmSA561,688::myc transgene, the mobile fraction for E-cadherin::GFP determined using FRAP is 47% ± 2.2% (Figures 4H and 4I), which is almost identical to that we measured in *mbt* mutant cells (Figures 2O and 2P). Altogether, the range of phenotypes we obtained when overexpressing ArmSA561,688::myc is similar to that seen in *mbt* mutant photoreceptors. These data therefore support a model in which Mbt regulates the stability of E-cadherin at the membrane as well as the cortical accumulation of Arm and Baz through phosphorylation of Arm at serine 561 and 688.

Mbt Promotes the Retention of Baz at the Developing ZA

Next, we sought to probe the relationship between *mbt*, ZA morphogenesis, and Baz localization. Our results so far suggest a model in which *mbt* might promote the retention of Baz at the developing ZA. To test this model, we overexpressed a wild-type version of Baz (Baz::GFP) in *mbt* mutant cells and tested for the presence of ectopic accumulation of Baz::GFP at the lateral cortex of the photoreceptors. Baz::GFP expressed in an otherwise wild-type retina localizes at the ZA in 98% of photoreceptors quantified (n = 528; Figures 5A and 5E). In contrast, expressing Baz::GFP in *mbt* mutant cells leads to the formation of Baz::GFP microdomains in 33% of the lateral cortices examined (n = 231; Figures 5B and 5E). These lateral cortices can contain up to three ectopic Baz domains that also contain aPKC and

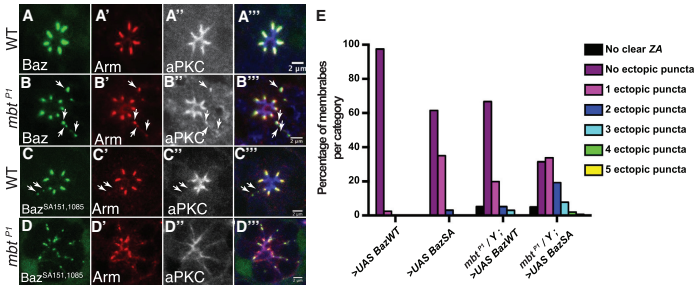

Figure 5. Mbt Promotes Baz Retention at the Developing ZA

(A–A''') Baz::GFP (green; A) in a wild-type ommatidium. Arm (red, A'), aPKC (gray; A''), merge (A'''). Note that the aPKC channel is in blue in the merged panel.

(B–B''') Expression of Baz::GFP (green; B) in an mbt^{P1} ommatidium. Arm (red, B'), aPKC (gray; B''), merge (B'''). Note that the aPKC channel is in blue in the merged panel. White arrows point to ectopic Baz aggregates.

(C–C''') Expression of BazSA151,1085::GFP (green; C) in a wild-type ommatidium. Arm (red; C') aPKC (gray; C''), merge (C'''). Note that the aPKC channel is in blue in the merged panel. White arrows point to ectopic Baz aggregates.

(D–D''') Expression of BazSA151,1085::GFP (green; D) in an mbt^{P1} mutant. Arm (red; D'), aPKC (gray; D''), merge (D'''). Note that the aPKC channel is in blue in the merged panel. The scale bar represents 2 μm.

(E) Quantification of the number of GFP puncta at the photoreceptor lateral membranes. On the x axis, BazSA stands for BazSA151,1085.

Arm. In addition, up to 88% of the ommatidia (n = 1,286 from four retinae) present poorly developed apical membranes compared to 40% in the case of mbt^{P1} (n = 2,662 from nine retinae). These data demonstrate that *mbt* limits the ability of Baz to form microdomains at the photoreceptor lateral cortex. They also provide a genetic link between *mbt*, the developing ZA and *baz*, indicating that a defect in ZA retention of Baz leads to the ectopic recruitment of aPKC and Arm at the lateral membrane.

Mbt and Par1 Function Redundantly to Prevent Baz Accumulation at the Lateral Cortex

A requirement for *mbt* in preventing Baz from accumulating at the lateral cortex raises the issue that the function of Mbt might be related to that of Par1. During polarity remodeling, Par1 expression is restricted to the lateral cortex of the photoreceptor (Figures S5A and S5B). In addition, expressing a Par1 transgene that escapes aPKC phosphorylation (Par1[AEM]::GFP) leads to its ectopic localization at the apical membrane (Doerflinger et al., 2010), thus indicating that apical exclusion of Par1 is mediated by aPKC phosphorylation (Figures S5C and S5D). Therefore, the localization pattern of Par1 is consistent with this kinase promoting lateral exclusion of Baz. In addition, similar to the developing follicular epithelium (Doerflinger et al., 2010), we measure an increase in the quantity of microtubules present in the soma of *par1* mutant photoreceptors (Figures S5E and S5F).

Quantifications performed on mature photoreceptors show that the *par1* loss-of-function polarity phenotype is very mild and consists of cells that present slightly longer sub-apical membranes (Figures S5G–S5J). Such a mild phenotype might be due to the presence of other redundant kinases phosphorylating Baz at serines 151 and 1085. In order to bypass such possible redundancy, we made use of the BazSA151,1085::GFP transgene (Benton and St Johnston, 2003b). Expressing this fusion protein in a wild-type retina leads to the formation of at least one ectopic BazSA151,1085::GFP microdomain in 35% of photoreceptor lateral cortices (n = 734; Figures 5C and 5E). However, BazSA151,1085::GFP is localized exclusively at the developing ZA in the majority (65%) of photoreceptors and ZA localization is observed when expressed in baz^4 mutant cells, which rules out a recruitment of BazSA151,1085::GFP via Baz oligomerization (Benton and St Johnston, 2003a; Figure S5K). From these experiments, we conclude that *par1*-dependent lateral exclusion of Baz is largely dispensable during photoreceptor polarity remodeling.

To test whether *mbt* functions redundantly with *par1*, we expressed BazSA151,1085::GFP in *mbt* mutant photoreceptors. In this condition, we observe an extensive ectopic localization of BazSA151,1085::GFP with lateral cortices containing up to five ectopic domains (n = 296; Figures 5D and 5E). This is accompanied by a very severe polarity phenotype, in that the aPKC and Arm expression domains extend laterally.

Altogether, these results indicate that Mbt-dependent ZA retention of Baz constitutes a main localization mechanism for this factor. This retention mechanism operates together with Par1-dependent lateral exclusion. Importantly, failure to limit Baz localization at the developing ZA leads to catastrophic defects during polarity remodeling.

DISCUSSION

Mbt Regulates the Accumulation of AJ Material at the Developing ZA

In the developing pupal photoreceptor and other popular model-developing epithelial cell types, the concomitant apical exclusion

of Baz and accumulation of Crb promotes the coalescence of AJ material during ZA remodeling (St Johnston and Ahringer, 2010). However, how AJ morphogenesis is regulated at the plasma membrane is not well understood. Here, we present complementary evidence indicating that Pak4/Mbt regulates this process. In the absence of *mbt* and when compared to wild-type cells, we measure less Arm at the ZA. The AJ domains that we observe in *baz* (or *baz*, *sdt*) mutant photoreceptors are no longer detected when *mbt* is also lacking. In addition, our FRAP experiments indicate that *mbt* limits the amount of E-cadherin::GFP that can be recovered at the remodeling ZA. Finally, expressing a version of Arm that cannot be phosphorylated by Mbt leads to a shortening of the ZA and a decrease in Baz levels similar to that measured in *mbt* mutant cells. The mobility that we measured for E-cadherin in these shorter ZA is comparable to that measured in *mbt* mutant cells. Therefore, our results indicate that, in vivo, Mbt promotes AJ morphogenesis at least in part through phosphorylation of Arm S561 and S688.

Mbt Function Is Linked to Arm Phosphorylation

Residues S561 and S688 are located in a domain of Arm that mediates part of the E-cadherin-catenin interface. Their phosphorylation destabilizes the E-cadherin-catenin interaction and cell-cell adhesion in non-polarized S2 cells (Menzel et al., 2008). Therefore, loss of *mbt* should lead to a stabilization of the E-cadherin-catenin interaction. We find that, at the developing photoreceptor ZA, loss of *mbt* promotes E-cadherin mobility as well as a decrease in Arm and Baz content. As E-cadherin is coupled to Arm, it also becomes coupled to the underlying F-actin cortex, which might influence AJ motility. Interestingly, Pak4/Mbt has been shown to promote the phosphorylation of the F-actin-severing protein cofilin at the conserved Ser3 (Dan et al., 2001; Menzel et al., 2007). Phosphorylation of cofilin inactivates it and leads to a slowing down of F-actin turnover (Bravo-Cordero et al., 2013). Reduced turnover of cortical F-actin has been associated with the stabilization of E-cadherin trans-interactions in vitro (Engl et al., 2014). We therefore propose that, upon loss of *mbt*, stabilization of the E-cadherin-catenin interface, perhaps combined with increased cofilin-dependent F-actin turnover, directs E-cadherin mobility. Altogether, our results indicate that the dynamic regulation of the E-cadherin-catenin interaction is important for ZA morphogenesis.

ZA Retention of Baz Is Required for Proper Apical Membrane Differentiation

In the remodeling photoreceptor, Baz, Par6, aPKC, and Crb all overlap with the apical 2/3 of the ZA, whereas the basal 1/3 presents very little staining for these proteins (Walther and Pichaud, 2010). In addition, we show here that the expression domain of Par1 abuts the basal boundary of the ZA. Therefore, the basal 1/3 of the developing ZA, which is approximately 350 nm in length, allows for a clear spatial separation of Baz and Par1 at the cortex. In *mbt* mutant cells, the length of the developing ZA along the apico-basal axis is significantly reduced, which largely abolishes this clear separation and might expose Baz to Par1 phosphorylation and promote its cortical exclusion. This might explain why we detect less Baz at the ZA of *mbt* mutant photoreceptors. In this model, Mbt would antagonize Par1 so to maintain an optimum pool of Baz at the ZA. Alternatively, a failure in retaining Baz at the ZA might lead to its ectopic localization at the lateral membrane, where it is targeted by Par1. In this second model, ZA retention and Par1 lateral exclusion of Baz function redundantly. This second model is supported by our finding that, when overexpressed in *mbt* mutant cells, Baz-SA151,1085::GFP accumulates at the lateral membrane. In any case, we find that Mbt-dependent AJ material accumulation influences apical membrane morphogenesis, and our genetic experiments indicate that this is through promoting the retention of Baz at the ZA. We note that both ArmSA561,688 and ArmSE561,688 support the recruitment of Baz at the developing ZA in rescue experiments. Thus, the phosphorylation status of Arm does not directly influence Baz recruitment at the ZA.

In vertebrate epithelial cells as well as in the photoreceptor, Pak4 functions downstream of the small GTPase Cdc42, which also regulates the Par6-aPKC module (Schneeberger and Raabe, 2003; Wallace et al., 2010; Walther and Pichaud, 2010). Therefore, our finding that Pak4 promotes the accumulation of Baz, a factor required for the accumulation of Par6-aPKC at the apical membrane, reveals an important functional cross-talk between AJ morphogenesis and apical membrane differentiation during polarity remodeling.

EXPERIMENTAL PROCEDURES

Antibodies and Immunological Methods

Whole-mount retinae were prepared as described in Walther and Pichaud (2006). The following antibodies were used: mouse anti-alpha tubulin 1/1,000 (Sigma); rabbit anti-PKCζ 1/200 (Santa Cruz Biotechnology); mouse anti-Arm 1/200 (N27-A1; Developmental Studies Hybridoma Bank); rabbit anti-Baz 1/2,000 (generated against C-terminal peptide H2N - CSQ YGS AAG SQP HAS KV - COOH; this work; Eurogentec SA); rat anti-Crb 1/200 (generated against C-terminal peptide H2N - H2N - CEM DNV LKP PPE ERL I - COOH; this work; Eurogentec SA); rat anti-E-cadherin 1/50 (DCAD2; Developmental Studies Hybridoma Bank); guinea pig anti-Mbt 1/200 (generated against peptides H2N - SSN RPLPLVDPSEIT C-CONH2 and H2N-PHHNNNKADTTSLNSC-CONH2; this work; Eurogentec SA); mouse anti-Myc 1/50 (9E10; Developmental Studies Hybridoma Bank); rabbit anti-Par1 1/200 (McDonald et al., 2008); guinea pig anti-D-Patj 1/400 (generated against C-terminal peptide H2N - SAS MGA EPD LIP DWR N - COOH; this work; Eurogentec SA); guinea pig anti-Par6 1/1000 (generated against C-terminal peptide H2N - CHH QQA ASN AST IMA SDV KDG VLH L - COOH; this work; Eurogentec SA); and rabbit anti-Sdt 1/250 (Berger et al., 2007), with the appropriate combination of mouse, guinea pig, rabbit, and rat secondary antibodies conjugated to Dy405, Alexa 488, Cy3, or Cy5 as appropriate at 1/200 each (Jackson ImmunoResearch). Retinae were mounted in VectaShield, and imaging was performed using a Leica SP5 confocal. Images were edited using ImageJ and Adobe Photoshop 7.0.

Fluorescent Recovery after Photobleaching

Pupal retinas were mounted at 40% after puparium formation (APF) by removing the pupal cuticle and carefully exposing the retina. Live imaging was performed on a Leica SP5 confocal with a 63× 1.4 numerical aperture (NA) oil immersion objective and the following settings: pixel resolution 512 × 512; speed 400 Hz; 10% 488-nm laser power at 20% argon laser intensity; and 5× zoom. The basal tip of the AJ was marked with a five-pixel-diameter circle region of interest (ROI) and photo-bleached with a single pulse using 90% 488-nm laser power at 20% argon laser intensity. AJ recovery was recorded every 1.293 s with the previously mentioned settings for 200 frames (E-cadherin::GFP).

Statistical Analyses

Length and pixel intensity measurements of Baz and Arm were determined by analyzing confocal images of *mbt* mosaic retina at 40% APF. For

quantification of Baz and Arm length and intensity in retina expressing Arm::myc, ArmSA561,688::myc and ArmSE561,688::myc images were acquired from samples processed simultaneously, using ubi-E-cadherin::GFP retinae as an internal control. In all cases, a threshold was applied to the original data files and then both the length of the Baz- or Arm-positive domain and the mean pixel intensity along this line were measured using the line tool in Fiji (Schindelin et al., 2012). To correct for differences in pixel intensity between retinas of the same genotype within an experiment, the measured average pixel intensity of signal of all junctions in control samples was determined. All individual pixel intensity measurements were then divided by this constant to determine the mean pixel intensity relative to control. In all cases, at least four independent retinae were used for each genotype and matched control.

Mean pixel intensity and area of α-tubulin immunofluorescence in wild-type and $par1^{D16}$ mutant ommatidia were determined by analyzing confocal images of $par1^{D16}$ mosaic retinae at 40% APF. A total of nine confocal images in which a wild-type ommatidium was found adjacent to an ommatidium fully mutant for $par1^{D16}$ were selected for analysis in Fiji. A threshold was applied to the α-tubulin channel and then the wand (tracing) tool was used to specify the regions of α-tubulin staining in wild-type and mutant tissue. The mean intensity and the total area of these paired regions were determined using the measure tool. This method was also used to quantify aPKC immunofluorescence in arm^{3} mutant ommatidia expressing ArmSA561,688.

To determine the percentage of ommatidia below the retinal floor, retinae of the indicated genotypes were dissected at 40% APF. Immunostaining was performed using antibodies against aPKC and Arm to mark the apical membrane and ZA, respectively. Confocal images of each whole retina were acquired, with z-sections taken at two microns intervals. Retinae were manually scored to determine the percentage of ommatidia with aPKC- and Arm-positive membrane domains below the retinal floor. A minimum of four retinae were scored for each genotype. Because in the genotype mbt^{P1}/Y ; *GMR-Gal4/UAS-*mbt^{KD} a proportion of ommatidia found below the retinal floor contained neither apical membrane nor ZA markers, for this genotype, the analysis was repeated using antibodies against E-cadherin, aPKC, and NaK (mouse a5 antibody; 1/50; Developmental Studies Hybridoma Bank [DSHB]) to mark the cell membrane.

For quantification of Baz::GFP puncta, the total number of ectopic Baz::GFP puncta was quantified in the following genotypes: (1) ; *GMR-Gal4/UAS-baz::GFP* ; (2) ; *GMR-Gal4/UAS-bazSA151,1085::GFP* ; (3) mbt^{P1}/Y ; *GMR-Gal4/UAS-baz::GFP* ; and (4) mbt^{P1}/Y ; *GMR-Gal4/UAS-bazSA151,1085::GFP;*. For each genotype, at least 230 cell interfaces from a minimum of five independent retinas were quantified. In all genotypes, it was assumed that one of the GFP-positive puncta scored corresponded to the ZA. All data were tested for normality with the D'Agostino-Pearson test. Parametric samples were tested for statistical significance using an unpaired two-tailed Student's t test. Nonparametric samples were tested for statistical significance using an unpaired two-tailed Mann-Whitney test. For experiments consisting of more than one experimental condition, statistical significance was determined with one-way ANOVA and Dunnett's multiple comparison test or the Kruskal-Wallis multiple comparison test for parametric or non-parametric samples, respectively. For the measurement of α-tubulin and aPKC, mean pixel intensity, and area, statistical significance was determined using the Wilcoxon matched pairs test.

Time series from FRAP experiments were drift corrected in Fiji (Schindelin et al., 2012) using the StackReg plugin, and for each experiment, three different z axis profiles were plotted: (1) from the photo-bleached area; (2) from an equivalent area of a neighboring non-photo-bleached AJ; and (3) from an equivalent area of background. The obtained data were normalized using easyFRAP (Rapsomaniki et al., 2012). E-cadherin::GFP (using ubi-cadherin::GFP) data were fitted to a one-phase association curve in GraphPad Prism. Mobile fractions (y value at infinite times) were determined with Prism based on the fitting curves obtained. The p values were calculated with an unpaired two-tailed Student's t test with Welch's correction. For all data, graphical representation and statistical analysis were performed in GraphPad Prism version 6.0 for Mac (GraphPad Software; http://www.graphpad.com). Columns represent mean, and error bars are the SEM of each dataset.

SUPPLEMENTAL INFORMATION

Supplemental Information includes Supplemental Experimental Procedures and five figures and can be found with this article online at http://dx.doi.org/10.1016/j.celrep.2016.03.014.

AUTHOR CONTRIBUTIONS

R.F.W., F.N.A., E.V., and J.J.B. conducted the experiments; F.P. and R.F.W. designed the experiments; and F.P. wrote the paper with the help of R.F.W.

ACKNOWLEDGMENTS

The authors are very grateful to Alan Hall and Dan Jin for sharing their work on Pak4 phosphorylation of hPar6b prior to publication. We also would like to thank Thomas Raabe, Daniel St Johnston, Andreas Wodarz, The Developmental Studies Hybridoma Bank, and Flybase for reagents. This work was funded by an MRC grant (award number 158745) to F.P. E.V. is the recipient of an MRC CDF.

Received: October 1, 2015
Revised: January 19, 2016
Accepted: February 26, 2016
Published: March 24, 2016

REFERENCES

Afonso, C., and Henrique, D. (2006). PAR3 acts as a molecular organizer to define the apical domain of chick neuroepithelial cells. J. Cell Sci. *119*, 4293–4304.

Benton, R., and St Johnston, D. (2003a). A conserved oligomerization domain in Drosophila Bazooka/PAR-3 is important for apical localization and epithelial polarity. Curr. Biol. *13*, 1330–1334.

Benton, R., and St Johnston, D. (2003b). Drosophila PAR-1 and 14-3-3 inhibit Bazooka/PAR-3 to establish complementary cortical domains in polarized cells. Cell *115*, 691–704.

Berger, S., Bulgakova, N.A., Grawe, F., Johnson, K., and Knust, E. (2007). Unraveling the genetic complexity of Drosophila stardust during photoreceptor morphogenesis and prevention of light-induced degeneration. Genetics *176*, 2189–2200.

Bravo-Cordero, J.J., Magalhaes, M.A., Eddy, R.J., Hodgson, L., and Condeelis, J. (2013). Functions of cofilin in cell locomotion and invasion. Nat. Rev. Mol. Cell Biol. *14*, 405–415.

Dan, C., Kelly, A., Bernard, O., and Minden, A. (2001). Cytoskeletal changes regulated by the PAK4 serine/threonine kinase are mediated by LIM kinase 1 and cofilin. J. Biol. Chem. *276*, 32115–32121.

Doerflinger, H., Vogt, N., Torres, I.L., Mirouse, V., Koch, I., Nüsslein-Volhard, C., and St Johnston, D. (2010). Bazooka is required for polarisation of the Drosophila anterior-posterior axis. Development *137*, 1765–1773.

Engl, W., Arasi, B., Yap, L.L., Thiery, J.P., and Viasnoff, V. (2014). Actin dynamics modulate mechanosensitive immobilization of E-cadherin at adherens junctions. Nat. Cell Biol. *16*, 587–594.

Ha, B.H., Morse, E.M., Turk, B.E., and Boggon, T.J. (2015). Signaling, Regulation, and Specificity of the Type II p21-activated Kinases. J. Biol. Chem. *290*, 12975–12983.

Harris, T.J., and Peifer, M. (2004). Adherens junction-dependent and -independent steps in the establishment of epithelial cell polarity in Drosophila. J. Cell Biol. *167*, 135–147.

Hutterer, A., Betschinger, J., Petronczki, M., and Knoblich, J.A. (2004). Sequential roles of Cdc42, Par-6, aPKC, and Lgl in the establishment of epithelial polarity during Drosophila embryogenesis. Dev. Cell *6*, 845–854.

Jin, D., Durgan, J., and Hall, A. (2015). Functional cross-talk between Cdc42 and two downstream targets, Par6B and PAK4. Biochem. J. *467*, 293–302.

Krahn, M.P., Bückers, J., Kastrup, L., and Wodarz, A. (2010). Formation of a Bazooka-Stardust complex is essential for plasma membrane polarity in epithelia. J. Cell Biol. *190*, 751–760.

McDonald, J.A., Khodyakova, A., Aranjuez, G., Dudley, C., and Montell, D.J. (2008). PAR-1 kinase regulates epithelial detachment and directional protrusion of migrating border cells. Curr. Biol. *18*, 1659–1667.

McKinley, R.F., and Harris, T.J. (2012). Displacement of basolateral Bazooka/PAR-3 by regulated transport and dispersion during epithelial polarization in Drosophila. Mol. Biol. Cell *23*, 4465–4471.

Menzel, N., Schneeberger, D., and Raabe, T. (2007). The Drosophila p21 activated kinase Mbt regulates the actin cytoskeleton and adherens junctions to control photoreceptor cell morphogenesis. Mech. Dev. *124*, 78–90.

Menzel, N., Melzer, J., Waschke, J., Lenz, C., Wecklein, H., Lochnit, G., Drenckhahn, D., and Raabe, T. (2008). The Drosophila p21-activated kinase Mbt modulates DE-cadherin-mediated cell adhesion by phosphorylation of Armadillo. Biochem. J. *416*, 231–241.

Morais-de-Sá, E., Mirouse, V., and St Johnston, D. (2010). aPKC phosphorylation of Bazooka defines the apical/lateral border in Drosophila epithelial cells. Cell *141*, 509–523.

Nam, S.C., Mukhopadhyay, B., and Choi, K.W. (2007). Antagonistic functions of Par-1 kinase and protein phosphatase 2A are required for localization of Bazooka and photoreceptor morphogenesis in Drosophila. Dev. Biol. *306*, 624–635.

Rapsomaniki, M.A., Kotsantis, P., Symeonidou, I.E., Giakoumakis, N.N., Taraviras, S., and Lygerou, Z. (2012). easyFRAP: an interactive, easy-to-use tool for qualitative and quantitative analysis of FRAP data. Bioinformatics *28*, 1800–1801.

Schindelin, J., Arganda-Carreras, I., Frise, E., Kaynig, V., Longair, M., Pietzsch, T., Preibisch, S., Rueden, C., Saalfeld, S., Schmid, B., et al. (2012). Fiji: an open-source platform for biological-image analysis. Nat. Methods *9*, 676–682.

Schneeberger, D., and Raabe, T. (2003). Mbt, a Drosophila PAK protein, combines with Cdc42 to regulate photoreceptor cell morphogenesis. Development *130*, 427–437.

Selamat, W., Tay, P.L., Baskaran, Y., and Manser, E. (2015). The Cdc42 Effector Kinase PAK4 Localizes to Cell-Cell Junctions and Contributes to Establishing Cell Polarity. PLoS ONE *10*, e0129634.

Shahab, J., Tiwari, M.D., Honemann-Capito, M., Krahn, M.P., and Wodarz, A. (2015). Bazooka/PAR3 is dispensable for polarity in Drosophila follicular epithelial cells. Biol. Open *4*, 528–541.

St Johnston, D., and Ahringer, J. (2010). Cell polarity in eggs and epithelia: parallels and diversity. Cell *141*, 757–774.

Tian, Y., Lei, L., and Minden, A. (2011). A key role for Pak4 in proliferation and differentiation of neural progenitor cells. Dev. Biol. *353*, 206–216.

Totong, R., Achilleos, A., and Nance, J. (2007). PAR-6 is required for junction formation but not apicobasal polarization in C. elegans embryonic epithelial cells. Development *134*, 1259–1268.

Wallace, S.W., Durgan, J., Jin, D., and Hall, A. (2010). Cdc42 regulates apical junction formation in human bronchial epithelial cells through PAK4 and Par6B. Mol. Biol. Cell *21*, 2996–3006.

Walther, R.F., and Pichaud, F. (2006). Immunofluorescent staining and imaging of the pupal and adult Drosophila visual system. Nat. Protoc. *1*, 2635–2642.

Walther, R.F., and Pichaud, F. (2010). Crumbs/DaPKC-dependent apical exclusion of Bazooka promotes photoreceptor polarity remodeling. Curr. Biol. *20*, 1065–1074.

Wei, S.Y., Escudero, L.M., Yu, F., Chang, L.H., Chen, L.Y., Ho, Y.H., Lin, C.M., Chou, C.S., Chia, W., Modolell, J., and Hsu, J.C. (2005). Echinoid is a component of adherens junctions that cooperates with DE-Cadherin to mediate cell adhesion. Dev. Cell *8*, 493–504.

Zihni, C., Munro, P.M., Elbediwy, A., Keep, N.H., Terry, S.J., Harris, J., Balda, M.S., and Matter, K. (2014). Dbl3 drives Cdc42 signaling at the apical margin to regulate junction position and apical differentiation. J. Cell Biol. *204*, 111–127.

Cell Reports, Volume *15*

Supplemental Information

Pak4 Is Required during Epithelial Polarity Remodeling through Regulating AJ Stability and Bazooka Retention at the ZA

Rhian F. Walther, Francisca Nunes de Almeida, Evi Vlassaks, Jemima J. Burden, and Franck Pichaud

Supplementary Figure 1: Apico-basal polarity remodeling in the developing photoreceptor

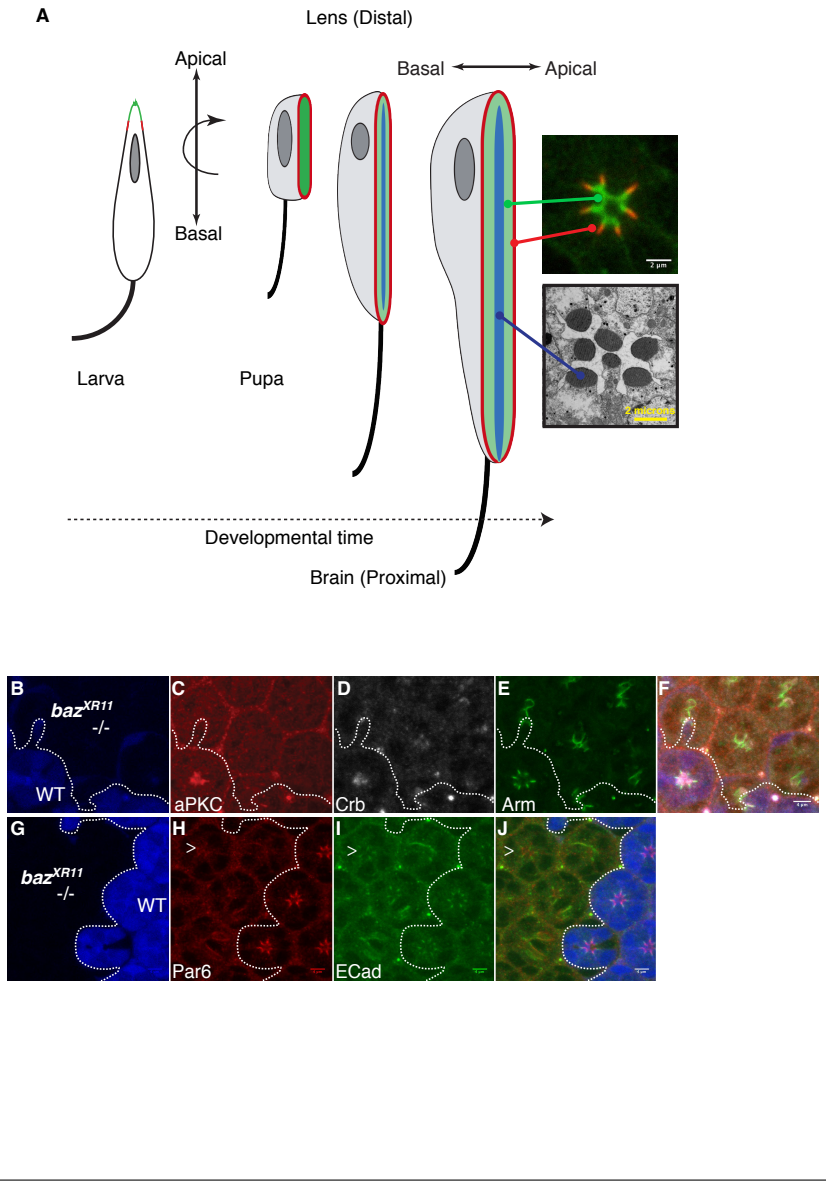

Supplementary Figure 2: *mbt* regulates apical membrane differentiation

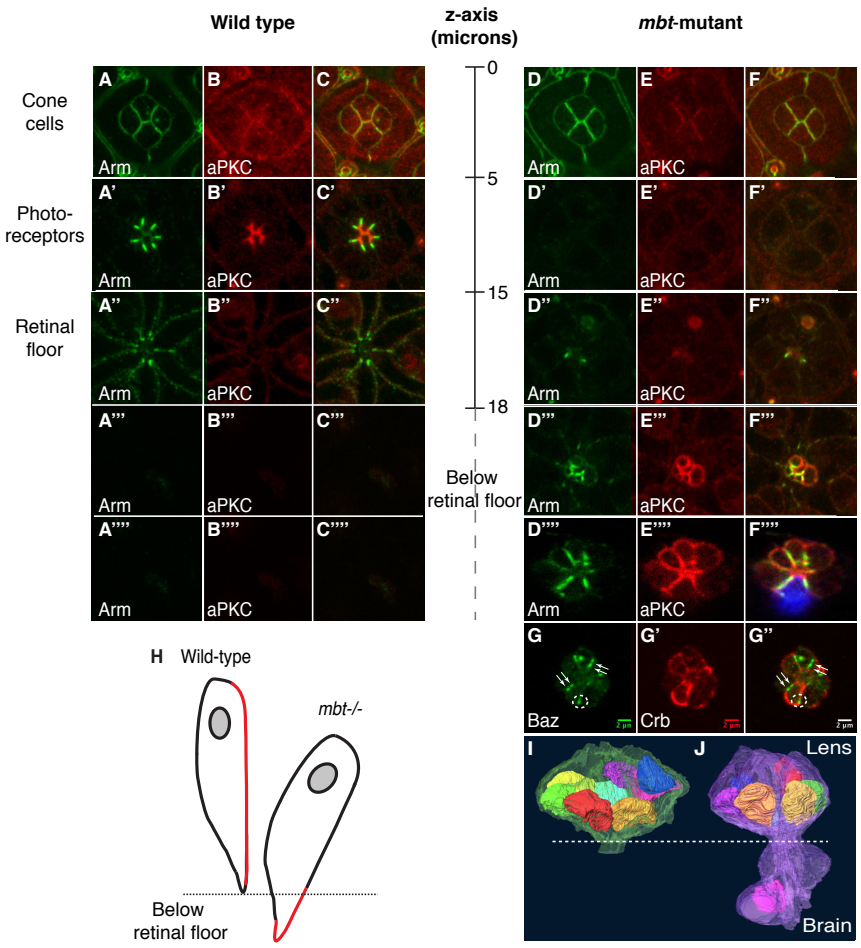

Supplementary Figure 3: Regulated Mbt kinase activity is required during apical membrane differentiation

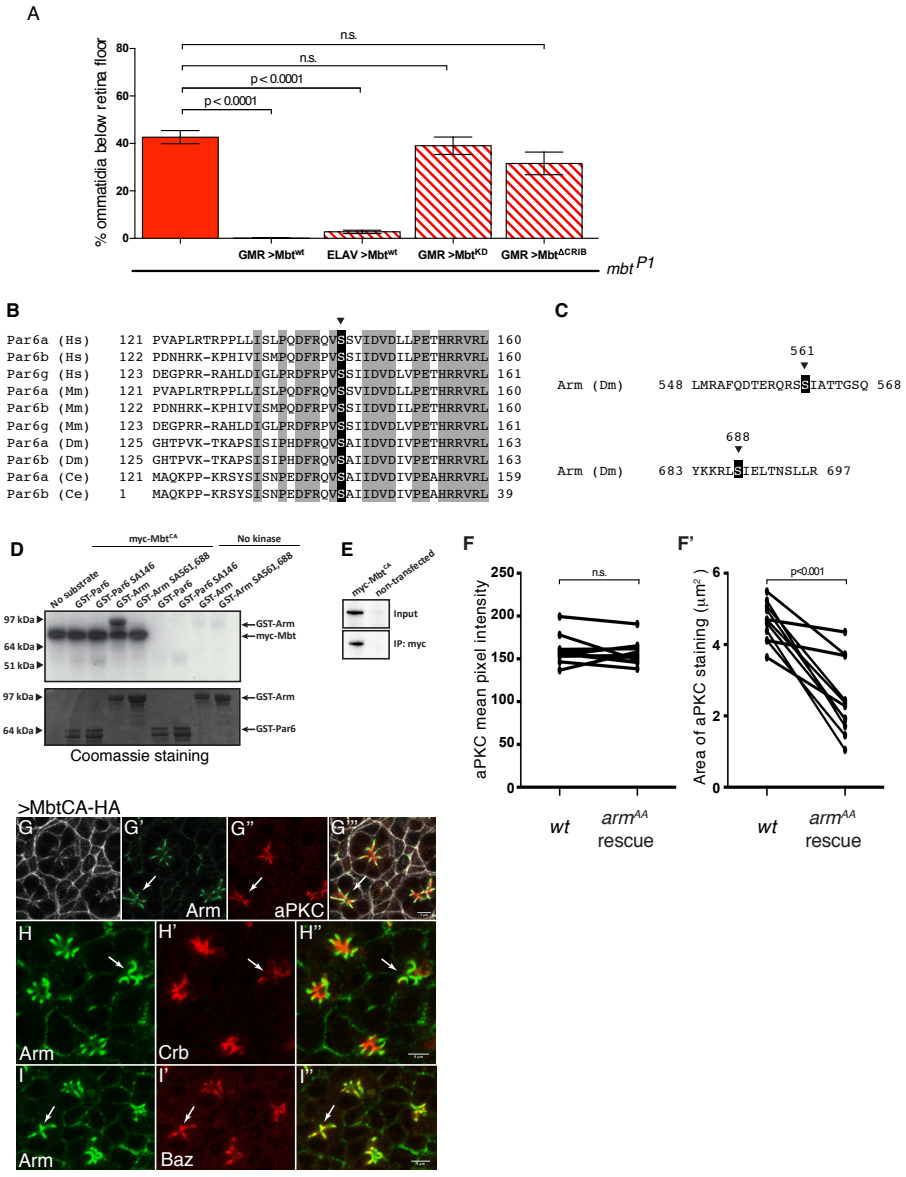

Supplementary Figure 4: Arm phosphorylation regulates *AJ* material stability

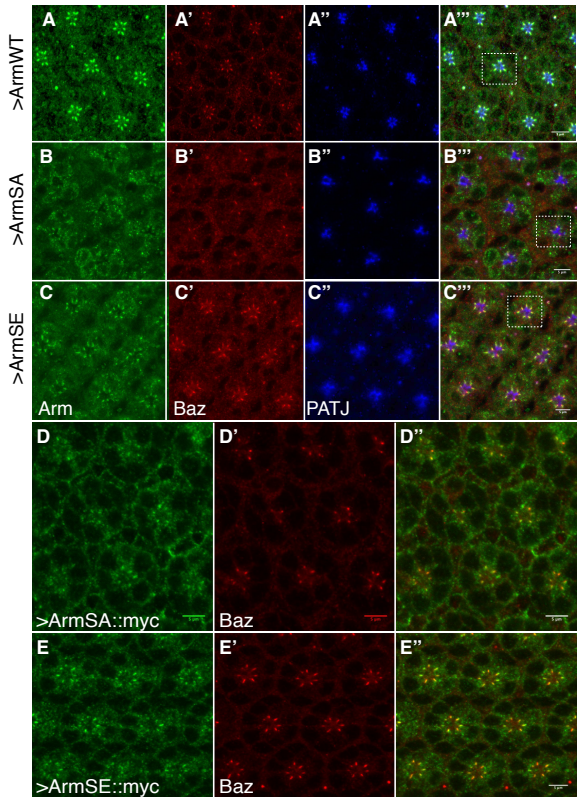

Supplementary Figure 5: Par1 localization and function during photoreceptor morphogenesis

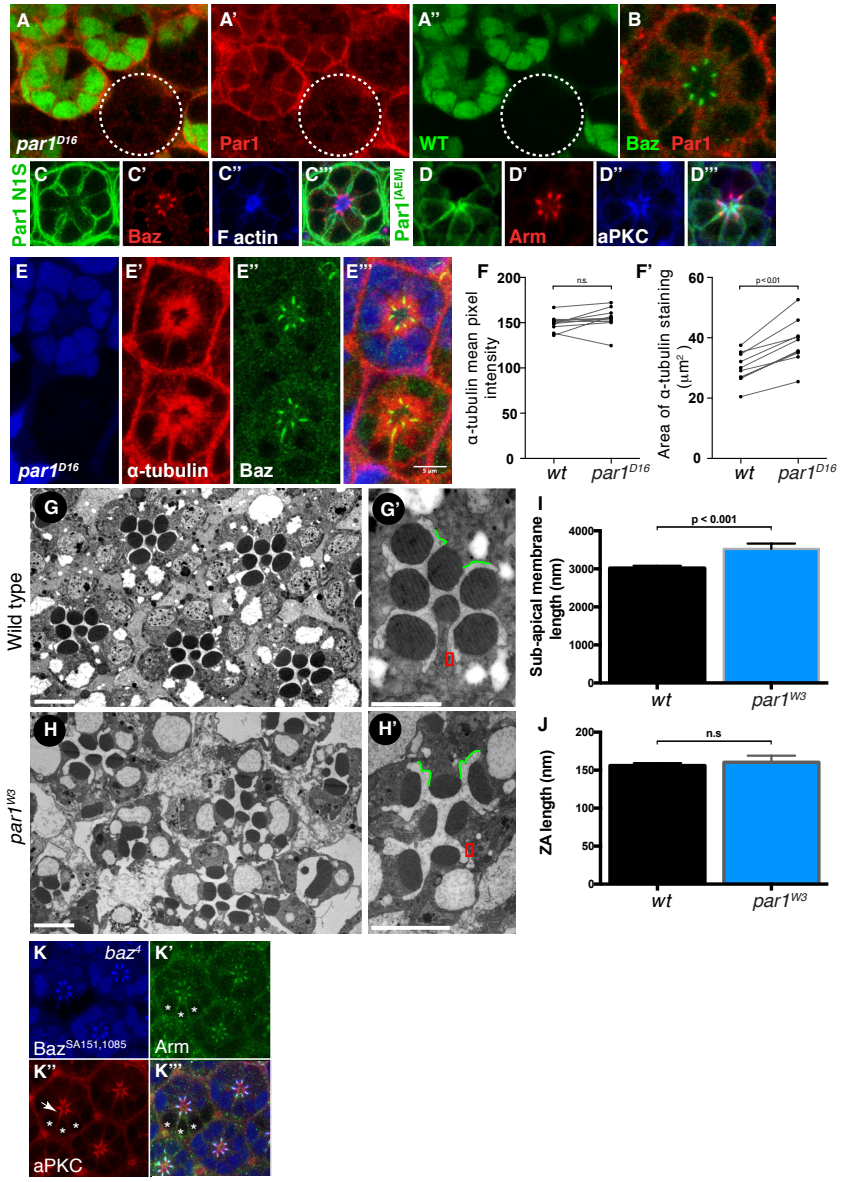

Supplementary Figure 1: Apico-basal polarity remodeling in the developing photoreceptor (A) During pupation, the apico-basal axis of the photoreceptor rotates 90 degrees as the cell undergoes morphogenesis. During pupal development, the new apical membrane domains are subsequently formed over time. *ZA* (red), sub-apical membrane (green) and stack of microvilli (blue). A representative confocal section of a wild type pupal ommatidium and electron micrograph of an adult ommatidum are shown, indicating the respective apical membrane domains. (B-F) baz^{XR11} mutant clone in the pupal retina. Mutant cells lack GFP (blue). aPKC (red), Crb (gray) and Arm (green). (G-J) baz^{XR11} mutant clone in the pupal retina. Par6 (red), E-cadherin (green). A white arrowhead points to residual Par6 staining (H) and *AJ* domains (I). Scale bars = 4 microns.

Supplementary Figure 2: *mbt* regulates apical membrane differentiation (A-F) Series of confocal sections along the lens to brain axis of a wild type ommatidium (A-C) and an mbt^{P1} mutant (D-F). Arm (green), aPKC (red) and merged images are shown in (C-C'''' and F– F''''). (A-F) Cone cell *AJ*. (A'-F') Confocal sections taken at the level of the photoreceptors. (A''-F'') Confocal sections of the retinal floor. In (D'''- F''' and D''''- F'''') consecutive sections below the retina are labeled BRF (Below Retinal Floor). (G-G'') Confocal section of an ommatidium mutant for mbt^{P1} stained for Baz (green) and Crb (red) imaged below the retinal floor. White arrows indicate tandem accumulations of *AJ* material while basally shifted *AJ* material is highlighted by a dashed circle. A merged image is shown in (G''). Scale bars = 2 microns.

(H) Representation of a wild type (left) and *mbt*^{P1} mutant ommatidium (right). The floor of the retina is represented as a dashed line. The apical membrane (i.e sub-apical membrane and *ZA*) is represented as a red line. (I-J) 3D rendering of serial electron microscopy (3View) performed on a wild type (I) and *mbt*^{P1} mutant (J) developing ommatidium at 45% after puparium formation. Photoreceptor nuclei are in solid colors. Cell membranes are in green (wild type) and purple (*mbt*^{P1}). The floor of the retina is highlighted by a dashed white line.

Supplementary Figure 3: Regulated Mbt kinase activity is required during apical membrane differentiation (A) Delamination phenotype in *mbt*^{P1} retina and *mbt*^{P1} expressing the wild type, kinase dead (KD) or ΔCRIB form of Mbt. For each genotype a minimum of 4 retinas were quantified. Columns represent mean and error bars are the SEM of each data set. Statistical significance was determined with one-way ANOVA and Dunnett's multiple comparison test for parametric samples. (B) Alignment of Par6 (Jin et al., 2015). (C) Serine residues 561 and 688 in Arm (Menzel et al., 2008). (D) *In vitro* phosphorylation assay. (E) Myc::Mbt^{CA} was expressed and isolated from S2 cells. (F) Mean pixel intensity of aPKC (F) and aPKC area (F') in paired wild type and *arm*^{3} mutant ommatidia expressing ArmSA561,688::myc. Statistical significance was determined using the Wilcoxon matched pairs test. (G-I) Overexpression of MbtCA (gray). (G') Arm (green) and (G'') aPKC (red). White arrows in G' and G'' indicate an apical domain where no separation of Arm from aPKC occurs. (H) Arm (green) and

(H') Crb (red). (I) Arm (green) and (I') Baz (red). (H-H') A white arrow highlights a poorly differentiated apical domain. (I-I'') A white arrow highlights an ommatidium with defects in apical-basal polarity. Scale bars: 4 microns.

Supplementary Figure 4: Arm phosphorylation regulates *AJ* material stability (A) Overexpression of Arm::myc. In (A-C), Arm (green), Baz (red), PATJ (blue). (B) Overexpression of ArmSA561,688::myc and (C) ArmSE561,688::myc. (D) Overexpression of ArmSA561,688::myc and (E) ArmSE561,688::myc. Myc (green), Baz (red). Scale bars 5 microns.

Supplementary Figure 5: Par1 localization and function during photoreceptor morphogenesis (A-A'') $par1^{D16}$ mutant cells lack nuclear GFP (green). Par1 (red). (B) Par1 (red) and Baz (green). (C-C''') Par-N1S::GFP transgene (green), Baz (red) and F-Actin (blue). (D-D''') Par1-N1S::GFP (AEM) (green), Arm (red) and aPKC (blue). (E-E''') Photoreceptors mutant for $par1^{D16}$ lack nuclear GFP (blue). α-tubulin (red), Baz (green). (F-F') Mean pixel intensity of α-tubulin immunofluorescence (F) and total area of α-tubulin fluorescence (F') in paired wild type and $par1^{D16}$ mutant ommatidia. In (F) and (F'), statistical significance was determined using the Wilcoxon matched pairs test. (G-H) Electron microscopy of a wild type retina (G-G') and a $par1^{W3}$ mutant retina (H-H'). A *ZA* is boxed in red and a sub-apical membrane is highlighted in green in (G') and (H'). Scale bars = 2 microns. (I-J) Length of the sub-apical membrane (I) and *ZA* (J) in wild type and $par1^{W3}$ retina. Columns represent mean and error bars are the SEM of each data set.

(K) *baz*^{4} mutant cells lacking GFP (blue) are highlighted by a white star. The blue channel is also used to show the BazSA151,1085::GFP protein. Arm (green), aPKC (red). A white arrow points to the rescue of aPKC localization.

Fly strains and genetics

The following genotypes were used:

Both the null allele *mbt^{P1} and* hypomorphic allele *mbt^{P3}* (Schneeberger and Raabe, 2003) were used all through this study.

mbt^{P1}FRT19A/FRT19AUbiGFP;eyflp (this work), (Newsome et al., 2000). *w,baz^{4}FRT9.2/ FRT9.2 UbiGFP;eyflp*. (Nusslein-Volhard et al., 1987). *w,baz^{XR11}FRT19A/ FRT19A UbiGFP;eyflp* and *w,baz^{EH747}FRT19A/ FRT19A UbiGFP;eyflp* (Shahab et al., 2015). *w,baz^{4},sdt^{XP96} FRT9.2/ FRT9.2 UbiGFP;eyflp* (Muller and Wieschaus, 1996). *mbt^{P1}, baz^{4} FRT9.2/FRT9.2 UbiGFP;eyflp* (this work). *w,hsflp;;crb^{11A22}FRT82B/ FRT82B UbiGFP* (Tepass et al., 1990); *w, eyflp ; aPKC^{k06403} FRT42D/ FRT42D UbiGFP* (Wodarz et al., 2000). *w,arm^{3} FRT101/FRT101 UbiGFP;eyflp* (Peifer et al., 1991). *w; EGUF, par1^{w3} FRT42D/FRT42D GMR-hid,cl* (Shulman et al., 2000). *eyFLP/+;par1$^{\Delta 16}$FRTG13/FRTG13 UbiGFP. GMR-Gal4/UAS-par1N1S::GFP; GMR-Gal4/UAS-par1::N1S GFP (AEM);* (Doerflinger et al., 2007); *GMR-Gal4/UAS-baz::GFP; and bazSA151,1085::GFP* (Benton and St Johnston, 2003). *;GMR-Gal4/ UAS-bazSA151,1085::GFP; mbt^{P1}/Y*; *GMR-Gal4/UAS-baz::GFP;. mbt^{P1}/Y; GMR-Gal4/UAS-bazSA151,1085::GFP;. UAS-mbt^{CA}/CyO; GMR-Gal4/TM2.* (Menzel et al., 2007). *mbt^{P1}/Y; GMR-Gal4/+;UAS-mbt^{WT}/+. mbt^{P1}/Y; ELAV-Gal4/+;UAS-mbt^{WT}/+. mbt^{P1}/Y; GMR-Gal4/UAS-mbt^{CA};. mbt^{P1}/Y*; *GMR-Gal4/+;UAS-mbt$^{\Delta CRIB}$/+* (Menzel et al., 2007). *GMR-Gal4/+; UASt-arm::myc/+* (this work). *GMR-Gal4/+; UASt-armSA561,688::myc/+* (this work). *GMR-Gal4/+ ; UASt-armSE561,688::myc/+* (this work). *w,arm^{3} FRT101/FRT101*

UbiGFP;eyflp/GMR-Gal4; UASt-arm::myc/+;. w,arm^{3} *FRT101/FRT101 UbiGFP;eyflp/GMR-Gal4; UASt-armSA561,688::myc/+;. w,arm*^{3} *FRT101/FRT101 UbiGFP;eyflp/GMR-Gal4*; *UASt-armSE561,688::myc/+*;. General fly cultures and crosses were carried out at 25°C.

Transgenic flies

Clone LD23131 encoding Armadillo cDNA was obtained from the Drosophila Genomics Resource Center and then subcloned into the pENTR™/D-TOPO® vector (Invitrogen). Residues S561 and S688 were mutated to alanine or glutamic acid using the QuikChange Lightning Multi Site-Directed Mutagenesis Kit. Following sequence verification (MWG Eurofins), the wild-type, SA561,688 and SE561,688 entry clones were used for Gateway cloning (Invitrogen) into the pTWM destination vector (Murphy lab) for expression of a C-terminally Myc tagged protein under the control of the UAST promoter. Injections were performed by BestGene (Chino Hills, CA).

Kinase Assay

GST-tagged Par6, Par6SA146, Arm and ArmSA561,688 were cloned into a pDEST15 vector containing an N-terminal GST tag using the Gateway Cloning System (Invitrogen). Bacteria were lysed by sonication in Lysis Buffer (50 mM Tris HCl pH7.6, 50 mM NaCl, 5 mM $MgCl_2$, 0.5% Triton X-100, 10 mM DTT) in the presence of protease inhibitor (EDTA-free Complete Protease Inhibitor [Roche]). GST fusion proteins were purified using Glutathione Sepharose 4 Fast Flow beads (GE Healthcare) and then washed (50 mM Tris HCl pH 7.4, 50 mM NaF, 300 mM NaCl, 1 % Triton X-100, 1 mM DTT, EDTA-

free Complete Protease inhibitor), eluted (40 mM Glutathione, 50 mM Tris HCl, pH 8.0), and dialyzed against lysis buffer with 40 % glycerol.

Drosophila Schneider S2 cells (DGRC) were transiently transfected with pActin-Myc::Mbt^{CA} (S492N, S521E) and lysed in 50 mM Tris HCl pH 7.5, 150 mM NaCl, 1 % Triton X-100, 5 mM DTT, EDTA). The lysates were incubated with 4 µg of anti-myc agarose beads (Sigma) for 1h at 4°C. The beads were washed with the kinase buffer (20 mM HEPES, pH 7.6, 150 mM NaCl, 20 mM $MgCl_2$, 10 µL/mL phosphatase inhibitor [Sigma], 20 µM ATP). Beads with kinase were split in 20 µL fractions and then mixed with 30 µg of each substrate GST fusion protein as well as 1 µL of [ɣ-^{32}P]-ATP (5 µCi). Each condition was incubated at 30^{o}C for 30 min. The proteins were separated by SDS-PAGE and visualized by autoradiography.

Electron microscopy

Electron microscopy was performed as in (Pinal et al., 2006) using a Tecnai G2 Spirit transmission electron microscope (FEI, The Netherlands) equipped with a Morada CCD camera (Olympus Soft Imaging Systems). Image quantification was performed using iTEM software.

For serial block face scanning electron microscopy, samples were prepared using a combinatorial heavy metal staining protocol involving thiocarbohydrazide, double osmication and *en bloc* Walton's lead aspartate as described by Ellisman and colleagues; http://ncmir.ucsd.edu/sbfsem-

protocol.pdf. Embedded samples were oriented, re-embedded, and regions of interest were identified from 70nm sections examined by TEM. The region of interest was then excised and mounted with cyanoacrylate glue onto specimen pins. These samples were further trimmed before being coated with gold palladium and mounted in the 3View microtome (Gatan, USA). Once aligned, the sample and microtome were returned to the SEM chamber and put under vacuum. The regions of interest on the block face were re-located in the SEM using backscattered electron detection and the imaging and cutting parameters were optimised for each sample. Data sets of 999 sections were collected with section thickness 75-100nm in a Zeiss Sigma FEG-SEM coupled to the Gatan 3View. Data was imported into Amira (VSG, France), where the cells of interest were manually segmented, reconstructed and rendered in 3D.

References

Benton, R., and St Johnston, D. (2003). Drosophila PAR-1 and 14-3-3 inhibit Bazooka/PAR-3 to establish complementary cortical domains in polarized cells. Cell *115*, 691-704.

Menzel, N., Schneeberger, D., and Raabe, T. (2007). The Drosophila p21 activated kinase Mbt regulates the actin cytoskeleton and adherens junctions to control photoreceptor cell morphogenesis. Mech Dev *124*, 78-90.

Muller, H.A., and Wieschaus, E. (1996). armadillo, bazooka, and stardust are critical for early stages in formation of the zonula adherens and maintenance of the polarized blastoderm epithelium in Drosophila. J Cell Biol *134*, 149-163.

Newsome, T.P., Asling, B., and Dickson, B.J. (2000). Analysis of Drosophila photoreceptor axon guidance in eye-specific mosaics. Development *127*, 851-860.

Nusslein-Volhard, C., Frohnhofer, H.G., and Lehmann, R. (1987). Determination of anteroposterior polarity in Drosophila. Science *238*, 1675-1681.

Peifer, M., Rauskolb, C., Williams, M., Riggleman, B., and Wieschaus, E. (1991). The segment polarity gene armadillo interacts with the wingless signaling pathway in both embryonic and adult pattern formation. Development *111*, 1029-1043.

Pinal, N., Goberdhan, D.C., Collinson, L., Fujita, Y., Cox, I.M., Wilson, C., and Pichaud, F. (2006). Regulated and polarized PtdIns(3,4,5)P3 accumulation is essential for apical membrane morphogenesis in photoreceptor epithelial cells. Current biology : CB *16*, 140-149.

Schneeberger, D., and Raabe, T. (2003). Mbt, a Drosophila PAK protein, combines with Cdc42 to regulate photoreceptor cell morphogenesis. Development *130*, 427-437.
Shahab, J., Tiwari, M.D., Honemann-Capito, M., Krahn, M.P., and Wodarz, A. (2015). Bazooka/PAR3 is dispensable for polarity in Drosophila follicular epithelial cells. Biology open *4*, 528-541.
Shulman, J.M., Benton, R., and St Johnston, D. (2000). The Drosophila homolog of C. elegans PAR-1 organizes the oocyte cytoskeleton and directs oskar mRNA localization to the posterior pole. Cell *101*, 377-388.
Tepass, U., Theres, C., and Knust, E. (1990). crumbs encodes an EGF-like protein expressed on apical membranes of Drosophila epithelial cells and required for organization of epithelia. Cell *61*, 787-799.
Wodarz, A., Ramrath, A., Grimm, A., and Knust, E. (2000). Drosophila atypical protein kinase C associates with Bazooka and controls polarity of epithelia and neuroblasts. J Cell Biol *150*, 1361-1374.